FERROCENE CONJUGATED DNA FOR BIOSENSING AND ANTISENSE APPLICATIONS

by

HOLLY ROBERTS

A thesis submitted to the University of Birmingham for the degree of:

DOCTOR OF PHILOSOPHY

School of Chemistry

College of Engineering and Physical Sciences

University of Birmingham

April 2018

Abstract

Deoxyribose nucleic Acid (DNA) is the building block of life and, as such, has been investigated for a wide range of uses. In particular, DNA has been investigated for use in biosensing applications and the treatment of diseases involving DNA replication or protein synthesis. In order to enhance the sensing capabilities of DNA, an array of tags and modified nucleic acids have been synthesised and trialled. This thesis studies both the sensing capabilities and the stability of electrochemical reporters based on the redox active molecule ferrocene.

The four topics investigated in this thesis are as follows:

1. Two synthetic ferrocene nucleic acid (FcNA) mimics were incorporated into the backbone of a DNA strand in a central position. These probes were then attached to the surface of gold electrodes through thiols incorporated at the 3' position to form mixed monolayers with 6-mercaptohexan-1-ol. These monolayers were used to detect target DNA with the aim of increasing sensitivity and decreasing the amount of probe required for sensing. The monolayers were also assessed for their long-term and electrochemical stability as well as their resilience towards multiple uses. Target detection was possible with square wave voltammetry due to the reliance of this technique on the 'critical frequency' of the redox active molecule and how this changes on duplexation.
2. DNA probes containing thymine-modified FcNA reporter groups were investigated further due the ability of mercuric ions (Hg^{2+}) to bind covalently to two opposite thymine groups. Detection of these ions was possible through

both cyclic voltammetry and square wave voltammetry although the latter gave the most profound distinction.

3. A 5’ DNA tag based on two covalently connected ferrocene molecules was compared and contrasted with a tag containing a single ferrocene molecule in terms of its DNA target sensing and stability to electrochemical interrogation. Interestingly, the presence of two redox active centres in close proximity gave rise to two redox waves, one of which displayed solution based electrochemical behaviour and one which displayed surface bound behaviour due to the potential of zero charge of the gold electrode.
4. The FcNA-conjugated DNA probes are assessed for their potential as therapeutic antisense agents by exposing the single stranded and duplexed probes to a DNase and two types of exonuclease enzyme. The ability of the FcNA molecules to withstand enzymatic digestion, and so prevent release of the target DNA strand when in duplex form, was monitored using polyacrylamide gel electrophoresis.

For my husband, Andrew, my forever and always, and my daughter, Eleanor, without whom the sun would not shine.

Acknowledgments

Where to begin? There are so many people who have had an influence on this thesis whether it was an enlightening conversation at a conference or an impromptu Costa Coffee moment when it seems like the world had caved in. It would be impossible to thank them all individually but there are some specific people I would like to mention here.

First thanks must, of course, go to Professor Jim Tucker for allowing me to complete my Ph. D course under his supervision. It has been a thoroughly enjoyable experience through your guidance, both academic and personal, your support and calming influence. I always managed to come out your office smiling no matter what the issue. The same thanks go to Dr Sarah Horswell for being so enthusiastic about unexpectedly becoming my second supervisor. Your patience with my lack knowledge and common sense has been outstanding and I would not have got very far without you!

These four years would not have gone so quickly if it wasn't for the good humour and fantastic support of the entirety of the Tucker group past and present. There are some people who have really made this time the best of my life. Huy and John, I could not have coped without your wonderful teaching, patience and friendship. Aysha, Ed, Klaudia, Media, Georgina and Francia, thanks for making the final two years such a laugh and providing a friendly environment to work in. Also to Sanaz, Louise, Sarah and Phil for the moral support! Apologies to the countless undergraduates I have used and abused over the years!

Thanks to the analytical facilities staff for their sterling work, in particular Dr Chi Tsang, Peter Ashton and Dr Allen Bowden for dealing with my regular 'emergencies'.

Thanks to Dr Paula Mendes and her group for use of the SPR instruments and their technical knowledge.

Thanks to the School of Chemistry and EPSRC for funding this studentship as well as Advantage West Midlands and Science City for providing the equipment.

On a more personal note, Siobhan, Becky and Johnathon, honestly the best friends anyone could ask for, we've been through a lot, good and bad, and I'm sure there will be many happy times ahead.

There are some people without whom I would genuinely not be here. Mom and Dad, without your support and selfless commitment to looking after Ella I would not have been able to have the time or money to follow my dreams. I am truly eternally grateful (and promise to provide you with more grandchildren!). Thanks to the rest of my family, particularly Nan, Laura, Callum, Mary and the Bethels for the all good times and pretending to look interested when I talk about my project!

Finally, there are two people who make the sun rise. My wonderful, patient, loving, long-suffering husband: Andrew, where would I be without you? And my beautiful daughter Eleanor: you have taught me the true value of life; you make me so proud every day and have had more influence on this volume than you will ever know. I love you both so much.

Table of Contents

List of Abbreviations

Abbreviation	Full term
Γ	Surface Coverage / molecules cm^{-2}
ΔE_p	Peak Separation
A	Adenine
AFM	Atomic Force Microscopy
AMCA	Trans-4-(Aminomethyl) cyclohexanecarboxylic Acid
AU	Absorption Units
AuNP	Gold Nanoparticle
BPB	Bromo-phenol Blue
C	Cytosine
CBS	Corey Bakshi Shibata
CD	Circular Dichroism Spectroscopy
Cp	Cyclopentadiene Ring
CV	Cyclic Voltammetry
D	Diffusion Coefficient / cm^2s^{-1}
DCM	Dichloromethane
DIPEA	N,N-Diisopropylethylamine
DMT	Dimethoxytrityl
DNA	Deoxyribose Nucleic Acid
$E_{1/2}$	Redox Potential / V
EDTA	Ethylenediaminetetraacetic acid
EI	Electron Impact
EIS	Electrochemical Impedance Spectroscopy
E_p^a	Anodic Peak Potential / V
E_p^c	Cathodic Peak Potential / V
$E_{1/2}$	Half wave potential
ES	Electrospray
ESI MS	Electrospray Ionisation Mass Spectrometry
Exo I	*Exonuclease I*
Exo III	*Exonuclease III*

Fc	Ferrocene
FcNA	Ferrocene Nucleic Acid
G	Guanosine
HD	Huntingdon's Disease
HIV	Human Immuno Virus
HPLC	High Performance Liquid Chromatography
ICP MS	Inductively Coupled Plasma Mass Spectrometry
I_p^a	Anodic Peak Current / A
I_p^c	Cathodic Peak Current / A
LOD	Limit of Detection
LNA	Locked Nucleic Acid
M-DNA	Metallated DNA
m/z	Mass to charge ratio
MB	Methylene Blue
MB	Molecular Beacon
MCH	6-mercaptohexan-1-ol
MRI	Magnetic Resonance Imaging
mRNA	Messenger RNA
MS	Mass Spectrometry
NMR	Nuclear Magnetic Resonance
NP	Nanoparticle
NT	Non-thiolated
PAGE	Polyacrylamide Gel Electrophoresis
PCR	Polymerase Chain Reaction
PMO	Phosphorodiamidate Morpholino Oligomer
PNA	Peptide Nucleci Acid
Ppb	Part Per Billion
PS	Phosphorothioate
PTFE	Polytetrafluoroethylene
R_f	Retardation Factor
RNA	Ribose Nucleic Acid
SAM	Self Assembled Monolayer

SNP	Single Nucleotide Polymorphism
SPR	Surface Plasmon Resonance
SPS	Solvent Purification System
SWV	Square Wave Voltammetry
T	Thymine
TBE	Tris Borate EDTA
TEA	Triethylamine
TEAA	Triethylammonium Acetate
T_m	Thermal Melting Temperature
TOF	Time of Flight
tRNA	Transfer RNA
U	Uracil
UV	Ultraviolet
Vis	Visible
XCFF	Xylenecyanol FF
XPS	X-Ray Photoelectron Spectroscopy

Chapter 1

Introduction

1.1 Deoxyribonucleic Acids (DNA)

It is perhaps unsurprising, as one of the central molecules upon which all life is based,[1] that possible modifications to the natural deoxyribonucleic acid (DNA) molecule have been widely explored since its structure was elucidated by Watson and Crick in 1953.[2] The ability to artificially design and fine tune novel properties for analogues based on DNA have implications for medicine, defence from biological warfare, forensics and nanotechnology in terms of biological sensing and bionanotechnology.[3–5]

1.1.1 DNA Components

DNA is comprised of three main building blocks: a phosphate backbone, deoxyribose sugar units and nucleobases (Figure 1.1). The ends of the DNA strand are labelled 3' or 5' depending on which carbon on the deoxyribose sugar the phosphate group is attached to (labelling shown in Figure 1.2). Natural DNA exists as a duplex and is formed when complementary nucleobases on opposite strands hydrogen bond and pull the strands together; adenine binds to thymine and cytosine binds to guanine. In ribose nucleic acid (RNA: single stranded molecules similar in structure to DNA but with a ribose sugar) the thymine is replaced with uracil. In order to accommodate the bond angles of the sugar-phosphate backbone on hydrogen bonding, DNA regularly forms the double helix structure characterised by Watson and Crick (Figure 1.2).[2]

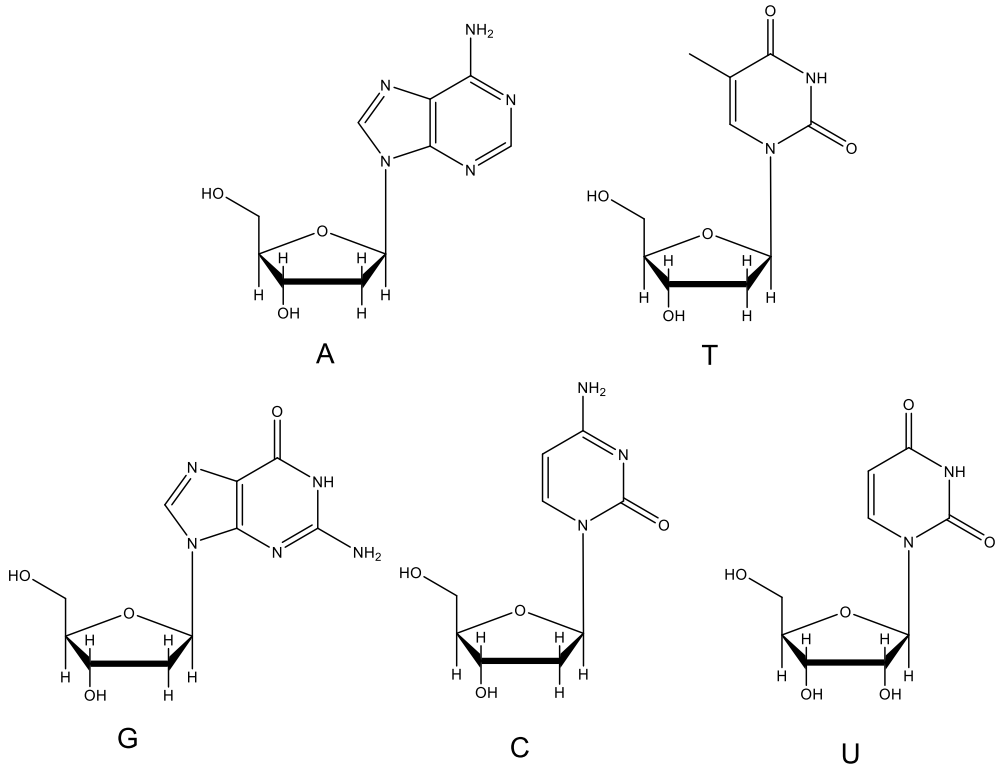

Figure 1.1: The nucleobases. Top: left: adenosine, right: thymidine. Bottom: left: guanosine, centre: cytosine, right: uracil.

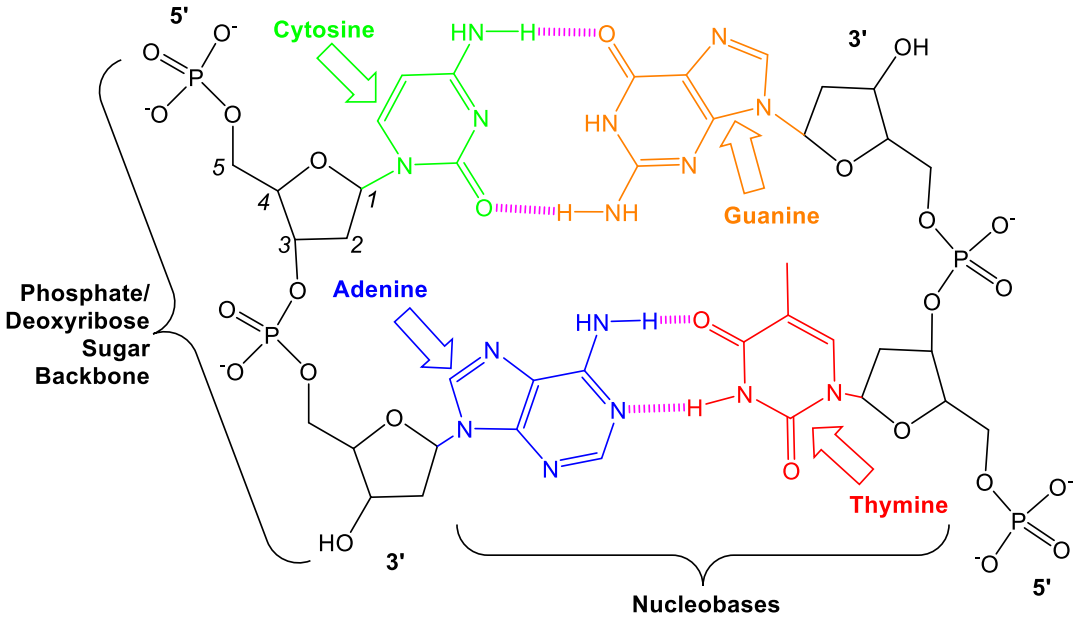

Figure 1.2:Structure of DNA and double helix[6]

1.1.2 DNA Stability

The strength of the interactions between two strands of DNA can be determined through thermal melting studies, a technique in which the temperature at which 50% of the DNA duplex (ds DNA) has denatured and reverted back to single stranded DNA (ss DNA) is determined by monitoring the change in UV absorption at 260 nm. Essentially, stronger interactions result in the need for a higher temperature to separate the strands. The strength of DNA duplexes is an important issue to consider and can be affected by a number of factors.[7]

The nucleobases themselves have two contributing factors. The most obvious is the complementarity afforded by the hydrogen bonding between corresponding bases. As well as stability, the complementary nature of the hydrogen bonding base pairs allows for sequences to form in the correct order necessary to code for the 100,000 proteins required by the body.[8] However, it has been noted on a number of occasions that the presence of π-π stacking which exists between the aromatic rings present in each nucleobase has a larger effect on stability than the hydrogen bonding alone. [9–12] Other factors include the hydrophobicity, salt composition and concentration in the environment of the DNA. For example, divalent salts are more stabilising than monovalent salts due to the formers increased ability to negate the multiple negative charges which exist along the DNA backbone and so reduce repulsion between the strands.[7]

The ordering of the bases also has an effect on stability since base pairs have varying dipoles and differing interactions with the pairs positioned above and below.

1.1.3 DNA Structure

Natural DNA generally exists as 'B-DNA'. The presence of multiple C-G pairs (with three consecutive C-G base pairs as a minimum[13]) results in a looser system known as 'Z-DNA'. It also has a left helical structure as oppose to the right twist of natural DNA and its major and minor grooves are similar in size (Figure 1.3). It is not yet known to exist in any biological system and is generally an unfavourable conformation.[6]

Another natural form of DNA is A-DNA which is common in RNA duplexes and is more similar to B-DNA but forms tighter helices as shown in Figure 1.3. It generally forms under dehydrating conditions and so is commonly seen in crystal structures generated for DNA due to the methods required to make crystals.[6]

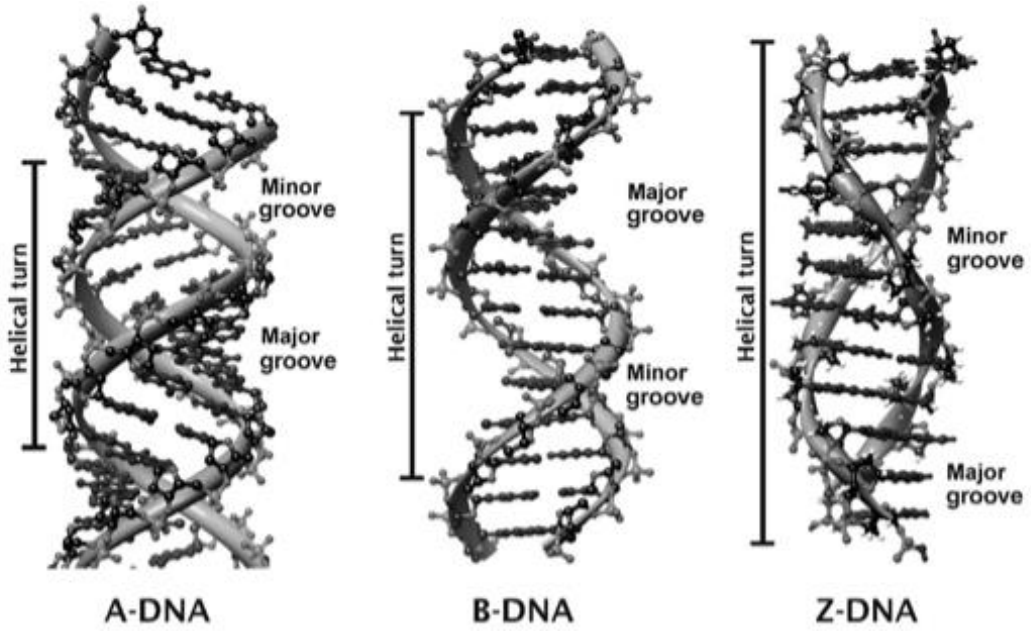

Figure 1.3: Structure of the three major types of DNA. The image was taken from Nakamoto and co-workers.[6]

1.2 Biosensing with DNA

It has been shown that alternatives of all the main building blocks can be synthetically produced and incorporated into DNA strands. Pinheiro and Holliger[1] have briefly reviewed this expansive area of research, giving examples of alternative nucleotide, sugar and backbone linkers.

A major focus for DNA modification is biosensing. The ability to sense a range of species including but not limited to small molecules, proteins or single nucleotide polymorphisms (SNP; variations in the genetic sequence of one nucleotide at a specific position[14] which is present in less than 1% population and can indicate predisposition towards contracting a disease and/or health issues) is important in the shift towards individual 'tailor-made' health care.[15] Before considering the role of ferrocene, it is prudent to discuss the more commonly used biosensing methods first.

Biosensing with a DNA strand probe is possible when a target strand or molecule hybridises or binds to a probe which is specific for the target.[16] The hybridisation is then detectable by a reporter molecule. There are a number of different types of reporter molecules used. Radioactive isotopes have been used due to their low limits of detection; [17] it has been possible to detect DNA in the tens of picomoles.[18] However, the intrinsic health and safety issues as well as the short usable life span of the compounds[17] have led to a recent decline in their use. As a result, fluorescent labels are more commonly used, as outlined below.

1.2.1 Fluorescent Methods

There are a wide variety of fluorescent dyes and systems, some of which have sensitivities in the region of attomoles,[19] that can be used for DNA hybridisation and

SNP detection and so this discussion will focus on a few common systems which will be described for illustration. Abel and co-workers[20] used fluorescein to detect hybridisations of complimentary strands of DNA where the dye was attached directly to the target strand. A capture probe was attached to a fibre optic sensor, the labelled complimentary strand added and then the fluoroscein was excited at 488 nm by an argon laser. The increase in emission in the area surrounding the fibre optic sensor was then recorded. While this showed a detection limit of 24 fmol, it took 60 min to reach this sensitivity and it was not tested with targets with a base mismatch. Since DNA can still bind with mismatches it might be expected that there was little or no reduction in emission by the fluoroscein. Other fluorescent dyes include rhodamine-based dyes and AMCA.[21]

There are a number of fluorescent probes which can be used to detect SNP sites such as Taqman, Scorpion and Molecular Beacon. These probes all depend on a technique which amplifies DNA called the polymerase chain reaction (PCR) invented by Mullis and co-workers in 1987.[22] This works through cycling heating steps (which denature and separate the DNA target into single strands) and elongation steps using primers and DNA polymerases to allow synthesis of a new complementary strand[22]. The repetition of this procedure allows for logarithmic replication of DNA meaning that only small amounts of target (theoretically 1 strand) is required in the first instance. However, errors in the DNA sequences increase after approximately thirty denaturing cycles. PCR can also be a lengthy process; techniques which are sensitive enough to detect target DNA directly would save time and be more cost effective.

1.2.1.1 Fluorescent Probes

Taqman probes (Figure 1.4) are stretches of DNA complementary to a target with a fluorescent reporter group on the 5' end of the strand and a quencher on the 3' end. The quencher acts to stop fluorescence by a process called fluorescent resonance energy transfer (FRET) whereby the excitation energy is transferred to the quencher in a distance dependent fashion through non-radiative processes. When the probe binds to the complementary strand the fluorophore is cleaved by DNA polymerase and so can fluoresce. In order to detect SNP sites two probes are required (one complementary to the mismatch sequence and one to the normal sequence) with different fluorescent reporters for each sequence.[23] However, Tom Brown and co-workers[24] have shown that it is possible to use only one probe to detect SNP sites by monitoring the fluorescence at a temperature where the probe is dissociated from the SNP strand (due to weaker binding) and the complementary strand is still bound to detect the presence of the 'mutant' strand. This technique requires highly accurate instrumentation.

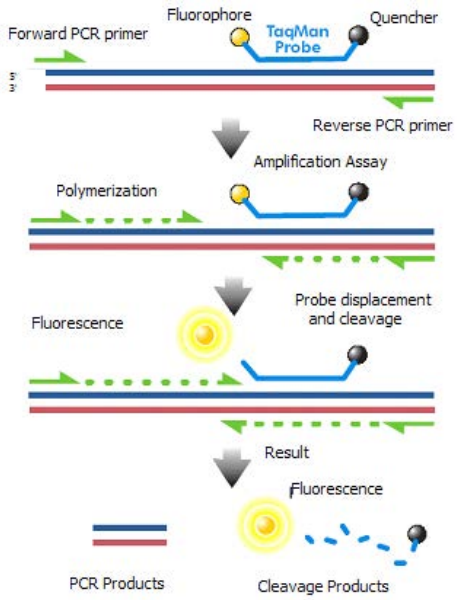

Figure 1.4: Schematic of action of Taqman Probes[25]

Molecular Beacons (Figure 1.5) consist of a stem loop probe which contains a complementary sequence to the target within the loop and a stem which has complementary bases close to the probe.[26] When in the loop formation the fluorescence is quenched but on addition of a target, the hairpin opens up to allow binding to the complementary strand.[24] This separates the fluorophore and the quencher so emission can be recorded.[26] As with the Taqman probe, two different sequences and fluorophores (specific for the natural and SNP variation) are required to detect the presence of a SNP site or it can be performed with one probe in a fine temperature window.

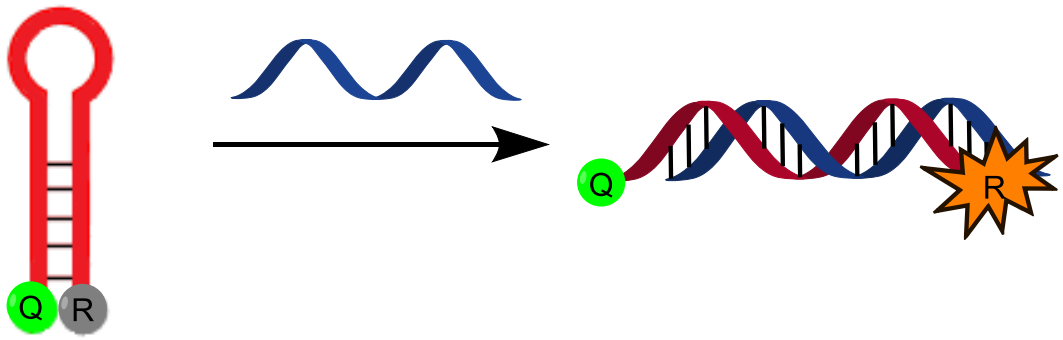

Figure 1.5 Schematic representation of the mode of action of a molecular beacon where Q refers to the quencher and R refers to the fluorescent reporter.

A Scorpion probe (Figure 1.6) is similar to a molecular beacon as there is a fluorescent reporter on the 5' end of the DNA stem, a quencher on the 3' end but the probe is also bound to the DNA strand of interest via a primer. This gives the advantage of faster assay times[23] compared to the probes previously described. The probe will bind to a DNA sequence with a SNP site but once again it is possible to subject the experiment to a narrow temperature window to allow the SNP strand to dissociate whilst the complementary stays bound

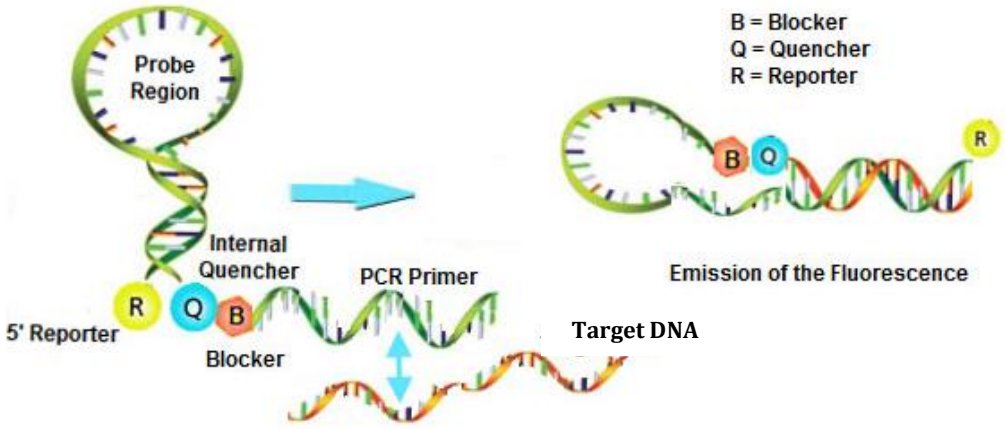

Figure 1.6 Schematic of the action of Scorpion Probes (Image taken from www.biosyn.com)[27]

While these methods have been shown to provide low limits of detection there are some issues which have yet to be overcome. The procedures can be complicated, long detection times[28] are normal, the analysis with probes is usually used in conjunction with PCR making miniaturisation difficult and samples must be reduced in volume, causing contamination and loss.[29] In light of this much research has focussed on producing sensors based on electrochemistry.

Fritz and co-workers[16] showed it is actually possible to detect the presence of hybridization and single base mismatches with 'label-free' DNA (i.e. no artificially inserted reporter compound). The DNA probe was bound to an electrode and the change in surface potential of the electrode on binding of the target was compared with that of the surface-bound DNA probe alone. However, the sensitivity for this technique was relatively poor with a detection limit of 2 nM. As a result, electrochemical species that utilise redox active reporter groups which can be incorporated in DNA are now becoming widely explored.

1.2.2 Electrochemical Methods

Electrochemistry is quickly becoming an important area of research in terms of biosensing. This method depends on the presence of a redox active species which is able to readily donate or accept electrons (oxidation and reduction respectively). This occurs at a particular potential (or voltage) and relies on the reporter group being in close proximity to an electrode enabling it to complete, in essence, an electrical circuit. The movement of electrons to and from the electrode results in an increase in current which can be monitored. The potential at which the species is reduced or oxidised can also be used to glean vital information. The theory of this will be covered further in Chapter 2. Commonly, Cyclic Voltammetry is used to probe a system when using electrochemical reporters. The electrode potential is scanned back and forward resulting in peaks showing where the compound oxidises and reduces. However, there are a range of electrochemical techniques which are widely used, including Square Wave Voltammetry, Electrochemical Impedance and Chronoamperometry.

The varying environments in which the reporter molecule exists will result in different redox potentials depending on the effect it has on the molecules ability to oxidise or reduce. Clearly, hybridisation of a target DNA strand would constitute a large change in environment for the redox active species, thus resulting in a change in redox potential.[4] The presence of SNP sites may cause changes in potential (as the environment will change marginally) and may allow for sensing. It is also possible to gain some insight into the reaction kinetics by varying the scan rate of the potential.

1.3 Ferrocene

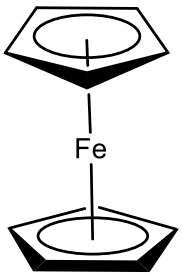

Figure 1.7 The Structure of Ferrocene

Ferrocene (shown in Figure 1.7) is used regularly as a redox reporter within DNA because it is easily manufactured within the lab, functionalisable, stable and has well defined electrochemical behaviour.[4] It has also been shown to be more air and moisture stable compared to alternative metallocenes.[30]

1.3.1 Incorporation of Ferrocene into DNA

Ferrocene has been incorporated into a number of regions within the DNA molecule. These are discussed below:

1.3.1.1 Attachment to DNA Terminals

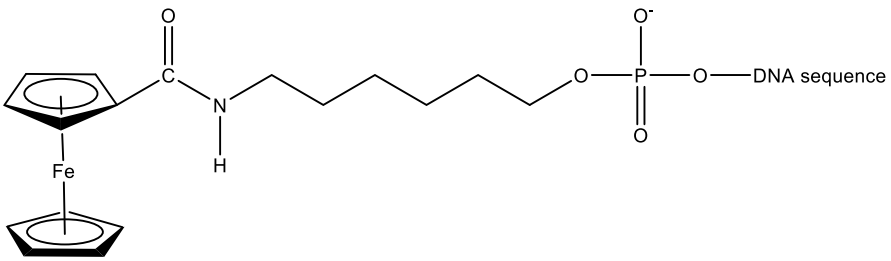

Figure 1.8 Ferrocene attached to DNA by an amino hexyl group.[31]

The first attempts at attaching ferrocene to DNA molecules for the purpose of electrochemical sensing were performed by Ihara and co-workers.[31] They initially

attached a ferrocene molecule, post synthetically, to the 5' end of DNA with an aminohexyl terminal (Figure 1.8). The electrochemical behaviour of this molecule was interrogated using an electrochemical detector (ECD) which induces electrochemical reactions with active species as the reaction mixture is eluted with high performance liquid chromatography (HPLC). The current change at the electrode can then be detected during the electrochemical reaction. They were able to detect hybridisation of the ferrocene labelled probe with a DNA target with sensitivity of detection between 1 and 20 fmol with this technique.[31] Ihara and co-workers note that the sensitivity is not as low as that possible with fluorescence methods which utilise enzyme amplification methods (although it was equivalent to that of radiolabelling methods) and the sensitivity largely depended on the stability of the hybrid molecule. In particular, it was observed that longer probe strands resulted in lower limits of detection. They also state that using HPLC had its disadvantages. The probes caused damage to the columns by clogging them and although the hybrids eluted off, it was more difficult to remove and regenerate the original probe. There were also concerns that for some of the columns tested, the DNA hybrid eluted too quickly so could be confused with artefact peaks inherent to the HPLC technique.[31] Ferrocene appeared to be an adequate reporter molecule but the detection method needed some development.

Subsequent investigations into ferrocene labels have generally used cyclic voltammetry since it is the conventional technique for electrochemical studies. Letsinger and co-workers used cyclic voltammetry to show the attachment of a DNA strand labelled at the 5' end of DNA with a ferrocene molecule to a gold surface. The

probe was synthesised using phosphoramidite chemistry (Figure 1.9) allowing for the automated synthesis of the DNA strand.[32]

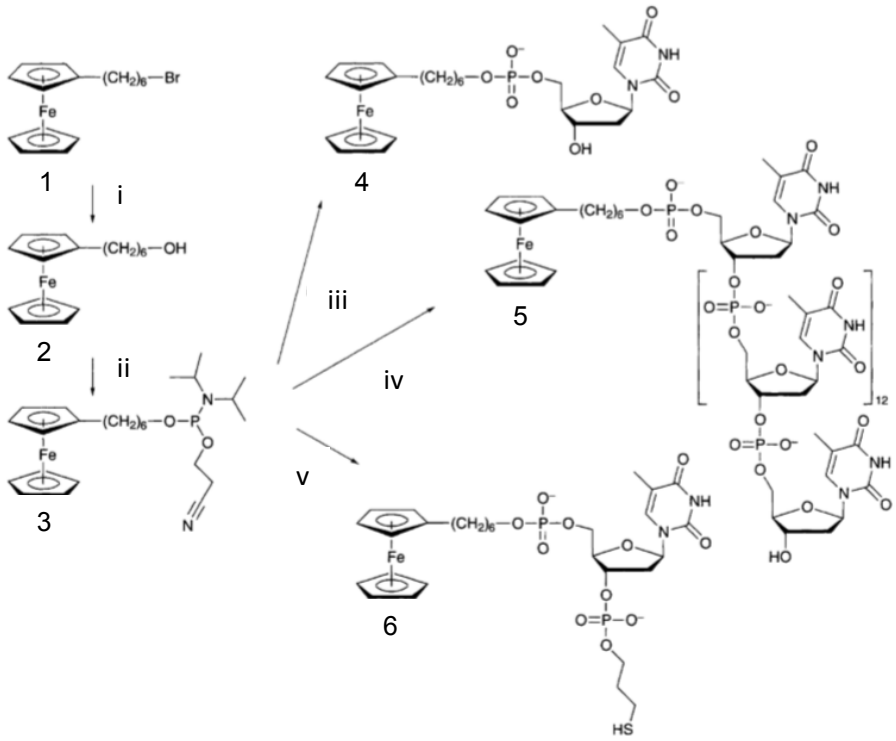

Figure 1.9: Reagents and conditions: i, H_20/HMPA, reflux, 6 h; ii, p-cyanoethyl-N, N-diisopropyl-chlorophosphoramidite: N, N-diisopropylethylamine: THF, room temp., 3 h; iii, thymidine modified CPG: DNA synthesizer; iv, thymidine modified CPG: DNA synthesizer; v, 3'-thiol modified CPG: DNA synthesizer[32]

Since then, ferrocene molecules have been attached to the ends of DNA on multiple occasions. This has been achieved in a number of ways, such as via a reaction of ferrocene with a nitrogen phosphate group and reaction of ferrocene a carboiimide group which goes on to combine with the imino groups on the T, U and G nucleosides.[4]

Hillier and co-workers showed it was possible to demonstrate nuclease enzyme activity on a 5' labelled DNA strand. It was found that the current increased as the strand was digested as the labelled digested DNA section was able to diffuse closer to the electrode. There is only one label on a strand which produces many nucleotides when digested raising the issue of competition by diffusion for the

electrode. As a result the sensitivity was not very high; 5μM of oligonucleotide was required for accurate detection.[33]

The attachment of the labelled oligonucleotide to a surface may remove the problems associated with diffusion. Anne and co-workers showed it was possible to attach a ferrocene molecule to the 3' end of DNA whilst attaching it to a gold electrode via a thiol unit on the 5' end. The aim was to measure the difference in elasticity of the single and hybridised DNA molecule strand. They conclude it may be possible to detect mismatches in base pairs as they affect the elasticity of the molecule, although this has not yet been tested.[34]

Plaxco and co-workers have used the principle of attaching a single DNA strand with 5' ferrocene probe to a gold electrode and combined it with a molecular beacon type stem loop detector. When in the stem loop the ferrocene is held close to the electrode, allowing for electron transfer. When the target strand hybridises with the stem loop the resultant duplex straightens and moves the ferrocene away from the electrode. The authors report that the ferrocene electrochemical signal disappears within 30 mins of adding 5 μM of DNA target and with less concentrated target solutions the signal reduces. Despite the high concentration of target required it was shown that the probes were recyclable, showing promise for the future creation of reusable detectors (Figure 1.10).[35]

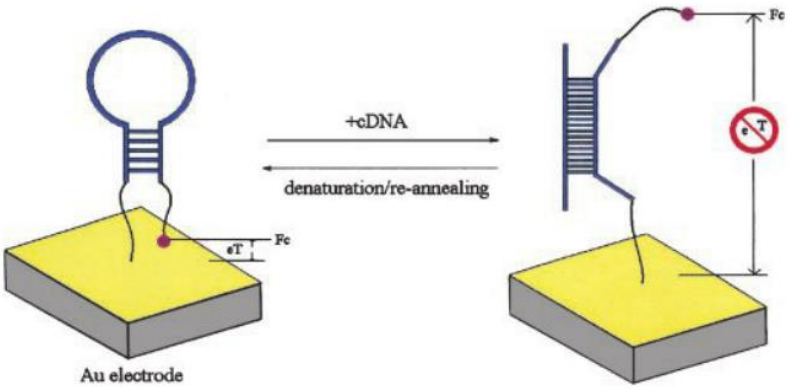

Figure 1.10: Monitoring target DNA detection through structural changes of a molecular beacon like probe with a ferrocene reporter group.[35]

1.3.1.2 Attachment to Nucleotides

Some groups have attempted to incorporate ferrocene molecules into the core structure of DNA so the electrochemical reporter is closer to the site of interest and the electrode, hopefully enhancing the electrochemical sensitivity.

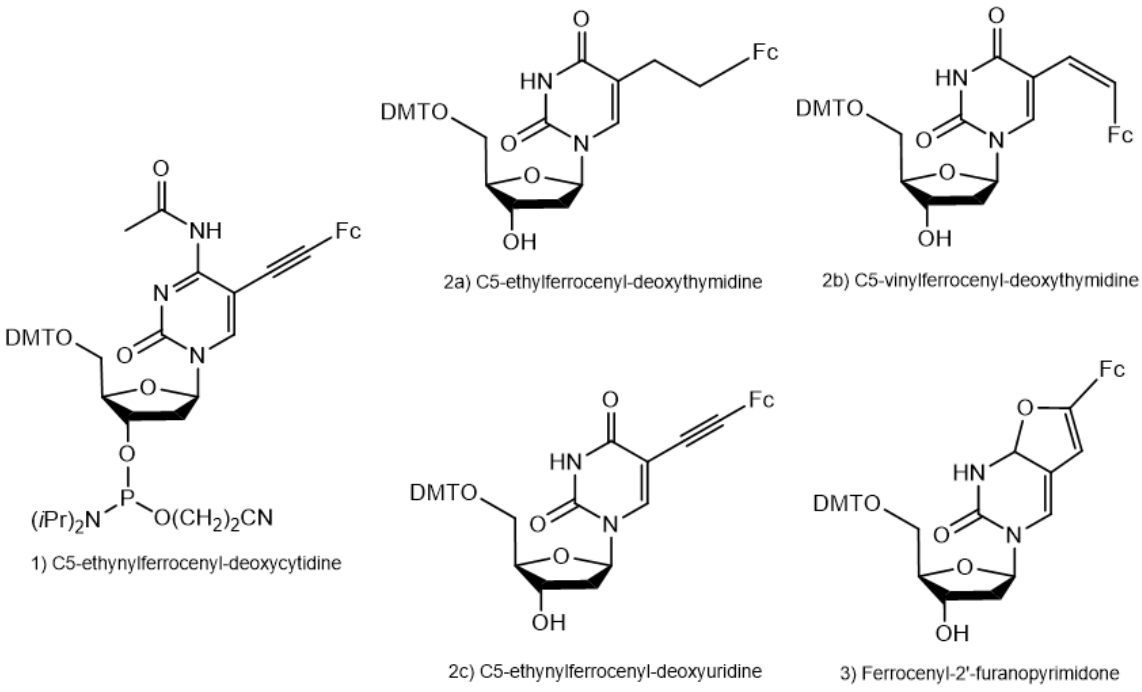

Figure 1.11 1) Conjugated cytidine monomer 2a-c) monomers containing single, double and triple bonded (respectively) alkyl linkers to a thymidine (or in the case of the triple bond uridine) nucleoside. 3) The cyclisation product from 2c.

To this end, many groups have incorporated ferrocene into DNA nucleosides and a few examples are discussed here. Houlton and co-workers have functionalised cytidine via a triple bond [36] and thymine via single and double bonds[37] (all with a 2 carbon linker) with ferrocene at the 5-position. The former was successfully integrated into a DNA strand and hybridised with a target producing reversible redox behaviour both in solution and immobilised on a silicon electrode. The ferrocene molecule was shown to be situated in the major groove and as a result had little effect on the natural DNA structure but did result in a small loss in stability (~2^{o}C by thermal denaturation ($T_{m)}$).[36] Thymine is a more conjugated system due to the triple bond to the ferrocene and so should have facilitated greater electron transfer between the reporter group and the nucleoside making it a more sensitive probe. However, it readily cyclised and formed a more stable duplex with a guanine residue rather than with adenine as the base opposite.[37] This was also observed by Yu and co-workers when working with uridine conjugated to ferrocene via triple bonds (Figure 1.11).[38]

Kraatz and co-workers worked around this issue by binding the ferrocene directly to the 5-position of uridine (and cytidine) by a 1 carbon link.[39] This was done using a Stille coupling and the resultant residues produced redox behaviour when in a 3 base DNA strand. The authors hope to combine this with a natural DNA strand in the future to determine whether the electrochemical signal change is enhanced on hybridisation.

Following their work on thymidine, Yu and co-workers then went on to attach ferrocene to the 2' OH position in both cytosine[40] and adenosine.[14] The adenosine version was used in a dual probe set up by adding a functional group to the ferrocene

molecule which altered the potential and enabled sensing of single nucleotide polymorphisms (SNP; variations in the genetic sequence of one nucleotide at a specific position which is regularly present in a population and can indicate predisposition towards contracting a disease and/or health issues[14]). One probe matched the target strand and one probe matched the strand with a mismatched base so the SNP was discernible by electrochemistry. The probe without the added group on the ferrocene was shown not to affect the stability of the duplex (by T_m: modified probe = 50.5°C vs. unmodified probe = 51.2°C). However, this setup required an anchor strand to the gold electrode, two probes in solution and the target strand. It is therefore unlikely that this probe will be reusable and requires more synthesis than using a single probe, adding to cost and time.

The ferrocene modified cytosine nucleotides were not used to detect SNPs but did show that the position of the ferrocene moiety within the nucleotide is important. At the 2' OH site of the cytosine thermal denaturation showed stability of the 15mer duplex with a matching target strand was very similar. Furthermore, using two ferrocene modified nucleosides reduced the T_m by 0.9°C from which the authors deduce that there is no significant change in duplex stability but could increase the sensitivity. However, placing the ferrocene in the 3' OH position gave a lower T_m indicating that the introduction of ferrocene was destabilising the duplex. The authors suggested this was because the ferrocene in the 3' OH position resulted in a change in geometry on hybridisation of the target. Clearly the effect of ferrocene on the structure of a DNA duplex needs to be considered when judging the viability of a new probe for target sensing.[40]

Interestingly all of the above groups note that the nucleoside to which the ferrocene is attached has a marked effect on the redox potential obtained. For example, the potential shift for Kraatz and co-workers[39] cytidine vs uridine trimer is 87mV (470mV vs. 387mV redox potentials respectively). While the authors offer no explanation for such a large shift, this author questions whether it may be possible to incorporate two or more modified nucleotides (since in certain positions the stability of the duplex is not affected by insertion of 2 ferrocene moieties, as discussed above) in order to detect multiple SNP sites by studying multiple redox potentials at once.

Ferrocene redox reporters can also be used as DNA backbone modifications. This will be discussed further in Chapter 3.

1.4 Metals in DNA

Various metals have been considered for input into the DNA structure in order to impart properties such as magnetism and conductivity which could facilitate the production of nano molecular machines and self-organising nano objects[41]. Lee and co-workers[42] showed that above pH 8, Zn^{2+}, Ni^{2+}, and Co^{2+}‡ could all form metal-DNA (M-DNA) where these ions are suggested to be coordinating to natural bases in a pair. This was done with the main aim of increasing DNA conductivity[43] which was achieved to the extent where an M-DNA SAM was as conductive as a gold surface.[44]

Hg^{2+} has been shown to coordinate mismatched thymines base pairs within an unmodified DNA duplex (Figure 1.12).[41] While the exact mechanism is not completely understood , Katz noticed that the viscosity of a natural DNA molecule increased on binding of Hg^{2+} and, after subsequent UV studies were carried out by Thomas,[46] Katz proposed that slippage was occurring between the two DNA strands in order for T

bases to align and facilitate T-Hg^{2+}-T binding.[41] This will be discussed in more detail in Chapter 4.

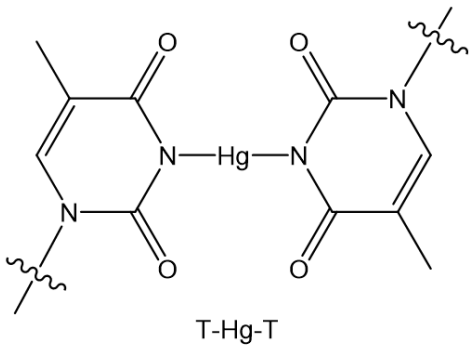

Figure 1.12: Thymine-Mercury-Thymine bonding within natural DNA[45]

It has also been shown to be possible to design artificial nucleosides with groups which bind specific metals. This increases duplex stability, an example being the complexation of Cu^{2+} with nucleosides which resemble the N, N'-bis (salicylidene) ethylenediamine ligand (Figure 1.13).[41] The ligand replaces the cytosine bases on opposing sides of a DNA duplex and forms a structure with a similar geometry. This allows for easy incorporation into natural DNA and has excellent implications for DNA as a nanoarchitecture material.

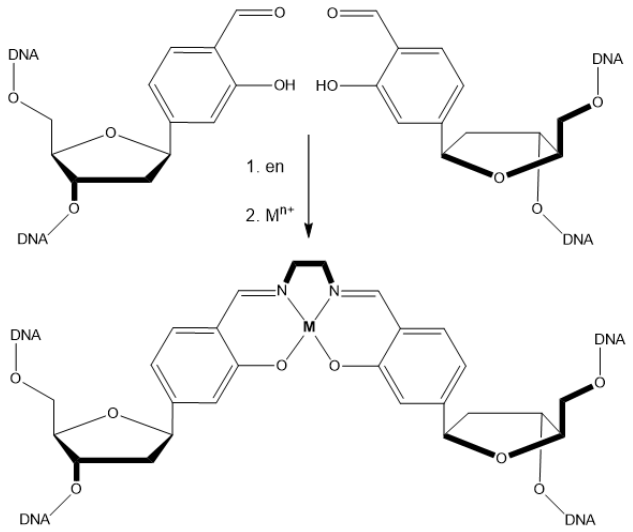

Figure 1.13: N,N'-bis(salicylidene) ethylenediamine ligand[6]

Despite the wide applications for metal addition to DNA there are a number of issues in terms of biosensing. Many metals are toxic within the body, including some which are most commonly used with DNA such as Hg^{2+}, Fe^{2+} (in large amounts), Zn^{2+} and Cu^{2+}, making studying them hazardous. Metals can also be incredibly expensive and, as mentioned above, the sensitivity is often poor. As a result, electrochemical methods of detection have received little focus with more attention placed on alternative sensors, which utilise radioactivity and fluorescence. However, the recent improvements in sensitivity, the discovery that metal binding can be directly facilitated by natural DNA (as described above) and the ability to create portable electrochemical sensors is rejuvenating this area of research.

1.5 Conclusion

A number of the electrochemical DNA based sensor systems described above used surfaces to form self-assembled monolayers (SAMs). This method has many advantages; the electrodes modified with SAMs can potentially be reusable, the sensitivity of the systems can be increased since the reporter groups are held closer to the electrode surface and the effect of hybridisation on a sensor can be monitored.[34] The SAMS are formed readily and with the need for little starting material due to the affinity of sulphur for gold.

However, there are issues. Brisset[35,47] and Plaxco[35] both showed that as their systems hybridised, the ferrocene reporter group moved away from the electrode and the electrochemical signal was either turned off or reduced. While this was taken to prove hybridisation, it may also mean that the probe is degrading, particularly in the case where the signal 'switches off' as the reporter molecule no longer functions.

This is known as a 'false-positive' and is an inherent problem with current electrochemical methods for interrogating SAMs, particularly as ferrocene is known to degrade in aqueous conditions.[48]

The versatility of ferrocene as an electrochemical reporter group has been clearly demonstrated on multiple occasions and while the limits of detection are not currently applicable for non PCR methods or comparable with fluorescence methods, great strides are being made in that direction. Electrochemistry offers a faster, reusable, reliable, tuneable, safer (compared to radioactive methods) and more portable route to DNA and SNP detection. In recent decades the scope of this field has burgeoned dramatically and, this author believes, will continue to do so.

1.6 Thesis Outline

This thesis comprises of a series of projects linked by the modification of oligonucleotides with redox active ferrocene incorporated mid strand or tagged to the 5' end of the strand. Due to the range of topics covered by this thesis a detailed introduction will be included at the beginning of each Chapter.

Chapter 2 includes a description of the uses and theory behind the various techniques used throughout the research carried out during this Ph.D. These include electrochemistry, methods for surface characterisation, gel electrophoresis and automated DNA synthesis.

Chapter 3 investigates the electrochemical characteristics, stabilities and sensing abilities of mixed self-assembled monolayers of two Ferrocene Nucleic Acid (FcNA) conjugated DNA probes and their respective enantiomers. This is carried out using cyclic voltammetry and square wave voltammetry.

Chapter 4 expands the investigations carried out on the FcNA conjugated DNA in the previous chapter. Duplexes consisting of a target DNA strand with thymine bases positioned opposite the FcNA units in the probe strand are considered for use as an electrochemical sensor for mercuric (Hg^{2+}) ions.

Chapter 5 compares the stability and sensing abilities of a biferrocenylene molecule, being used as an electrochemical reporter attached to the 5' end of a DNA probe, with that of a single ferrocene unit in the same position. This is assessed using cyclic voltammetry and square wave voltammetry.

Chapter 6 investigates the possibility of using FcNA conjugated DNA for anti-sense therapeutics. Enzymes were used to digest the single stranded and duplexed

modified oligonucleotides which were then analysed by gel electrophoresis and mass spectrometry.

1.7 References

(1) Pinheiro, V. B.; Holliger, P. *Curr. Opin. Chem. Biol.* **2012**, *16*, 245–252.

(2) Watson, J. D.; Crick, F. H. *Cold Spring Harb. Symp. Quant. Biol.* **1953**, *18*, 123–131.

(3) Wang, J. *Chem. Eur. J.* **1999**, *5*, 1681–1685.

(4) Duprey, J.-L. H. A.; Tucker, J. H. R. *Chem. Lett.* **2014**, *43*, 157–163.

(5) Stulz, E. *Chem. Eur. J.* **2012**, *18*, 4456–4469.

(6) Nakamoto, K.; Tsuboi, M.; Strahan, G. D. *Drug-DNA interactions: structures and spectra*; John Wiley & Sons Inc., 2008.

(7) Mergny, J. L.; Lacroix, L. *Oligonucleotides* **2003**, *13*, 515–537.

(8) JC Morales, K. G. .

(9) Hunter, C. A. *J. Mol. Biol.* **1993**, *230*, 1025–1054.

(10) Yakovchuk, P.; Protozanova…, E. *Nucleic Acids Res.* **2006**, *34*, 564–574.

(11) Pang, Y.-P.; Miller, J. L.; Kollman, P. A. *J. Am. Chem. Soc.* **1999**, *121*, 1717–1725.

(12) Guckian, K. M.; Schweitzer, B. A.; Ren, R. X.-F.; Sheils, C. J.; Tahmassebi, D. C.; Kool, E. T. *J. Am. Chem. Soc.* **2000**, *122*, 2213–2222.

(13) Herbert, A.; Rich, A. *J. Biol. Chem.* **1996**, *271*, 11595–11598.

(14) Yu, C. J.; Wan, Y.; Yowanto, H.; Li, J.; Tao, C.; James, M. D.; Tan, C. L.; Blackburn, G. F.; Meade, T. J. *J. Am. Chem. Soc.* **2001**, *123*, 11155–11161.

(15) Paleček, E.; Bartošík, M. *Chem. Rev.* **2012**, *112*, 3427–3481.

(16) Fritz, J.; Cooper, E. B.; Gaudet, S.; Sorger, P. K.; Manalis, S. R. *Proc. Natl. Acad. Sci.* **2002**, *99*, 14142–14146.

(17) Ihara, T.; Nakayama, M.; Murata, M.; Nakano, K.; Maeda, M. *Chem. Commun.* **1997**, 1609–1610.

(18) Wolf, S. F.; Haines, L.; Fisch, J.; Kremsky, J. N.; Dougherty, J. P.; Jacobs, K. *Nucleic acids Res.* **1987**, *15*, 2911–2926.

(19) Smith, L. M.; Sanders, J. Z.; Kaiser, R. J.; Hughes, P.; Dodd, C.; Connell, C. R.; Heiner, C.; Kent, S. B.; Hood, L. E. **1986**.

(20) Abel, A. P.; Weller, M. G.; Duveneck, G. L.; Ehrat, M.; Widmer, H. M. *Anal. Chem.* **1996**, *68*, 2905–2912.

(21) Chehab, F. F.; Kan, Y. W. *Proc. Natl. Acad. Sci.* **1989**, *86*, 9178–9182.

(22) Arnheim, N.; Erlich, H. A.; Horn, G. T.; Mullis, K. B.; Saiki, R. K.; Scharf, S. J. Process for amplifying, detecting, and/or-cloning nucleic acid sequences, July 1987.

(23) Vega, F. M.; Lazaruk, K. D.; Rhodes, M. D.; Wenz, M. H. *Mutat. Res. Mol. Mech. Mutagen.* **2005**, *573*, 111–135.

(24) Thelwell, N.; Millington, S.; Solinas, A.; Booth, J.; Brown, T. *Nucleic Acids Res.* **2000**, *28*, 3752–3761.

(25) Tapp, I.; Malmberg, L.; Rennel, E.; Wik, M.; Syvanen, A. C. *Biotechniques* **2000**, *28*, 732–739.

(26) Tyagi, S.; Kramer, F. R. *Nat. Biotechnol.* **1996**, *14*, 303–308.

(27) Bio-Synthesis Inc. Scorpions® Primers and Probes http://www.biosyn.com/scorpions-primers.aspx (accessed Feb 2018).

(28) Korri-Youssoufi, H.; Garnier, F.; Srivastava, P.; Godillot, P.; Yassar, A. *J. Am. Chem. Soc.* **1997**, *119*, 7388–7389.

(29) Kuhr, W. G. *Nat. Biotechnol.* **2000**, *18*, 1042–1043.

(30) Ziółkowski, R.; Olejniczak, A. B.; Górski, Ł.; Janusik, J.; Leśnikowski, Z. J.; Malinowska, E. *Bioelectrochemistry* **2012**, *87*, 78–83.

(31) Takenaka, S.; Uto, Y.; Kondo, H.; Ihara, T.; Takagi, M. *Anal. Biochem.* **1994**, *218*, 436–443.

(32) Mucic, R. C.; Herrlein, M. K.; Mirkin, C. A.; Letsinger, R. L. *Chem. Commun.* **1996**, 555–557.

(33) Hillier, S. C.; Frost, C. G.; Jenkins, A. T. A.; Braven, H. T.; Keay, R. W.; Flower, S. E.; Clarkson, J. M. *Bioelectrochemistry* **2004**, *63*, 307–310.

(34) Anne, A.; Demaille, C. *J. Am. Chem. Soc.* **2005**, *128*, 542–557.

(35) Fan, C.; Plaxco, K. W.; Heeger, A. J. *Proc. Natl. Acad. Sci.* **2003**, *100*, 9134–9137.

(36) Pike, A. R.; Ryder, L. C.; Horrocks, B. R.; Clegg, W.; Connolly, B. A.; Houlton, A. *Chem. - Eur. J.* **2005**, *11*, 344–353.

(37) Pike, A. R.; Ryder, L. C.; Horrocks, B. R.; Clegg, W.; Elsegood, M. R.; Connolly, B. A.; Houlton, A. *Chem. Eur. J.* **2002**, *8*, 2891–2899.

(38) Yu, C. J.; Yowanto, H.; Wan, Y.; Meade, T. J.; Chong, Y.; Strong, M.; Donilon, L. H.; Kayyem, J. F.; Gozin, M.; Blackburn, G. F. *J. Am. Chem. Soc.* **2000**,

122, 6767–6768.

(39) Song, H.; Li, X.; Long, Y.; Schatte, G.; Kraatz, H.-B. *Dalton Trans.* **2006**, 4696–4701.

(40) Yu, C. J.; Wang, H.; Wan, Y.; Yowanto, H.; Kim, J. C.; Donilon, L. H.; Tao, C.; Strong, M.; Chong, Y. *J. Org. Chem.* **2001**, *66*, 2937–2942.

(41) Clever, G. H.; Kaul, C.; Carell, T. *Angew. Chem. Int. Ed.* **2007**, *46*, 6226–6236.

(42) Aich, P.; Labiuk, S. L.; Tari, L. W.; Delbaere, L. J.; Roesler, W. J.; Falk, K. J.; Steer, R. P.; Lee, J. S. *J. Mol. Biol.* **1999**, *294*, 477–485.

(43) Wettig, S. D.; Wood, D. O.; Lee, J. S. *J. Inorg. Biochem.* **2003**, *94*, 94–99.

(44) Wettig, S. D.; Wood, D. O.; Aich, P.; Lee, J. S. *J. Inorg. Biochem.* **2005**, *99*, 2093–2101.

(45) Laviron, E. *J. Electroanal. Chem. Interfacial Electrochem.* **1979**, *100*, 263–270.

(46) Thomas, C. A. *J. Am. Chem. Soc.* **1954**, *76*, 6032–6034.

(47) Brisset, H.; Navarro, A.-E.; Spinelli, N.; Chaix, C.; Mandrand, B. *Biotechnol. J.* **2006**, *1*, 95–98.

(48) Breuer, R.; Schmittel, M. *Organometallics* **2012**, *31*, 6642–6651.

Chapter 2

Techniques

2.1 Synthesis of Oligonucleotide Sequences

The synthesis of DNA is now a routine affair within many commercial companies and research laboratories. The ability to reliably design and make DNA quickly has partially led to the explosion in research into sensing applications since Marvin Caruthers research group developed the phosphoramidite chemistry, now the most commonly used method, in 1981.[1–5]

This method utilises a 2-cyanoethyl protecting group for the phosphate group and a variety of protecting groups are required for the A, G and C bases (Figure 2.1) due to their nucleophilic nature. This ensures the nucleotides are stable enough to survive the synthesis process whilst the protecting groups are still relatively easily removed under basic conditions (30% ammonia). This allows for minimal loss of the required DNA product, combined with the ease provided by automated methods of production.[6]

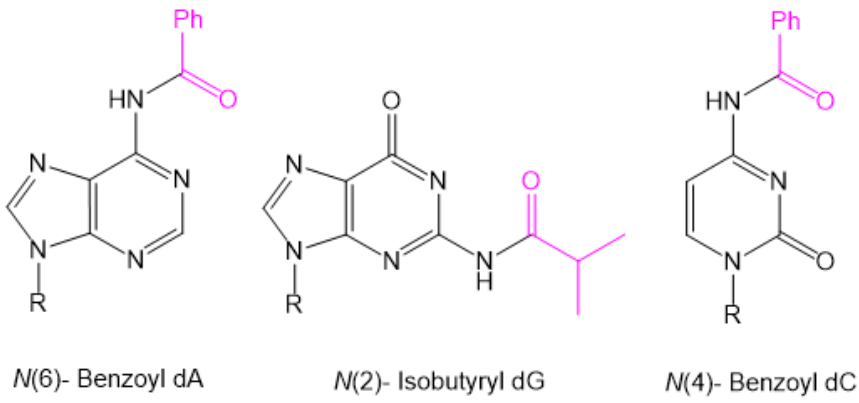

Figure 2.1: Protecting groups (highlighted) of the bases (from left to right) adenosine, guanine and cytosine. R represents the pentose sugar ring.

The synthesis of DNA can, in theory, be repeated as many times as necessary to create the required sequence. In practice, there are restrictions to the sequence length, not least the solid support necessary to secure the DNA strand whilst it is

being extended. The most commonly used supports are CPG or controlled pore glass columns that have the first base pre-mounted. As suggested by the name, these supports have a particular pore size. Once a sequence outgrows its pore, reactants are no longer capable of reaching the reactive sites on the molecule and yield drops off dramatically.

2.1.1 Automated DNA Synthesis

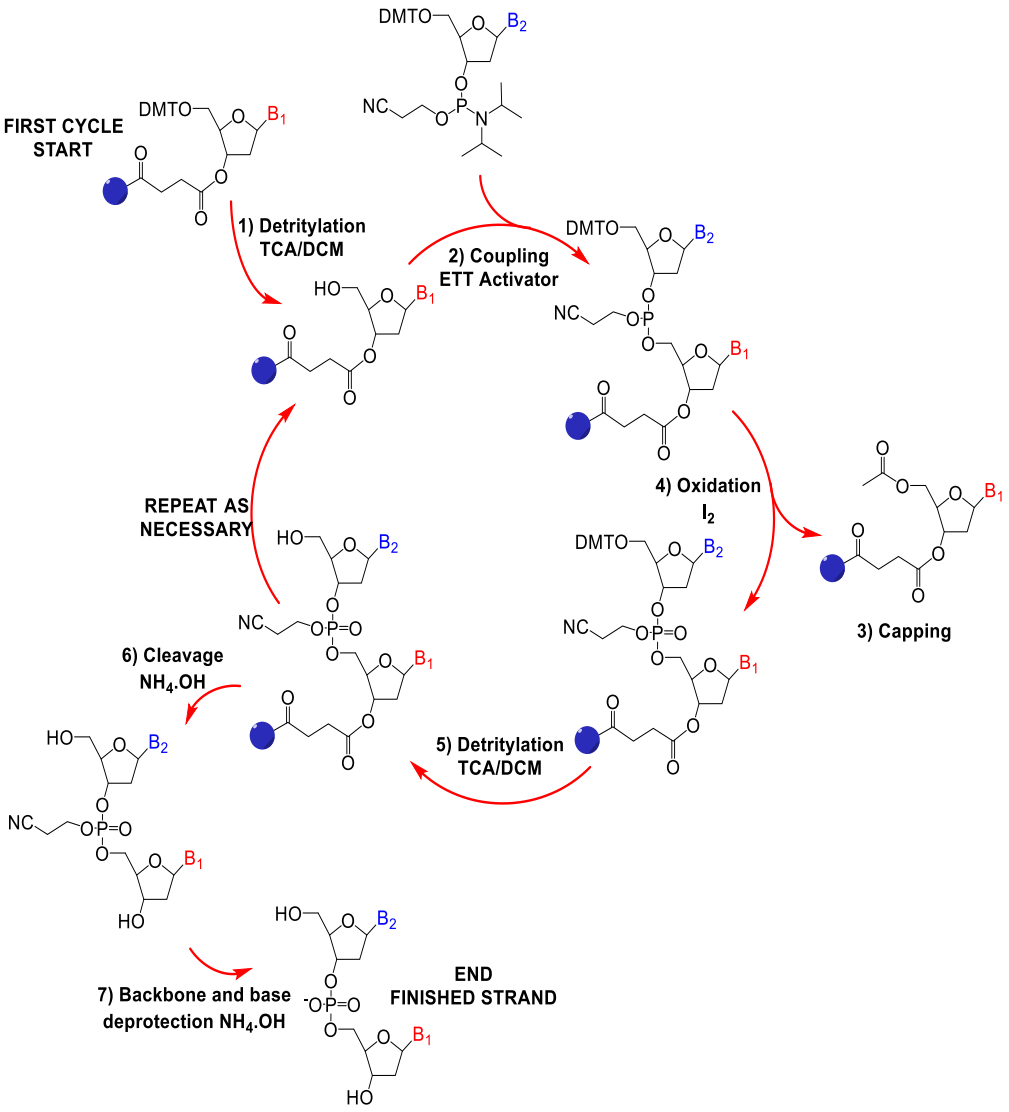

Figure 2.2 Schematic of automated DNA synthesis. [6] *Reproduced from Reference 6.*

Oligonucleotide synthesis is carried out on an automated DNA/RNA synthesiser and follows a series of steps (Figure 2.2) which are then repeated for each nucleotide addition. The strands are generally synthesised in the 3' to 5' direction and reactants are dissolved and delivered in acetonitrile. The process of DNA synthesis is now extremely standardised and the following discussion briefly outlines the chemical procedure:

2.1.1.1 Deprotection of the 5' OH

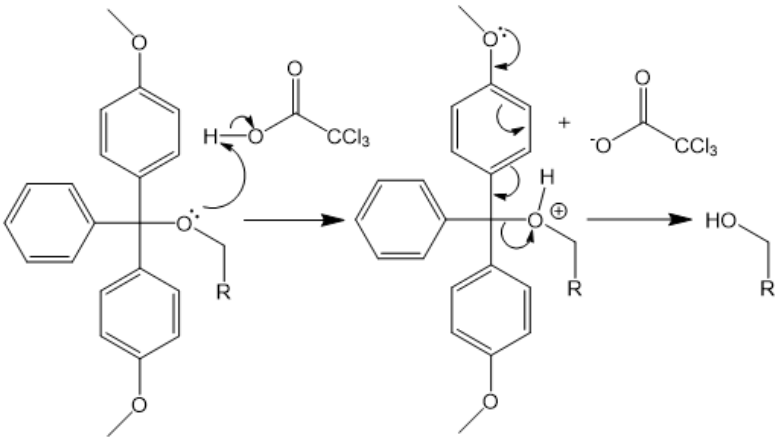

Figure 2.3 Removal of the DMT protecting group from the remainder of the nucleoside (denoted by R)

The cycle begins with the removal of the 4, 4'-dimethoxytrityl (DMT) group which protects the free alcohol before use. This is done using trichloroacetic acid (TCA) and the mechanism is given above (Figure 2.3). The DMT group has two roles in that it acts as an excellent leaving group, allowing for the further reaction of the 5' OH group, and, owing to the highly coloured nature of the compound and its subsequent ability to be easily detected by UV-absorption, can be used to monitor the nucleotide addition efficiency for every cycle.

2.1.1.2 Base Coupling

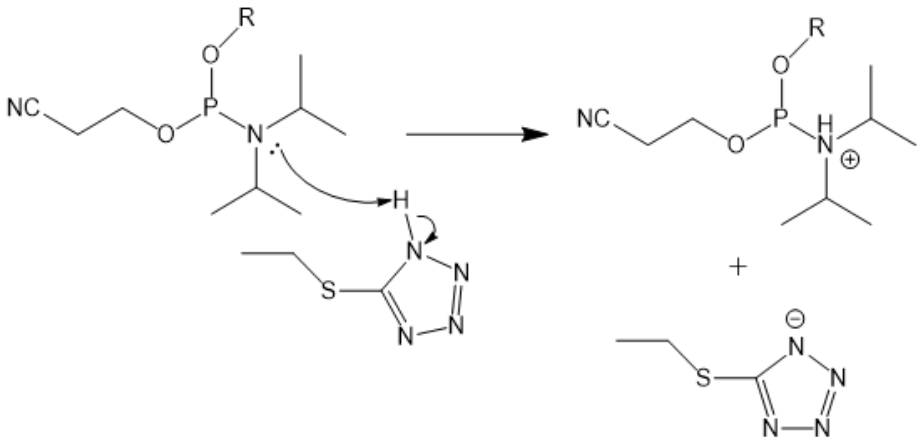

Figure 2.4 Activation of the phosphoramidite (R represents the nucleoside)

Removal of the DMT group leaves the more reactive 5' OH group free to react with the next base available. To ensure coupling steps are high yielding, an activator, 5-(ethylthio) tetrazole (ETT), is used to protonate the new phosphoramidite and so improve the leaving group (Figure 2.4).

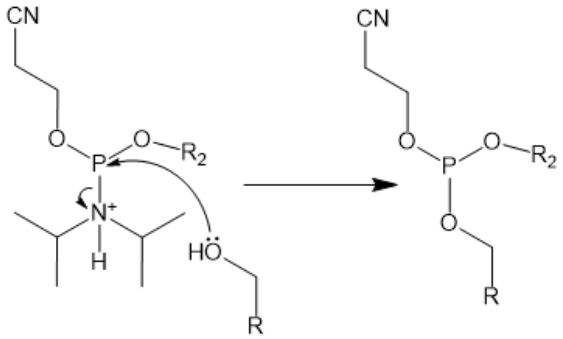

Figure 2.5 Addition of the next base in the sequence using an activated base (R denotes the initial nucleoside, R_2 denotes the nucleoside added)

The activated base is then exposed to the CPG support with the pre-mounted nucleoside where the exposed 5'OH can rapidly react with the phosphorous atom via nucleophilic attack. This results in the formation of a phosphite triester (Figure 2.5).

2.1.1.3 Capping

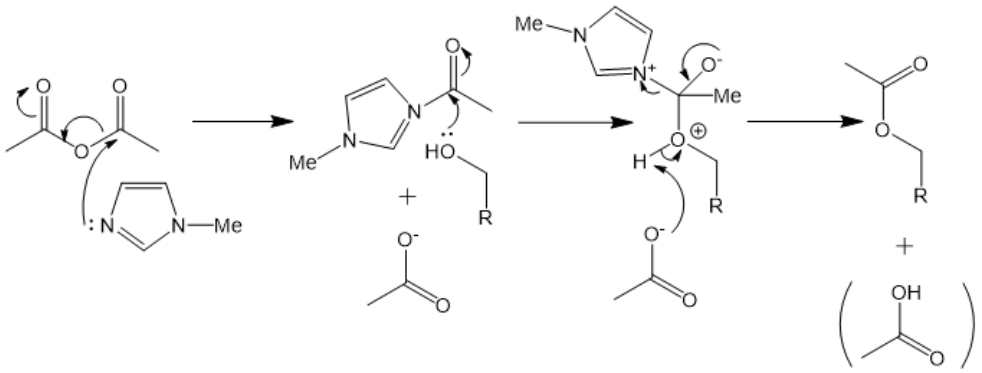

Figure 2.6 Mechanism by which unreacted DNA sequences are capped (R denotes the nucleoside)

Although the DNA synthesis process is high yielding (yields of 99% or more are regularly achieved for each coupling step)[6] it is inevitable that there will be sequences where a coupling has failed. If these sequences were allowed to continue to react in subsequent cycles, a large range of similar length strands would be produced. This would make purification of the final sample very difficult.

Instead of allowing these sequences to continue, they are 'capped'. Two capping mixtures are present on the synthesiser and then combined just before exposure to the CPG column. 'Cap Mix A' contains acetic anhydride and 'Cap Mix B' contains n-methylimidazole, both dissolved in tetrahydrofuran.

In combination, Cap Mix A and B react to form a highly electrophilic species which enables the acetylation of the free 5' OH of unreacted strand. The strands with the correct sequence are immune to this process due to the presence of the DMT group of the successfully reacted base.

2.1.1.4 Oxidation of the Phosphate Backbone

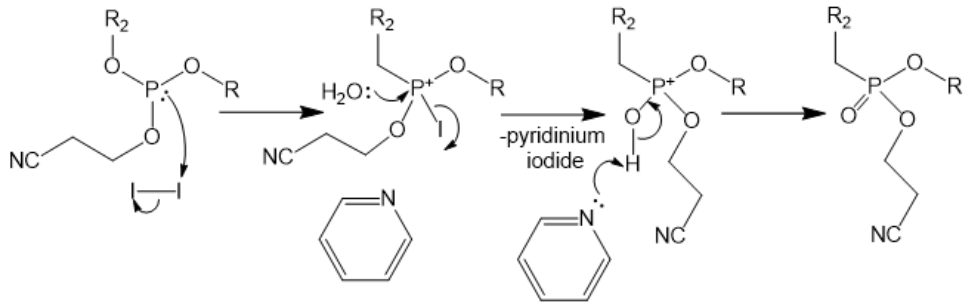

Figure 2.7 Mechanism of phosphate backbone oxidation using iodine and pyridinium (R denotes initial nucleoside, R_2 denotes recently added nucleoside)

The final oxidation state of the phosphorous atom is now converted from the less stable 3+ oxidation state to 5+, which is also the final oxidation state present in the backbone of natural DNA. This oxidation is achieved using iodine in water as shown in Figure 2.7. A pyridinium species must also be present to oxidise the remaining alcohol group in order to form the final required phosphate group. The newly added base can then be detritylated, as described above in Section 2.1.1.1 and is ready to be subjected to the DNA synthesis cycle again to be repeated as necessary.

2.1.1.5 Cleavage and Base Deprotection

After the cycle has been repeated and the oligonucleotide has reached the desired length and sequence, there are two more essential processes. The sequences must be removed from the CPG resin and the protecting groups for the phosphate backbone and the nucleobases must be removed in order for the DNA to be purified and useable.

Both of these steps are carried out in $NH_4.OH$. The basic conditions allow for the reduction of the ester bond which connects the initial base to resin, leaving a 3' OH in

place as for natural DNA. This mixture is then flushed through to a glass vial. This is removed manually and heated to 60 ^{o}C for 6 hours.

The need to heat for this amount of time is largely due to the isobutyryl protecting group present on the guanine nucleobase. The benzoyl groups attached to both A and C are cleaved relatively quickly but the isobutyryl needs much more encouragement to cleave. It is not uncommon for impurities collected during the purification method to actually have the correct DNA sequences but with 1 or more guanine bases still protected. However, this is currently a very efficient and high yielding method owing to the reduced need to transfer solutions regularly. The NH_4.OH is then removed *in vacuo* and the DNA is ready for purification.[6]

2.1.2 Thiol Incorporation

A widely used technique to enable attachment of oligonucleotides to gold surfaces is to employ a thiol end terminus to the DNA linker, to exploit the strong affinity of the sulphur-gold bond.[7] Thiols are also easily incorporated using automated DNA synthesis by replacing the resin bound nucleoside first used in the synthesis with a resin bound DMT protected disulphide.[6] The disulphide can later be reduced to give free thiols to allow for reaction with the gold layer.

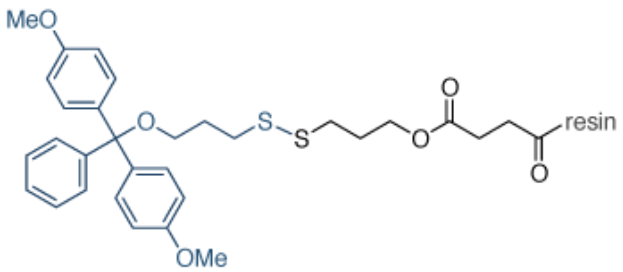

Figure 2.8 Resin bound disulphide for attachment at the 3' terminus of FcNA

2.1.3 Modified Phosphoramidites

Since the advent of the use of the phosphoramidite chemistry described above, many attempts have been made to insert species modified with a DMT protecting group, phosphitylated region or both as appropriate. Many of these can now be included in the automated synthesis, making modification of DNA relatively easy.

This thesis focuses on the incorporation of ferrocene-based, electrochemically active species into DNA. Some examples of this type of tag and how can it can be incorporated into DNA have already been covered, in depth, previously (section 1.3).

2.2 Self-Assembled Monolayer (SAM) Formation

Another area of interest in this thesis is the electrochemical investigation of surface bound species. The incorporation of a disulphide group to the 3' end of the DNA probe, as discussed in section 2.1.2, allows for the attachment of the species of interest to the surface of a gold electrode in a predictable and well understood manner. Figure 2.9 outlines the process involved.

The free DNA with disulphide attachment is exposed to 10 mM tris(2-carboxyethyl)phosphine (TCEP) which selectively reduces S-S bonds to thiols. This step is necessary since the free thiol itself is both reactive and unstable. The presence of the disulphide allows for storage of the probe in solution until it is required.

Thiol chemistry is not well understood but the formation of a S-Au bond is known to be highly favourable, resulting in spontaneous monolayer formation on exposing the gold electrode to the thiolated probe.[8] It is important to 'back-fill' the remaining free

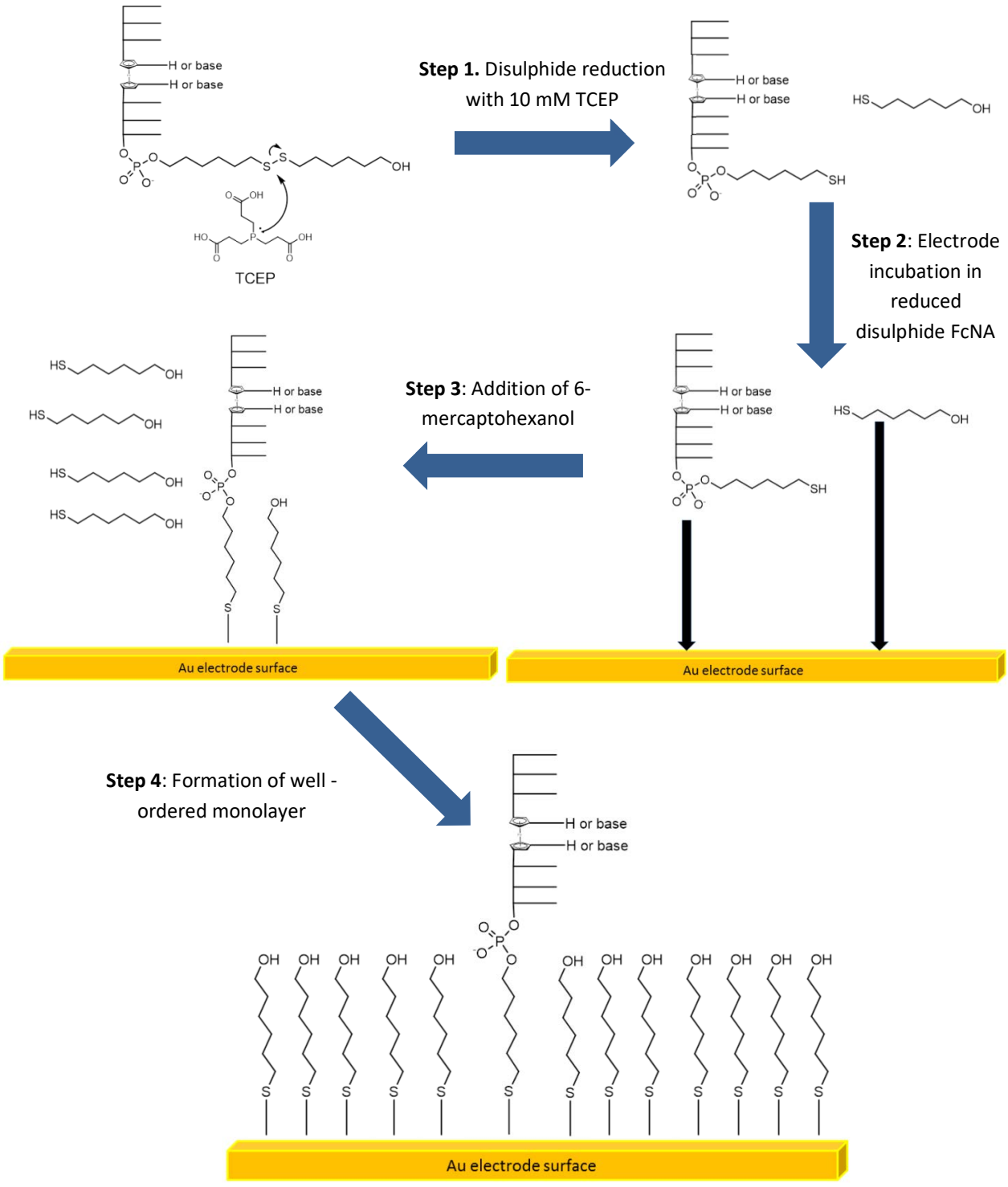

Figure 2.9 Formation of Self-Assembled Monolayers

surface of the electrode with a species which is not electrochemically active and will not interact directly with the probe, such as 6-mercaptohexan-1-ol. This is to prevent non-specific absorption of targets or signal interferences from electrochemical interactions between the gold and species in solution such as water and oxygen, and also provides well ordered self-assembled monolayers (SAMs).[9] By careful selection of the disulphide phosphoramidite to be incorporated during automated DNA synthesis, the thiolated by-product from the reduction of the disulphide will be the same as the species being used to pack the rest of the surface, again ensuring a well ordered SAM.

Plaxco and co-workers carried out a detailed study of the effect of the packing species and showed that there is a fine balance between signal acquisition and surface stability. The optimum species was found to be 6-mercaptohexan-1-ol (MCH) since the DNA probe was flexible enough to interact with the electrode surface whilst the MCH maintained a surface thick enough to prevent direct interaction of the solution species with the bare gold. As a result of this study MCH was used throughout this thesis. However, variations in packing species is an area which should be investigated in the future since optimum conditions may vary between differing redox active groups and DNA chain lengths.[9]

2.3 Electrochemistry

Electrochemistry is the study of the effect on electrical outputs of a chemical reaction or vice versa. As a result this branch of chemistry encompasses a large range of topics and applications from hydrogen production[10–12] to electroplating[13,14] to

biosensing[15–18]. It is this final application which is utilised heavily in this thesis and so a brief description of the fundamentals and setup for this use are necessary.

An electrochemically or redox active species is one that can be reduced (gain electrons) or oxidised (lose electrons) under certain conditions, whether that be by applying a particular voltage or through a chemical reaction. This movement of electrons (known as current) can be measured and is harnessed as electricity.

2.3.1 Electrochemical Set-Up

Throughout this thesis a three electrode set-up was employed (Figure 2.10).

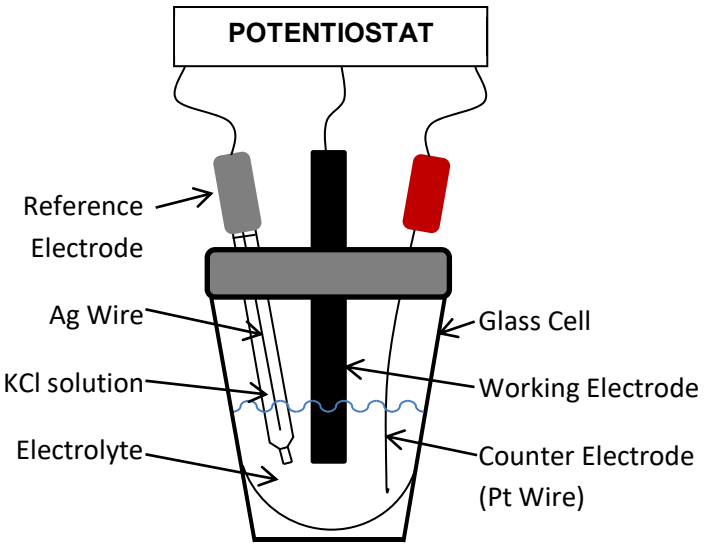

Figure 2.10: Three electrode cell set-up

This consists of:

- A Ag|AgCl reference electrode (RE)
- A gold microdisc working electrode (of diameter 0.2 cm) (WE)
- A platinum wire counter electrode (CE)

These electrodes are inserted into a sealed, argon flushed cell (normally made of glass) and the tips are submerged below a solution which contains charge carrying species (this solution is known as the electrolyte). Electrons can then pass between the electrodes, through the solution, and so create an electric circuit.

The WE is used to monitor the substance of interest at a particular potential. The CE is present to complete the circuit by accommodating the movement of electrons or redox active substance at the applied potential.

The RE is required since attempts to directly measure potential changes at the WE involve the flow of a current, which could result in perturbing the electrochemical half-reaction at the RE and produce variance in the applied potential. A reference electrode contains a stable electrochemical half-reaction, in this case NaCl with a AgCl-coated Ag wire, with constant composition. As a result its potential is constant. Therefore any changes in potential versus this standard must be due to changes at the working electrode whilst monitoring the reaction. In this way, the potential with respect to the RE can be reproducibly determined.[19]

This set-up is widely used for the basis of many different electrochemical experiments. While there are many variations of electrochemical techniques only those used during the production of this thesis will be discussed; cyclic voltammetry and square wave voltammetry.

2.3.2 Cyclic Voltammetry (CV)

Cyclic voltammetry is one of the most broadly used techniques for electrochemical analysis, largely due to the amount of information that can be derived with relatively cheap equipment and simple, fast procedures.[20] The potential is scanned linearly

over a defined range and then reversed to form a cycle (Figure 2.11). The current produced is then plotted vs the potential applied to give peaks for the oxidation and reduction of the redox active species of interest.[19,21]

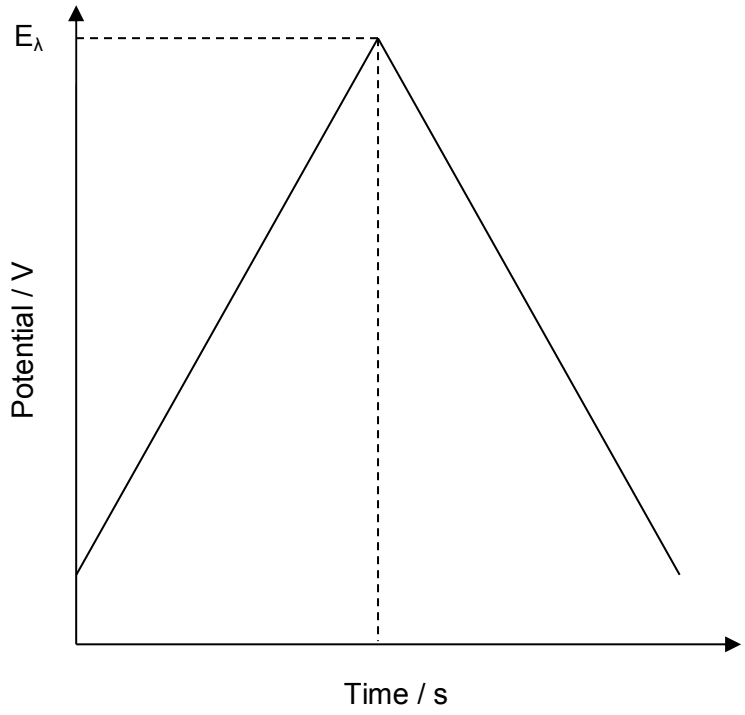

Figure 2.11 Potential sweep diagram for CV showing the switching potential, E_λ

It is possible to deduce a wealth of information from a voltammogram (Figure 2.12). From the forward oxidation or anodic peak maximum the anodic peak potential (E_p^a) and peak current (I_p^a) can be determined while the return reduction or cathodic peak minima provides the cathodic peak potential (E_p^c) and cathodic peak current (I_p^c). The half-wave potential ($E_{1/2}$) can be calculated by taking the average of (E_p^a) and (E_p^c) to give a standard, comparable potential for each redox process. For a fully reversible system, with no underlying electrochemical reactions occurring, the number of electrons oxidised must be the same as the number of electrons being reduced.

Therefore, for a reversible system, where the diffusivities of reacting species are similar, the ratio of I_p^a to I_p^c must be approximately equal to 1.[19]

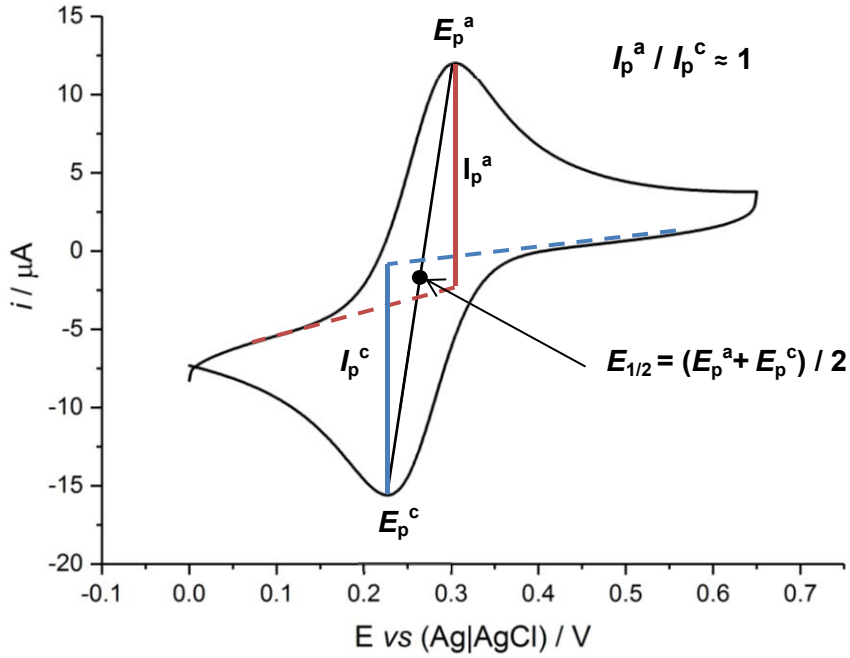

Figure 2.12 CV showing anodic peak potential (E_p^a), cathodic peak potential (E_p^c), anodic peak current (I_p^a), cathodic peak current (I_p^c) and $E_{1/2}$ potential

2.3.2.1 Solution-Based Electrochemistry

While the method of data acquisition is the same, the shape of the cyclic voltammograms, depending on whether the analyte is in solution or bound to the electrode surface, varies quite considerably as shown in Figure 2.13. The reason for this will be briefly discussed here, but this thesis focusses solely on the use of surface bound electrochemically active species.

In both of the above cases, it is necessary for the charged species to be transported to the WE. For solution-based electrochemistry this requires mass transport and diffusion through the electrolyte. Since the compounds in solution need to overcome the resistance of the electrolyte and diffuse to the surface greater kinetic energy is required. As a result the potential at which the most amount of current is detected is

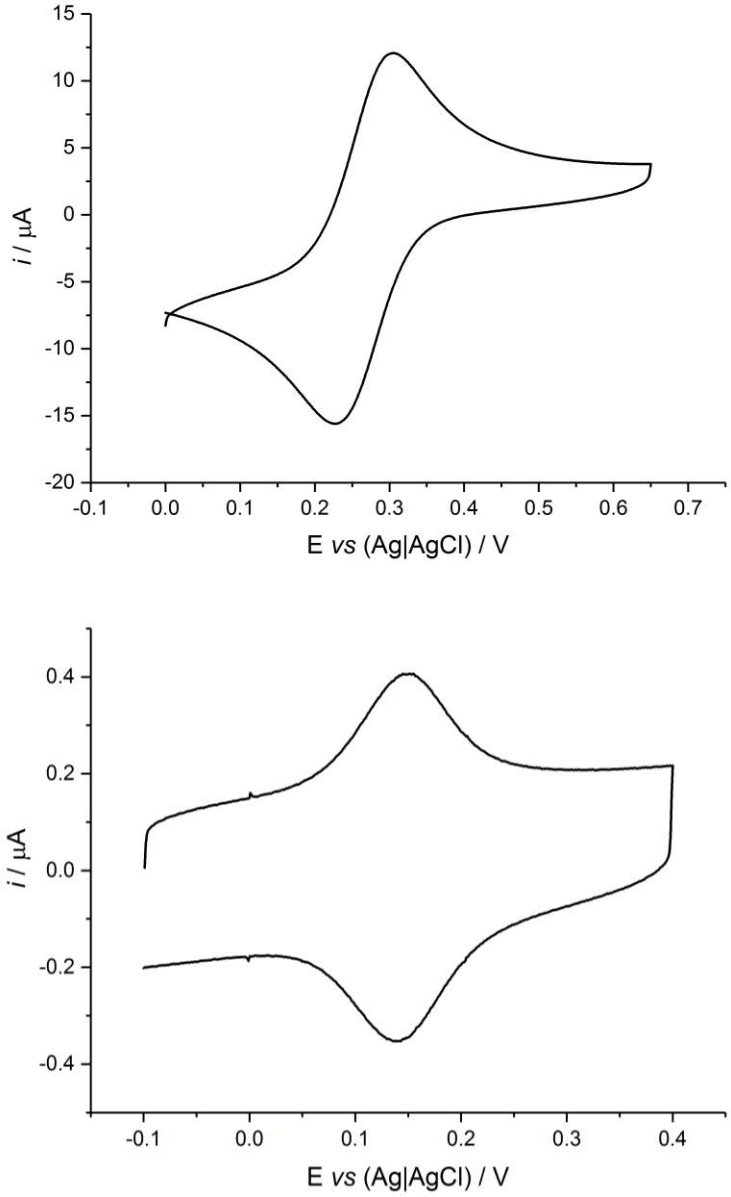

Figure 2.13 Top: CV of 2 M $K_3Fe(CN)_6$ in 1mM phosphate buffer and 1 M $NaClO_4$, solution-based analyte. Bottom: CV of FcTT conjugated DNA in a mixed monolayer with mercaptohexan-1-ol analysed in 10 mM phosphate buffer, 1 M $NaClO_4$

more than the potential at which the reaction actually occurs. This is known as an 'over-potential'. For a fully reversible system (which exhibits so called 'Nernstian'

behaviour) the resulting peak separation for a one electron process will be approximately 59 mV.[19]

It is possible to predict the diffusion coefficient of the species of interest by varying the scan (or sweep) rate at which the CV is recorded. Increasing scan rate increases the magnitude of the change in applied potential per second and CVs recorded over a set potential window are recorded much quicker, meaning the diffusion layer (or the distance from the electrode affected by the applied potential) is smaller.

The Randles-Ševčik equation (Equation 2.1) predicts that for a reversible, solution-based electrochemical redox process current is directly proportional to the square root of the scan rate and a plot of these two factors should produce a linear graph. From this the diffusion coefficient can be determined.[22,23]

Equation 2.1: $$\boldsymbol{i_{\mathrm{p}} = 2.69\, x\, 10^{5} n^{3/2} A D^{1/2} C v^{1/2}}$$

Where:

i_p = peak current (A)

n = no of electrons transferred per molecule in redox process

A = microscopic electrode surface area (cm^2)

D = diffusion coefficient ($cm^2\ s^{-1}$)

C = bulk concentration of electrolyte ($mol\ dm^{-3}$)

v = Sweep rate ($V\ s^{-1}$)

2.3.2.2 Surface-Based Electrochemistry

Electrochemical analysis of surface bound redox active species varies significantly from solution-based species. As the redox active system is now bound to close to the electrode it is no longer reliant on diffusion to allow for electron transfer. As a result

anodic and cathodic peaks should have a peak separation very close to 0 mV (Figure 2.13) and current should increase with linear dependence on the scan rate and not the square root of the scan rate due to the following relationship:[19]

$$\textit{Equation 2.2} \qquad \boldsymbol{i_{\mathrm{p}} = \frac{n^2F^2}{4RT} v A_{\mathrm{sur}} \Gamma}$$

Where:

i_p = peak current (A)

n = no of electrons transferred per molecule in redox process

F = Faraday's constant

R = gas constant

T = temperature (assumed to be 25 ^{o}C)

v = Sweep rate (V s^{-1})

A_{sur} = microscopic electrode surface area (cm^2)

Γ = surface coverage

From Equation 2.2 it is possible to determine the number of electrochemically active species on the working electrode. This equation requires the microscopic area of an electrode to first be determined.

2.3.3 Determining Microscopic Area

In order to draw meaningful comparisons between data, the reactive or microscopic area of the gold electrode must be determined for each experiment.[24,25] In the case of gold, electrodes are polycrystalline and natural variation in polishing or electrochemical cleaning can leave a rough surface with more sites available for reaction. This can add additional peaks in the CV resulting from the variance in the formal potential of oxide formation for the different gold sites. Very low microscopic

area can also imply contaminants left on the surface of the electrode which may affect experimental outcomes.

Gold oxide layers form readily to completely cover the electrode surface when it is placed in an acidic solution. The charge transfer is calculated by integrating the cathodic peak which represents the reduction of gold oxide from the electrode surface, shown in Figure 2.14.

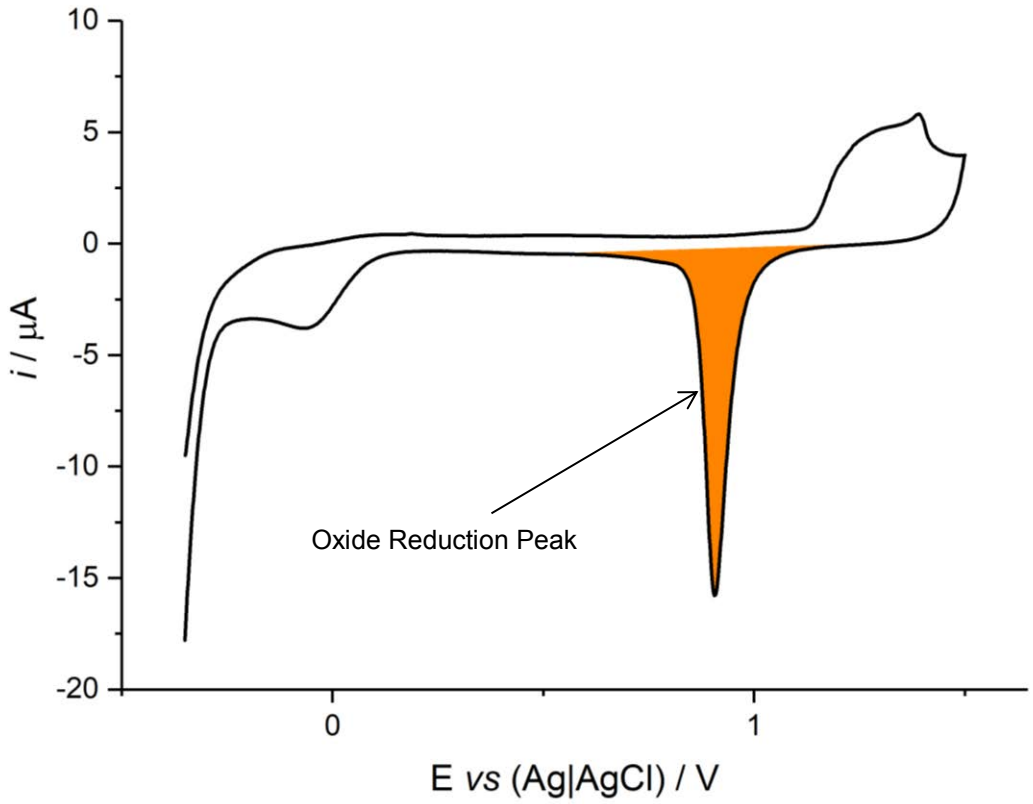

Figure 2.14 CV of bare gold electrode in 0.5 M H_2SO_4, recorded between -350 and 1500 mV at 500 mV s^{-1}. The oxide reduction peak is highlighted.

The charge required to remove the layer can then be compared with the literature value (482 µC cm^{-2})[26] for removing a monolayer of adsorbed oxygen using the following equation to give a roughness factor[24,25,27]:

Equation 2.3 $$\Gamma = {}^{\frac{Q}{A}}\!/_{482\ \mu C\ cm^{-2}}$$

Where:

Γ = surface roughness

Q = charge / μC

A = geometric electrode surface area / cm^2

The roughness factor can then be multiplied by the geometric surface area to give the microscopic area. This procedure was carried out for all experiments and the surface roughness factors were generally between 1 and 2.

2.3.4 Square Wave Voltammetry

While CV is excellent for obtaining large amounts of information about the characteristics of redox system it has some limitations. The large background currents that are observed are due to non-faradaic processes (also known as capacitance current). These currents occur due to the movement and build-up of charged species towards the electrode and occur on changing the potential of the electrode (since changing the charge of the electrode will attract or repel charged species). This current decays quickly after being held at a particular potential as the movement of the charged species ceases.

In 1952, George Barker developed 'square wave polarography' in an attempt to overcome this issue.[28] This technique involved overlaying a staircase wave form with a square wave form as shown in Figure 2.15. At the time, the complexity of the calculations needed to acquire useable data meant that this technique was too difficult to use.[29]

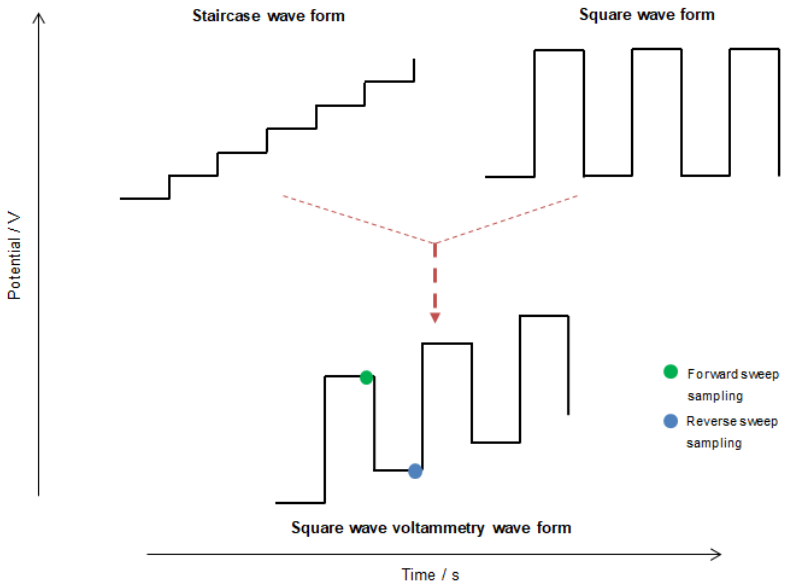

Figure 2.15 Square wave voltammetry potential vs time profile

However, the advent of the microprocessor in the 1980s meant that this technique, which is now known as square-wave voltammetry (SWV), has seen a rise in popularity. This is largely due to the speed with which data can be acquired (less than 1 minute but more often in a few seconds), reduction in the magnitude of the capacitance current and enhanced sensitivity.[29–32]

The current is sampled twice: immediately before reversing the potential on both the forward and reverse potential sweep (Figure 2.15). This ensures that the capacitance charging has decayed significantly before a measurement is taken. Since the waveform is sampled twice, two peaks are obtained. The differential of these is then taken which enhances the peak and so the sensitivity (by at least two orders of magnitude compared to cyclic voltammetry) (Figure 2.16). The SWV technique is used throughout this thesis, in combination with cyclic voltammetry, in order to obtain as much information about the sensor systems as possible.[28,29,33]

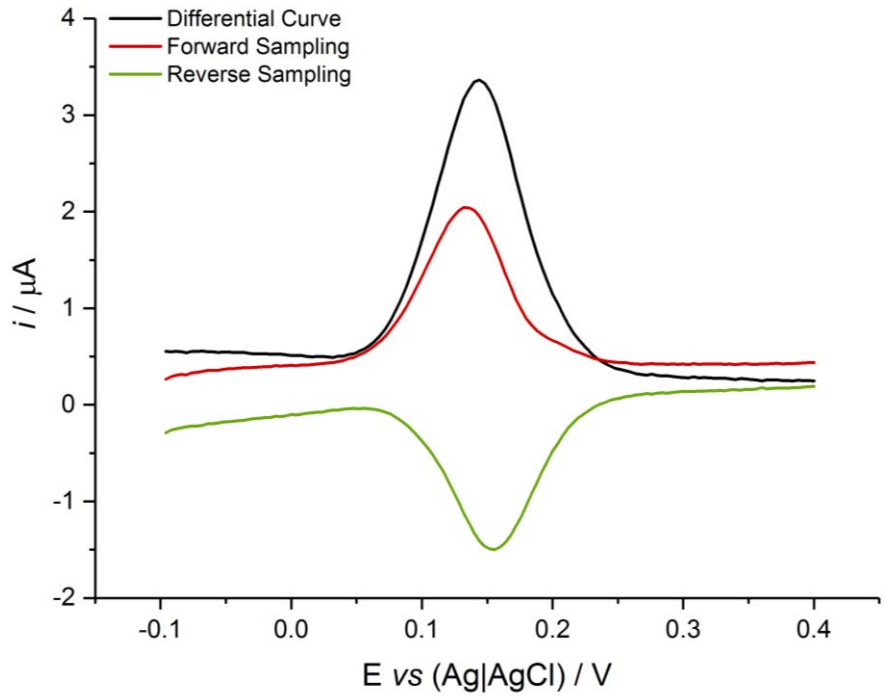

Figure 2.16 Example of peak enhancement in SWV (Thymine based FcNA SAM in 1 M $NaClO_4$, 10 mM phosphate buffer at 200 Hz)

2.4 Surface Characterisation

A number of different techniques were used to identify and analyse the various characteristics of the SAMs created in order to try to better understand the results observed. A brief description of the theory and uses of each technique are outlined below:

2.4.1 Ellipsometry

The principles of ellipsometry have been used and understood for over 100 years but the complex calculations and modelling required to glean data made it a relatively rare technique.[34] It has only been with the explosion in modern computing that this technique has been more widely explored and is now regularly used to determine monolayer thicknesses and to investigate how a material interacts with light.[35–38]

Ellipsometry utilises these interactions by monitoring the resultant change in amplitude and phase of polarised light. The incident beam of linearly polarised light is first directed at the surface of interest. The light will both reflect and refract at each of the different layers (i.e. the surface of interest and the substrate) causing the light to both lose intensity and change phase (Figure 2.17). The reflected light (also called elliptically polarised light) is detected by the analyser. The difference between the incident and reflected light can then be determined.[39]

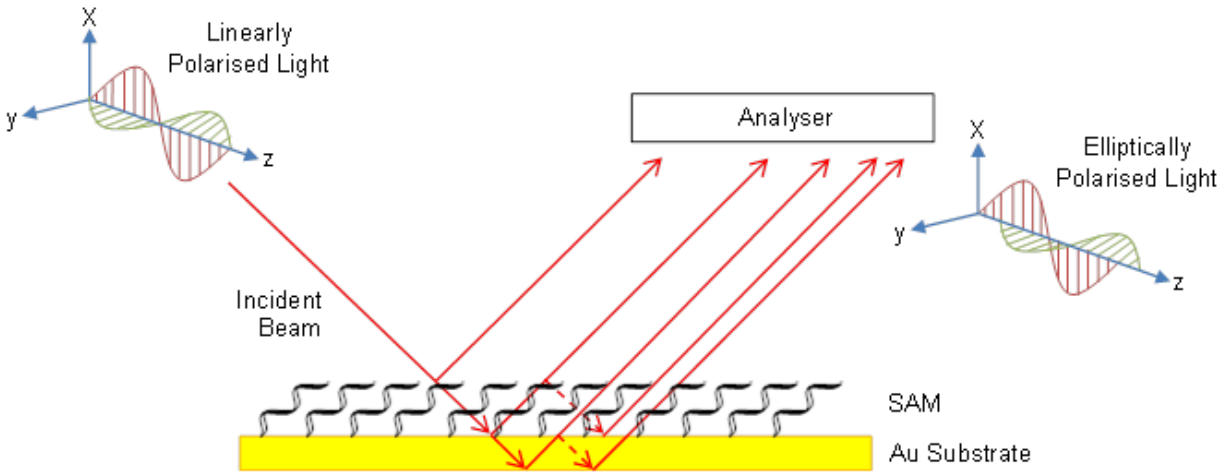

Figure 2.17 Schematic of the Principles of Ellipsometry showing the interactions of the beam with the sample and substrate and the resultant change in phase and amplitude of the reflected light[39]

Since the interactions with the substrate, the molecules themselves and the layer boundaries must be accounted for, a modelling program is utilised, where previously determined constants for each component can be used to fit the data. A program can then determine the surface thickness from this model.

For the purposes of this thesis, ellipsometry was used to determine the variation of SAM thickness in order to try to determine the density of the surface packing. If the molecules are more densely packed they will tend to be directed more orthogonal to the plane of the surface and so give a larger film thickness (Figure 2.18).[40,41] If the

length of molecule is known and the surface thickness can be derived, then the angle at which the molecule lies on the surface can be determined (Equation 2.4).

Equation 2.4: $$Tilt\ Angle\ (A) = \cos\left(\frac{Surface\ Thickness\ (B)}{Molecule\ Length\ (C)}\right)$$

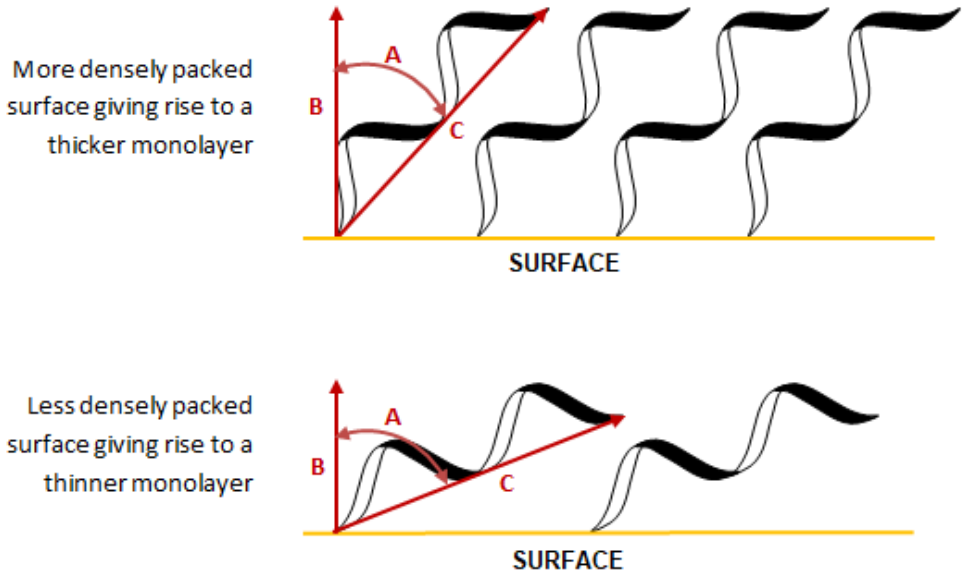

Figure 2.18 Diagram of the relationship between monolayer packing density and thickness. The required parameters for Equation 2.4 are also labelled.

2.4.2 X-Ray Photoelectron Spectroscopy

X-Ray photoelectron spectroscopy (XPS) has been referred to as the 'mass spectrometry of surfaces'. The technique involves the ejection of core electrons (i.e. those not in the valence shell of an atom) by irradiating the surface of interest with a beam of X-rays (Figure 2.19).

The energy of the X-ray beam enables the ejection of core electrons and, by knowing the intensity of the X-ray beam, the energy required to remove these electrons can be determined. Since the binding energy is characteristic for each electron in a specific energy level in each species (since each element interacts differently with

the X-Ray beam), the detected energy difference (equating to the binding energy) can be used to determine the elements present on a surface.[42,43] The resultant kinetic energy generated is indicative of the atomic species from which the electron has been ejected.

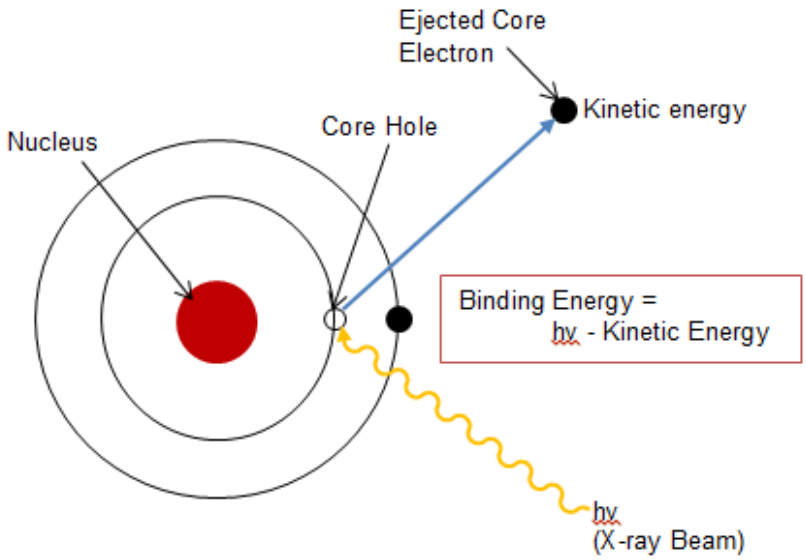

Figure 2.19 The principles of XPS analysis

Since the number of electrons detected by the analyser must be directly proportional to the number of the species present on the surface, the ratios of the respective elements to each other can also be determined.[43] This can give an indication of the average molecule distribution (i.e. whether the probe molecules in a SAM are well packed or not) but not the specific architecture of the SAM (i.e. is it uniform or are there small islands of the molecule of interest?).

2.5 Polyacrylamide Gel Electrophoresis (PAGE)

Gel electrophoresis is a technique designed for the separation of small species, mainly proteins or oligonucleotide fragments. This thesis uses PAGE for the

separation of oligonucleotides and so the methodologies discussed are appropriate for that practice, though these only vary marginally for use with proteins.[44]

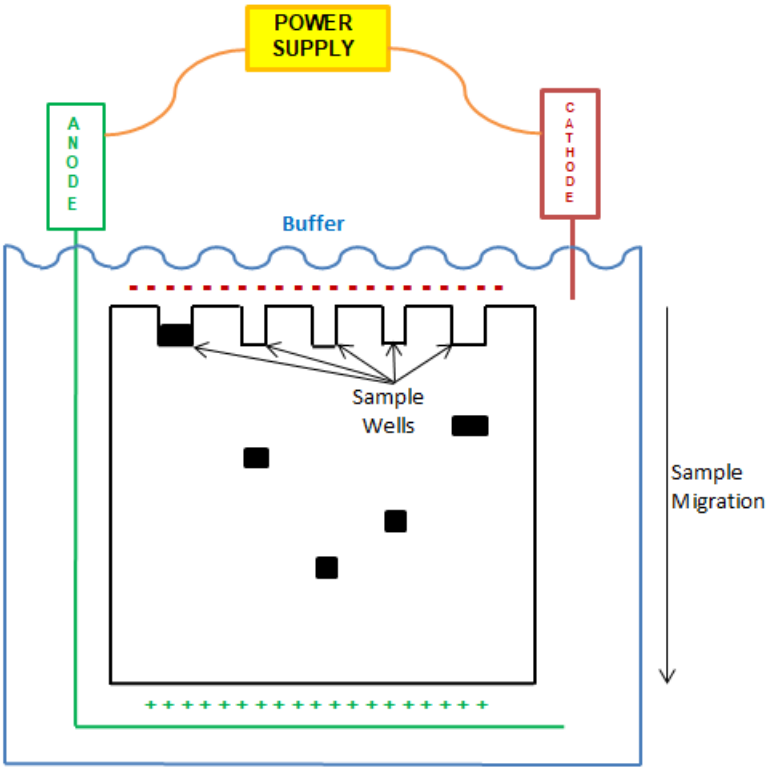

Figure 2.20 Schematic representing the working principles of PAGE

An electric current is applied such that the resultant cathode resides at the top of the gel and the more positive anode rests at the bottom. DNA is naturally negatively charged due to the phosphate backbones and so is dragged through the gel material towards the anode (Figure 2.20). The speed at which the species travel through the gel material depends on their charge, shape and size.[44] The highly charged and smaller sized strands can travel more quickly through the gel, allowing the user to separate DNA samples. The resultant gels can then be analysed by applying a dye which binds to the DNA and can be visualised using fluorescence or, if the

concentration of sample used is high enough, through UV shadow where the gel is placed on a substrate which does not absorb UV light. The sample absorbs UV light at 260 nm, resulting in the presence of dark spots on an otherwise illuminated gel.[45,46]

The latter of these two methods requires no additional treatment or modification of the sample. This is greatly advantageous; since the PAGE technique is a 'gentle' and does not damage the sample, the DNA or its fragments can be excised from the gel and analysed further.

2.6 References

(1) Caruthers, M. H. *React. Polym. Ion Exch. Sorbents* **1987**, *6*, 159–174.

(2) Caruthers, M. H. *Science* **1985**, *230*, 281–285.

(3) Caruthers, M. H.; Beaucage, S. L.; McBride, L.; Matteucci, M.; deHaseth, P.; Goldman, R.; Galluppi, G.; Fisher, E. F.; Efcavitch, J. W.; Becker, C. *Gene Amplif. Anal.* **1983**, 1–26.

(4) Caruthers, M. H.; Barone, A. D.; Tang, J.-L.; Stabinsky, Z.; Matteucci, M.; McBride, L. J.; Fisher, E. F.; Dodds, D. R.; Beaucage, S. L. *Methods Enzymol.* **1987**, *154*, 287–313.

(5) Dorman, M. A.; Noble, S. A.; McBride, L. J.; Caruthers, M. H. *Tetrahedron* **1984**, *40*, 95–102.

(6) Brown, T.; Brown Jr., T.; ATDbio Ltd. Nucleic Acids Book.

(7) Volkert, A. A.; Subramaniam, V.; Ivanov, M. R.; Goodman, A. M.; Haes, A. J. *ACS Nano* **2011**, *5*, 4570–4580.

(8) Pensa, E.; Cortés, E.; Corthey, G.; Carro, P.; Vericat, C.; Fonticelli, M. H.; Benítez, G.; Rubert, A. A.; Salvarezza, R. C. *Accounts Chem. Res.* **2012**, *45*, 1183–1192.

(9) Ricci, F.; Zari, N.; Caprio, F.; Recine, S.; Amine, A.; Moscone, D.; Palleschi, G.; Plaxco, K. W. *Bioelectrochemistry* **2009**, *76*, 208–213.

(10) Rossmeisl, J.; ZW Qu, H. Z., GJ Kroes…. .

(11) McCambridge, M. Electrolysis of water, February 1988.

(12) Harrison, K.; Levene, J. I. In *Solar Hydrogen Generation*; Springer, 2008; pp. 41–63.

(13) Schlesinger, M.; Paunovic, M. *Modern electroplating*; John Wiley & Sons, 2011; Vol. 55.

(14) Lowenheim, F. A.; Senderoff, S. Modern electroplating, 1964.

(15) Carpini, G.; Lucarelli, F.; Marrazza, G.; Mascini, M. *Biosens. Bioelectron.* **2004**, *20*, 167–175.

(16) Wang, J. *Chem. Eur. J.* **1999**, *5*, 1681–1685.

(17) Chen, S.; Dou, Y.; Zhao, Z.; Li, F.; Su, J.; Fan, C.; Song, S. *Anal. Chem.* **2016**, *88*, 3476–3480.

(18) Eissa, S.; Zourob, M. *Anal. Chem.* **2017**, *89*, 3138–3145.

(19) Bard, A. J.; Faulkner, L. R. *Electrochemical methods: fundamentals and applications*; Wiley New York, 1980; Vol. 2.

(20) Eckermann, A. L.; Feld, D. J.; Shaw, J. A.; Meade, T. J. *Coord. Chem. Rev.* **2010**, *254*, 1769–1802.

(21) Kissinger, P. T.; Heineman, W. R. *J. Chem. Educ.* **1983**, *60*.

(22) Randles, J. E. _. B. _. *Trans. Faraday Soc.* **1948**, *44*, 327–338.

(23) Ševčik, A. *Collect. Czechoslov. Chem. Commun.* **1948**, *13*, 349–377.

(24) Carvalhal, R. F.; Freire, R. S.; Kubato, L. T. *Electroanalysis* **2004**, *17*.

(25) Hoogvliet, J. C.; Dijksma, M.; Kamp, B.; van Bennekom, W. P. *Anal. Chem.* **2000**, *72*, 2016–2021.

(26) Oesch, U.; Janata, J. *Electrochimica Acta* **1983**, *28*, 1237–1246.

(27) Douglass Jr., E. F.; Driscoll, P. F.; Liu, D.; Burnham, N. A.; Lambert, C. R.; McGimpsey, W. G. *Anal. Chem.* **2008**, *80*, 7670–7677.

(28) Barker, G. C.; Jenkins, I. L. *Analyst* **1952**, *77*, 685–696.

(29) Osteryoung, J. G.; Osteryoung, R. A. *Anal. Chem.* **1985**, *57*, 101–110.

(30) Lovrić, M. In *Electroanalytical Methods*; Springer, 2010; pp. 121–145.

(31) Ramaley, L.; Krause Jr, M. S. *Anal. Chem.* **1969**, *41*, 1362–1365.

(32) Economou, A.; Fielden, P. R. *Anal. Chim. Acta* **1993**, *273*, 27–34.

(33) Scholz, F. *Electroanalytical methods*; Springer, 2002.

(34) Fujiwara, H. *Spectroscopic Ellipsometry: Principles and Applications*; John Wiley & Sons, 2007.

(35) Sigal, G. B.; Mrksich, M.; Whitesides, G. M. *Langmuir* **1997**, *13*, 2749–2755.

(36) Zhu, B.; Eurell, T.; Leckband, D.; Gunawan, R. *J. Biomed. Mater. Res.* **2001**, *56*, 406–416.

(37) Offord, D. A.; John, C. M.; Linford, M. R.; Griffin, J. H. *Langmuir* **1994**, *10*, 883–889.

(38) McGillivray, D. J.; Valincius, G.; Loscheb, M.; Kasianowicz, J. J.; Heinrich, F.; Woodward, J. T.; Febo-Ayala, W.; Vanderah, D. J. *Biointerphases* **2007**, *2*, 21–33.

(39) Woollam, J. H. What is Ellipsometry? https://www.jawoollam.com/resources/ellipsometry-tutorial/what-is-ellipsometry (accessed May 11, 2017).

(40) Phan, H. T. M.; Bartelt-Hunt, S.; Rodenhausen, K. B.; Schubert, M.; Bartz, J. C. *PLOS ONE* **2015**, *10*, 0141282.

(41) Porter, M. D.; Bright, T. B.; Allara, D. L.; Chidsey, C. E. D. *J. Am. Chem. Soc.* **1987**, *109*, 3559–3568.

(42) Heide, P. V. der. *X-ray photoelectron spectroscopy: an introduction to principles and practices*; John Wiley & Sons, 2012.

(43) X-Ray Photoelectron Spectroscopy http://www.npl.co.uk/science-technology/surface-and-nanoanalysis/surface-and-nanoanalysis-basics/introduction-to-xps-x-ray-photoelectron-spectroscopy (accessed May 16, 2017).

(44) Nature Education. Gel Electrophoresis http://www.nature.com/scitable/definition/gel-electrophoresis-286 (accessed Apr 7, 2017).

(45) Gel electrophoresis: Visualising and interpreting the results https://www.sciencelearn.org.nz/videos/1271-gel-electrophoresis-visualising-and-interpreting-the-results (accessed Apr 7, 2017).

(46) Hassur, S. M.; Whitlock, H. W. *Anal. Biochem.* **1974**, *59*, 162–164.

Chapter 3

Ferrocene Nucleic Acids for Surface Bound DNA Sensing

3.1 Introduction

Ferrocene is one of the mostly widely used redox tags for electrochemical analysis, as discussed in section 1.3. One of the attractions of ferrocene is that it is amenable to functionalisation, which allows for the tuning of electrochemical properties and the variation of its position within a probe molecule or DNA sequence.[1]

In addition to the DNA modifications described in Chapter 1, a redox-active backbone modification can be inserted as close to the site of a base pair mismatch as possible. It was therefore envisaged that using this approach with a ferrocene redox active tag would produce a more sensitive probe for single nucleotide polymorphism (SNP) detection, giving an improvement over more flexible 3' and 5' modified redox tags that would be situated further away from a SNP site.

In addition to this, redox tags based on ferrocene are prone to degradation through nucleophilic attack on the oxidised ferrocenium ion (this is discussed further in Chapter 5).[2–6] The exposed nature of the 3' and 5' tags results in sensors that exhibit large losses in current over time and when subjected to multiple interrogations, unlike alternative redox active species such as methylene blue.[2] However, it was anticipated that placing the ferrocene reporter unit into the DNA backbone would make the unit less susceptible to attack, and so increase the stability of the probe strand.

DNA backbone modifications also have an advantage over nucleoside modifications. The reporter group is no longer an extension of the original structure but directly replaces an entire unit. Attachments to a nucleoside have previously resulted in the ferrocene unit being forced to sit outside the duplex or block the hydrogen bonding between bases.[7,8] This can cause a reduction in the stability of base pairs within the

duplex whereas the addition of unmodified nucleobases directly to the Fc backbone group could allow for a sensor directly attached to groups taking an active part in hydrogen bonding.[9] This was considered to be a further opportunity to increase the sensitivity towards SNPs.

3.1.1 Ferrocene as a DNA Backbone Mimic

There have been previous attempts at making a ferrocene unit part of a DNA backbone. The first example of a ferrocene monomer used for this approach is shown in Figure 3.1.[10] The alcohol groups were DMT-protected and phosphitylated to allow for automated synthesis of 22 base DNA probes via standard solid-phase synthesis methods. The authors first inserted this at the 5' and 3' ends for solution work[11,12] and at the 3' end only for surface work.[10] The thermal melting temperature or T_m (the temperature at which 50% of the DNA duplex (ds DNA) has denatured and reverted back to single stranded DNA (ss DNA)) measurements for the probes in solution showed a small destabilisation of the duplex upon hybridisation with the 3' modified probe (a reduction of ~1^{o}C) but not with the 5' modified probe when compared to natural DNA. The authors suggested that this was due to the ferrocene altering the duplex conformation on hybridisation and so reducing its binding strength. They also noted that having ferrocene monomers at both ends of the strand appeared to increase the electrochemical activity (89% increase in CV area) on binding to a fully complementary target, possibly due to a favourable orientation of the 3' end towards the electrode, which aligned the probe in a uniform direction ensuring that the 5' ferrocene is more accessible to the base pairs.[11]

Attachment to a Au surface using a 3'-modifed probe also showed that hybridisation of the complementary target reduced the electrochemical signal due to the probe no longer being aligned parallel to the surface.[10] The sensitivity limit of this detection was calculated to be 3 μM, which is generally higher than fluorescence methods. It also, once again, illustrates the problem of 'on-off' signalling where the reason for the reduction in electrochemical signal is ambiguous i.e. it could be due to either hybridisation or probe degradation.

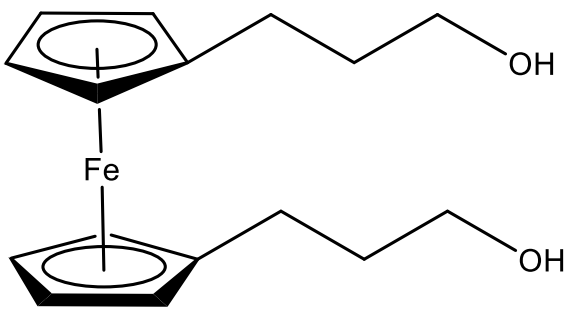

Figure 3.1: Ferrocene DNA backbone monomer[11]

Brisset and co-workers then used this work to introduce the ferrocenyl monomer into a hairpin molecular beacon-type molecule.[13] They showed that multiple reporter groups could be incorporated at both the ends and mid-strand. Increasing the number of ferrocene units caused duplex stability to reduce slightly (conversely it increased for the unhybridised beacon) but the sensitivity of the probe increased. The authors estimated a sensitivity limit of 1 μM when 8 ferrocene monomers were included in the loop but suggested that they could improve on this by immobilising the probe on a gold surface.[13]

Despite the possible advantages of having a redox-active reporter incorporated into a DNA backbone, the work described above was, to this author's knowledge, the only example of insertion of a redox active species into a DNA backbone until the synthesis of a ferrocene nucleic acid mimic by Tucker and co-workers, first reported in 2012.[9]

3.1.2 Ferrocene Nucleic Acid (FcNA)

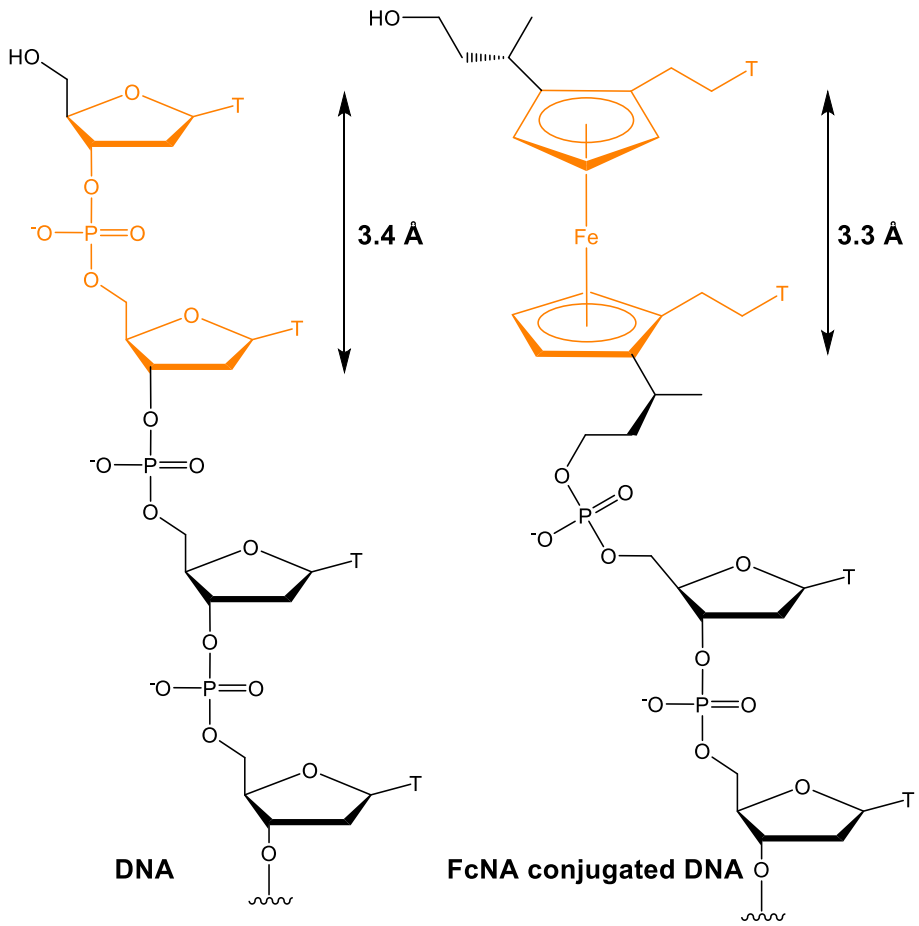

Figure 3.2 Structures of DNA (left) and FcNA conjugated DNA (right) exemplifying how FcNA can replace two sugar phosphate units.

Furthering their previous work on ferrocene-nucleobase conjugates[14] and based on computational modelling carried out by Dr John Wilkie (University of Birmingham)[9], Tucker and co-workers functionalised a ferrocene with nucleobases for backbone

insertion with the aim of developing a sensitive and stable redox reporter tag. It was hoped that, because of the similar Cp-Cp ring distance in ferrocene compared to the distance between the sugar rings in DNA (3.3 vs 3.4 Å respectively) (Figure 3.2), the nucleobases would be oriented such that hydrogen bonding would still be able to occur, thus linking the redox tag directly to the SNP binding event whilst retaining the duplex structure.[9]

The structures of a thymine and an abasic FcNA unit (FcTT and FcHH, respectively) are shown in Figure 3.3. Adenine (FcAA) and cytosine (FcCC) versions have also been synthesised and inserted into DNA but have not been investigated in the course of this work.[15] Guanine has consistently proven to be the more challenging substitution due to solubility issues and, to date, has not been successfully incorporated into DNA.[15]

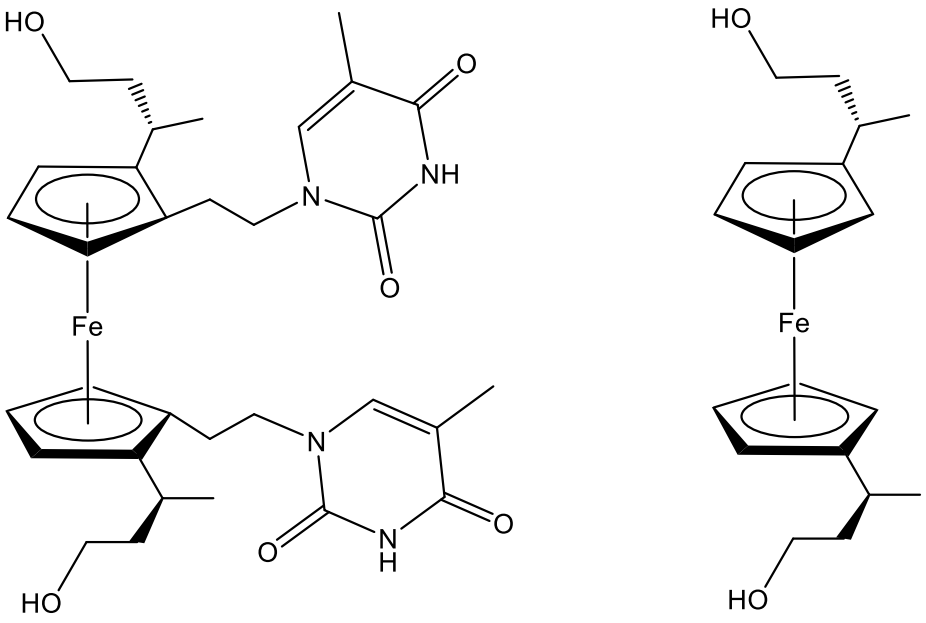

FcTT **FcHH**

Figure 3.3 Structure of FcTT[9] (Left) and FcHH (right). The synthesis of the FcHH monomer is currently unpublished.

The tetra-substituted unit consists of two thymine nucleobases attached to the ferrocene through a two carbon chain and two primary alcohols attached through linkages consisting of three carbon atoms and an alpha methyl group.

The chirality induced at the α-carbon position allows for the diastereoselective ortho-directed addition of the bases during the synthesis and their appropriate linkage. This, in turn, induces planar chirality within the ferrocene unit, since the di-substituted Cp rings result in non-superimposable mirror images (Figure 3.4).[16] For these molecules, if the stereochemistry around the α-carbon is (*R*), the planar chirality arrived at from this synthesis is (*S*) and vice versa for the (*R*) central stereochemistry. Use of the two enantiomers has proved to have quite an influence on the properties of the strand which will be discussed in both the summary of previous work and in the results described during the course of this thesis.[15]

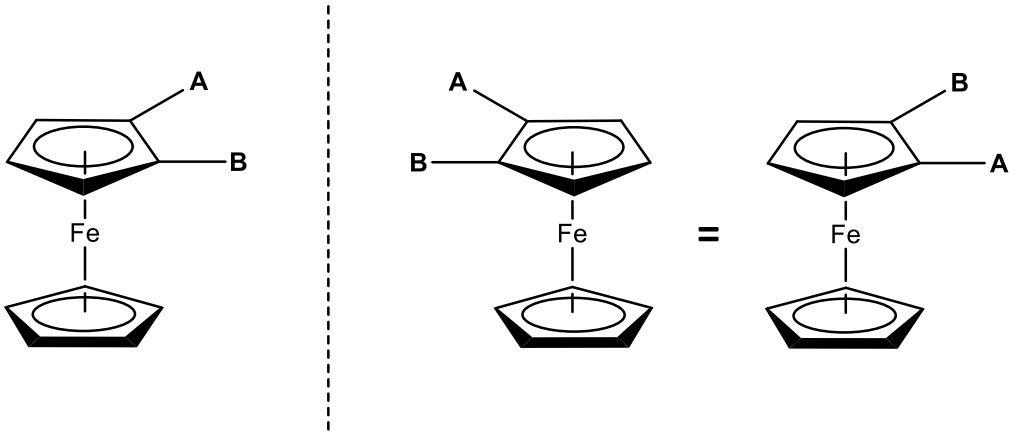

Figure 3.4 Planar Chirality of Ferrocene molecules due to the non-superimposable nature of groups attached to the di-substituted Cp Rings.

The full labelling of the FcNA molecules is as follows:

Fcn**X**c**ZBB**$_{\mathbf{XXpYpY}}$

Where:

BB = nucleobases

n**X** = number of carbons between the Cp ring and the phosphate group

c**Z** = number of carbon atoms between the Cp ring and the nucleobase

XX = chirality of the methyl group stereocentre (central chirality) = (*R,R*) or *(S,S*)

pYpY = planar chirality = (*pR,pR*) or (*pS,pS*)

The majority of this work focusses on Fcn3c2TT and Fcn3HH which, for clarity and simplicity, are referred to as FcTT and FcHH in the results and discussion, with only the label for the central chirality being included e.g. $FcTT_{(S,S)}$.

Insertion into DNA was made possible by the addition of a 4,4'-dimethoxytrityl (DMT) group to one primary alcohol whilst the other was phosphitylated, giving the resulting phosphoramidite (Figure 3.5) for use in automated DNA synthesis:

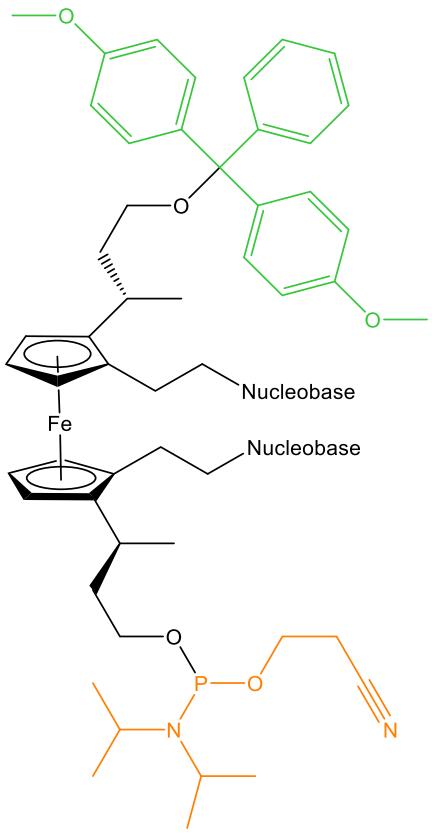

Figure 3.5 FcNA Phosphoramidite with DMT (highlighted green) and phosphitylation (highlighted orange) groups

A thymine-conjugated FcNA octamer was synthesised using this method (Figure 3.6). However, it was not able to form duplexes with its complementary target, under normal conditions.[9] This may be due to the slight difference in size between the FcNA and its equivalent DNA structure. However, the TA base match is the weakest of the complementary base sets and so even long chains of these would not be expected to have that high stability. The T_m for 5 μM of the natural DNA equivalent of this sequence in 50 mM NaCl is only 35.4°C.[17]

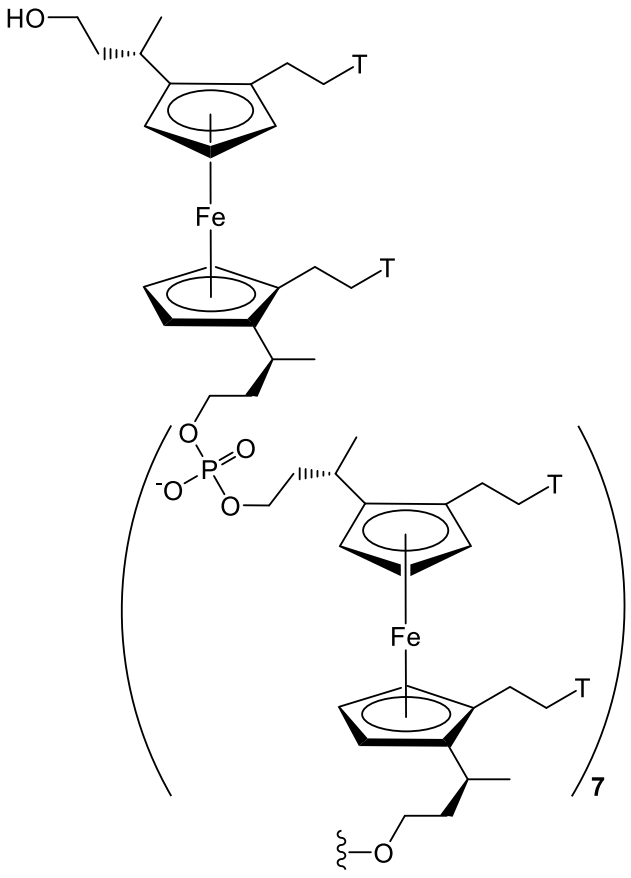

Figure 3.6 FcNA octamer

It was possible to obtain electrochemical data for this species. The cyclic voltammograms displayed a clear, quasi-reversible redox wave pair (Figure 3.7). Its quasi reversibility was attributed to the multiple electron transfer processes.[9,15,18]

The inability of the octamer to form stable duplexes with DNA led to subsequent studies using FcNA-DNA conjugates, where the FcNA was inserted as a single monomer into a central position in the DNA backbone.

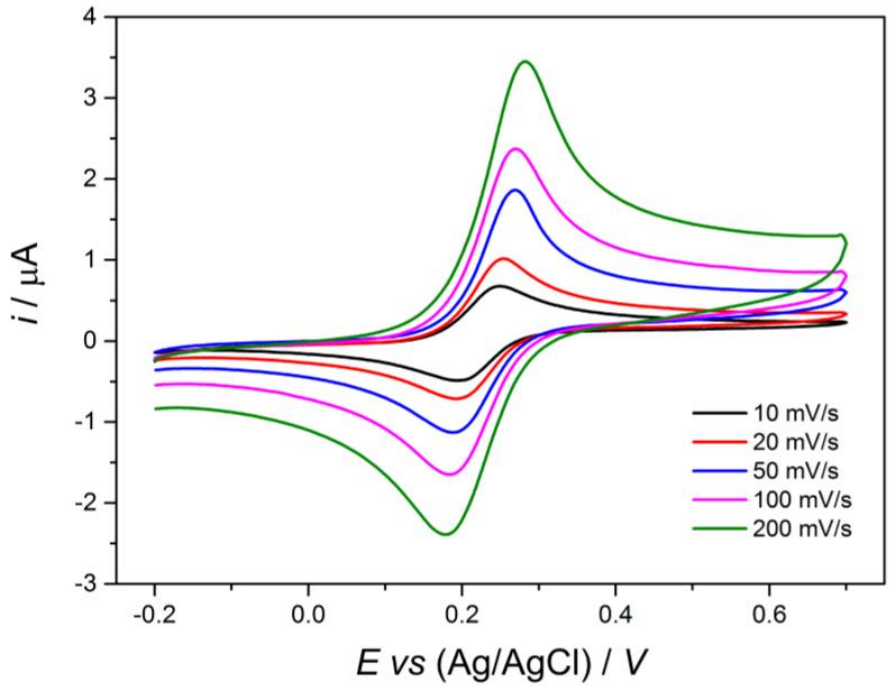

Figure 3.7 Cyclic voltammograms of $(FcTT_{SS})_8$ in 1 M $NaClO_4$, 10 mM phosphate buffer[9]

3.1.3 Previous Studies

Studies carried out by previous researchers have investigated the effect on DNA duplex stability of varying the linker lengths from the FcNA unit to both the nucleobase and the phosphate group. The work involved the characterisation of the FcNA-conjugated DNA through a variety of techniques and an assessment of the

electrochemical behaviour of the optimised structure in solution. The conclusions relevant to the following work are summarised here:

3.1.3.1 Optimisation of the FcNA structure

A range of different linker lengths to both the nucleobase and phosphate group were investigated by Dr James Carr-Smith.[15] The thymine nucleobases were primarily used throughout to ensure that a direct comparison was possible. Sequences used throughout previous work described here were the same as those used during the subsequent work described during this thesis and are given in Table 3.3.

As detailed below, the FcNA structure was optimised by monitoring the effect of changing the linker lengths on the T_m value when the FcNA conjugated DNA was part of the same fully complementary duplex.

3.1.3.1.1 Effect of Fc on Duplex Stability

Initially, a FcHH control (see Figure 3.3) was investigated to assess the impact of the Fc and was compared to a natural DNA strand with two abasic sites (Figure 3.8) in the equivalent FcNA position. The target was fully complementary except for two adenine bases opposite the abasic sites. For both *(R,R)* and *(S,S)* chirality there was a 0.5 ^{o}C increase in T_m compared with the equivalent natural DNA (37.0 ^{o}C vs 37.5 ^{o}C for S1AbAb vs both S1FcHH$_{(S,S)}$ and S1FcHH$_{(R,R)}$, respectively) suggesting that the presence of Fc did little to impact duplex stability.[15]

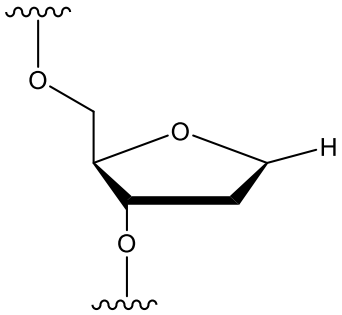

Figure 3.8 Abasic monomer for insertion into DNA

Interestingly, despite both $FcHH_{(R,R)}$ and $FcHH_{(S,S)}$ giving the same T_m values, molecular modelling (carried out by Dr Jean-Louis Duprey) suggested that the FcNA units orient themselves quite differently within the duplex. In order to ensure both enantiomers have the methyl groups situated within the hydrophobic core of the duplex, the *(S,S)* isomer orients itself perpendicular to the base stacking motif whereas *(R,R)* more closely follows the helical structure of natural DNA.[15]

3.1.3.1.2 FcTT: Varying Linker Length to the Nucleobase

The effect of changing the length of the linker to the nucleobase from two carbon atoms to three carbon atoms for thymine-based FcNA was investigated. The T_m values of these and of the natural DNA equivalent are given in Table 3.1.

Table 3.1 T_m values for both stereoisomers of Fcn3c2TT and Fcn3c3TT natural DNA when duplexed with a fully complementary target. 5 μM of each strand in 10 mM sodium phosphate buffer pH 7.0, 100 mM $NaClO_4$. Modifications (and TT in natural DNA) were placed at positions 8 and 9 in a 16 base DNA strand (where the FcNA unit replaces two natural nucleotides).[15] Sequence is as S1 in Table 3.3.

Modification	Thermal Melting Temperature (T_m) / °C
Fcn3c**2**TT_{RRpSpS}	43.0
Fcn3c**2**TT_{SSpRpR}	41.0
Fcn3c**3**TT_{RRpSpS}	41.5
Fcn3c**3**TT_{SSpRpR}	43.0
TT	56.0

The presence of any of the FcTT variations in the DNA strand had a detrimental impact on the stability with reductions in T_m between 13 and 15 ^{o}C, though these were still improvements on the FcHH units. This was explained by the additional rigidity of the Fc unit compared with the corresponding DNA dinucleotide. In particular, the ferrocene is only able to rotate its Cp rings in two parallel planes. This, coupled with the slight decrease in size of the Fc compared with that of the dinucleotide it is replacing, is likely to produce some strain in the base stacking motif, so reducing the stability of the structure. Further to this, circular dichroism (CD) spectroscopy showed that duplexed FcTT-conjugated DNA produced less intense bands at 275 and 245 nm: the bands normally associated with B-DNA.[19,20] This implies that the duplex is distorted somewhat compared to natural DNA, and which is consistent with the observed reductions in stability.[15]

The presence of an additional carbon atom in the nucleobase linker reversed the stability trend (Table 3.1) with units with *(R,R)* chirality now being more stable (2 ^{o}C increase in $T_{m)}$) than the *(S,S)* version. Molecular modelling, shown in Figure 3.9, was used to determine the cause of this.

For the 2 carbon linker, the *(S,S)* version appears to kink out of the duplex whereas the *(R,R)* unit more closely follows the natural line of the double helix backbone, presumably giving rise to a less strained duplex. For the three carbon atom linker system, neither chirality can align well with the sugar phosphate backbone. However, the *(S,S)* variant can orient the thymine bases so that a more natural base stacking motif is supported; hence the stability is slightly higher than the other stereochemistry.

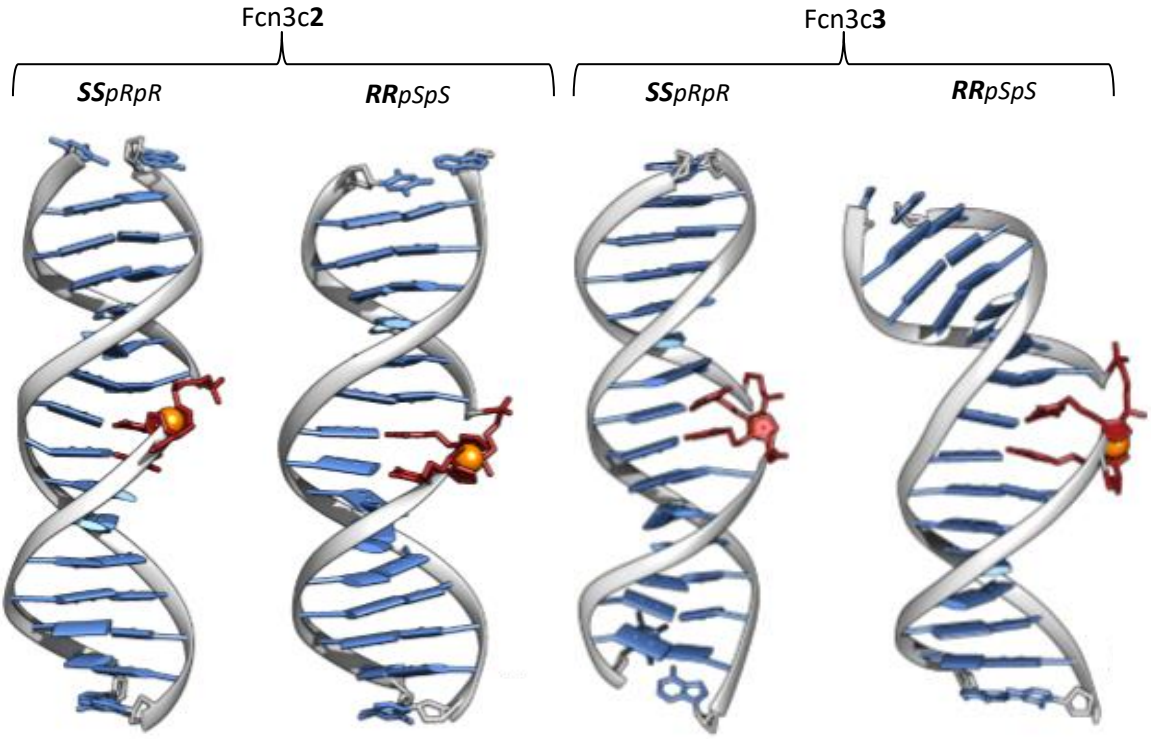

Figure 3.9 Molecular dynamic simulations (5 ns) of both isomers of Fcn3c2TT and Fcn3c3TT duplexed with fully complementary DNA target (i.e. AA opposite the FcNA units). Visualised using Chimera II and carried out by Dr Jean-Louis Duprey. Images courtesy of Dr James Carr-Smith.[15,21]

It was also noted that the multiple denaturing and annealing steps usually carried out during the acquisition of T_m measurements resulted in a gradual increase in T_m value for both of the units with 3 carbon atom linkers to the nucleobase. This implies the partial oxidation of the FcNA unit and it was theorised that the additional +I inductive effect of the extended alkyl linker allowed for its more facile oxidation of the Fc. Partly as a result of this, as well as the insignificant improvement in T_m (0.5°C for Fcn3c**3**TT$_{\boldsymbol{RR}pSpS}$ compared to Fcn3c**2**TT$_{\boldsymbol{RR}pSpS}$) on extending the alkyl chain, the two carbon atom linker to the nucleobase was used in all subsequent experiments.[15]

3.1.3.1.3 FcTT: Presence of the Methyl Group

Investigations into the loss of central chirality by removal of the methyl group from the phosphate linker group revealed a decrease in T_m value of 1.5 °C for the duplex with the Fcn3c**2**TT$_{\boldsymbol{RR}pSpS}$ equivalent, labelled Fcn3c**2**TT$_{pRpR}$ (the loss of the methyl group results in a change in the priorities used to derive planar chirality and so the chirality is now reversed) (T_m values given in Table 3.2). There was no change in T_m on changing Fcn3c**2**TT$_{\boldsymbol{SS}pRpR}$ to Fcn3c**2**TT$_{pSpS}$. The structures of Fcn3c**2**TT$_{\boldsymbol{SS}pRpR}$ and the equivalent Fcn3c**2**TT$_{pSpS}$ are given in Figure 3.10 for illustration.

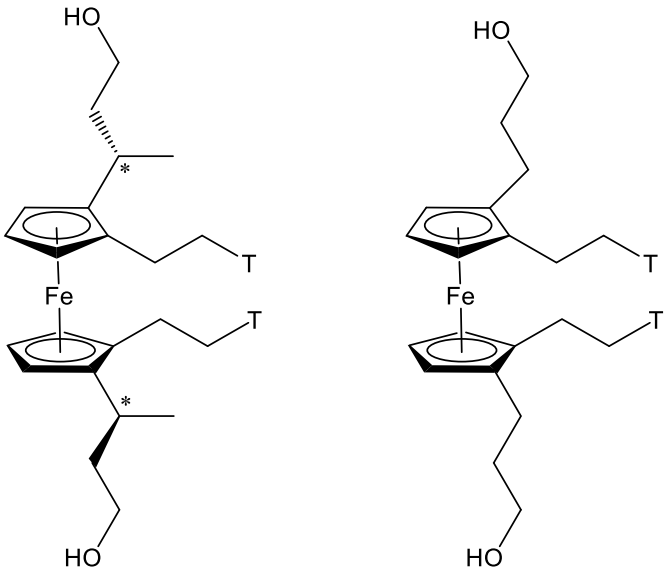

*Figure 3.10 Comparison of equivalent Fcn3c2TT monomers with and without a methyl group including in the phosphate linker group (*S,SpRpR *and* pSpS, *respectively)*

Further studies revealed that central chirality is important for base discrimination for the *(R,R)* isomer. The two bases opposite the FcNA unit were varied and the effects on the T_m values were investigated (Table 3.2).

Table 3.2 T_m values for Fcn3c2TT$_{R,RpSpS}$, Fcn3c2TT$_{pRpR}$ and natural DNA when duplexed with various targets (targets were fully complementary except for bases 8 and 9 which are indicated by XX in the table below). 5 μM of each strand in 10 mM sodium phosphate buffer pH 7.0, 100 mM NaClO4. Modifications (and TT in natural DNA) were placed at positions 8 and 9 in a 16 base DNA strand (where the FcNA unit replaces two natural nucleotides).[15]

Modification	**Thermal Melting Temperature (T_m) / ^oC** XX = Bases Opposite FcNA		
	AA	AG	GG
Fcn3c2TT$_{RRpSpS}$	43.0	42.0	41.0
Fcn3c2TT$_{pRpR}$	41.5	41.0	41.0
TT	56.0	44.5	44.5

For Fcn3c2TT$_{RRpSpS}$, increasing complementarity resulted in increasing T_m values which implies an H-bonding interaction with the bases opposite. This was not observed with Fcn3c2TT$_{pRpR}$. Molecular modelling suggested that this was due to the duplex unravelling slightly to form a large cavity where bases are too far apart to interact. This would also account for the slight reduction in stability of the duplexes.[15]

3.1.3.1.4 FcTT: Varying Linker Length to Phosphate Group

Reducing the number of carbon atoms in the linker to the phosphate group and retaining the methyl group was too challenging synthetically. As a result, a two carbon atom linker to the phosphate was investigated with only planar chirality (Fcn2c2TT). Although the resultant fully complementary duplex maintained the base discrimination trends previously discussed, the stability was lower (42.0 ^oC Fcn**2**c2TT$_{pRpR}$ *v.* 43.0 ^oC for Fcn**3**c2TT$_{RRpSpS}$) and so the presence of the methyl group was deemed to be the more important addition to the structure.[15]

Consequently, the optimised structure was judged to be a ferrocene molecule with a two carbon atom alkyl linker to the nucleobase and a three-carbon alkyl linker containing a methyl group on the α-carbon with *(R,R)* stereochemistry.

3.1.3.2 Hydrogen Bonding

Some of the evidence presented above was explained by there being hydrogen bonding between bases attached to the FcNA units and those of the DNA targets.

To investigate this further, Fcn2c3CC$_{(R,R)pSpS}$ (FcCC$_{(R,R)}$) was synthesized and incorporated into DNA of the same sequence as in the previous studies. Its structure is shown in Figure 3.11.

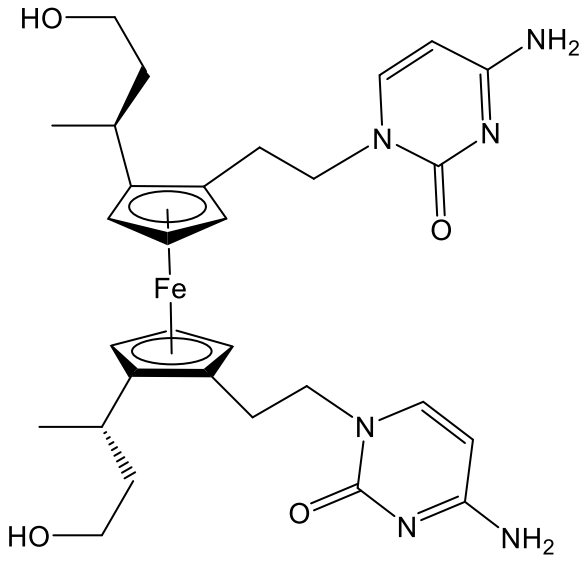

Figure 3.11 Structure of Fcn2c3CC$_{RRpSpS}$ (FcCC$_{RR}$)

The CC derivative was expected to be the more stable due to the increase from two hydrogen bonds possible with T-A base pairs to three with C-G base pairs. Gratifyingly, duplex stability increased (as evidenced by a by 8.5 ^{o}C and 2.5 ^{o}C increase in T_m) when FcCC$_{(R,R)}$ conjugated DNA was bound to a fully complementary target compared to targets with an AA or AG mismatch (respectively). The trend of increasing stability with increasing number of mismatched bases opposite strongly supports hydrogen bonding.[15]

CD data showed a significant change in duplex structure on binding complementary DNA as evidenced by a hypsochromic (blue) shift in the B-DNA bands, a decrease in

the positive band intensity and an additional peak present at 290 nm. Since the spectra of $FcCC_{(R,R)}$ bound to an AA mismatch target more closely resembled that of the unmodified DNA controls (see Figure 3.12), it was concluded that these observations were most likely due to the untwisting and even flipping out of a base from the duplex to accommodate the hydrogen bonding. This, and the relative ease with which FcNA is incorporated into DNA, raised the possibility of using these compounds for biosensing applications. This was subsequently investigated with electrochemical methods.[15]

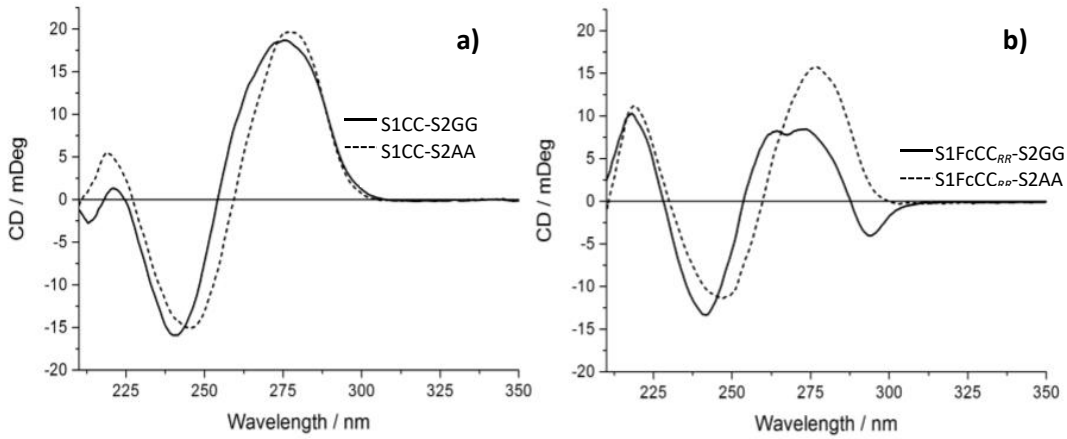

Figure 3.12 CD spectra of a) unmodified DNA control probe (S1CC) bound to targets with GG (S2GG) (solid line) and AA (S2AA) (dashed line) bases opposite and b) $FcCC_{RR}$ modified probe strands bound to targets with GG (S2GG) (solid line) and AA (S2AA) (dashed line) bases opposite. Spectra acquired using 5 μM of each strand in 10 mM sodium phosphate buffer pH 7.0, 100 mM NaClO4. Spectra courtesy of Dr James Carr-Smith.[15]

3.1.3.3 Electrochemistry

The electrochemical characteristics of DNA strands containing $FcHH_{(R,R)}$, $FcTT_{(R,R)}$, $FcCC_{(R,R)}$ and $Fcn2c3AA_{SSpRpR}$ ($FcAA_{(S,S)}$) were compared using cyclic voltammetry (CV) and square wave voltammetry (SWV) at a concentration of 50 μM probe strand in 1 M $NaClO_4$, 10 mM sodium phosphate buffer at pH 7. As calculated from the CV

data, all gave a linear relationship between current and the square root of the scan rate, typical of reversible systems in the limit of linear diffusion. An example of this is given in Figure 3.13. However, a fully reversible system has a peak separation (ΔE_p) of 59 mV and a cathodic to anodic peak ratio (i_p^c/i_p^a) of 1.[22,23] Both $FcHH_{(R,R)}$ and $FcTT_{(R,R)}$ strands had ΔE_p of 62 mV which is within error of the ideal 59 mV whereas ΔE_p for $FcCC_{(R,R)}$ and $FcAA_{(S,S)}$ were 75 and 77 mV respectively, implying that the cytosine and adenine derivatives were slightly less reversible. For all systems i_p^c/i_p^a was less than one, ranging from 0.86-0.98, indicative of quasi reversible behaviour.[15]

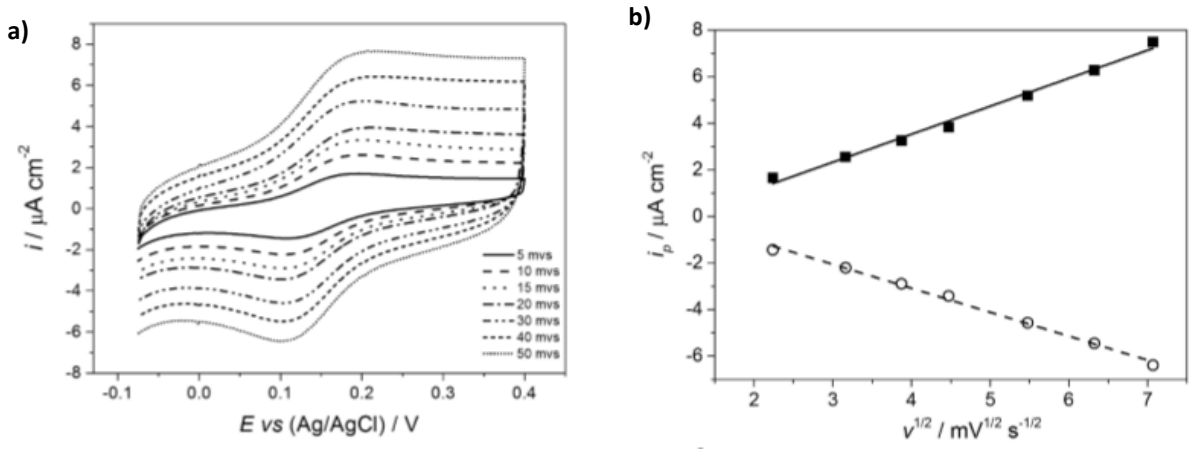

Figure 3.13 a) Cyclic voltammograms of $FcTT_{(R,R)}$ conjugated DNA recorded at various scan rates in 1M $NaClO_4$, 10 mM sodium phosphate buffer pH 7.0. b) the corresponding Randles- Sevcik plots showing linear dependence of current on square root of scan rate. ■=anodic current, ○=cathodic current.Graphs courtesy of Dr James Carr-Smith.[15]

The half wave potential, $E_{1/2}$, varied between the different Fc derivatives due to the electron withdrawing abilities of the bases, as had been previously noted by Houlton and co-workers.[24] For example, $FcHH_{(R,R)}$ was oxidised at the least positive potential (112 mV), since there are no bases attached to influence the oxidation. The ferrocenes with bases attached followed a predictable oxidation trend: $FcTT_{(R,R)}$ (148 mV) < $FcCC_{(R,R)}$ (155 mV) < $FcAA_{(S,S)}$ (173 mV). This corresponds to the calculated

electron affinities of the appropriate bases when attached to ferrocene.[25] While the highly electron withdrawing purine rings dramatically increase the potential required for oxidation of $FcAA_{(S,S)}$, a guanine derivative would be expected to require the least positive potential due to the presence of the electron donating oxygen atom.

Fully complementary targets were added to each FcNA conjugated probe strand and heat annealed to allow for hybridisation. All systems showed a suppression of current on binding in both SWV and CV and a slight shift of $E_{1/2}$ to more negative potentials (example given in Figure 3.14). The suppression can be explained by a duplexed system being larger, which decreases its diffusivity to and from the electrode. The increase in charge (due to the additional phosphate groups in the target backbone) would also affect its diffusivity as well as stabilising the oxidised ferrocenium species, allowing for oxidation to occur at a more negative potential.[15]

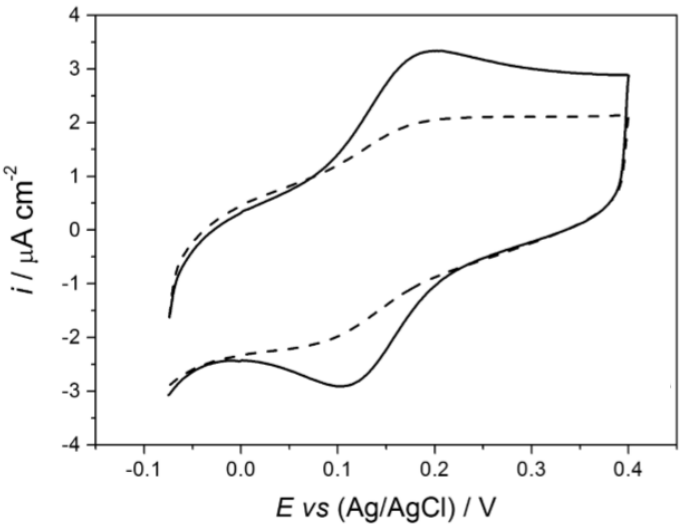

Figure 3.14 Cyclic voltammetry of single stranded $FcTT_{(R,R)}$ conjugated DNA (solid line) and duplexed with a fully complementary target (dashed line). CV recorded in 1 M $NaClO_4$, 10 mM sodium phosphate buffer, pH 7.0. 50 μM of each strand used. Graph courtesy of Dr James Carr-Smith.[15]

Detection of mismatched probes was carried out with the $FcTT_{(R,R)}$ derivative. Addition of 1 molar equivalents of the target strand containing a double mismatch

(GG opposite FcNA unit) resulted in 76% depletion in current compared with 88% for fully complementary DNA. It was suggested that this may be a method for base discrimination. However, the large concentrations of target and probe required for peaks to be detected above the capacitance current rendered solution-based electrochemistry a relatively insensitive detection method.

3.1.4 Conclusions and Project Aims

Despite the wide range of ferrocene- based modifications to the core DNA structure, very few studies have focussed on replacing the entire sugar phosphate unit. Ferrocene is an ideal candidate for this type of substitution since it is a very similar size to two consecutive sugar phosphate units.[9] This reduces destabilisation of the duplex and allows for the placement of nucleosides at positions close to that of natural DNA, to promote hydrogen bonding.[15] This, coupled with the ease of functionalisation and the well understood electrochemical properties of ferrocene, make it an excellent prospect for a sensitive DNA sensor.[9]

To this end, and following on from work by Brisset and co-workers, the Tucker group designed and synthesised a tetra-substituted ferrocene nucleic acid designed to mimic natural DNA. It possesses reactive groups which make it suitable for insertion into DNA through automated synthesis and a nucleobase attachment on each Cp ring to allow for hydrogen bonding.[9,10,12,13,15]

Previous work by the group has focussed on optimisation of the structure through varying the linker lengths and inclusion of planar and central chirality. A combination of duplex melting studies, CD spectroscopy and molecular modelling has been used to compare duplex stabilities of enantiomers of FcTT, FcHH, FcCC and FcAA in

DNA. A combination of these techniques has provided evidence that the FcNA units are indeed capable of hydrogen bonding despite there being a decrease in stability compared with natural DNA.[15]

Solution-based electrochemical studies showed quasi-reversible behaviour for these compounds and a reduction in current on binding a target, which may be usable as a way of detecting base mismatches opposite the FcNA unit.[15]

In a continuation of this work and in an attempt to increase the sensitivity of this system, it was decided to investigate FcNA-DNA conjugates as surface-bound probes in self assembled monolayers (SAMs). Both enantiomers of FcHH and FcTT were to be explored since these species were shown to display good Nernstian behaviour and electrochemistry in solution. As well as their ability to detect base mismatches, the stability of the SAMs were to be considered in depth with a long-term view to develop an electrochemical SNP detection device.

3.2 Results and Discussion

3.2.1 Oligonucleotides Used

The DNA sequences used throughout this chapter are shown in Table 3.3. The following FcNA units were incorporated into DNA: $FcHH_{(R,R)}$, $FcHH_{(S,S)}$, $FcTT_{(R,R)}$ and $FcTT_{(S,S)}$. S0 is the natural DNA probe control with a thiol group attached to the 3' terminus (incorporated as outlined in Section 7.2). S1 is the FcNA conjugated DNA equivalent of S0. S2 denotes the target strand which is fully complementary except for bases 8 and 9. These are the bases opposite the FcNA unit and varying these allows for assessment of the FcNA unit in its capacity for SNP detection.

Table 3.3 Oligonucleotide sequences used throughout Chapter 3

Oligonucleotide	Sequence (5' – 3')
S0	TGG ACT CTT CTC AAT G **-SH**
S1(**$TT_{(S,S)}$ *or* $TT_{(R,R)}$**	TGG ACT C (**$FcTT_{(S,S)}$ *or* $FcTT_{(R,R)}$** CTC AAT G **-SH**
S1(**$HH_{(S,S)}$ *or* $HH_{(R,R)}$**	TGG ACT C (**$FcHH_{(S,S)}$ *or* $FcHH_{(R,R)}$** CTC AAT G **-SH**
S2(**AA, GG, CC, TT *or* TA**)	CAT TGA G(**AA, GG, CC, TT *or* TA)** GAG TCC A

3.2.2 Preparation of SAMs

SAMs were prepared as outlined in sections 2.2 and 7.4.1. The concentration and volume of both thiolated probe (200 μL of 1 μM DNA) and 6-mercapto-1-hexanol (1.46 mL at 2 mM) used to form the SAMS were not varied throughout this work. This procedure and the amounts used were outlined by Plaxco and co-workers following on from their work on maximising surface stability and signal acquisition with electrochemically active SAMs.[26,27] Whilst it is noted that the ideal conditions for each system will vary, it was decided to continue with those outlined by Plaxco and co-workers to demonstrate a proof of principle before further optimisation studies were carried out.

One change was made to the suggested method, for all subsequent experiments, following initial electrochemical studies. The current was shown to increase with successive interrogations by SWV as shown in Figure 3.15. This was unexpected and implied that surface rearrangement was occurring on the electrode. This reorganisation of the surface on application of a potential has been reported previously and would be an issue when determining differences between the signals produced for bound and unbound probes as well as when monitoring degradation of the redox-active species.[28–31] Subsequently it was found that extending the exposure time of the electrode to MCH from 4 hours to 20 hours on SAM preparation,

prevented this effect, with the current reducing slightly over 150 scans. It is likely that the longer time period allowed DNA probes to migrate away from one another due to the repulsion between the negatively charged phosphate backbones. The resulting SAM was expected to have more spread out probes sequences, enabling facile electron transfer and so maximise current acquisition.

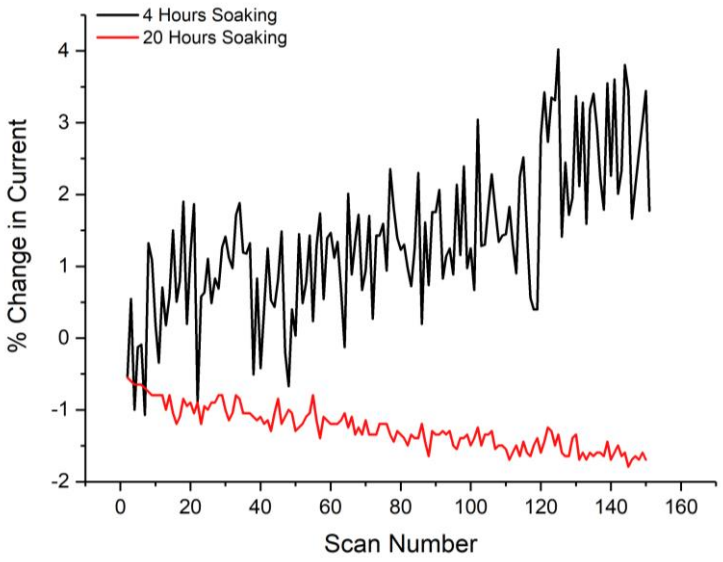

Figure 3.15 Percentage change in current (as measured from the SWV peak maximum) on successive electrochemical scans of mixed monolayers of S1TT$_{(S,S)}$ where the SAM was prepared with MCH exposure of 4 hours (black line) and 20 hours (red line). SWV recorded at a frequency of 200 Hz, amplitude of 25 mV and step of 1 mV in 1 M $NaClO_4$, 10 mM phosphate buffer.

3.2.3 Characterisation of SAMs

In order to establish whether the redox-active species in the SAMs were indeed well dispersed, attempts were made to characterise them by ellipsometry and X-ray photoelectron spectroscopy (XPS).

3.2.3.1 Ellipsometry

The principles behind ellipsometry are described in section 2.4.1. Briefly, the interaction of an incident light beam with the various components of the surface

(including the gold substrate, MCH, DNA and air interfaces) results in both the reflection and refraction of the light and a subsequent change in the intensity of that light. From the energy and phase of the reflected light (or elliptically polarised light) and its difference from the incident beam, these interactions can be modelled to determine the thickness of the SAM present.[32]

Mixed monolayers of S1TT$_{(S,S)}$, S1TT$_{(R,R)}$, S1HH$_{(S,S)}$, S1HH$_{(R,R)}$, S0 and monolayers of MCH alone were investigated. In solution, the length of an MCH molecule has been calculated by molecular modelling to be 1.068 nm.[33] The Au-S bond has been shown to vary between 2.2 and 2.6 Å which would correspond to a maximum MCH SAM thickness of 1.29-1.33 nm.[34,35] The experimental ellipsometry data are shown in Table 3.4.

Table 3.4 Experimentally derived surface thicknesses using ellipsometry using Cauchy modelling method where a = 1.45. Thicknesses are an average of 3 measurements taken on each of three slides.

SAM	Surface Thickness / nm
MCH	1.7 ± 0.1
S0	1.8 ± 0.2
S1**TT**$_{(S,S)}$	1.6 ± 0.2
S1**TT**$_{(R,R)}$	1.5 ± 0.1
S1**HH**$_{(S,S)}$	1.4 ± 0.3
S1**HH**$_{(R,R)}$	1.5 ± 0.3

The MCH only monolayer is thicker than the calculated maximum for this species. This may be due to the SAM formation process or the modelling system used to calculate the thicknesses. The value used to measure the concordance between the model and the experimental results is known as χ^2, with χ^2 = 1 being fully matched. For the data derived above, χ^2 was between 1.3 and 1.7, which is within acceptable

limits.[36] It is possible that hydrogen bonding is occurring between MCH attached to the gold surface and a small number of free MCH molecules that are not removed during the rinsing process. This would result in a packed surface bound layer with a diffuse double layer. Further studies, such as extended washing times or AFM should be undertaken to determine the cause.

The modified SAMs all possess very similar thicknesses, close to that of the thickness of the MCH alone. This would suggest that the concentrations of probe used to form these monolayers do indeed result in a packed layer of MCH with a sparse distribution of DNA probe, ideal for electrochemical sensing.[26,37,38] This allows the DNA strands to lie parallel to the surface of the monolayer as they are unhindered by closely packed neighbouring molecules. The values are consistent for each variation of the probe, suggesting that the FcNA has little impact on the structure of the SAM surface.

3.2.3.2 X-Ray Photoelectron Spectroscopy (XPS)

Often referred to as the 'mass spectrometry of the surface', XPS measures the kinetic energy and number of electrons being ejected from an atom by an incident laser beam (section 2.4.2 contains more detailed theory). The difference in energy between the incident beam and resultant kinetic energy corresponds to the energy required to remove that electron (i.e. the binding energy) and is indicative of the species in the sample since each atom will have its own unique set of binding energies. The final spectrum consists of a plot of the number of electrons vs binding energy (in eV) from which peaks can be integrated and used to determine the ratios

of atoms present.[39,40] An example of an XPS spectrum of gold, with the relevant binding energies labelled, is given in Figure 3.16.

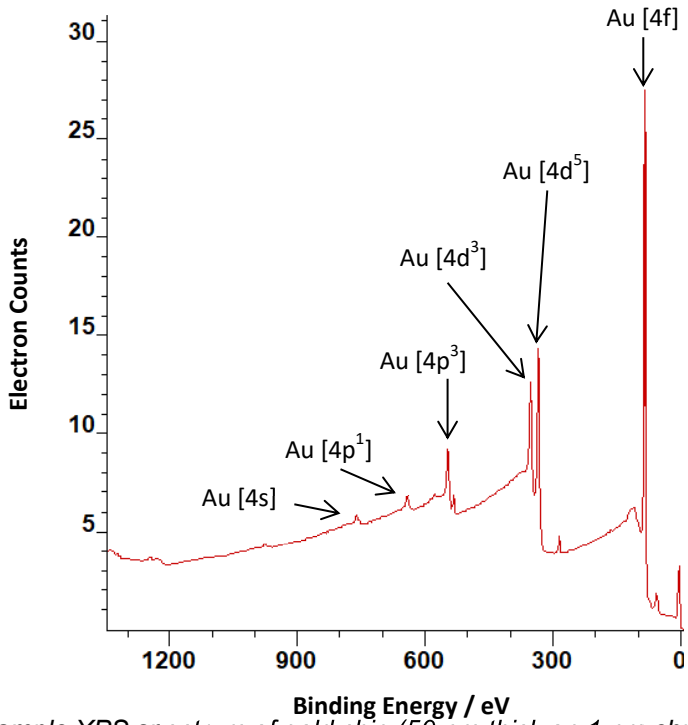

Figure 3.16 Example XPS spectrum of gold chip (50 nm thick on 1 nm chromium coated glass) with the relevant binding energies labelled. Data recorded at the National EPSRC XPS Users' Service (NEXUS) at Newcastle University.

XPS measurements (performed at the NEXUS facility in Newcastle University) were carried out on SAMs consisting of MCH only and on mixed monolayers of S0, $S1TT_{(S,S)}$, $S1TT_{(R,R)}$, $S1HH_{(S,S)}$ and $S1HH_{(R,R)}$. The amount of an element present can be determined form the integral of the peak. Fitting the spectra enables the ratios of elements present to be determined.[39] For this reason specific elements were analysed in detail to give an indication of the surface characteristics. For example, the percentage of the electrons which were resulting from ejection from the 2p sulphur orbital was used as a base measurement since every molecule bound to the surface should contain one sulphur atom. To confirm the accuracy of the peak modelling, the experimentally determined ratio of C 1s : S 2p electrons in MCH only (13.8 ± 1.4%) was compared with the calculated percentage composition (6:1 or

14.3%) and were concordant, which gave confidence in investigation of the remaining SAMs of interest.[41]

Unfortunately, due to a low total percentage of iron compared with other elements, it was not possible to accurately fit the Fe 2p peak to give an indication of the number of FcNA reporters. Instead, the ratio of FcNA-DNA to MCH molecules was determined by comparing the percentage of electrons resulting from N 1s with those resulting from S 2p. The data are given in Table 3.5.

Table 3.5 The ratio of DNA strands to MCH molecules present on a surface for each of 5 different mixed monolayers, calculated from the percentage of electrons detected that are due to ejection from the S 2p and N 1s orbitals. Percentages and their associated errors are determined from the XPS analysis of three sample areas from each of three individually prepared SAMs. Experiments carried out at NEXUS, Newcastle University.

SAM	% S 2p	% N 1s	Calc'd No. of N atoms	DNA:MCH ratio
S0	3.5 ± 0.3	25.2 ± 0.4	54	1 : 6
S1**TT**$_{(S,S)}$	8.5 ± 1.3	7.3 ± 1.3	54	1 : 62
S1**TT**$_{(R,R)}$	8.7 ± 1.4	13.3 ± 2.5	54	1: 34
S1**HH**$_{(S,S)}$	3.9 ± 3.8	25.8 ± 1.0	50	1 : 7
S1**HH**$_{(R,R)}$	3.5 ± 0.1	27.1 ± 2.1	50	1 : 6

S0 and both S1FcHH variations show good concordance, with 1 DNA strand per approximately 6 MCH molecules present on the surface. This would suggest a relatively densely packed distribution of DNA, where strands could be expected to interfere with each other if diffusion to the surface was to occur, particularly when the strands were duplexed (due to the increased rigidity).[42] This is contrary to what was found by ellipsometry, which suggested that the DNA probes were dispersed enough to lie flat on the surface. Further repeats of both experiments will be required to ascertain the reasons for this.

Both S1TT variants were shown to be much more diffusely packed than the S0 and S1HH SAMs. This is not consistent with the ellipsometry data and the difference is difficult to explain. It is possible that these SAMs are more prone to degradation in air and thus are more greatly affected by the increased time required to transport the samples to the XPS facility. These experiments should be repeated to confirm the results.

Ideally, further studies, such as STM, could be carried out in an attempt to visualise the SAM structure and provide further insight into the diffusivity of the DNA strands within the surface. By recording these measurements at regular intervals, it may also be possible to observe whether the FcTT units are more prone to degradation or whether the higher ratios are actually indicative of the surface.

3.2.4 Electrochemistry

3.2.4.1 Initial Control Studies

The mixed monolayers were further characterised using cyclic voltammetry. Initially, CVs of bare Au, MCH only and mixed monolayers of S0 were recorded to ensure the peaks to be interpreted were indeed resulting from the FcNA units, as was expected. The resulting CVs are shown as overlays in Figure 3.17.

As predicted by the literature, CVs of the bare Au electrode, due to the adsorption and desorption of species from the electrolyte, possessed enhanced current and a large negative peak.[43] These were not present in the MCH and S0 mixed monolayer since the SAMs act to block the interaction between the gold surface and ions in solution. As expected for these systems, there was no issue with interference peaks.

Accordingly, peaks present in the CVs of SAMs of both variants of S1HH and S1TT were assumed to arise from the FcNA units themselves.

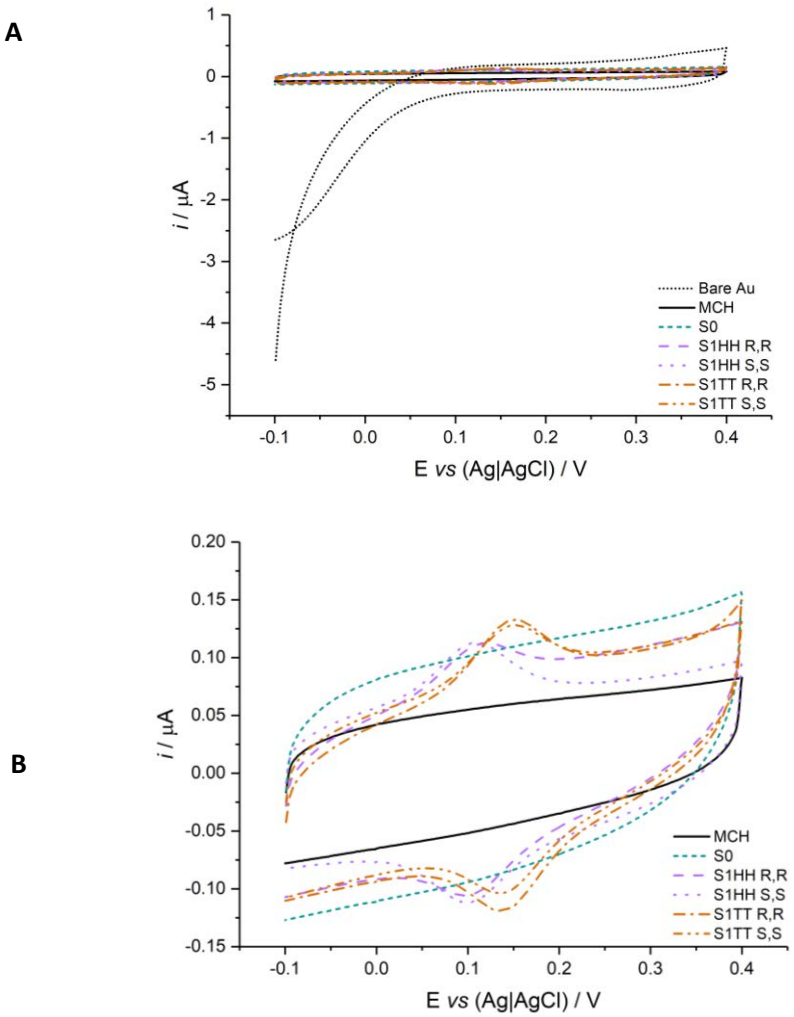

Figure 3.17 Cyclic voltammograms of A: Bare gold, MCH only, S0, S1HH$_{(R,R) \text{ and } (S,S)}$ and S1TT$_{(R,R) \text{ and } (S,S)}$ mixed monolayers (B: without Bare Au to allow for ease of comparison). CVs recorded at 100 mV s^{-1} in 1 M $NaClO_4$, 10 mM phosphate buffer

3.2.4.2 Characterisation by CV

The mixed monolayers of S1HH$_{(R,R) \text{ and } (S,S)}$ and S1TT$_{(R,R) \text{ and } (S,S)}$ were characterised by recording CV at varying scan rates and plotting the resultant relationship between scan rate and current. The corresponding graphs and data are given in Figure 3.18 and Table 3.6, respectively.

The calculated surface coverages for these systems indicate sparsely populated surfaces and correspond well to surface coverages reported within the literature which allow for full DNA hybridisation. It also increases the probability that the redox centre will be able to reach the electrode surface and that the systems could produce sensitive electrochemical devices with fully reversible redox behaviour.[37,38]

*Table 3.6 Electrochemical behaviour of DNA:FcNA SAMs derived from Figure **3.18**. All values are an average of three replicate measurements. $E_{1/2}$, ΔE_p and I_p^c / I_p^a are determined form the 100 mV s^{-1} redox wave. Γ is determined from the gradient of the square root of the scan rate vs current graph. (Figure 3.18)*

SAM	$E_{1/2}$ / mV	ΔE_p / mV	I_p^c / I_p^a	Γ / x 10^{11} molecules cm^{-2}
A: S1**HH**$_{(R,R)}$	108 (± 0.2)	5.4 (± 3.0)	1.04 (± 0.08)	4.83 (± 0.38)
B: S1**HH**$_{(S,S)}$	104 (± 1.0)	2 (± 3.1)	1.01 (± 0.06)	5.66 (± 0.37)
C: S1**TT**$_{(R,R)}$	144 (± 0.9)	1.5 (± 2.8)	1.22 (± 0.05)	6.15 (± 0.57)
D: S1**TT**$_{(S,S)}$	144 (± 0.5)	2 (± 2.7)	1.26 (± 0.03)	5.52 (± 0.59)

For all systems, peak separation ($\Delta E_p = E_p^a - E_p^c$) is consistently low and plots of scan rate vs current display excellent linear dependence, corresponding to that which is expected for a typical surface-bound electrochemically active species with fully reversible, Nernstian behaviour. However, whilst the cathodic to anodic peak ratio (I_p^c / I_p^a) for both FcHH enantiomers is close to 1 and therefore a further indication of fully reversible behaviour, the FcTT enantiomers are not, with slightly higher cathodic currents.[22,23]

This is most likely due to the increased error associated with the increased currents observed for the FcTT enantiomers and difficulty extrapolating an accurate baseline for cathodic peak (see Figure 3.18). An alternative explanation is the presence of the thymine groups. As discussed in section 3.1.3.3, the electron withdrawing ability of

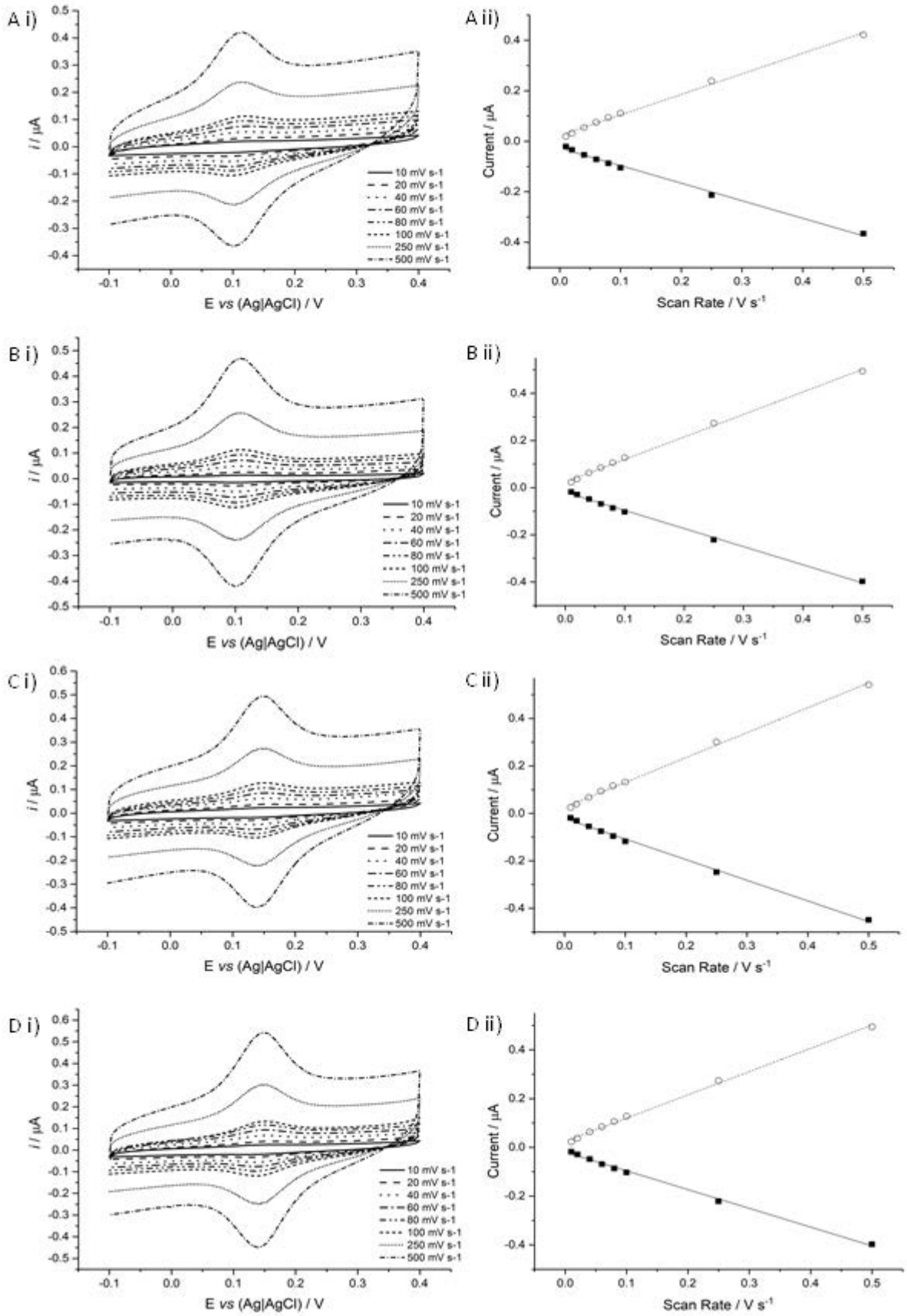

Figure 3.18 i) CVs of A: S1HH(R,R), B: S1HH(S,S), C: S1TT(R,R) and D: S1TT(S,S), CVs recorded at varying scan rates, between -100 and 400 mV in 1 M $NaClO_4$, 10 mM phosphate buffer. ii) Linear dependence of current on scan rate for A, B, C and D.

the nucleobase results in a positive shift of the oxidation potential (as exemplified by the $E_{1/2}$ values listed in Table 3.6) and this may also affect the reversibility of the system.[25]

However, it may also be due to underlying electrochemical reactions, reduced electron transfer kinetics or even slight degradation of the FcTT units, resulting in the reduction in height of the anodic peak. These explanations are unlikely to be the case since subsequent cycles do not induce any further reduction in current.

3.2.4.3 Optimisation of and Characterisation by SWV

As discussed in section 2.3.4, SWV is often favoured as a sensing technique due to the inherent removal of capacitance current and enhancement of the peak of interest, resulting in increased sensitivity compared with CV.[44–46] As such, CV was used to characterise the surface at the beginning and end of every experiment to ensure the SAMs were consistent but the sensing investigations were carried out using SWV.

Plaxco and co-workers have discussed, at length, the possibility for tuning SWV parameters to maximise the signal.[27] For these SAMs, varying the amplitude (height in mV of the square wave form) and step (increase in potential for each iteration of the wave form in mV) had little effect on the overall peak shape but changing the frequency produced data of varying quality. A range of frequencies were trialled with $S1TT_{(S,S)}$ (Figure 3.19).

As shown in Figure 3.19, a frequency of 200 Hz results in the most substantial peak which does not also possess any of the artefacts (negative peaks and peak folds) associated with SWV recorded at higher frequencies.[2,27] This observation, in combination with Osteryoung and Osteryoung's comparison of the various

frequencies, led to the selection of 200 Hz as a standard frequency. This frequency is a 'trade-off' between the more sensitive but less consistent data attained with lower frequencies and the reduced sensitivity but more reproducible SWV obtained with higher frequencies.[44]

The resultant SWV of each of the SAMs is given in Figure 3.20.

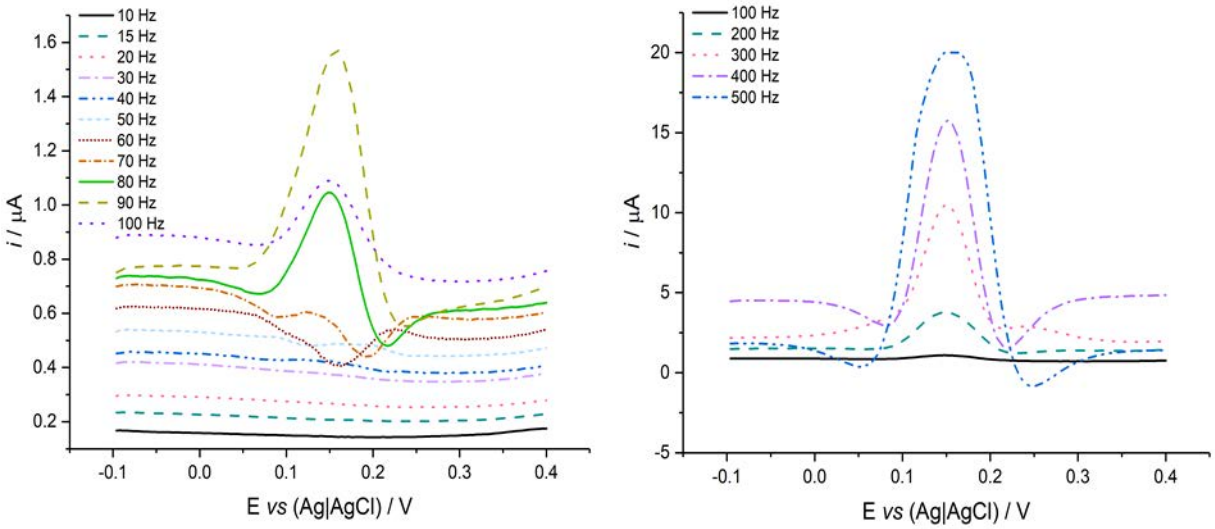

Figure 3.19 SWV of $S1TT_{(S,S)}$ recorded at various frequencies (Left: 10-100 Hz Right: 100-500 Hz). SWV were recorded at amplitude of 25 mV and step of 1 mV. SWV recorded in 1 M $NaClO_4$, 10 mM phosphate buffer

The $E_{1/2}$ values derived from Figure 3.18 and Figure 3.20 are given in Table 3.7 and show good agreement between CV and SWV. SAMs containing FcHH derivatives produced currents on oxidation as low as ~30% of the FcTT probes. A likely explanation relies on the sensitivity of SWV to the "critical frequency" of the molecule being interrogated. White and Plaxco showed that surface bound, redox-active molecules exhibit maximum signal at a frequency which is individual to that species.[47] The differences in structure between the FcHH and FcTT derivatives may result in the selected SWV parameters not being optimal for both systems. This is

supported by the fact that a similar difference in maximum current in not reflected in the respective CVs.

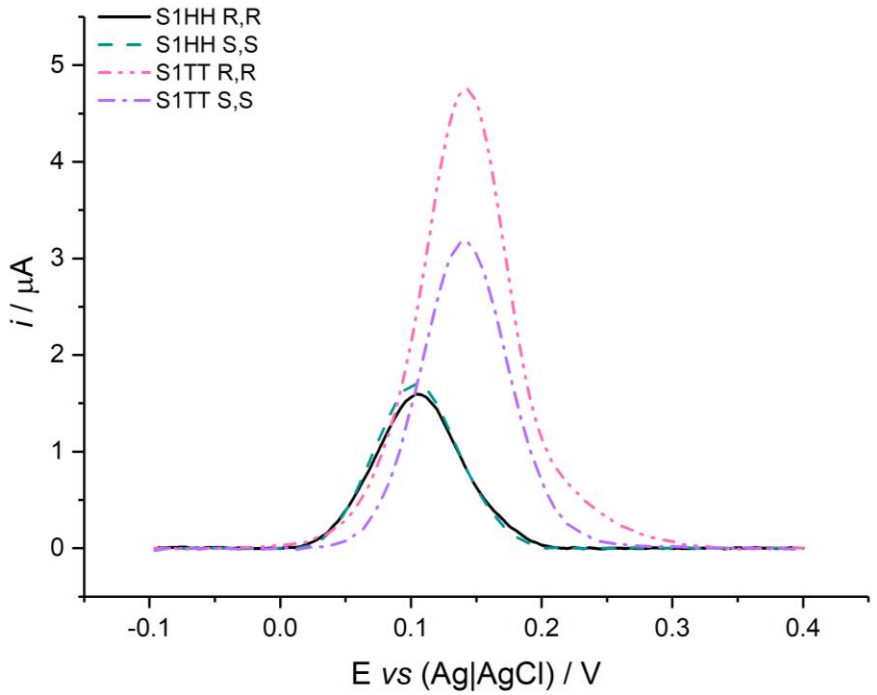

Figure 3.20 SWV of S1HH$_{(R,R) \text{ and } (S,S)}$ and S1TT$_{(R,R) \text{ and } (S,S)}$. SWV were recorded at a frequency of 200 Hz, amplitude of 25 mV and step of 1 mV in 1 M $NaClO_4$, 10 mM phosphate buffer.

Table 3.7 Comparison of the values for $E_{1/2}$ derived from CV and SWV. All values are an average of three replicate measurements.

SAM	CV $E_{1/2}$ / mV	SWV $E_{1/2}$ / mV
S1**HH**$_{(R,R)}$	108 (± 0.2)	111 (± 1.7)
S1**HH**$_{(S,S)}$	104 (± 1.0)	110 (± 2.0)
S1**TT**$_{(R,R)}$	144 (± 0.9)	144 (± 3.3)
S1**TT**$_{(S,S)}$	144 (± 0.5)	146 (± 3.4)

There is also a ~30% decrease in the current of S1FcTT$_{(S,S)}$ compared with S1FcTT$_{(R,R)}$ which was consistent with the surface distribution measured by the XPS data for these probes. The low distribution of probes containing the *(S,S)* enantiomer

compared with the *(R,R)* enantiomer (as evidenced in data acquired from both of these techniques) would imply there are fewer redox sites present in the SAMs to undergo electron transfer, thus resulting in lower current. However, as for the FcHH derivatives, the differences in structure between the *(S,S)* and *(R,R)* derivatives may result in the SWV parameters' corresponding more closely to the critical frequency of the *(R,R)* enantiomer, causing an enhanced signal.

Since one possible explanation for the XPS and SWV data trends was a lesser degree of degradation of the FcTT compared with the FcHH systems (as well as for $FcTT_{(S,S)}$ *vs* $FcTT_{(R,R)}$) it was decided to investigate the electrochemical stability of all four systems as a priority.

3.2.5 Stability

The instability of ferrocene (Fc) in its oxidised form (the ferrocenium ion) towards nucleophilic attack is well documented.[3,4,6,48] Whilst the mechanisms of degradation are discussed in more detail, in reference to improving redox tags based on Fc, in section 5.1.2.1, it was considered prudent to consider the stability of the FcNA at this point to evaluate the efficacy of it as a potential commercial device.

Following on from work comparing the stabilities of methylene blue (MB) and Fc redox tags, published by Plaxco and co-workers (and discussed in more detail in section 5.1.2),[2] the stabilities of the SAMs were assessed for:

- Long term stability
    - A CV and SWV were recorded once a day for seven (for $S1TT_{(S,S)}$ only due to constraints on material) or eight days and the percentage change in current monitored.

- Susceptibility to mechanical degradation
    - DNA SAMs were interrogated in their single stranded forms, when duplexed and when returned to single stranded after being soaked in urea to remove the target and washed. The loss of the redox active species due to the physical aspects of SAM reuse (i.e. washing, moving between storage vessels etc.) was monitored using this method.
- Susceptibility to degradation using electrochemical methods
    - SAMs were interrogated by SWV one hundred and fifty times, consecutively, and the percentage change in current monitored.

3.2.5.1 Long Term Stability

The stability of the SAMs immobilised on gold electrodes to long term storage was assessed by storing them in 1 M $NaClO_4$, 10 mM phosphate buffer exposed to air and at room temperature for a period of eight days (seven for $S1TT_{(S,S)}$. The sensors were interrogated once a day and the data compared. The acquired data for the long term stability studies are shown in Figure 3.21.

Plaxco and White showed that exposed Fc tags attached to the 3' end of DNA lost ~90% signal due to current over 7.5 days.[2] All of the systems evaluated above are an improvement on this previous observation, as shown by the data in Table 3.8. The error with these systems is high, a problem that has been previously associated with ferrocene-based electrochemical systems, though no explanation for why this is the case has been given.[2]

FcHH derivatives appear to degrade faster, losing ~50% in current signal, compared with ~30% loss for the FcTT derivatives; the chirality of the species appears to make

Table 3.8 The final current loss after 7 days for each SAM from SWV. Each is the average of three repeats. The error is calculated as the standard deviation of these three replicate measurements.

SAM	% Loss in Current after 7 days
S1**HH**$_{(R,R)}$	55 (± 17.2)
S1**HH**$_{(S,S)}$	47 (± 6.9)
S1**TT**$_{(R,R)}$	32 (± 34.2)
S1**TT**$_{(S,S)}$	35 (± 22.0)

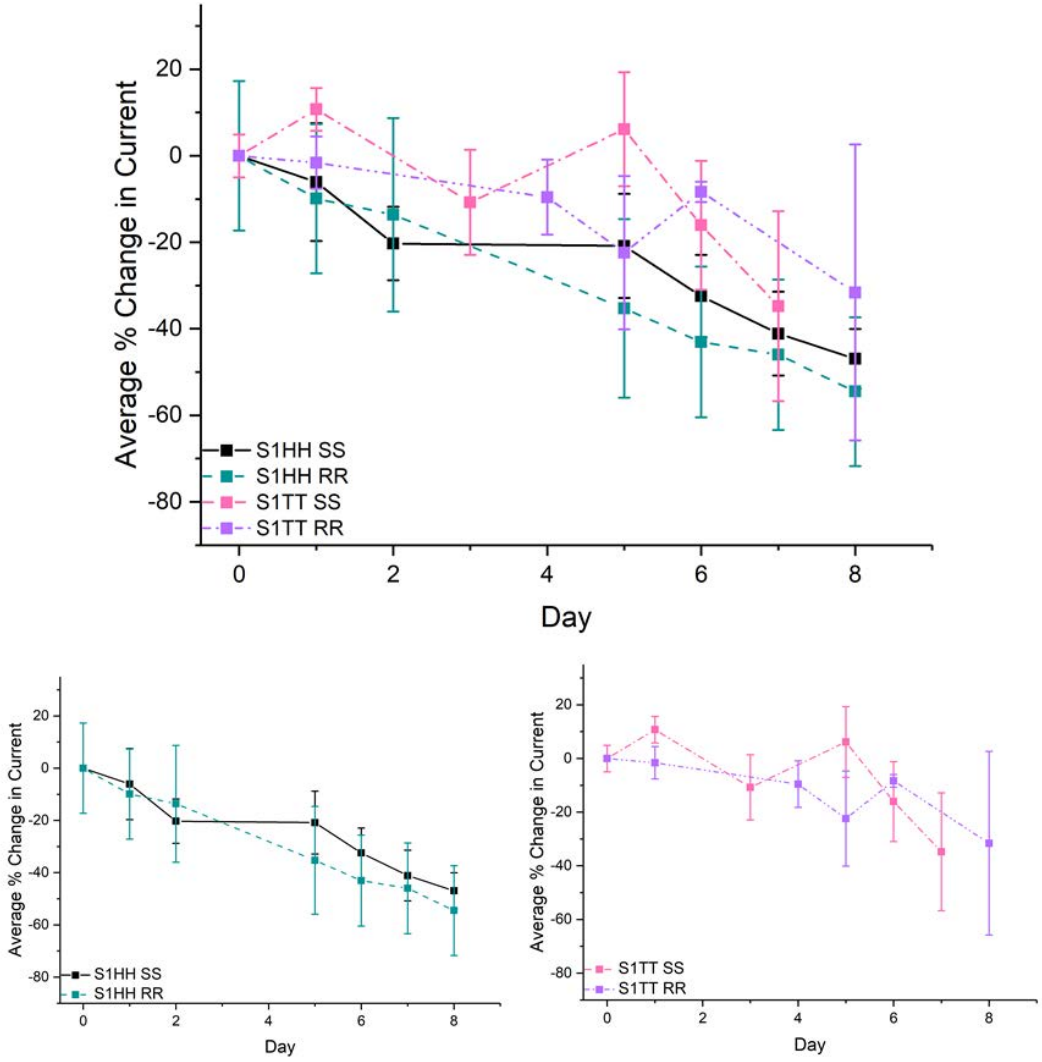

Figure 3.21 Top: Percentage loss in current as measured from the peak maxima of the SWV for S1HH(S,S) and (R,R) and S1TT(S,S) and (R,R) over 8 days (7 for S1TT SS) calculated from a minimum of 3 experiments. Data are split into S1HH$_{(S,S)}$ and $_{(R,R)}$ only (bottom left) and S1TT$_{(S,S)}$ and $_{(R,R)}$ only(bottom right) for ease of viewing. SWV measured at a frequency of 200 Hz, amplitude of 25 mV and a step of 1 mV in 1 M NaCl, 10 mM phosphate buffer.

little difference. The signal changes for the FcTT units are likely to be due to the generalised loss of thiols from the surface since the MB electrochemical redox tag is reported to show 35% signal loss over the same period (which was attributed almost solely to thiol loss).[2,49,50] The additional losses in signal shown by the FcHH units are probably due to the slightly enhanced degradation of the ferrocene units themselves.

It has been suggested that the improvement on stability compared to exposed, 5' tagged Fc unit, is due to the protection of the redox active centre by the negatively charged DNA backbone and the four appended groups, which increase steric hindrance and block any potential groups capable of nucleophilic attack (OH^-, halides etc.).[3,4,6,48] This may also explain why the stability decreases with the FcHH groups since these do not have the nucleobases attached, thus resulting in a less sterically hindered setting.

Interestingly, the error with the FcTT based SAMs is much higher than that of the FcHH based SAMs, despite the average level of degradation being lower.

3.2.5.2 Stability towards Mechanical Degradation

The stability of the SAMs to mechanical degradation was assessed by interrogating at each stage of the duplexation and regeneration process as described above in section 3.2.5. The sensors were interrogated at the initial single stranded stage and then after soaking in DNA target (S2AA for every experiment) for 20 min (hybridisation) and 8 M urea for 10 min (regenerating the single stranded probe) before repeating the hybridisation.[51] One cycle was assigned as a combination of one interrogation of the single stranded probe SAM and one of the duplexed SAM.

The acquired data for the mechanical stability studies, showing the current loss of the single stranded probe after each cycle, is shown in Figure 3.22.

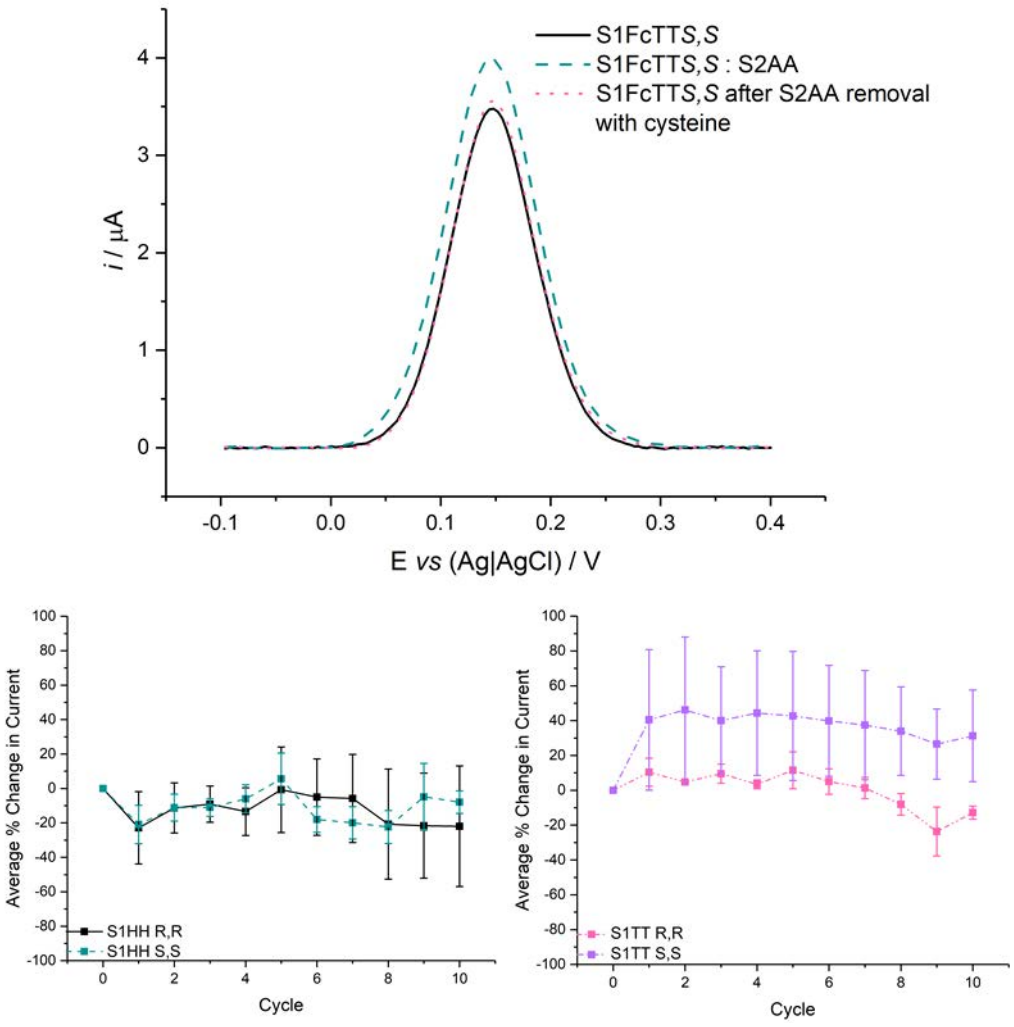

Figure 3.22 Top: Example of the SWV resulting from the multiuse cycles with single stranded $S1FcTT_{(S,S)}$, $S1FcTT_{(S,S)}$:S2AA and single stranded $S1FcTT_{(S,S)}$ after removal of the S2AA target by soaking the SAM in 10 µM cysteine for 20 min. Target was added by soaking the single stranded SAMs in 100 nM target for 10 min. Bottom: Percentage loss in current as measured from the peak maxima of the SWV for $S1HH_{(S,S) \text{ and } (R,R)}$ and $S1TT_{(S,S) \text{ and } (R,R)}$ over 10 cycles, calculated from a minimum of 3 experiments. The data are split into $S1HH_{(S,S) \text{ and } (R,R)}$ only (bottom left) and $S1TT_{(S,S) \text{ and } (R,R)}$ only (bottom right) for ease of viewing. SWV measured at a frequency of 200 Hz, amplitude of 25 mV and a step of 1 mV in 1 M NaCl, 10 mM phosphate buffer.

All the FcNA systems are an improvement on 5' attached Fc redox probes, which exhibit overall losses in current signal of 50% under these conditions, and are not

dissimilar from the losses in current displayed with MB (10% loss in current signal over 15 cycles). The overall losses in current signal are given in Table 3.9.[2]

Table 3.9 The final current loss after 10 cycles for each SAM. Each is the average of three replicate measurements.

SAM	% Loss in Current after 10 cycles
S1**HH**$_{(R,R)}$	22 (± 35.1)
S1**HH**$_{(S,S)}$	8 (± 6.6)
S1**TT**$_{(R,R)}$	12 (± 3.7)
S1**TT**$_{(S,S)}$	-31 (± 26.3)

It is clear from the graphs in Figure 3.22 and final loss of current given in Table 3.9, that there is large variation and error in the data obtained for S1TT$_{(S,S)}$ and S1HH$_{(R,R)}$. The currents obtained resulted in an increase in average current for S1TT$_{(S,S)}$ and an accompanying average error of 26% across all the cycles. For S1HH$_{(R,R)}$ the average error was 35% across every cycle. Clearly, these values represent systems which cannot provide consistent data on reuse.

However, SAMs formed from S1TT$_{(R,R)}$ and S1HH$_{(S,S)}$ displayed a higher level of consistency across each measurement, with average errors across the 10 cycles of 6 and 10%, respectively, suggesting the rigours of duplexing, denaturing and washing the SAMs are not the cause of the degradation. The final percentage losses of current of S1TT$_{(R,R)}$ and S1HH$_{(S,S)}$ are also very similar to the 10% shown by MB in the literature.[2] It is not easy to explain the difference between these FcNA-based SAMs and the less consistent systems (S1HH$_{(R,R)}$ and S1TT$_{(S,S)}$. However, the molecular modelling showed that both S1TT$_{(R,R)}$ and S1HH$_{(S,S)}$ (Figure 3.9 and section 3.1.4.1.1 respectively) orient themselves within the DNA duplex in a manner

which reduces distortion. $S1TT_{(R,R)}$ aligns closely with the natural helix shape, allowing for hydrogen bonding, and $S1HH_{(S,S)}$ is buried within the duplex structure, allowing for base stacking interactions. The enhanced rigidity associated with these orientations when duplexed, may reduce the degradation due to nucleophilic ions as well as resulting in single stranded DNA of similar structure on denaturation. Further repetition of these measurements could be carried out in order to ascertain whether this is a true phenomenon.[15]

3.2.5.3 Stability towards Electrochemical Interrogation

The stability of the SAMs to electrochemical interrogation was assessed by subjecting the SAMs, with the probes in single stranded form, to 150 consecutive SWV at 200 Hz and in 1 M $NaClO_4$, 10 mM phosphate buffer. The acquired data for the successive electrochemical interrogation studies, showing the current loss for each scan, is shown in Figure 3.23.

Every FcNA-DNA conjugate probe tested showed a remarkable improvement on the stability of 5' tagged Fc probes, which has previously been shown to lose 50% current signal after 100 SWV scans.[2] They were also all comparable with the degradation shown with MB in the literature (2% over 100 scans) with very little error in each measurement. The final % loss of current after 150 scans is given

Table *3.10*. These systems appear to be highly stable to successive oxidation and reduction cycles.[2]

It should be noted that, although the error values are all less than 5%, the error for the FcHH systems are marginally higher than those for the FcTT systems. This may be due to the increased flexibility afforded the FcHH units since they do not have the opportunity to stack with neighbouring bases. This could increase the range of orientations a single stranded probe could adopt and, consequently, slightly broaden the range of oxidation potentials at which the electron transfer occurs.

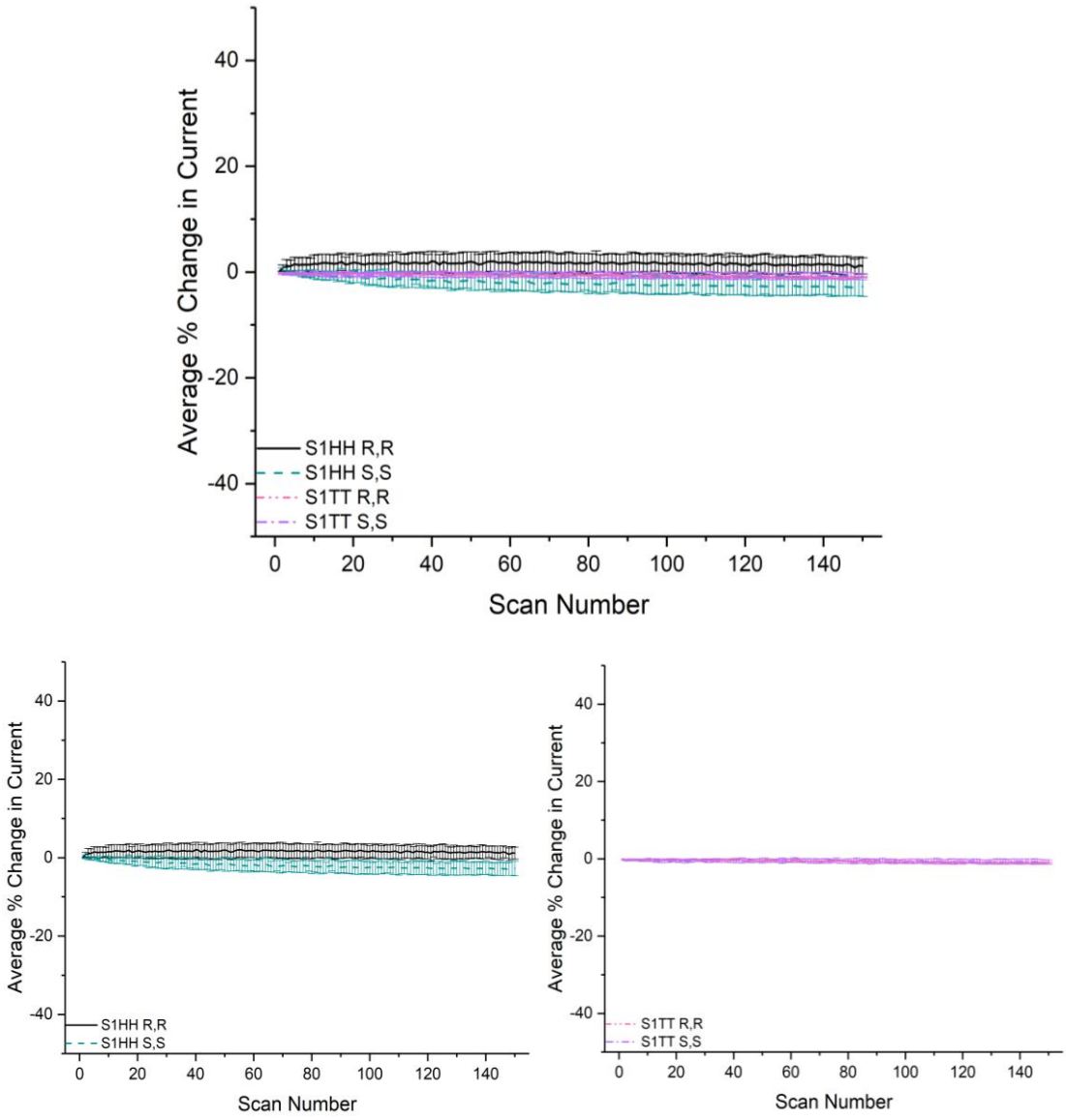

Figure 3.23 Top: Percentage loss in current as measured from the peak maxima of the SWV for $S1HH_{(S,S) \text{ and } (R,R)}$ and $S1TT_{(S,S) \text{ and } (R,R)}$ over 150 consecutive SWV scans, calculated from a minimum of 3 experiments. Data are split into $S1HH_{(S,S) \text{ and } (R,R)}$ only (bottom left) and $S1TT_{(S,S) \text{ and } (R,R)}$ only (bottom right) for ease of viewing. SWV measured at a frequency of 200 Hz, amplitude of 25 mV and a step of 1 mV in 1 M NaCl, 10 mM phosphate buffer.

Table 3.10 % Loss in Current after 150 SWV scans. Measurements are given as an average of at least 3 replicate measurements.

SAM	% Loss in Current after 150 scans
S1**HH**$_{(R,R)}$	-1.2 (± 1.5)
S1**HH**$_{(S,S)}$	2.7 (± 1.8)
S1**TT**$_{(R,R)}$	1.0 (± 0.2)
S1**TT**$_{(S,S)}$	0.9 (± 0.6)

3.2.5.4 Stability Conclusions

Overall, all the surface-bound FcNA:DNA conjugated systems investigated here are a vast improvement on 5' tagged Fc DNA probes investigated by Plaxco and co-workers.[2] All the systems are stable to successive electrochemical interrogation and S1FcHH$_{(S,S)}$ and S1TT$_{(R,R)}$ in particular show high stability towards mechanical degradation with low associated error. This suggests that it may be possible to develop a reusable sensor with these systems, saving both time and expense.[2]

The longevity of these systems is also an improvement on the previous 5' redox tags, with the FcTT enantiomers showing the greatest resistance to degradation.[2] It is possible to attribute signal loss from these systems to the generalised loss of thiols from the surface rather than of the FcTT units themselves.[2]

Whilst the FcHH based probes appear to degrade slightly more readily than the FcTT probes over time, it could be argued that S1FcHH$_{(S,S)}$ is the most promising candidate for a reusable sensor in terms of stability. It displays consistently low error and stability towards both consecutive SWV scans and the physical damage caused by multiple uses and although S1FcHH$_{(S,S)}$ is not as stable to long term storage as either of the FcTT enantiomers, it is still shows 8% less current loss than the FcHH$_{(R,R)}$ enantiomer and does not possess the high error associated with the FcTT units.

3.2.6 DNA Sensing

The improvement in stability afforded by all the FcNA systems led to an assessment of the DNA sensing capability of all the FcNA-DNA conjugate SAMs. This was done by exposing the SAMs to 100 nM target DNA (S2AA, GG, CC, TT, TA or a random strand) for 20 min before washing away excess target with a stream of Millipore water to prevent its adsorbing to the SAM surface. Non-specific adsorption of the target can affect both the conformation of the duplexes and the ease with which they form.[52]

3.2.6.1 CV vs SWV

Initially, CVs of the S1TT$_{(S,S)}$ were recorded when the probes were single stranded and when the probes were hybridised with S2AA. These were then compared.

Since previous solution based electrochemical experiments had shown both a decrease in observed current and a negative shift in $E_{1/2}$ in the CVs, it was of interest to discover whether there would also be an observable difference in the CVs for the surface bound systems. However, as shown by the example overlay in Figure 3.24 here was no significant variation between the two CVs.

This can be explained by considering the differing behaviour of surface-bound species compared with solution-based, redox-active molecules. The system is no longer heavily reliant on diffusion of the electroactive species to the surface. As a result, the extra mass, and thus resistance to movement in solution, afforded by the formation of a duplex, is not a factor in the electron transfer, which takes place between the surface and an Fc unit already in proximity to the surface. Therefore, a decrease in current is not observed in CV.[22,23]

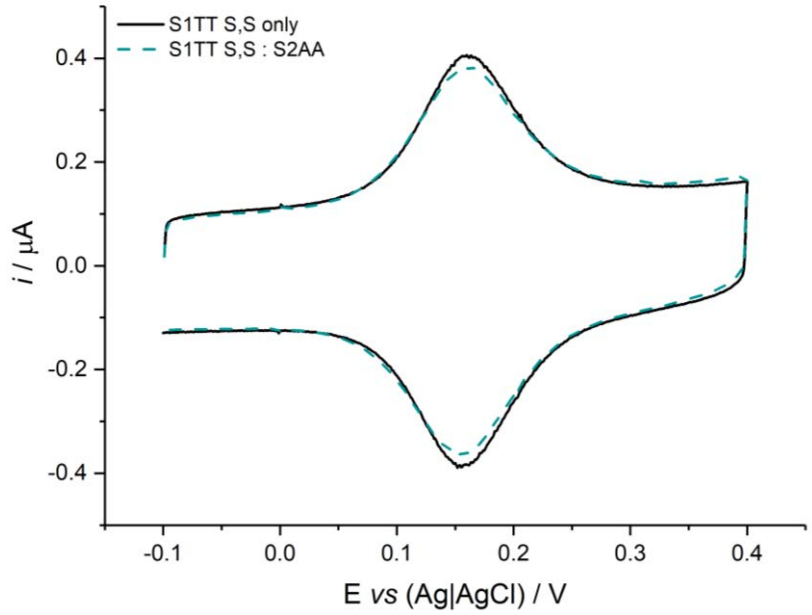

Figure 3.24 CV of S1TT$_{(S,S)}$ only and S1TT$_{(S,S)}$: S2AA for comparison of the effect of duplexation on the characteristics of the CV. 10 mM CVs recorded at 500 mV s^{-1}, between -100 and 400 mV in 1 M $NaClO_4$, 10 mM phosphate buffer. Target was added by soaking the single stranded SAMs in 100 nM target for 10 min.

Although a change in oxidation potential was expected (more so than a change in current), it was not observed. This could be due to the probes being held in a more constrained orientation on a surface (since the FcNA units are held relatively closely to the surface, with only 7 nucleobases between it and the MCH layer) rather than the flexibility it is afforded in solution. As such, the environment of the FcNA unit may change very little on duplexation, preventing the further stabilisation of the ferrocenium ion that is evidenced in solution-based studies by a decrease in the $E_{1/2}$. SWV was next trialled since, as detailed previously, it has been shown to be a more sensitive technique than CV and the 'critical frequency' effect, as highlighted by the variation in currents displayed in Figure 3.20, could also play a role in the sensing behaviour. The result for the S1TT$_{(S,S)}$ system is shown in Figure 3.25.

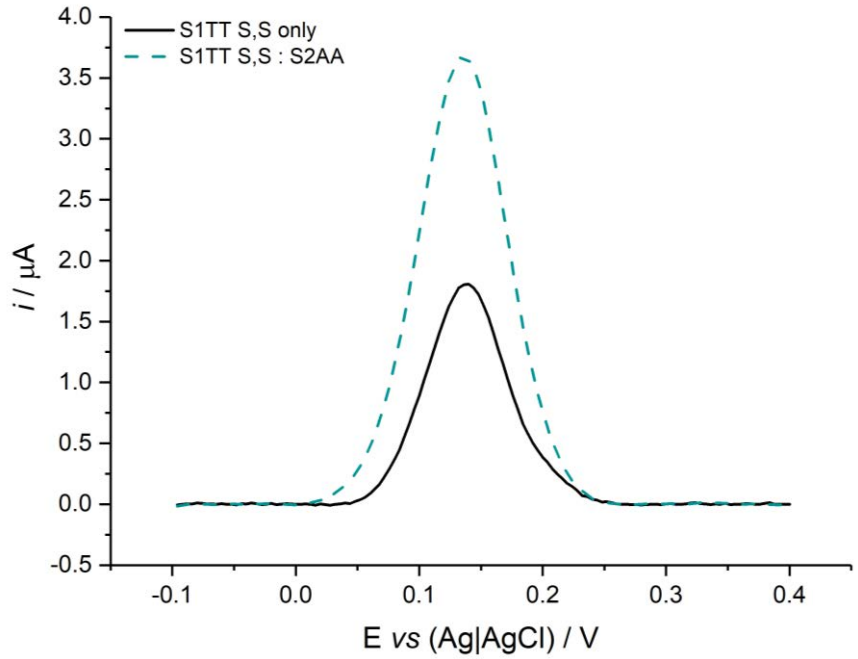

Figure 3.25 SWV of S1TT(S,S) only and S1TT(S,S) : S2AA for comparison of the effect of duplexation on the characteristics of the SWV. SWV measured at a frequency of 200 Hz, amplitude of 25 mV and a step of 1 mV in 1 M NaCl, 10 mM phosphate buffer. Target was added by soaking the single stranded SAMs in 100 nM target for 10 min.

Compared with the single stranded S1TT$_{(S,S)}$ there is a 65 ± 11% current *increase* upon binding S2AA . For the majority of ferrocene-based probes in the literature the current decreases upon duplex formation, as a consequence of the probe's rigidity increasing. This results in the redox active site being held further from the electrode surface which, in turn, slows the diffusion of the redox centre towards the surface and so reduces electron transfer rate.[2,10,12,31,37,38,47,53–55]

However, as shown by Plaxco and co-workers, tuning the square wave frequency to below ~20 Hz for strands with electrochemical tags attached to the 5' end of the DNA can reverse this effect, giving an enhanced signal on binding. The process is outlined in Figure 3.26.[27]

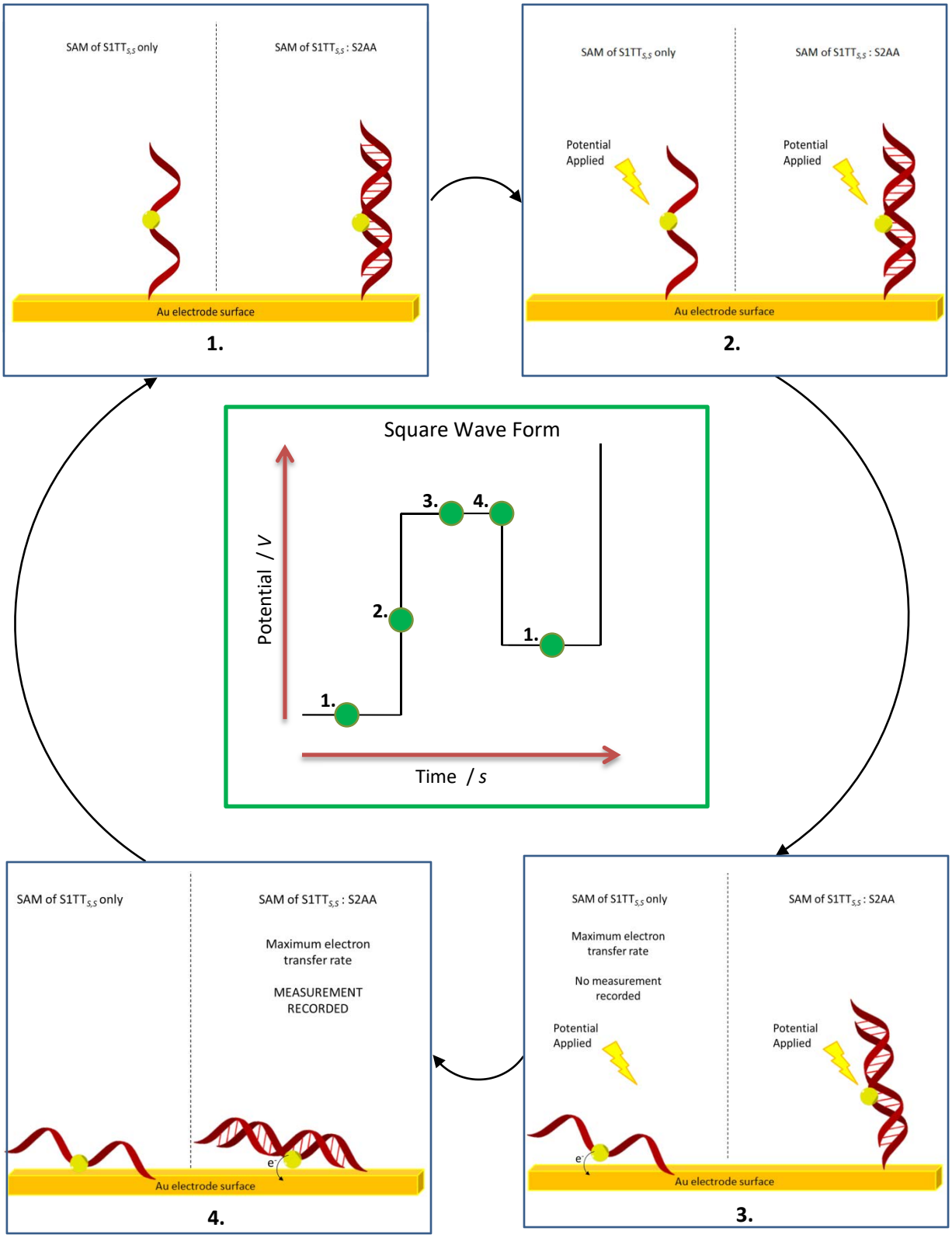

Figure 3.26 Schematic reflecting the movement of surface bound FcNA:DNA conjugates as single stranded and duplexed (1-4) and how that relates to the square wave form (centre)

The faster rate of electron transfer, due to the decreased strand rigidity associated with the single stranded DNA, means the current has largely been depleted when a measurement is recorded, owing to the waiting step in the square wave form (steps 3 and 4 in Figure 3.26). In contrast, the slower rate produced by the less mobile duplex due to the reduction in movement of the redox-active site towards the surface means the electron transfer is at its peak at this point.

It has been suggested that, since the FcNA unit is placed centrally in the S1 strand, it is very much closer to the electrode surface than a 5' tagged Fc species, allowing the signal enhancement to occur at higher frequencies. Both duplexed and single stranded species are moving towards the surface readily but the single stranded species remains more mobile.

The ability of SWV to distinguish between single stranded and duplexed probe FcNA-DNA conjugates allowed for further study into whether it could also be used to distinguish base mismatches.

3.2.6.2 (R,R) vs (S,S)

The ability of each system to distinguish between a target containing two base mismatches and, in one case, one base mismatch, was assessed for each system and the effect of the stereochemistry of the FcNA units and the base pairing ability compared. The results for the FcHH and FcTT enantiomers are shown in Figure 3.28and Figure 3.29, respectively.

It is clear for both FcTT and FcHH systems that the inclusion of *(S,S)* chirality produces a greater percentage increase in current compared with the *(R,R)* enantiomers. This is particularly prominent for S1FcTT$_{(R,R)}$, where any percentage

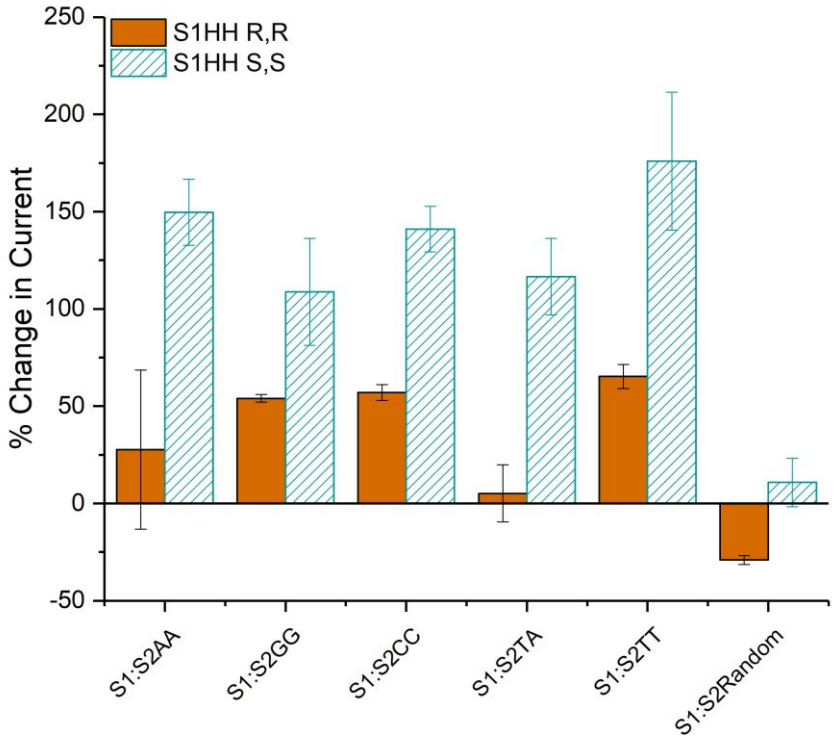

Figure 3.28 Percentage change in current on duplexation of both S1HH enantiomers with various targets. The results are calculated from a minimum of three replicate measurements of SWV measured at a frequency of 200 Hz, amplitude of 25 mV and a step of 1 mV in 1 M NaCl, 10 mM phosphate buffer. Target was added by soaking the single stranded SAMs in 100 nM target for 10 min.

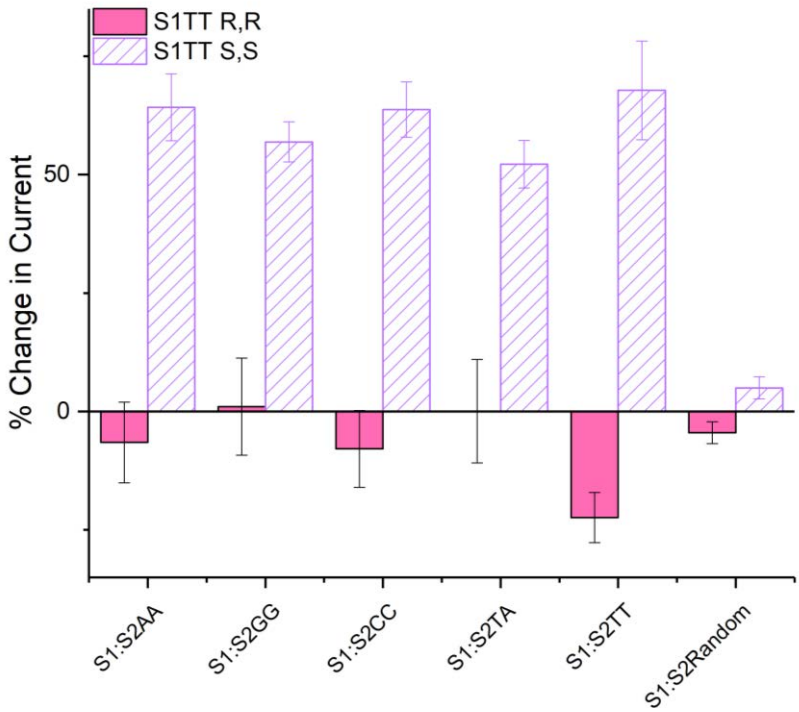

Figure 3.29 Percentage change in current on duplexation of both S1TT enantiomers with various targets. The results are calculated from a minimum of three replicate measurements of SWV measured at a frequency of 200 Hz, amplitude of 25 mV and a step of 1 mV in 1 M NaCl, 10 mM phosphate buffer. Target was added by soaking the single stranded SAMs in 100 nM target for 10 min.

change (interestingly is it the only system where the current change is almost consistently negative) is also accompanied by a large variation in error.

Since in the previous molecular modelling studies, described in section 3.1.4, it was suggested that the FcNA units with *(R,R)* stereochemistry align more closely to the structure of the natural DNA helix backbone, it could be expected that the orientation of units with *(R,R)* stereochemistry is predisposed to duplex formation. Therefore, the environment of the FcNA unit varies very little on hybridisation, which is reflected in very little variation in electron transfer rate compared with for the *S,*S enantiomers and less percentage change in current as a result.

The increased alignment with the natural DNA backbone can also explain why S1FcTT$_{(R,R)}$ has the lowest percentage change out of all four systems. For this stereochemistry, the FcTT moiety is capable of base stacking even in a single stranded DNA sequence, predisposing it further to duplexation.

The data shown above (Figure 3.28 and Figure 3.29) indicated that S1TT$_{(R,R)}$ and S1HH$_{(R,R)}$ would not be suitable as DNA sensors because the percentage change in current was too low and error was too high, making conclusive DNA sensing impossible. As a result, further experiments were carried out with the *(S,S)* enantiomers only.

3.2.6.3 FcHH vs FcTT

S1HH$_{(S,S)}$ and S1TT$_{(S,S)}$ were compared to determine the effect of base pairing on the DNA sensing ability of the FcNA units on a surface. The comparison is shown in Figure 3.30. As expected, there is no variation in current on exposure of either SAM

to a random sequence DNA target, suggesting there is no binding and ensuring that the increase in current arises from duplexation and not non-specific binding.

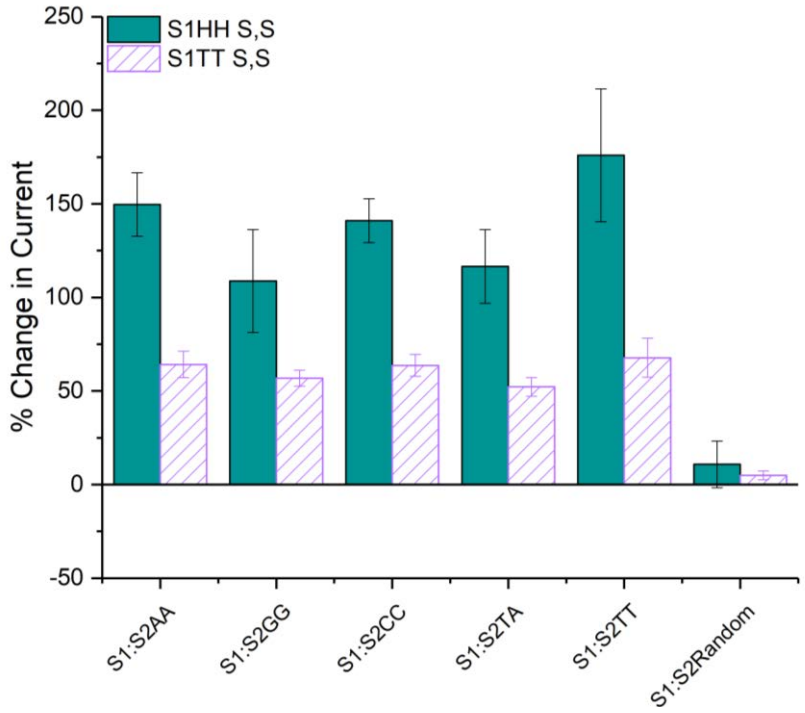

Figure 3.30 Percentage change in current on duplexation of S1TT$_{(S,S)}$ and S1HH$_{(S,S)}$ with various targets. The results are calculated from a minimum of three replicate measurements of SWV measured at a frequency of 200 Hz, amplitude of 25 mV and a step of 1 mV in 1 M NaCl, 10 mM phosphate buffer. Target was added by soaking the single stranded SAMs in 100 nM target for 10 min.

S1HH$_{(S,S)}$ produces the highest percentage increase in current on duplexation, more than double the percentage for the S1TT$_{(S,S)}$ in nearly all cases.

There are two explanations for this observation. Firstly, as described previously, the presence of the nucleobases allows for base stacking within the DNA strands thus minimising the change in the environment of the FcTT unit on duplexation and having a reduced effect on the ease of electron transfer.

However, these data were determined using the percentage change in current and the raw SWV showed generally lower currents for S1HH moieties. The increased

percentage change in current may therefore be an artefact of the data treatment. To confirm this is not the case, the raw currents of the single stranded SAMS were normalised to 1 to give comparable data between the systems. These data are shown in Table 3.11.

Table 3.11 Normalised Currents for S1TT$_{(S,S)}$ and S1HH$_{(S,S)}$ when duplexed with various targets, where S1XX only = 1. Data reported are an average of at least three replicate measurements.

	Normalised Current (Where S1XX = 1)					
SAM	**S2AA**	**S2GG**	**S2CC**	**S2TT**	**S2TA**	**S2Random**
S1**TT$_{(S,S)}$**	1.52	1.45	1.51	1.41	1.55	0.98
S1**HH$_{(S,S)}$**	1.80	2.07	2.39	2.15	2.73	1.10

As shown in Table 3.11, the greater increase in current for S1HH$_{(S,S)}$ compared with S1TT$_{(S,S)}$, though not as marked in the normalised data, is still present, indicating that S1HH$_{S,S}$ does indeed, give the more marked response to duplex formation

For the S1TT$_{(S,S)}$ system there is no significant variation in the current increase upon changing the sequence of the target strand. For the S1HH$_{(S,S)}$ system there are less even changes although the large errors associated with the data renders the system, in its current state, unable to differentiate between different bases. However, when the pattern of current increases is compared for both S1HH$_{(S,S)}$ and S1TT$_{(S,S)}$ across all the targets there appears to be similarities (i.e. S1XX:S2TT gives the highest percentage increase in current, S1XX:S2TA gives the lowest percentage change in both cases). To be sure that this is a real phenomenon, an in-depth, methodical assessment of every aspect of SAM formation (DNA concentration and exposure time, MCH concentration and exposure time, temperature etc.) would have to be carried out to optimise the SAMs and reduce the errors in the data.

3.2.6.4 Limit of Detection (LOD)

All experiments carried out so far were carried out using a target concentration of 100 nM. Preliminary data suggest that a percentage change in current is still discernible with a target concentration of 10 nM. Further study is required to determine whether detection of the target at sub-nanomolar levels is possible.

3.3 Conclusions

In a continuation of previous solution-based investigations and following optimisation of the FcNA structures using thermal melting points, mixed monolayers of MCH and $FcHH_{(S,S)}$, $FcHH_{(R,R)}$, $FcTT_{(S,S)}$ and $FcTT_{(R,R)}$ were explored. Each SAM was assessed for longevity, resistance to mechanical degradation, sustained electrochemical interrogations and its ability to detect DNA targets. In addition to this, each SAM underwent surface characterisation with XPS and ellipsometry.

The surface characterisation will need to be repeated and STM carried out to confirm the results. Ellipsometry suggested that all the systems were diffusely packed, in line with previous literature.[37,56] However, XPS data suggested that the distribution of S0 and S1HH based probes was more compact in comparison with the S1TT probes and so an assessment of electrochemical stability was conducted.

All systems showed improvements on the 5' tagged Fc reporters previously described by Plaxco and co-workers.[2] For 150 consecutive electrochemical scans, all SAMs showed near-zero changes in current and low error. S1TT systems showed ~20% improvement on S1HH in terms of longevity over 8 days with S1TT systems showing only a ~30% reduction in signal overall. However, the error associated with the FcTT systems was much greater.

Conversely, resistance to mechanical degradation seemed to depend more on the orientation of the FcNA within the duplex environment. $FcTT_{(R,R)}$ and $FcHH_{(S,S)}$-based SAMs showed levels of mechanical degradation consistent with that previously shown for MB and had lower error across the measurements.[2]

Following these experiments, it was concluded that $S1FcHH_{(S,S)}$ represented, marginally, the most promising candidate for DNA sensing. Whilst the displayed longevity was not as great as for the FcTT units, $FcHH_{(S,S)}$ performed consistently well in terms of low error, consecutive electrochemical interrogations and reduced damage through reuse compared with the other variations.

The sensing ability of the $FcHH_{(S,S)}$ monomer was further corroborated during the assessment of the different systems abilities to detect target DNA. While significant differences were not obtained in CV, the additional sensitivity afforded by SWV allowed for DNA target detection and the 'frequency effect'. Both FcNA units containing the *(R,R)* chirality produced SAMs which resulted in percentage changes in current on binding that were high in error and less applicable, since some targets produced zero change in current.

On the other hand, mixed monolayers containing *(S,S)*-based FcNA units consistently produced increases in current on binding. This is a very unusual occurrence and a feature of the ability to tune the frequency of SWV. This is an improvement on most electrochemical systems, which rely on a reduction in current and run the risk of a 'false positive' result.[2,10,12,31,37,38,47,53–55]

$S1HH_{(S,S)}$ showed consistently higher percentage increases on binding for all the targets. This was subsequently shown to be a real phenomenon rather than an artefact of the way in which the data were analysed.

Interestingly, a pattern began to emerge for both units containing the *(S,S)* chirality on binding the different targets. However, due to the error in the systems, it was not possible to determine whether this was a true result or an artefact. Further reduction of the error in the systems, through optimisation of SAM formation, may enable identification of the specific mismatches in a target if this pattern was confirmed.

3.4 Further Work

To further the investigations of the FcNA species as a potential commercial SNP sensing device, the following work is suggested:

- STM measurements to explain the differences between the different species and to visualise the surface distribution of the probes.
- Determine the LOD
- Optimise every aspect of SAM formation and SWV frequency to attempt to improve the LOD.
- After improvement of the LOD, attempts should be made to detect DNA targets that represent true SNPs and not double base mismatches.
- Carry out a trial application of the best FcNA-DNA conjugate system on a disposable electrochemical chip to begin to assess the efficacy of the FcNA units as potential commercial/clinical sensing devices.

3.5 References

(1) Duprey, J.-L. H. A.; Tucker, J. H. R. *Chem. Lett.* **2014**, *43*, 157–163.

(2) Kang, D.; Zuo, X.; Yang, R.; Xia, F.; Plaxco, K. W.; White, R. J. *Anal. Chem.* **2009**, *81*, 9109–9113.

(3) Hurvois, J. P.; Moinet, C. *J. Organomet. Chem.* **2005**, *690*, 1829–1839.

(4) Holeček, J.; HandlíŖ, K.; Klikorka, J.; Bang, N. D. *Collect. Czechoslov. Chem. Commun.* **1979**, *44*, 1379–1387.

(5) Breuer, R.; Schmittel, M. *Organometallics* **2012**, *31*, 1870–1878.

(6) Abbott, N. L.; Whitesides, G. M. *Langmuir* **1994**, *10*, 1493–1497.

(7) Pike, A. R.; Ryder, L. C.; Horrocks, B. R.; Clegg, W.; Elsegood, M. R.; Connolly, B. A.; Houlton, A. *Chem. Eur. J.* **2002**, *8*, 2891–2899.

(8) Yu, C. J.; Wang, H.; Wan, Y.; Yowanto, H.; Kim, J. C.; Donilon, L. H.; Tao, C.; Strong, M.; Chong, Y. *J. Org. Chem.* **2001**, *66*, 2937–2942.

(9) V. Nguyen, H.; Zhao, Z.; Sallustrau, A.; Horswell, S. L.; Male, L.; Mulas, A.; Tucker, J. H. R. *Chem. Commun.* **2012**, *48*, 12165–12167.

(10) Brisset, H.; Navarro, A.-E.; Spinelli, N.; Chaix, C.; Mandrand, B. *Biotechnol. J.* **2006**, *1*, 95–98.

(11) Navarro, A.-E.; Spinelli, N.; Moustrou, C.; Chaix, C.; Mandrand, B.; Brisset, H. *Nucleic acids Res.* **2004**, *32*, 5310–5319.

(12) Navarro, A.-E.; Spinelli, N.; Chaix, C.; Moustrou, C.; Mandrand, B.; Brisset, H. *Bioorganic & Med. Chem. Lett.* **2004**, *14*, 2439–2441.

(13) Chatelain, G.; Brisset, H.; Chaix, C. *New J. Chem.* **2009**, *33*, 1139–1147.

(14) Nguyen, H. V.; Sallustrau, A.; Male, L.; Thornton, P. J.; Tucker, J. H. R. *Organometallics* **2011**, *30*, 5284–5290.

(15) Carr-Smith, J. Modified nucleic acids: structural studies and applications in biosensing, University of Birmingham, 2015.

(16) Moss, G. P. *Pure Appl. Chem.* **1996**, *68*.

(17) Integrated DNA Technologies Inc. OligoAnalyzer 3.1 https://www.eu.idtdna.com/calc/analyzer (accessed 2017).

(18) Ramaley, L.; Krause Jr, M. S. *Anal. Chem.* **1969**, *41*, 1362–1365.

(19) MACQUET, J.-P.; BUTOUR, J.-L. *Eur. J. Biochem.* **1978**, *83*, 375–387.

(20) Kypr, J.; Kejnovska, I.; Renciuk, D.; Vorlickova, M. *Nucleic Acids Res.* **2009**,

37, 1713–1725.

(21) Pettersen, E. F.; Goddard, T. D.; Huang, C. C.; Couch, G. S.; Greenblatt, D. M.; Meng, E. C.; Ferrin, T. E. *J. Comput. Chem.* **2004**, *25*, 1605–1612.

(22) Scholz, F. *Electroanalytical methods*; Springer, 2002.

(23) Bard, A. J.; Faulkner, L. R. *Electrochemical methods: fundamentals and applications*; Wiley New York, 1980; Vol. 2.

(24) Houlton, A.; Isaac, C. J.; Gibson, A. E.; Horrocks, B. R.; Clegg, W.; Elsegood, M. R. J. *J. Chem. Soc. Dalton Trans.* **1999**, 3229–3234.

(25) Dutta, A. K.; Sengupta, T.; Vaval, N.; Pal, S. *Int. J. Quantum Chem.* **2015**, *115*, 753–764.

(26) Xiao, Y.; Lai, R. Y.; Plaxco, K. W. *Nat. Protoc.* **2007**, *2*, 2875–2880.

(27) Dauphin-Ducharme, P.; Plaxco, K. W. *Anal. Chem.* **2016**.

(28) Stranick, S. J.; Parikh, An.; Allara, D. L.; Weiss, P. S. *J. Phys. Chem.* **1994**, *98*, 11136–11142.

(29) Wu, Z.-S.; Chen, C.-R.; Shen, G.-L.; Yu, R.-Q. *Biomaterials* **2008**, *29*, 2689–2696.

(30) Zhang, Q. D.; March, G.; Noel, V.; Piro, B.; Reisberg, S.; Tran, L. D.; Hai, L. V.; Abadia, E.; Nielsen, P. E.; Sola, C.; Pham, M. C. *Biosens. Bioelectron.* **2012**, *32*, 163–168.

(31) Ricci, F.; Zari, N.; Caprio, F.; Recine, S.; Amine, A.; Moscone, D.; Palleschi, G.; Plaxco, K. W. *Bioelectrochemistry* **2009**, *76*, 208–213.

(32) Woollam, J. H. What is Ellipsometry? https://www.jawoollam.com/resources/ellipsometry-tutorial/what-is-ellipsometry (accessed May 11, 2017).

(33) Huang, T.; Nallathamby, P. D.; Xu, X.-H. N. *J. Am. Chem. Soc.* **2008**, *130*, 17095–17105.

(34) Pakiari, A. H.; Jamshidi, Z. *J. Phys. Chem.* **2010**, *114*, 9212–9221.

(35) Andreoni, W.; Curioni, A.; Grönbeck, H. *Int. J. Quantum Chem.* **2000**, *80*, 598–608.

(36) Tompkins, H.; Irene, E. A. *Handbook of ellipsometry*; William Andrew, 2005.

(37) Anne, A.; Demaille, C. *J. Am. Chem. Soc.* **2006**, *128*, 542–557.

(38) Anne, A.; Bouchardon, A.; Moiroux, J. *J. Am. Chem. Soc.* **2003**, *125*, 1112–

1113.

(39) Heide, P. V. der. *X-ray photoelectron spectroscopy: an introduction to principles and practices*; John Wiley & Sons, 2012.

(40) X-Ray Photoelectron Spectroscopy http://www.npl.co.uk/science-technology/surface-and-nanoanalysis/surface-and-nanoanalysis-basics/introduction-to-xps-x-ray-photoelectron-spectroscopy (accessed May 16, 2017).

(41) Christ, B. V. *Elem. Nativ. Oxides* **2000**.

(42) Anne, A.; Demaille, C. *J. Am. Chem. Soc.* **2005**, *128*, 542–557.

(43) Wei, Y.; Yang, R.; Li, X.-Z.; Wang, L.; Huang, X.-J. *Anal.* **2011**, *136*, 3997.

(44) Osteryoung, J. G.; Osteryoung, R. A. *Anal. Chem.* **1985**, *57*, 101–110.

(45) Lovrić, M. In *Electroanalytical Methods*; Springer, 2010; pp. 121–145.

(46) Economou, A.; Fielden, P. R. *Anal. Chim. Acta* **1993**, *273*, 27–34.

(47) White, R. J.; Plaxco, K. W. *Anal. Chem.* **2009**, *82*, 73–76.

(48) Breuer, R.; Schmittel, M. *Organometallics* **2012**, *31*, 6642–6651.

(49) Willey, T. M.; Vance, A. L.; Van Buuren, T.; Bostedt, C.; Terminello, L. J.; Fadley, C. S. *Surf. Sci.* **2005**, *576*, 188–196.

(50) Mani, G.; Johnson, D. M.; Marton, D.; Dougherty, V. L.; Feldman, M. D.; Patel, D.; Ayon, A. A.; Agrawal, C. M. *Langmuir* **2008**, *24*, 6774–6784.

(51) Herskovits, T. T. *Biochemistry* **1963**, *2*, 335–340.

(52) Ravan, H.; Kashanian, S.; Sanadgol, N.; Badoei-Dalfard, A.; Karami, Z. *Anal. Biochem.* **2014**, *444*, 41–46.

(53) Fan, C.; Plaxco, K. W.; Heeger, A. J. *Proc. Natl. Acad. Sci.* **2003**, *100*, 9134–9137.

(54) González-Fernández, E.; Avlonitis, N.; Murray, A. F.; Mount, A. R.; Bradley, M. *Biosens. Bioelectron.* **2016**, *84*, 82–88.

(55) Hasegawa, Y.; Takada, T.; Nakamura, M.; Yamana, K. *Bioorganic & Med. Chem. Lett.* **2017**.

(56) Anne, A.; Demaille, C. *J. Am. Chem. Soc.* **2008**, *130*, 9812–9823.

Chapter 4

FcNA for Electrochemical Mercury Detection

4.1 Introduction

The ability of nucleic acids to bind various metal ions has prompted investigation into a wide range of diverse applications for metallated DNA (M-DNA). From natural phenomena, such as the catalysis of the hydrolysis of RNA and DNA by ribozymes[1] and DNAzymes[2], to attempts to improve conductance through a DNA 'wire'[3–7], to the development of nanoarchitectures[8–10], many groups have explored and utilised the incorporation of metal ions into DNA either to understand biological processes or to encourage the development of nanomachines.[11]

DNA is an ideal building block due to its biological relevance, the ease with which it can be synthesised and, as shown in Chapter 3, the variety of artificial nucleosides which can be incorporated. Much previous research has focussed on the incorporation of modified, chelating nucleosides (such as the N,N'bis salicylidene) ethylenediamine ligand used to chelate Cu^{2+}, as discussed in section 1.4)[9] in order to enhance the electronic and structural properties of DNA.[4,5,8–10,12,13] Until recently, the use of direct interactions of metal ions with unmodified nucleic acids had been limited. However, a growing need to sense metal ions for medical and environmental applications, and the recognition that some metal-base pairing can be facilitated by base mismatches, has led to a resurgence in research in this area.[2,14–16] The detection of mercury ions through thymine-thymine mismatches has been particularly prevalent and is the focus of this chapter.

4.1.1 Metals in DNA

A number of different metal ions have been shown to bind to natural DNA. Lee and co-workers termed the phrase '*M-DNA*´ after showing that some divalent metal cations could form complexes with DNA in conditions above pH 8. The inclusion of

these ions provided conductivity such that the DNA helices could act as wires.[5–7,17] The resulting systems have been shown to be usable as electrochemical sensors for single nucleotide mismatches, with detection limits as low as 10 fM.[18–21]

Titration of the metals in question, Zn^{2+}, Co^{2+} and Ni^{2+}, into target duplexed DNA, were shown, through NMR studies, to result in the loss of the T and G imino proton signals. This and subsequent modelling studies, led Lee and co-workers to suggest the binding mode given in Figure 4.1.[5,17] However, elucidation of the true nature of the metal binding has not yet been achieved. Mechanisms involving the binding of the metal to the major and minor grooves, involving no deprotonation and deprotonation, have also been suggested.[22,23]

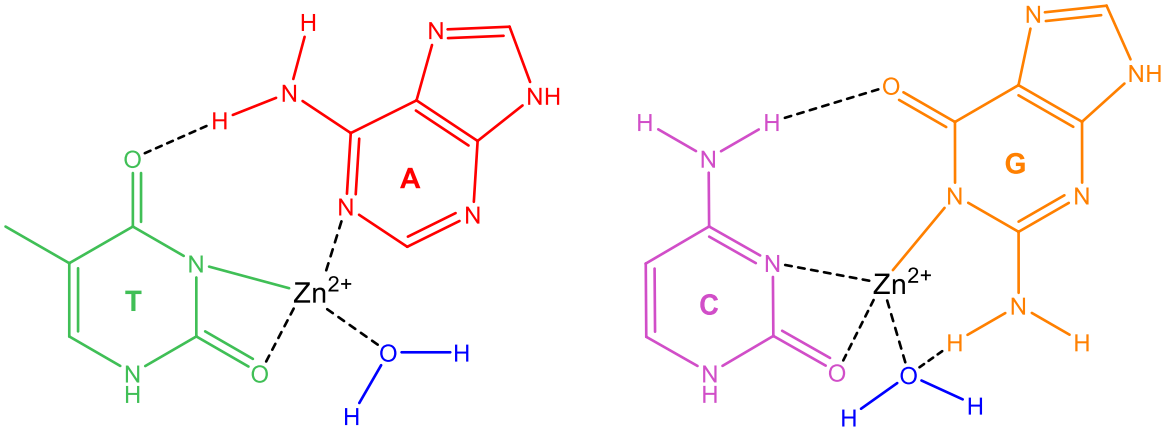

Figure 4.1 Zn^{2+} mode of binding in DNA duplexes as suggested by Lee and co-workers.[6]

Whilst the examples given above require basic conditions in order to bind DNA, Cu^{2+} is known to bind to DNA under biological conditions, causing irreparable damage through the facilitation of the formation of reactive oxygen species.[24,25] Conditions associated with high level of copper in the body include Wilson's disease, where accumulation in the brain and liver result in organ failure and neurological issues.[26]

The interaction of Cu^{2+} and nucleic acids is not well understood, although there is some evidence for site-specific intercalation and a higher specificity for Cu^{2+} in duplexed DNA compared to single-stranded DNA. This would suggest a need for geometrically controlled intercalation with the major or minor grooves, or coordination between opposite bases to be present, as is the case for Zn^{2+}.[24,27,28]

The health implications of excess Cu^{2+} display a need for the sensitive and accurate detection of these, and similar, metal ions and raise the possibility that interactions with nucleic acids could be used to detect and quantify their presence in a biological setting.

4.1.1.1 Lanthanides

More recently, lanthanides have been shown to be able to bind to 5-hydroxyuracil (U^{OH}). The formation of U^{OH} occurs naturally upon the oxidative deamination of cytosine. U^{OH} has been shown to form stable base pairs with A, G, C and T nucleobases. Its introduction into natural DNA is often the precursor to point mutations within the DNA strand, primarily through the conversion of C to U^{OH}. U^{OH} has a very similar structure to A and thus results in a T base being inserted opposite the U^{OH} rather than the required G base.[13,29,30]

The lanthanides, ytterbium, europium and gadolinium have all been shown to bind between mismatched pairs of U^{OH} in their trivalent state. The duplex stability was shown to increase when three neighbouring U^{OH} were centrally incorporated into one 15 base DNA strand within a complementary duplex. This was attributed to the lanthanide ions coordinating to neighbouring bases as well as those directly adjacent to them, in order to satisfy their coordination spheres. Subsequent NMR and CD

studies also showed that natural B-DNA structure was retained. The proposed binding mode is shown in Figure 4.2.[13]

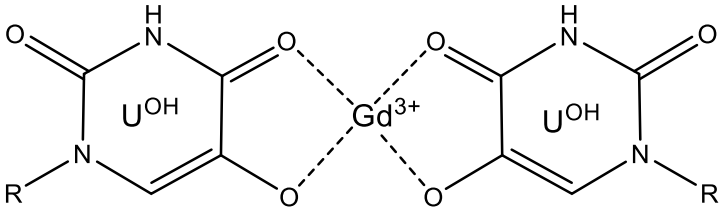

Figure 4.2 Binding mode of Lanthanide ions between U^{OH} mismatches

Since lanthanides have a wide range of applications, including catalysis, as part of luminescent compounds and as MRI contrast agents, the structural control of the positioning of the ions could have promise for the development of DNA based products with industrial applications.[31]

4.1.1.2 Silver

In 2008, Ono and co-workers unexpectedly discovered that addition of Ag^+ to DNA duplexes with a cytosine-cytosine mismatch resulted in enhanced duplex stability, in terms of varied temperature and pH. The T_m measurements showed an increase in stability of 8 ^oC on addition of Ag^+ ions and the resultant metallated DNA duplexes were more stable between pH 5 and 9. The C-C mismatch was also shown to be highly specific for Ag^+ ions.[15]

^1H NMR studies showed the formation of a new imino proton peak upon the titration of Ag^+ and ESI MS studies suggested that one cation binds per mismatched C-C pair. Currently, the binding mode is not fully understood, though ^{15}N NMR studies are

being used to try to ascertain more structural information. Ono and co-workers tentatively suggest the binding mode structure given in Figure 4.3.[15,32]

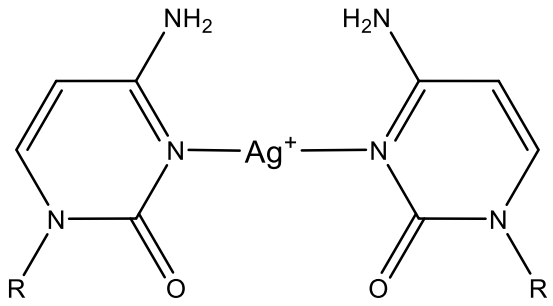

Figure 4.3 Suggested binding mode for C-Ag(I)-C[15]

Ono and co-workers went on to show that this system could be used as a Ag^+ sensor. By attaching a fluorescent group to one end of a cytosine rich single strand of DNA and a quencher group to the other, the reduction in fluorescent signal could be monitored as the metal ions were titrated into the DNA containing solution. Although this system did not prove highly specific, it was most sensitive to the addition of Ag^+, again suggesting that metal-binding DNA may be a route to sensitive metal detection.[15]

4.1.2 Mercury

One of the best known and utilised incidences of metal-nucleic acid binding pairs is thymine-mercury-thymine (T-Hg^{2+}-T). As this phenomenon is the focus of the following chapter, it will now be discussed in more detail.

4.1.2.1 Importance of Mercury Sensing

The ecological impact of heavy metal contamination within the environment cannot be underestimated. The ease with which toxic species such as mercury are

conducted through the food chain, through bioaccumulation, renders them one of the most deadly set of industrial by-products.[33–35] Mercury in particular, is a by-product of many large scale industrial processes, including the burning of fossil fuels and gold mining, and so is a common environmental pollutant.[36–39]

All forms of mercury are known to be toxic, with organic methylmercury and mercuric ions being the most potent. Both of these have been shown to bind to cysteine residues in proteins and prevent the action of enzymes. Methylmercury is particularly toxic since it is highly lipophilic and, as such, is able to cross the blood-brain barrier as well as to pass into most other organs.[39] Exposure to inorganic mercuric ions (Hg^{2+}), which cannot so easily pass through the body's barriers, results in accumulation of Hg^{2+} in the kidney and gut. This causes necrosis (the death of almost all cells in a given region) of those organs.[40]

Current methods of detection, such as ICP-MS[41,42], emission spectroscopy[43,44], nanoparticles[45,46], and fluorescent sensors[45,47,48], suffer from expensive procedures and equipment, poor sensitivity and inadequate selectivity.

Given the environmental and health impacts of mercuric ions, it is important to have a fast, sensitive and affordable method of detection.[49,50]

4.1.2.2 Thymine-Mercury-Thymine

As early as 1963, Katz theorised that Hg^{2+} ions are able to bind to thymine-thymine mismatches within a DNA duplex in a ratio of 1:2 (Hg^{2+}:T).[14] In 1952, Katz had noted that the viscosity of a solution of natural DNA molecules increased on addition of Hg^{2+} and had attributed this to a change in the size of the molecule, with Hg^{2+} binding to the negative phosphate backbone.[51] After subsequent UV studies were carried out

by Thomas[52], Katz proposed that slippage was occurring between the two DNA strands in order for T bases to align and facilitate T-Hg^{2+}-T binding.[14]

Later, Ono and co-workers confirmed that the incorporation of the Hg^{2+} ion was facilitated by the loss of the thymine imino protons, through ^{1}H NMR studies, and theorised that the Hg^{2+} is bound as shown in Figure 4.4.[53]

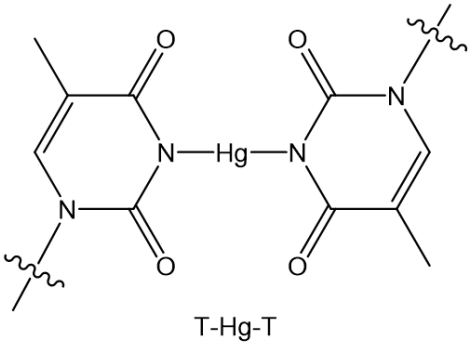

Figure 4.4 Thymine-Mercury-Thymine bonding motif[53]

Thymine-mercury-thymine interactions are highly favourable, both entropically and enthalpically. T_m studies showed that addition of Hg^{2+} ions stabilised duplexes containing T-T, as evidenced by an increase in thermal melting temperature of 10 ^{o}C. Interestingly, the Hg^{2+} stabilised T-T mismatch duplexes had a 3 ^{o}C higher T_m than complementary A-T base pairs.[53]

Ono and co-workers used solution based NMR to develop a 3D structure of the interactions which showed that the T-Hg^{2+}-T pairing is accommodated within the B-DNA structure. It also revealed that the Hg^{2+} releases water molecules in order to position itself within the hydrophobic duplex centre, thus explaining the increase in entropy on binding.[54,55] The enthalpic contribution is associated with the formation of covalent bonds between the bases and the metal ion.[55,56] In recent times, this

knowledge has enabled the development of a range of DNA based mercury sensors, as detailed in the following section.

4.1.2.3 Mercury Sensing with DNA Nanoparticles

DNA modified gold nanoparticles (Au-NPs) have been used for a range of sensing applications, including proteins[57,58], oligonucleotides[59,60] and small molecules.[61,62] The DNA is attached to the Au-NPs via thiol bonds as for SAMs on gold electrodes. The optical properties of nanoparticles are distance-dependent and can, in some cases, be tuned or changed by varying the interconnections between them, which results in a colour change in solution. Consequently, nanoparticles have been used as colorimetric sensors for a range of targets, including Hg^{2+} ions.[63]

The first example of a Hg^{2+} sensor based on DNA:AuNP was designed by Mirkin and co-workers, in 2007. The system involved the use of two different AuNPs, one functionalised with a polythymine strand and the other functionalised with a polyadenine strand which had one thymine base inserted in a central position. At 47 ^{o}C, introduction of 1 μM of Hg^{2+} ions resulted in the aggregation of the NPs and a colour change in the solution, facilitated through T-Hg^{2+}-T between the thymine bases on both sets of NPs. The methodology proved to be highly selective, with no other tested metal ion causing a colorimetric change (Figure 4.5). However, the temperature required careful control through expensive equipment. The sensitivity was also poor, with 1 μM being the minimum amount of Hg^{2+} detectable.[63]

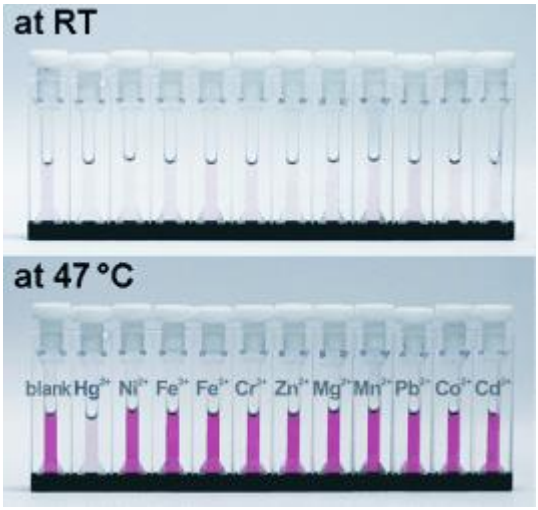

Figure 4.5 Temperature dependency and colorimetric selectivity of DNA:AuNPs for 1μM Hg^{2+}. Image taken from Mirkin and co-workers. [63]

Subsequent uses of DNA:AuNPs for Hg^{2+} detection have improved the sensitivity by introducing additional elements such as unbound DNA targets[64–66] and fluorescent tags[67] which gave limits of detection of 0.5 μM and 0.05 μM, respectively. Another method utilises the affinity of mercury for thiols, thus removing the DNA strands from the AuNPs and resulting in a colorimetric change.[68] However, AuNPs remain expensive and require toxic or highly corrosive chemicals to synthesise.[69] The addition of supplementary species to enable the increase in sensitivity also adds a level of complexity to the system and decreases the usability necessary for a simple and fast reporter system.

4.1.2.4 Mercury Sensing with Fluorescent DNA Probes

Mercury detection using fluorescence usually incorporates both a quencher and a fluorescent group at the terminals of single-stranded DNA, as for the Ag^{+} detection system described in section 4.1.1.1. The first example was again first reported by Ono and co-workers, but has been taken further by other groups.[70–75] Yang and co-

workers have applied it to a stem-loop molecular beacon. Molecular Beacons (MBs) are oligonucleotides probes which, when bound to a target, fluoresce. When not bound, a quencher comes into close contact with the fluorescing agent through the formation of a hairpin loop and prevents emission by energy transfer[76]).[77]

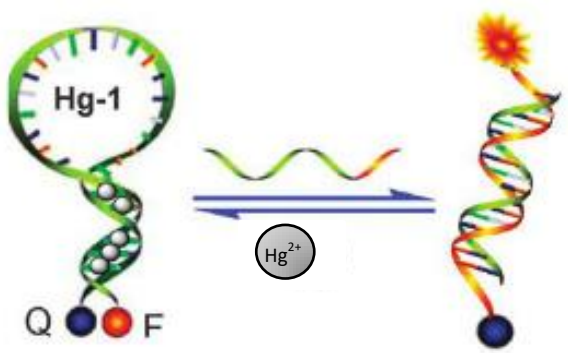

Figure 4.6 MB utilised by Yang and co-workers to detect mercury ions. Image taken from Yang and co-workers.[77]

Complementary targets were added to the free MB strand and the MB strand in the presence of Hg^{2+} and the effect on their fluorescence compared. When mercury ions were not present, the fluorescence changed very little, since the quencher was not held close in either case. In the presence of Hg^{2+}, a true MB was formed and the quencher was held close to the fluorescing agent, thus reducing the emission. Displacing the metal ions with a complementary target strand resulted in the fluorescent group moving away from the quencher and so the fluorescence increased. However, the hybridised DNA with SNP target fluorescence emission was approximately 72% lower compared with a complementary target strand duplex after initial addition of Hg^{2+} ions.[77] While the amount of Hg^{2+} tested (1 μM) is much higher than that required by some AuNP (see section 4.1.2.3) or other fluorescent systems[70,78], this approach may show some promise for signal enhancement when

combined with other labelling techniques, as well for producing dual-function systems for the detection of Hg^{2+} and SNPs.

4.1.2.5 Mercury Sensing with DNA Bound Redox Reporters

There has been little research in the area of electrochemical Hg^{2+} detection despite the potential advantages. Electrochemistry could offer a fast, non-toxic and portable method for the assessment of mercury contamination. Additionally, prefabricated electrode chips and their associated equipment, can be operated by non-specialists, leading to the potential for commercially available devices.[79,80]

The issue with the systems which have already been investigated is that they rely largely on structural change in the molecule and an associated loss in signal[81–85] or the need for a more complicated electrochemical technique, such as electrochemical impedance spectroscopy (a technique which measures the impedance of a system to the flow of current).[81,86,87]

Yu and co-workers attached a ferrocene reporter group to the 3' terminal of a surface bound DNA strand. When in the more flexible single stranded form, it was held closely to the electrode surface, facilitating fast electron transfer. The sequence contained regions with 8 adjacent thymine nucleosides. On the addition of Hg^{2+} and a target sequence also containing 8 thymine nucleosides, a stable and more rigid double stranded species was formed. The increased rigidity resulted in the ferrocene group being held further from the electrode surface, resulting in an associated loss in signal, as shown in Figure 4.7.[88]

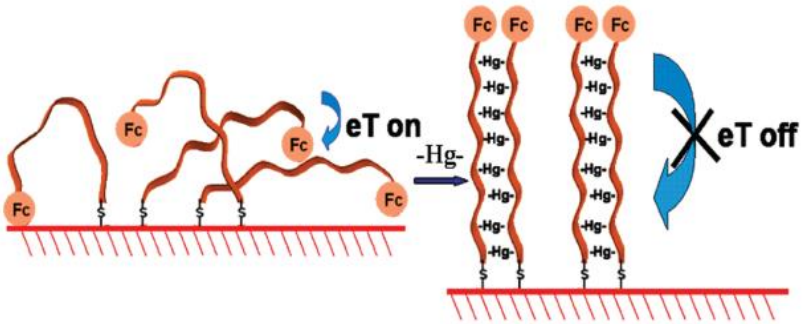

Figure 4.7 Overview of the mechanism of action of the electrochemical Hg^{2+} sensor designed by Yu and co-workers*. Image taken from Yu* and co-workers.[88]

This system showed excellent selectivity for Hg^{2+} over a range of other divalent metals (except Cu^{2+} which appeared to form complexes with the poly-T oligonucleotides) and was reusable when washed with ascorbic acid. It also had a detection limit of 0.5 nM, 10 times lower than the legal limit for Mercury contamination in British drinking water (5 nM).[89] However, the reliance of this system on a reduction in current and 'on-off' signalling can lead to false positives during analysis.[88]

Kim and co-workers improved upon this system by utilising a 21-mer with thymine rich regions at either end. The result was that the oligonucleotide folded back on itself and formed a hairpin structure upon the addition of Hg^{2+} ions. Again the ferrocene group was attached to the 3'-end of the DNA but a gain in signal strength was exhibited upon the binding of mercury. This was due to the reporter group's being brought into closer proximity with the electrode surface, in reverse of the system developed by Yu and co-workers and analogous to the molecular beacons described in section 4.1.2.4. This has a two-fold advantage: a less complicated system with fewer components and so lower associated error, and an 'off-on' signalling system which prevents false positives. The system was specific for Hg^{2+} ions and was reusable when washed with 10 μM cysteine, which is a highly selective mercury

binder.[90] However, the sensitivity of this system was not as low as that of the system described by Yu and co-workers and was not able to detect mercury at or below safe levels in drinking water, with a detection limit of 0.1 μM.[83,89] The reason for this is not given, but the system used by Yu and co-workers involves the movement of two redox active centres on the formation of one mercury facilitated duplex whereas the looped structure investigated by Kim and co-workers relies on the movement of only one redox centre.

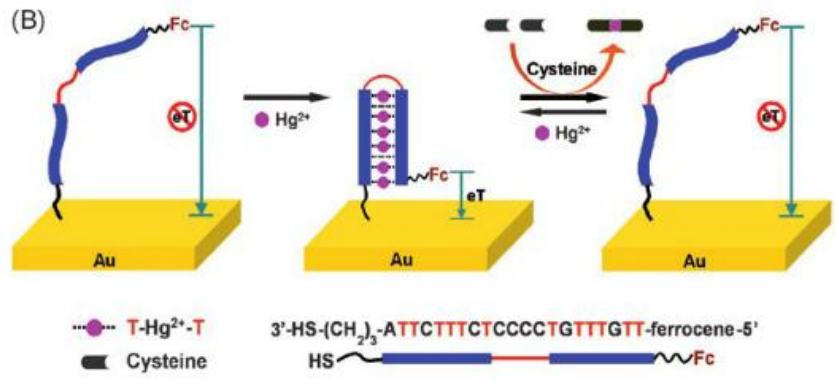

Figure 4.8 Overview of the mechanism of action of the electrochemical, Hg^{2+} sensor designed by Kim and co-workers. Image taken from Kim and co-workers.[83]

While electrochemical methods show great promise for mercury detection, further strides to achieve a reliable, accurate and sensitive system need to be made.

4.1.3 Previous Work

FcNA conjugated DNA has been shown to bind target DNA and induce an electrochemical signal response on a surface with a greater degree of sensitivity than in solution (Chapter 3). As described in section 4.1.2.5, current electrochemical methods for Hg^{2+} detection show promise but are restricted by their reliance on large

structural change to induce variations in current. Since the FcNA reporter is in the centre of the probe strand and would be directly attached to the thymine in a T-Hg^{2+}-T binding motif, it was investigated as a possible alternative to the systems described above. The hope was that sensitivity would increase and the need for movement of the reporter group towards and away from the electrode would be removed, thus eradicating 'on-off' signalling and its associated ambiguity. Initial work was carried out to characterise the nature of the FcTT-Hg^{2+} system in solution, as detailed below.

4.1.3.1 Binding and Stability

The binding of the FcTT unit with Hg^{2+} ions was first investigated by analysing the thermal melting temperature (T_m). 5 μM solutions of both the probe strand containing the central FcTT unit and unmodified target strand with two thymines or two adenines in the equivalent FcTT positions were hybridised in 10 mM sodium phosphate buffer pH 7.0, 100 mM $NaClO_4$. To the resulting duplex, 2 molar equivalents of $HgClO_4$ were added. The results are shown in Table 4.1.[91]

Table 4.1 T_m values of $FcTT_{(R,R)}$ and $FcTT_{(S,S)}$ vs TT and AA targets, with and without the addition of 2 molar equivalents of $Hg(ClO_4)_2$..5 μM of each strand, 10 mM sodium phosphate buffer pH 7.0, 100 mM $NaClO_4$. Data taken form the thesis of Dr James Carr-Smith.[91]

	T_m / °C , TT Target			T_m / °C, AA Target		
Modification	Without Hg^{2+}	With Hg^{2+}	Difference	Without Hg^{2+}	With Hg^{2+}	Difference
$FcTT_{RR}$	40.5	43.5	+3.0	43.0	41.5	-1.5
$FcTT_{SS}$	39.5	45.5	+6.0	41.0	34.0	-7.0
TT	41.5	53.0	+11.5	55.5	54.0	-1.5

When hybridised with a target with thymine mismatches, both FcTT stereoisomers showed an enhancement of duplex stability upon the addition of Hg^{2+}. The values were also greater than the duplexes when hybridised with a fully complementary target both with and in the absence of Hg^{2+}. This suggests that Hg^{2+} binding is more favourable than hydrogen bonding for FcTT systems. It should be noted, however, that the stabilisations were not as significant as that observed with the unmodified probe DNA and thus was attributed to the rigidity of the ferrocene units.[91]

The stabilising effect was found to be greatest with the *(S,S)* stereoisomer. The modelling studies shown in Chapter 3 (Figure 3.8) suggest that the *(S,S)* stereoisomer is less aligned with the natural DNA backbone than the *(R,R)* version. As such, the greater increase in T_m could result from the FcTT-Hg^{2+}-TT bonding realigning the *(S,S)* stereoisomer closer to the structure of natural DNA, thus stabilising it further. Due to this additional stability, subsequent experiments were carried out with the $FcTT_{(S,S)}$ modified probe only.[91]

Probe $FcTT_{(S,S)}$: Target AA duplexes were used to confirm that stabilisation was due to T-Hg^{2+}-T bonding rather than to stabilisation of the negatively charged backbone, which would result in stabilisation regardless of the presence of TT mismatches. While the T_m data (Table 4.1) confirms the stabilisation observed is not due to neutralisation of the backbone charge, interestingly, there was a reduction in stability (-7^{o}C) rather than the stability being unaltered. Circular Dichroism spectroscopy (CD), a technique which monitor the absorption of circularly polarised light. was used to determine the origin of this loss in stability and the result is shown in Figure 4.9.[91]

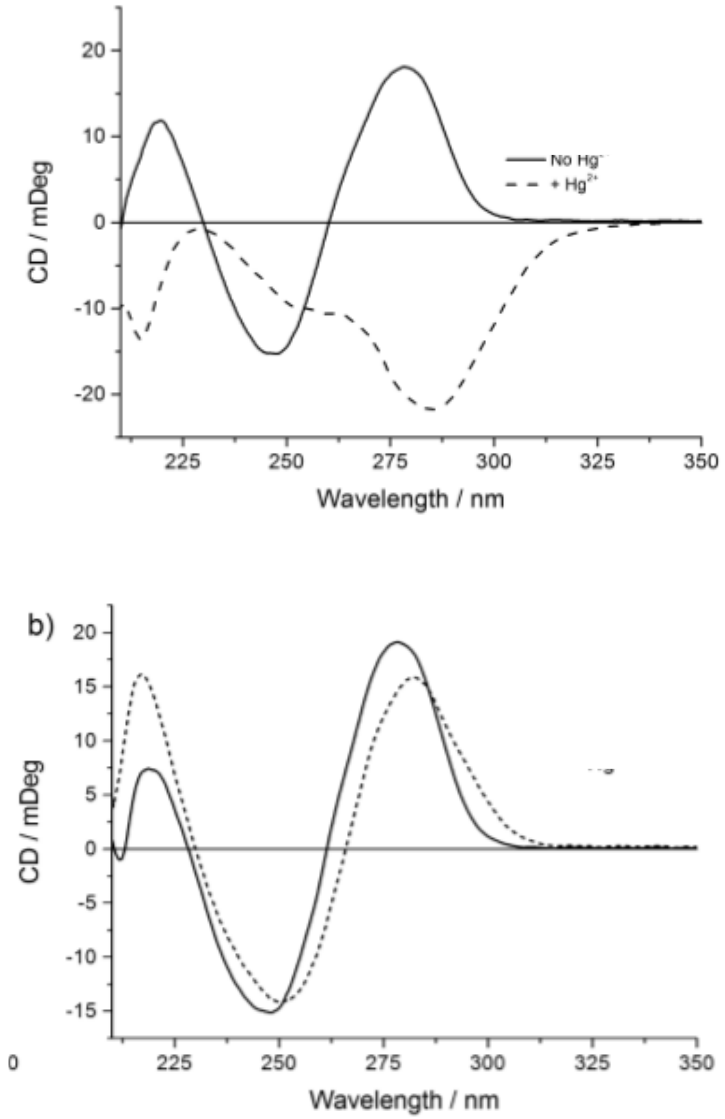

Figure 4.9 Top: CD spectra of $FcTT_{(S,S)}$ duplexed with an AA target before and after the addition of 2 molar equivalents of Hg^{2+}. Bottom: CD spectra of $FcTT_{(S,S)}$ duplexed with an TT target before and after the addition of 2 molar equivalents of Hg^{2+}. 5 μM of each strand, 10 mM sodium phosphate biffer pH 7.0, 100 mM $NaClO_4$. Courtesy of Dr James Carr-Smith.[91]

Addition of Hg^{2+} to duplexes of $FcTT_{(S,S)}$ modified probes bound to AA targets resulted in a complete loss of B-DNA structure, which explains the loss in stability for these duplexes. It was suggested that, due to the stabilising effect of the T-Hg^{2+}-T adduct, slippage occurs and the DNA rearranges to accommodate the formation of this binding motif.[14,91]

The same CD experiments with $FcTT_{(S,S)}$:TT duplexes (Figure 4.9) revealed that the B-DNA structure was retained upon the addition of Hg^{2+}. Additionally, mass spectrometry experiments (Figure 4.10) showed masses equivalent to the duplex alone and to the duplex with one and two Hg^{2+} ions, the latter of which corresponded to the total number of T-Hg-T bonds possible in the duplex. Together, these results were further evidence for the formation of a FcTT-Hg^{2+}-T binding motif rather than enhanced duplex stability through backbone neutralisation.[91]

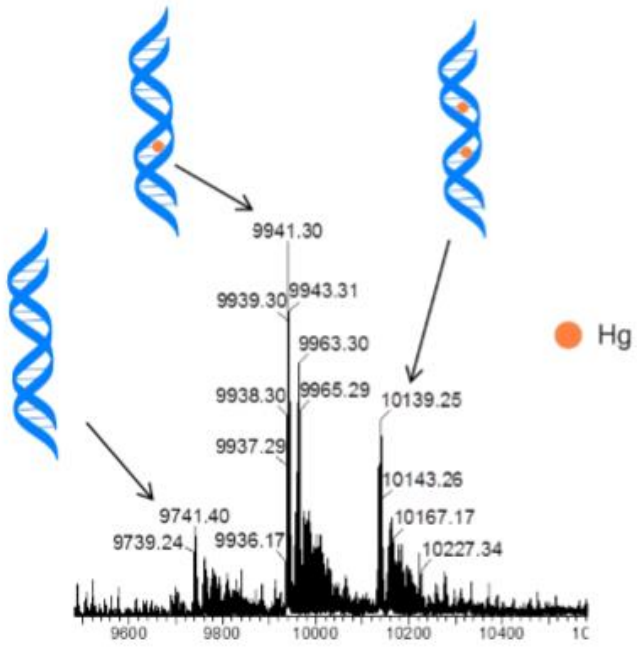

Figure 4.10 Deconvuluted ESI mass spectrum observed for $FcTT_{(S,S)}$ probe:AA target when bound to mercury showing the three main ions of the duplex alone and when bound to one and two mercury atoms. Courtesy of Dr James Carr-Smith.[91]

4.1.3.2 Sensitivity and Selectivity

The selectivity of the FcTT system towards Hg^{2+} was assessed using T_m and CD studies. The $FcTT_{(S,S)}$ DNA probe: unmodified TT target duplex was incubated with a range of different divalent ions. There was no significant change in T_m observed for

any the ions tested (Table 4.2), suggesting excellent selectivity with the FcTT system.[91]

Table 4.2 T_m values for FcTT probe : TT target duplexes after incubation in 2 molar equivalents of a range of divalent cations and the difference compared to a non-incubated duplex. 5 μM of each strand, 10 mM sodium phosphate buffer pH 7.0, 100 mM $NaClO_4$. Courtesy of Dr James Carr-Smith.[91]

Metal	T_m / °C	Difference
No Metal	39.5	
Hg^{2+}	46.5	+7.0
Zn^{2+}	41.0	+1.5
Pb^{2+}	40.5	+1.0
Cd^{2+}	40.0	+0.5
Fe^{2+}	40.5	+1.0
Cu^{2+}	41.5	+2.0
Ba^{2+}	40.0	+0.5
Ca^{2+}	41.0	+1.5
Mg^{2+}	40.0	+0.5

The effect of the addition of Cd^{2+}, Cu^{2+} and Zn^{2+} on the duplex structure was also assessed using CD spectroscopy, as shown in Figure 4.11. The was no change in the observed B-DNA structure for duplex incubated in Cd^{2+} or Zn^{2+} compared with a duplex alone. There was a slight decrease and bathochromic shift in the 275 nm band on the addition of Cu^{2+}, which was attributed to the fact that Cu^{2+} is known to interact with nucleobases as discussed in section 4.1.1. These results again suggest the FcTT – TT system has a high level of selectivity for Hg^{2+}.[24,27,28,91]

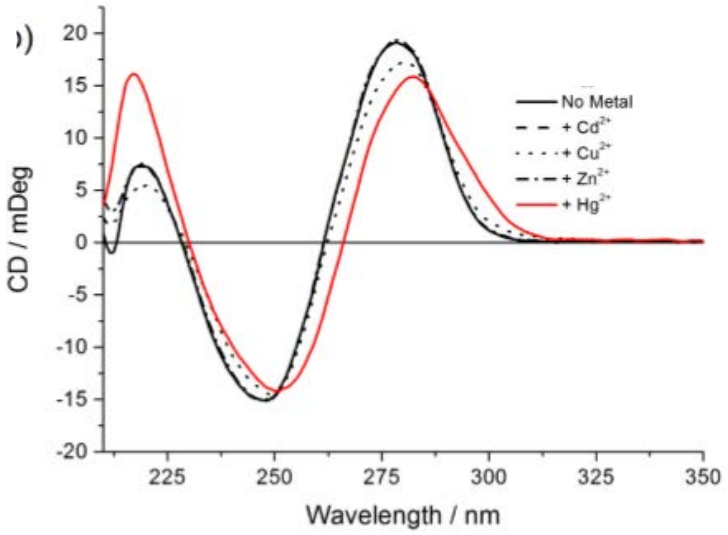

Figure 4.11 CD spectra of FcTT-TT duplex after incubation in Cd^{2+} (dashed line), Cu^{2+} (dotted line) and Zn^{2+} (dash-dot line). The same experiments with Hg^{2+} is given as a red line for comparison. Metals were added at 2 molar equivalents, 5 μM of each strand, 10 mM sodium phosphate buffer pH 7.0, 100 mM $NaClO_4$. Courtesy of Dr James Carr-Smith.[91]

UV titration studies were used to investigate the sensitivity of the FcTT-TT system towards Hg^{2+}. Additions of Hg^{2+} ranged from 0.125 to 2 molar equivalents and resulted in an increase in both the reduction in UV absorption and a red shift (shown in Figure 4.12), which was attributed to the tightening of the duplex upon adduct formation.[53,91,92] The focus of this work was to determine how many equivalents of Hg^{2+} were required for the UV absorption decrease to plateau rather than to find the limit of detection (2 equivalents, corresponding to the number of T-Hg-T bonding positions available). However, a change in the UV absorption was observed from the lowest concentration of mercury ions added, suggesting the system could be investigated further to determine its sensitivity and the limit of detection.[91]

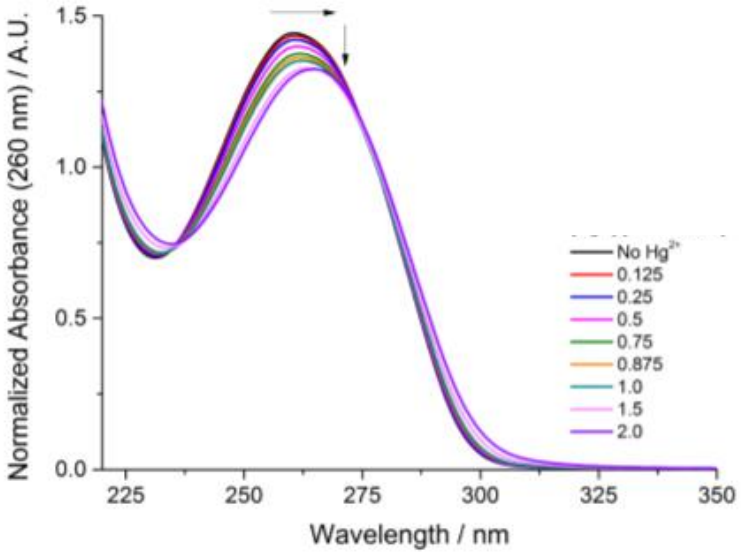

Figure 4.12 UV-vis spectra of $FcTT_{(S,S)}$ probe:TT target duplexes upon on the addition of $Hg(ClO_4)_2$. 5 μM of each strand, 10 mM sodium phosphate buffer pH 7.0, 100 mM $NaClO_4$.

4.1.3.3 Electrochemistry

For solution based electrochemical studies, it was necessary to use DNA and FcNA conjugated DNA at concentrations of 50 μM. The use of mercury at this concentration leads to its adsorption to the surface of gold electrodes, which interferes with the current signal. As a result it was not possible to accurately determine any electrochemical differences due to Hg^{2+} binding to the freely diffusing FcTT probes.[91,93]

4.1.4 Conclusions and Project Aims

The pollution of the environment with heavy metals, in particular mercury, can have devastating effects on the ecology of an area and on our health, either through direct contact with or the consumption of affected animals, crops and water. Many techniques have been used to detect mercury, but standard protocols currently utilise expensive, specialist and time inefficient instrumentation. To attempt to improve this

situation, and with the enhanced understanding of metal interactions with nucleic acids in recent times, sensors based on fluorescence, AuNP and electrochemistry have all been investigated. These have been shown to successfully detect Hg^{2+} ions at concentrations below the legal UK drinking water contamination limits. However, many of these techniques are either expensive or rely on structure changes and 'on-off' signalling, leading to the issue of potential false positive responses.

Chapter 3 has shown that electrode bound DNA-FcNA conjugates containing a $FcTT_{(S,S)}$ unit in a central position are capable of reproducibly detecting DNA targets, including targets with a TT mismatch. This, and the previous work carried out in solution, which strongly suggested that Hg^{2+} ions do bind to the $FcTT_{(S,S)}$–TT system, has led to the following investigations which focus on detecting mercuric ions using electrochemistry. The aim was to detect Hg^{2+} ions without the need to rely on structural changes in the DNA strand as the mercury is bound directly to the redox reporter group.

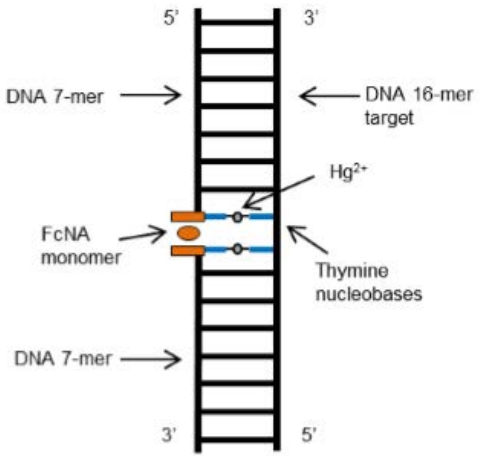

Figure 4.13 Representation of Hg^{2+} binding in an $FcTT_{(S,S)}$: TT duplex. Courtesy of Dr James Carr-Smith.

The use of mixed SAMS, where the reporter group is located close to the electrode surface, increasing sensitivity, and the surface is backfilled with 6-mercaptohexan-1-ol, preventing excessive Hg^{2+} adsorption to the surface, would allow for sensitive electrochemical detection which was not possible within a solution based experiment. The SAMs would also be investigated for their reusability, which again, is not possible with solution based experiments.

4.2 Results and Discussion

4.2.1 Oligonucleotides used

The DNA sequences used throughout this chapter are shown in Table 4.3. Due to the evidence in Chapter 3 and the previous work carried out by the Tucker group, which suggested that the FcNA units containing *(S,S)* chirality were more appropriate for sensing DNA targets, only $FcHH_{(S,S)}$ and $FcTT_{(S,S)}$ units were incorporated into DNA for these experiments. The strands used were the same as those used in Chapter 3. This ensured that it was possible to identify that target DNA has bound to the probe prior to detection of the Hg (II).

S1 is the FcNA conjugated DNA with a thiol group attached to the 3' terminus. NT denotes non-thiolated. S2 denotes the target strand which is fully complementary in the case of S1TT. The $FcHH_{(S,S)}$ unit was used for comparison purposes since it would not be able to bind the Hg^{2+} through the same T-Hg^{2+}-T binding motif as $FcTT_{(S,S)}$.

SAMs were prepared as outlined in sections 2.2 and 7.4.1. The concentration and volume of both thiolated probe (200 μL of 1 μM DNA) and 6-mercapto-1-hexanol (1.46 mL at 2 mM) used to form the SAMS were not varied throughout this work.

Table 4.3 Oligonucleotide sequences used throughout Chapter 4

Oligonucleotide	Sequence (5' – 3')
S1**TT**	TGG ACT C **FcTT$_{(S,S)}$** CTC AAT G **-SH**
S1**HH**	TGG ACT C **FcHH$_{(S,S)}$** CTC AAT G **-SH**
S1**HH-(NT)**	TGG ACT C **FcHH$_{(S,S)}$** CTC AAT G
S2	CAT TGA G**TT** GAG TCC A

4.2.2 Electrochemical Detection of Hg (II)

4.2.2.1 Detection by CV

The electrochemical effect of Hg^{2+} introduction on the redox activity of the FcTT$_{(S,S)}$ unit was first assessed using cyclic voltammetry. The duplexes were prepared as described in Chapter 3. Briefly the mixed SAMs were soaked in a 5 mL of 100 nM target in 10 mM phosphate buffer, 1 M $NaClO_4$. The subsequent duplexes were soaked in 2 μM $Hg(ClO_4)_2$ for 10 mins. The resulting CVs and data are shown in Figure 4.15 and Table 4.1, respectively.

The data indicate that there is little variation in the halfwave potential ($E_{1/2}$) of the FcNA unit, which would suggest that the binding of the mercury ions to the ferrocene bound thymine does not affect the electron withdrawing abilities of the nucleobase.[94] This supports the proposed binding structure given in Figure 4.4 in that the replacement of the imino proton with a Hg^{2+} ion, which is bound to two thymine bases, would not result in a net change in charge and therefore any significant effect on the electron density at the heterocycle.

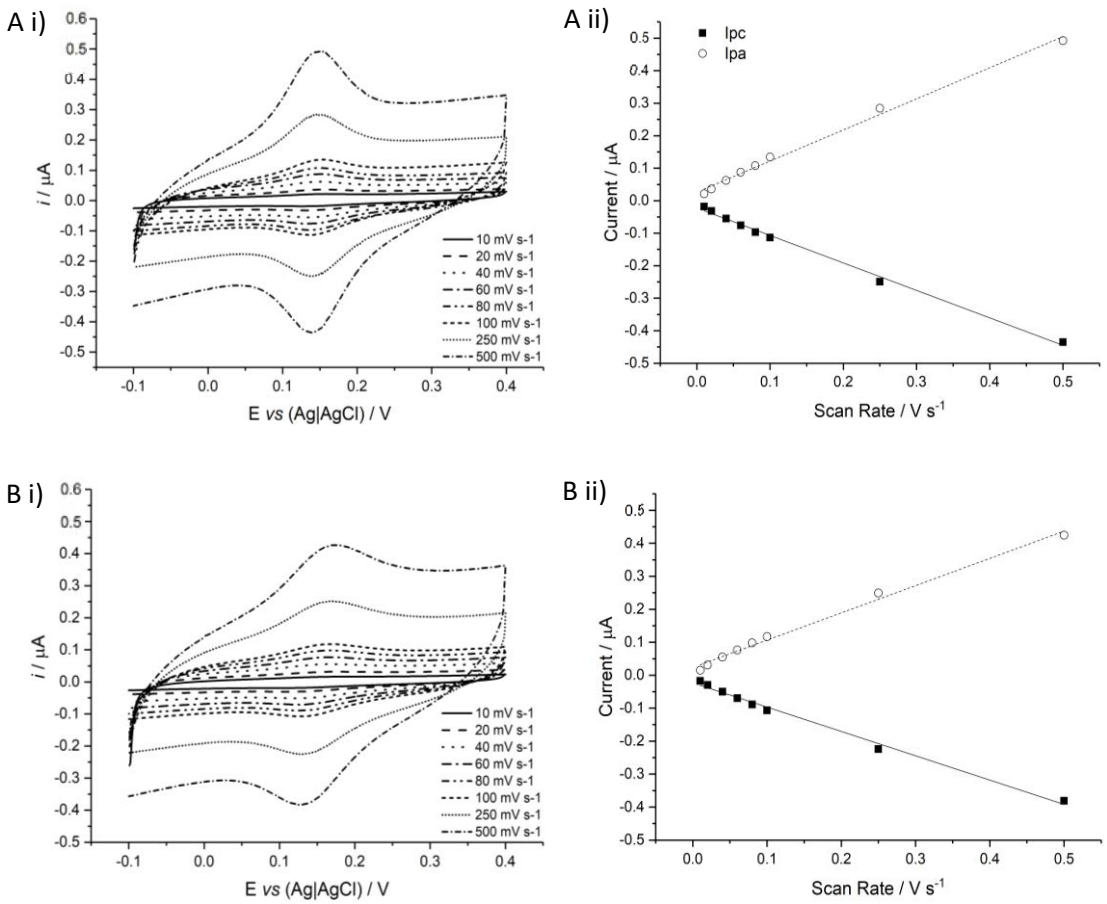

Figure 4.15 i) CVs of A: S1TT:S2 B: S1TT:S2 soaked in 2 µM $Hg(ClO_4)_2$. Target strands were used at a concentration of 100 nM. CVs recorded at varying scan rates, between -100 and 400 mV in 1 M $NaClO_4$, 10 mM phosphate buffer. ii) Linear dependence of current on scan rate for A and B.

Table 4.4 Electrochemical behaviour of S1TT:S2 SAMs with and without Hg^{2+} added. Data derived from Figure 4.14.

SAM	$E_{1/2}$ / mV	ΔE_p / mV	I_p^c / I_p^a
A: S1TT:S2	144	2	1.15
B: S1TT:S2 + Hg^{2+}	148	17.25	1.07

Note: *Due to the lack of material remaining from Chapter 3 and equipment malfunctions, this experiment was carried out once.*

The cathodic to anodic peak ratio (I_p^c/I_p^a) changed very little on the addition of Hg^{2+}, which indicates that the binding of Hg^{2+} does not induce any underlying electrochemical reactions.[95,96]

The only significant electrochemical difference observed was an increase in peak separation ($\Delta E_p = E_p^a - E_p^c$). Further analysis revealed that ΔE_p increased with increasing scan rate on the addition of Hg^{2+} (shown in Table 4.5). This implies a loss in the reversibility of the electrochemical behaviour.[95,96]

Table 4.5 The ΔE_p before and after addition of Hg^{2+} to the S1FcTT$_{S,S}$: S2 duplex, where A and B refer to Figure 4.14. Data derived from Figure 4.14.

	ΔE_p / mV	
Scan Rate	**A:** S1**TT**:S2	**B:** S1**TT**:S2 + Hg^{2+}
10 mV s^{-1}	-5	-2
20 mV s^{-1}	3	19
40 mV s^{-1}	5	13
60 mV s^{-1}	2	15
80 mV s^{-1}	3	20
100 mV s^{-1}	4	20
250 mV s^{-1}	2	23
500 mV s^{-1}	2	30

The cause of the increase in ΔE_p with scan rate is difficult to explain but is due to the introduction of the mercury ion. This may reduce the facileness of electron transfer through a greater resistance of the duplex movement towards the electrode surface.

4.2.2.2 Electrochemical Detection by SWV

As detailed above, detection of Hg^{2+} using CV was not immediately obvious from the CVs themselves. Since SWV had already proved more suitable for the detection of DNA targets (Chapter 3) it was now trialled for the detection of Hg^{2+} using the same SAMs, as shown in Figure 4.16.

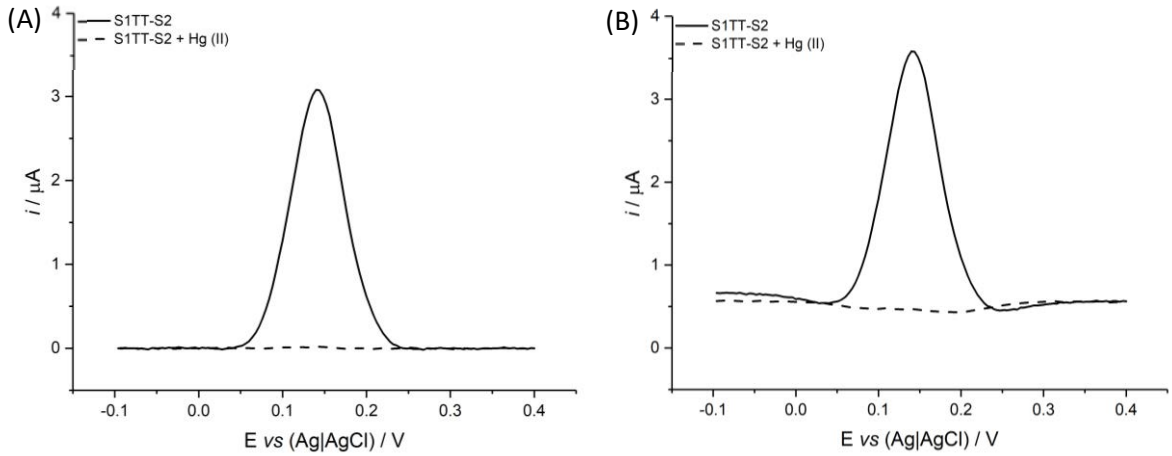

Figure 4.16 SWV of S1TT:S2 before and after soaking in 2 µM $Hg(ClO_4)_2$ recorded at 200 Hz, where A: background subtracted and B: SWV before background subtraction. SWV were recorded at amplitude of 25 mV and step of 1 mV. SWV recorded in 1 M $NaClO_4$, 10 mM phosphate buffer.

Soaking the S1TT-S2 SAM modified electrode in 2 µM $Hg(ClO_4)_2$ for 20 min, resulted in a 99.4% decrease in current at a frequency of 200 Hz. Clearly, such a dramatic effect was not observed by CV. However, since mercury ions had previously been shown to produce large currents across a wide range of potentials,[83,90,97,98] there was a concern that an increase in background current may have been high enough to obscure the FcTT related peak. Consequently, the reduction in signal may have been an artefact of the process of background subtraction, which is carried out to make peaks more comparable. To ensure that this was not the case, the non-subtracted data were checked and are given in Figure 4.16 (B). The background currents are comparable for both the SWVs recorded, suggesting that the current issues associated with Hg^{2+} adsorption on bare Au electrodes are negated by the reduced concentrations of mercuric ions required (compared with solution based work) and the presence of a closely packed monolayer across the Au surface.

The reason for the reduction in signal was then considered further. This type of 'on-off' signalling is associated with the induction of structural change, as in previous examples of DNA based electrochemical Hg^{2+} sensors.[81–85, 88] The T-Hg-T binding motifs are in a central position in the S1TT:S2 duplex and the previous CD experiments carried out by the Tucker group suggested that the natural DNA duplex structure is maintained on the binding of Hg^{2+} ions; therefore, this system should not induce a large conformational change. Furthermore, such a charge would be expected to be mirrored in the CV data, which is clearly not the case. This suggests that the '*critical frequency*' of the molecule, to which SWV is incredibly sensitive,[99] is affected by the increased rigidity of the T-Hg^{2+}-T binding motif. However, another, less likely, possibility was that Hg^{2+} was degrading the DNA probe rather than binding to the thymines.[100] The system was therefore explored further using S1FcHH$_{(S,S)}$ mixed monolayers.

4.2.2.3 Control Studies with FcHH$_{(S,S)}$

The use of S1FcHH$_{(S,S)}$ removed the possibility of Hg^{2+} bonding in close proximity to the ferrocene unit. Therefore it was expected that no reduction in current would be observed unless degradation of the redox tag was occurring. The resulting SWVs are given in Figure 4.17 and unexpectedly show a 90.7 ± 0.57% reduction in current upon the addition of Hg^{2+} ions to the S1HH:S2 duplex. This was coupled with a 48 ± 4 mV positive shift in potential, a difference which was not observed when investigating the S1TT system. These values are averages determined from a minimum of three experiments.

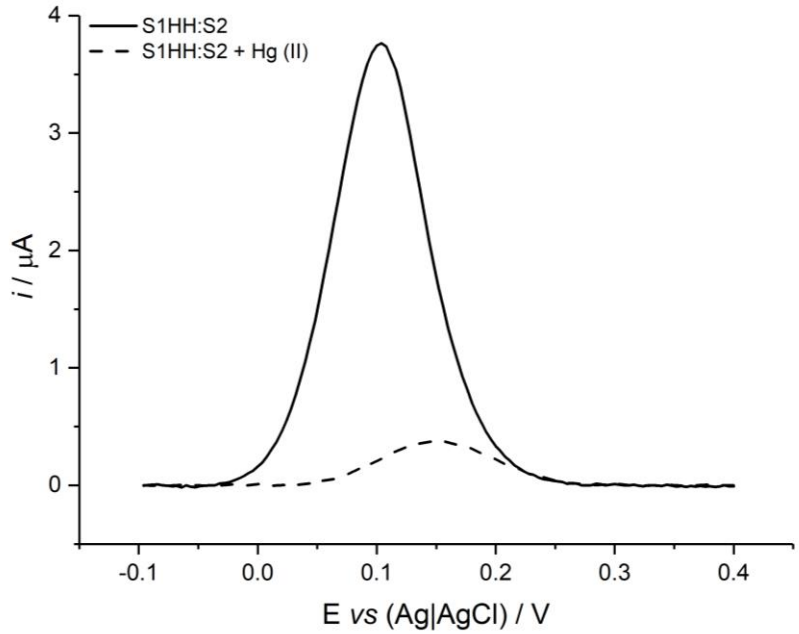

Figure 4.17 SWV of S1HH:S2 before and after soaking in 2 µM $Hg(ClO4)_2$ recorded at 200 Hz, at amplitude of 25 mV and step of 1 mV. SWV recorded in 1 M $NaClO_4$, 10 mM phosphate buffer.

These results would imply that there is a significant change in the environment of the redox reporter. FcTT-Hg^{2+}-T had previously proved to be a highly favourable interaction, stabilising the duplex to a greater extent than when the FcTT unit was opposite complementary AA bases. In contrast, the FcHH unit cannot hydrogen bond to bases and, which inherently reduces the structural stability of the duplex in this region. Additionally, the FcHH monomer is not sterically hindered and so is capable of rotating on its axis to some extent, acting as a 'hinge'. Therefore, it was suggested that the favourability of the T-Hg^{2+}-T bonding, the additional flexibility afforded by the FcHH unit compared with FcTT and the presence of a thymine as the final base at the 5' end and penultimate base at the 3' end, could result in the displacement of the target strand and folding of the probe to accommodate the mercury binding motif (see Figure 4.18). The reduction in current could then be explained by the rigidity of

such a structure and difficulty with which the FcHH unit can orient itself to allow for facile electron transfer.

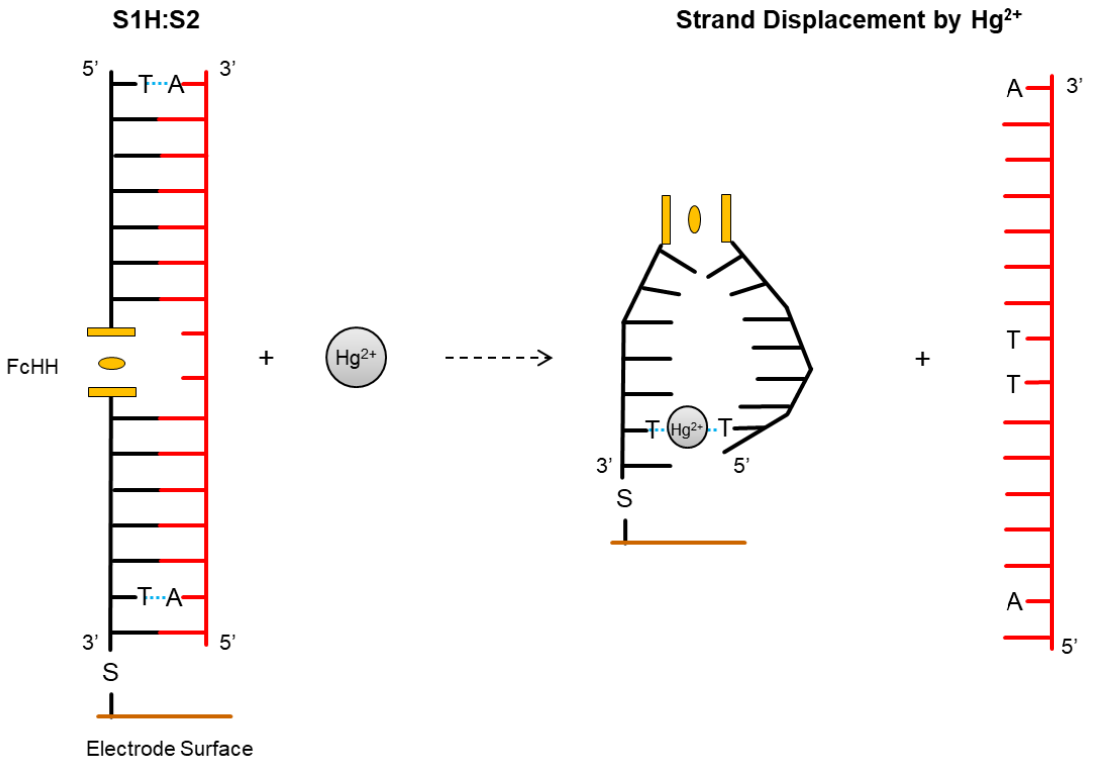

Figure 4.18 Schematic for the proposed displacement of S2 from an S1HH:S2 duplex by Hg^{2+}.

The possibility of this separate T-Hg-T interaction was investigated further using mass spectrometry (MS). 50 µL of 25 µM of FcHH(NT) in 2 µM $Hg(ClO_4)$ was prepared and left for 1 hour at room temperature before mass spectrometric analysis. The ratio of Hg^{2+} to DNA was 1:12.5. Although a 1:1 ratio or above would be preferred in order to maximise the number of strands participating in the mercury binding, there was a concern that the presence of excess Hg^{2+} may be hazardous to the instrument operators and subsequent users.

Despite the use of a reduced mercury concentration, an additional peak at 4831.7 m/z, which equates to the mass of the oligonucleotide (4630.7 g mol^{-1}) and one

additional mercury ion (200.6 g mol^{-1}) can be seen in the MS (*Figure 4.19*). This and the electrochemical data above support the proposal that the T-Hg-T motif is causing the oligonucleotide to fold, In the case of FcTT, the presence of two of these motifs in the centre of the duplex, allowing for base stacking, is more stabilising and so target strand displacement does not occur. Accordingly, the redox reporter environment changes very little and so no variation in potential is observed.

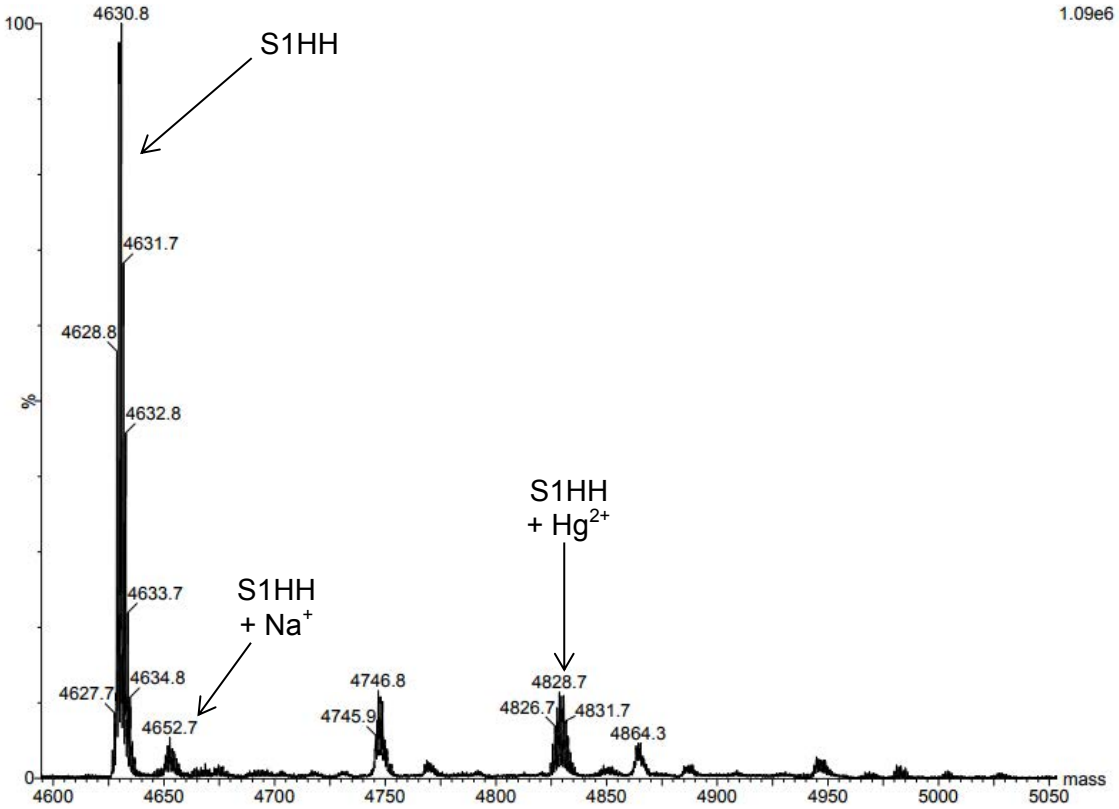

Figure 4.19 Deconvuluted ESI mass spectrum observed for S1HH in the presence of mercury showing the peaks for S1HH with no Hg^{2+} bound (with and without Na^{+}) and with one Hg^{2+} ion bound.

4.2.3 Sensor Reusability

Cysteine is known to competitively bind mercury and has been shown in the literature to allow for the reusability of mercury sensors.[83,90,97,98] To further ensure the signal reduction was not due to degradation of the DNA probe or redox reporter, the SAM was soaked in 10 μM cysteine for 10 min after exposure to $Hg(ClO_4)_2$. This was then

repeated multiple times in a cycle of Hg^{2+} and cysteine exposures to assess the stability of the system to reuse. The resulting SWV and bar chart analysing the loss in current are given in Figure 4.20.

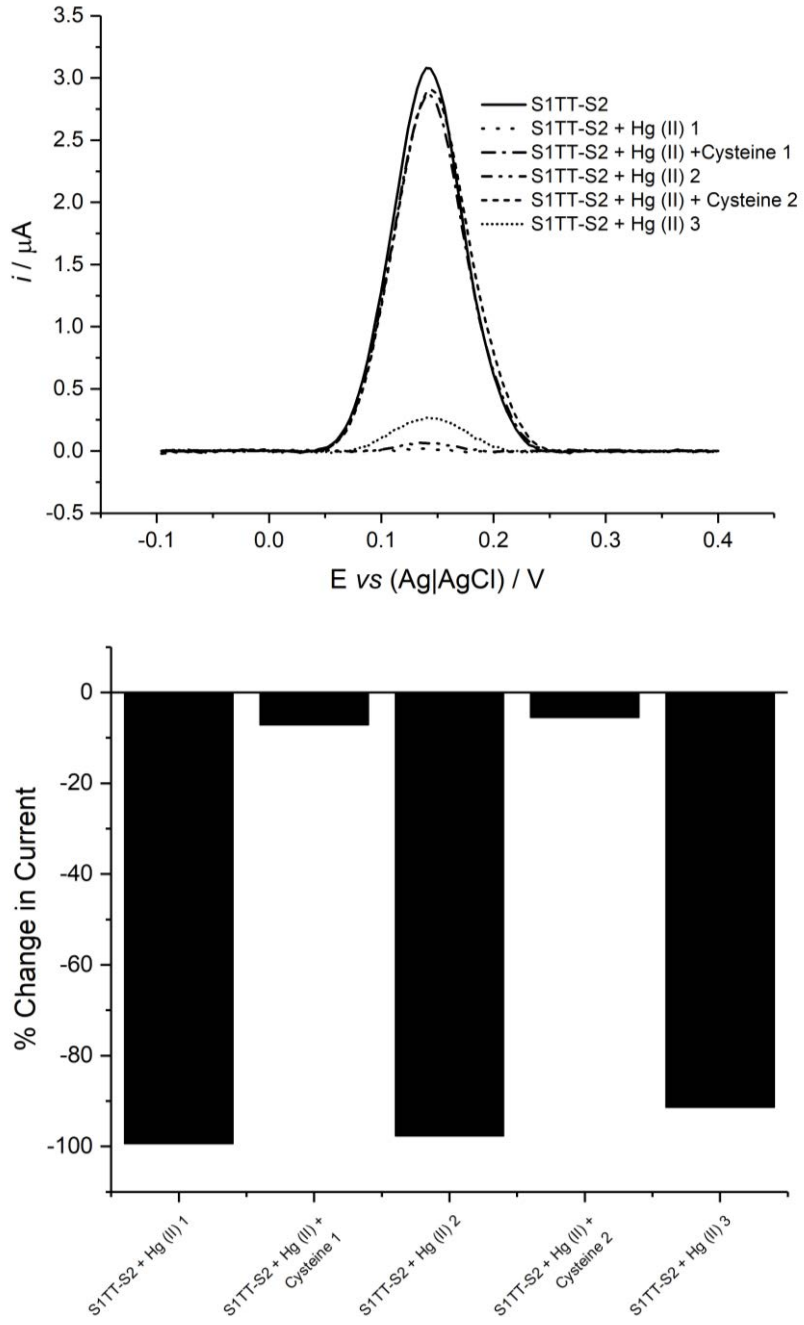

Figure 4.20 Top: SWV of S1TT:S2 before and during cycles of soaking in 2 µM $Hg(ClO_4)_2$ and 10 µM cysteine recorded at 200 Hz, at amplitude of 25 mV and step of 1 mV. SWV recorded in 1 M $NaClO_4$, 10 mM phosphate buffer. Bottom: Bar chart of the % change in current vs S1TT:S2 (taken from the peak maxima of the SWV above).

On the addition of cysteine, the FcNA redox reporter signal recovers to 98 and 91% of the original S1TT:S2 duplex current for the 1st and 2nd cycle respectively. This further corroborates the suggestion that the reduction in current on the addition of Hg^{2+} observed in the SWV is due to the binding of mercuric ions. As can be seen from the SWV, the oxidation potential does not vary from that of the initial duplex (144 mV) and the current returns very close to that of the initial duplex. This implies that the use of cysteine to remove the Hg^{2+} ions allows for the retention of the S1TT:S2 duplex. The high percentage signal recovery also indicates promise for the development of a reusable system.

4.2.4 Limit of Detection (LOD)

Initial studies to this end were confounded by instrument issues and a lack of sample.

4.3 Conclusions

Initial studies have been carried out into the ability of the FcTT conjugated DNA SAMs to detect mercuric ions when bound to a DNA target containing TT bases opposite the Fc unit. This was a continuation of solution based work previously carried out by the Tucker Group which had shown that mercury binding to bare electrodes had made electrochemical detection impossible.

The complete surface coverage of the SAMs and the reduction in the concentration of Hg^{2+} required compared with solution based studies prevented the high background currents associated with Hg^{2+} detection and enabled the detection of Hg^{2+} by both CV and SWV.

SWV proved to be the more sensitive detection technique, with a 99% decrease in signal. This decrease could then be attributed directly to binding of the mercury ions rather than the degradation of the FcNA probe through comparison with FcHH probes. FcHH probes do not possess the appropriate binding motif next to the redox reporter to facilitate mercury binding. However, a reduction in current was still observed on the addition of Hg^{2+} accompanied by a shift in the observed oxidation potential, not seen with FcTT. This and subsequent MS studies indicated that for the FcHH system, the target strand is displaced and the single stranded probe orients to facilitate the favourable T-Hg-T binding motif using thymines available at either end of the strand.

It had been hoped that the presence of the binding motif close to the redox reporter in a central position in the probe would prevent 'on-off' signalling, a prevalent issue within the literature. [81–85] However, this system displayed 'on-off' signalling as well. Nevertheless, it was shown to be reusable when using cysteine to competitively bind the Hg^{2+}, with an average 91.4% signal recovery over two cycles.

It was also not possible, in the time available, to determine the limit of detection for this system, which should be a focus of future work to determine whether the sensitivity of this system is comparable with those in the literature capable of detecting mercury below the legal concentration in drinking water (5 nM).[85,88,89]

4.4 Further Work

To further the investigations of the S1TT:S2 duplex as a potential commercial Hg^{2+} sensing device, the following could be investigated:

- Repeat all of the experiments above where only one repetition has been possible, with newly purified strands, to ensure the preliminary work is a true reflection of the system's behaviour.
- Determine the limit of detection to assess the viability of the system as a commercial sensor.
- Determine the selectivity of the system by investigating the effect on the electrochemistry in the presence of other metal ions.
- Vary the SWV frequency in an attempt to tune it to the critical frequency of the FcTT reporter when bound to the mercury ion, as described by Plaxco and co-workers.[99] This may prevent the system from being a 'on-off' sensor with almost 100% loss in signal on binding.
- Subsequent to the determination of the limit of detection, the system should be applied to a disposable electrochemical chip and exposed to mercury to begin to assess the efficacy of the S1TT:S2 duplex as potential commercial sensing device.

4.5 References

(1) Pyle, A. M. *Science* **1993**, *261*, 709–714.

(2) Zhan, S.; Wu, Y.; Wang, L.; Zhan, X.; Zhou, P. *Biosens. Bioelectron.* **2016**, *86*, 353–368.

(3) Kelley, S. O.; Barton, J. K.; Jackson, N. M.; McPherson, L. D.; Potter, A. B.; Spain, E. M.; Allen, M. J.; Hill, M. G. *Langmuir* **1998**, *14*, 6781–6784.

(4) Clever, G. H.; Söltl, Y.; Burks, H.; Spahl, W.; Carell, T. *Chem. Eur. J.* **2006**, *12*, 8708–8718.

(5) Wettig, S. D.; Wood, D. O.; Aich, P.; Lee, J. S. *J. Inorg. Biochem.* **2005**, *99*, 2093–2101.

(6) Wettig, S. D.; Wood, D. O.; Lee, J. S. *J. Inorg. Biochem.* **2003**, *94*, 94–99.

(7) Aich, P.; Labiuk, S. L.; Tari, L. W.; Delbaere, L. J.; Roesler, W. J.; Falk, K. J.; Steer, R. P.; Lee, J. S. *J. Mol. Biol.* **1999**, *294*, 477–485.

(8) Wagenknecht, H.-A. *Angew. Chem. Int. Ed.* **2003**, *42*, 3204–3206.

(9) Clever, G. H.; Kaul, C.; Carell, T. *Angew. Chem. Int. Ed.* **2007**, *46*, 6226–6236.

(10) Clever, G. H.; Shionoya, M. *Coord. Chem. Rev.* **2010**, *254*, 2391–2402.

(11) Stulz, E. *Chem. Eur. J.* **2012**, *18*, 4456–4469.

(12) Arkin, M.; Murphy, C. J.; Jenkins, Y. C.; Turro, N. J.; Barton, J. K. *J. Inorg. Biochem.* **1993**, *51*.

(13) Takezawa, Y.; Müller, J.; Shionoya, M. *Chem. Lett.* **2017**, *46*, 622–633.

(14) Katz, S. *Biochim. et Biophys. Acta* **1963**, *68*, 240–253.

(15) Ono, A.; Cao, S.; Togashi, H.; Tashiro, M.; Fujimoto, T.; Machinami, T.; Oda, S.; Miyake, Y.; Okamoto, I.; Tanaka, Y. *Chem. Commun.* **2008**, 4825–4827.

(16) Goren, R.; Siegel, S. M. *Plant Physiol.* **1976**, *57*, 628–631.

(17) Lee, J. S.; Latimer, L. J.; Reid, R. S. *Biochem. cell Biol.* **1993**, *71*, 162–168.

(18) Long, Y.-T.; Li, C.-Z.; Sutherland, T. C.; Kraatz, H.-B.; Lee, J. S. *Anal. Chem.* **2004**, *76*, 4059–4065.

(19) Long, Y.-T.; Li, C.-Z.; Kraatz, H.-B.; Lee, J. S. *Biophys. J.* **2003**, *84*, 3218–3225.

(20) Li, X.; Lee, J. S.; Kraatz, H.-B. *Anal. Chem.* **2006**, *78*, 6096–6101.

(21) Li, C.-Z.; Long, Y.-T.; Kraatz, H.-B.; Lee, J. S. *J. Phys. Chem. B* **2003**, *107*,

2291–2296.

(22) Roitzsch, M.; Lippert, B. *J. Am. Chem. Soc.* **2004**, *126*, 2421–2424.

(23) Alexandre, S. S.; Soler, J. M.; Seijo, L.; Zamora, F. *Phys. Rev. B* **2006**, *73*.

(24) Sagripanti, J.-L.; Goering, P. L.; Lamanna, A. *Toxicol. Appl. Pharmacol.* **1991**, *110*, 477–485.

(25) Linder, M. C. *Mutat. Res. Mol. Mech. Mutagen.* **2012**, *733*, 83–91.

(26) Ala, A.; Walker, A. P.; Ashkan, K.; Dooley, J. S.; Schilsky, M. L. *Lancet* **2007**, *369*, 397–408.

(27) Sagripant, J. L.; Kraemer, K. H. *J. Biol. Chem.* **1989**, *264*, 1729–1734.

(28) Moreno, L. I.; McCord, B. R. *Forensic Chem.* **2017**, *4*, 89–95.

(29) Thiviyanathan, V.; Somasunderam, A.; Volk, D. E.; Gorenstein, D. G. *Chem. Commun.* **2005**, 400.

(30) Greim, H.; Albertini, R. J. *The Cellular Response to the Genotoxic Insult: The Question of Threshold for Genotoxic Carcinogens*; Royal Society of Chemistry, 2012.

(31) McGill, I. *Ullmann's Encycl. Ind. Chem.* **2000**.

(32) Ono, A.; Torigoe, H.; Tanaka, Y.; Okamoto, I. *Chem. Soc. Rev.* **2011**, *40*, 5855.

(33) Deng, X.; Wilson, D. *Appl. Microbiol. Biotechnol.* **2001**, *56*, 276–279.

(34) Monteiro, L. R.; Costa, V.; Furness, R. W.; Santos, R. S. *Mar. Ecol. Prog. Ser.* **1996**, 21–25.

(35) Moreno-Jiménez, E.; Gamarra, R.; Carpena-Ruiz, R. O.; Millán, R.; Peñalosa, J. M.; Esteban, E. *Chemosphere* **2006**, *63*, 1969–1973.

(36) Wang, Q.; Kim, D.; Dionysiou, D. D.; Sorial, G. A.; Timberlake, D. *Environ. Pollut.* **2004**, *131*, 323–336.

(37) Tchounwou, P. B.; Ayensu, W. K.; Ninashvili, N.; Sutton, D. *Environ. Toxicol.* **2003**, *18*, 149–175.

(38) Eisler, R. Mercury hazards from gold mining to humans, plants, and animals. *Reviews of environmental contamination and toxicology*, 2004, 139–198.

(39) Tchounwou, P. B.; Yedjou, C. G.; Patlolla, A. K.; Sutton, D. J. *Exp. Suppl.* **2012**, 133–164.

(40) Park, J.-D.; Zheng, W. *J. Prev. Med. & Public Health* **2012**, *45*, 344–352.

(41) Krupp, E. M.; Milne, B. F.; Mestrot, A.; Meharg, A. A.; Feldmann, J. *Anal. Bioanal. Chem.* **2008**, *390*, 1753–1764.

(42) Legrand, M.; Lam, R.; Jensen-Fontaine, M.; Salin, E. D.; Chan, H. M. *J. Anal. At. Spectrom.* **2004**, *19*, 1287–1288.

(43) Han, F. X.; Patterson, W. D.; Xia, Y.; Sridhar, B. M.; Su, Y. *Water, air, soil Pollut.* **2006**, *170*, 161–171.

(44) Ceulemans, M.; Adams, F. C. *J. Anal. At. Spectrom.* **1996**, *11*, 201–206.

(45) Kawasaki, H.; Yoshimura, K.; Hamaguchi, K.; Arakawa, R. *Anal. Sci.* **2011**, *27*, 591–591.

(46) Darbha, G. K.; Ray, A.; Ray, P. C. *Acs Nano* **2007**, *1*, 208–214.

(47) Wang, J.; Qian, X.; Cui, J. *J. Org. Chem.* **2006**, *71*, 4308–4311.

(48) Chen, C.; Wang, R.; Guo, L.; Fu, N.; Dong, H.; Yuan, Y. *Org. Lett.* **2011**, *13*.

(49) Bernhoft, R. A. *J. Environ. Public Health* **2012**, *2012*.

(50) Proskuryakov, S. Y. a.; Konoplyannikov, A. G.; Gabai, V. L. *Exp. Cell Res.* **2003**, *283*, 1–16.

(51) Katz, S. *J. Am. Chem. Soc.* **1952**, *74*, 2238–2245.

(52) Thomas, C. A. *J. Am. Chem. Soc.* **1954**, *76*, 6032–6034.

(53) Miyake, Y.; Yamaguchi, H.; Ono, A.; Machinami, T.; Fujimoto, T.; Sawa, R.; Kondo, Y.; Tanaka, Y.; Kudo, M.; Oda, S.; Tashiro, M.; Togashi, H. *J. Am. Chem. Soc.* **2006**, *128*, 2172–2173.

(54) Kondo, J.; Yamada, T.; Hirose, C.; Okamoto, I.; Tanaka, Y.; Ono, A. *Angew. Chem. Int. Ed.* **2014**, *53*, 2385–2388.

(55) Šebera, J.; Burda, J.; Straka, M.; Ono, A.; Kojima, C.; Tanaka, Y.; Sychrovsk` y, V. *Chem. Eur. J.* **2013**, *19*, 9884–9894.

(56) Tanaka, Y.; Kondo, J.; Sychrovský, V.; Šebera, J.; Dairaku, T.; Saneyoshi, H.; Urata, H.; Torigoe, H.; Ono, A. *Chem. Commun.* **2015**, *51*, 17343–17360.

(57) Nam, J.-M.; Thaxton, C. S.; Mirkin, C. A. *Science* **2003**, *301*, 1884–1886.

(58) Cognet, L.; Tardin, C.; Boyer, D.; Choquet, D.; Tamarat, P.; Lounis, B. *Proc. Natl. Acad. Sci.* **2003**, *100*, 11350–11355.

(59) Cao, Y. C.; Jin, R.; Mirkin, C. A. *Science* **2002**, *297*, 1536–1540.

(60) Elghanian, R.; Storhoff, J. J.; Mucic, R. C.; Letsinger, R. L.; Mirkin, C. A. *Science* **1997**, *277*, 1078–1081.

(61) Maxwell, D. J.; Taylor, J. R.; Nie, S. *J. Am. Chem. Soc.* **2002**, *124*, 9606–9612.

(62) Liu, D.; Wang, Z.; Jiang, X. *Nanoscale* **2011**, *3*, 1421–1433.

(63) Lee, J.-S.; Han, M.; Mirkin, C. *Angew. Chem.* **2007**, *119*, 4171–4174.

(64) Xue, X.; Wang, F.; Liu, X. *J. Am. Chem. Soc.* **2008**, *130*, 3244–3245.

(65) Liu, C.-W.; Hsieh, Y.-T.; Huang, C.-C.; Lin, Z.-H.; Chang, H.-T. *Chem. Commun.* **2008**, 2242.

(66) Xu, X.; Wang, J.; Jiao, K.; Yang, X. *Biosens. Bioelectron.* **2009**, *24*, 3153–3158.

(67) Liu, C.-W.; Huang, C.-C.; Chang, H.-T. *Langmuir* **2008**, *24*, 8346–8350.

(68) Liu, D.; Qu, W.; Chen, W.; Zhang, W.; Wang, Z.; Jiang, X. *Anal. Chem.* **2010**, *82*, 9606–9610.

(69) Shah, M.; Badwaik, V.; Kherde, Y.; Waghwani, H. K.; Modi, T.; Aguilar, Z. P.; Rodgers, H.; Hamilton, W.; Marutharaj, T.; Webb, C. *Front. Biosci* **2014**, *19*, 10–2741.

(70) Miyake, Y.; Ono, A. *Tetrahedron Lett.* **2005**, *46*, 2441–2443.

(71) Ono, A.; Togashi, H. *Angew. Chem. Int. Ed.* **2004**, *43*, 4300–4302.

(72) Wang, Z.; Lee, J. H.; Lu, Y. *Chem. Commun.* **2008**, 6005–6007.

(73) Liu, C.-W.; Huang, C.-C.; Chang, H.-T. *Anal. Chem.* **2009**, *81*, 2383–2387.

(74) Liu, B.; Zeng, F.; Wu, G.; Wu, S. *Analyst* **2012**, *137*, 3717–3724.

(75) Che, Y.; Yang, X.; Zang, L. *Chem. Commun.* **2008**, 1413–1415.

(76) Tyagi, S.; Kramer, F. R. *Nat. Biotechnol.* **1996**, *14*, 303–308.

(77) Yang, R.; Jin, J.; Long, L.; Wang, Y.; Wang, H.; Tan, W. *Chem. Commun.* **2009**, 322–324.

(78) Ono, A.; Togashi, H. *Angew. Chem. Int. Ed.* **2004**, *43*, 4300–4302.

(79) Bernalte, E.; Sánchez, C. M.; Gil, E. P. *Anal. Chim. Acta* **2011**, *689*, 60–64.

(80) Carpini, G.; Lucarelli, F.; Marrazza, G.; Mascini, M. *Biosens. Bioelectron.* **2004**, *20*, 167–175.

(81) Cao, R.-G.; Zhu, B.; Li, J.; Xu, D. *Electrochem. Commun.* **2009**, *11*, 1815–1818.

(82) Ding, Y.; Niu, X.; Chen, C.; Zhao, H.; Lan, M. *Sensors Actuators B-chemical* **2011**, *158*, 383–387.

(83) Han, D.; Kim, Y.-R.; Oh, J.-W.; Kim, T. H.; Mahajan, R. K.; Kim, J. S.; Kim, H. *Anal.* **2009**, *134*, 1857–1862.

(84) Liu, X.; Sun, C.; Wu, H.; Zhang, Y.; Jiang, J.; Shen, G.; Yu, R. *Electroanalysis* **2010**, *22*, 2110–2116.

(85) Wu, D.; Zhang, Q.; Chu, X.; Wang, H.; Shen, G.; Yu, R. *Biosens. Bioelectron.* **2010**, *25*, 1025–1031.

(86) Orazem, M. E.; Tribollet, B. *Electrochemical Impedance Spectroscopy*; Wiley, 2011.

(87) Cai, W.; Xie, S.; Zhang, J.; Tang, D.; Tang, Y. *Biosens. Bioelectron.* **2017**.

(88) Liu, S.-J.; Nie, H.-G.; Jiang, J.-H.; Shen, G.-L.; Yu, R.-Q. *Anal. Chem.* **2009**, *81*, 5724–5730.

(89) Drinking Water Inspectorate. *What are the drinking water standards?*; DEFRA: Great Britain, 2017.

(90) Lee, J.-S.; Ulmann, P. A.; Han, M. S.; Mirkin, C. A. *Nano Lett.* **2008**, *8*, 529–533.

(91) Carr-Smith, J. Modified nucleic acids: structural studies and applications in biosensing, University of Birmingham, 2015.

(92) Gruenwedel, D. W. *J. Inorg. Biochem.* **1994**, *56*, 201–212.

(93) Watson, C. M.; Dwyer, D. J.; Andle, J. C.; Bruce, A. E.; Bruce, M. R. M. *Anal. Chem.* **1999**, *71*, 3181–3186.

(94) Dutta, A. K.; Sengupta, T.; Vaval, N.; Pal, S. *Int. J. Quantum Chem.* **2015**, *115*, 753–764.

(95) Scholz, F. *Electroanalytical methods*; Springer, 2002.

(96) Bard, A. J.; Faulkner, L. R. *Electrochemical methods: fundamentals and applications*; Wiley New York, 1980; Vol. 2.

(97) Chai, F.; Wang, C.; Wang, T.; Ma, Z.; Su, Z. *Nanotechnology* **2009**, *21*.

(98) Chekmeneva, E.; Díaz-Cruz, J. M.; Esteban, M.; Arino, C. *J. Electroanal. Chem.* **2010**, *644*, 20–24.

(99) Dauphin-Ducharme, P.; Plaxco, K. W. *Anal. Chem.* **2016**.

(100) Costa, M.; Christie, N. T.; Cantoni, O.; Zelikoff, J. T.; Wang, X. W.; Rossman, T. G. DNA damage by mercury compounds: An overview. *Advances in mercury toxicology*, 1991, 255–273.

Chapter 5

Biferrocenylene *vs* Ferrocene Redox Tags

5.1 Introduction

Despite its wide use within the electrochemistry field, ferrocene (Fc) has some disadvantages related to its stability, electrochemical reproducibility and sensing capabilities. The fact that, even with these issues, ferrocene remains one of the most popular redox tags for DNA biosensing is indicative of a lack of viable alternatives. Within this chapter, some of the attempts to improve ferrocene redox tags via synthetic modifications will be discussed as well as the advantages and disadvantages of the major alternatives.

5.1.1 Alternative Redox Tags

There have been many redox reporter groups considered for DNA sensing purposes. Indeed, natural nucleic acids themselves have been shown to be reduced at negative potentials on mercury electrodes (-1.5 V for cytosine and adenosine, -2.4 V for thymine and, in the case of guanine, at a potential so negative that the background current masks it, when compared with a Ag|AgCl reference electrodes). However, thus far, only guanine has been shown to exhibit reversible electrochemistry.[1,2] In practice, using the bases of DNA as a reporter group results in a range of problems. There is a lack of reproducibility as the nucleobase potentials are affected by their position within the DNA strand. The slight differences in environment often result in poorly resolved peaks and hybridisation of a target only acts to worsen this issue.[3] Also, the need to use a mercury drop electrode prevents sensor miniaturisation in addition to its being a potential health hazard and having a constantly varying electrode surface area.[4] As a result it is more common to attach and use a redox-

active tag, with well-defined and easily detectable electrochemistry, to the DNA probe strand.

A number of redox-active species have been used as tags on probes for DNA detection. Some of these are shown in Figure 5.1 and their characteristics are discussed below.

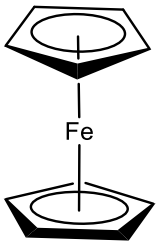

Ferrocene

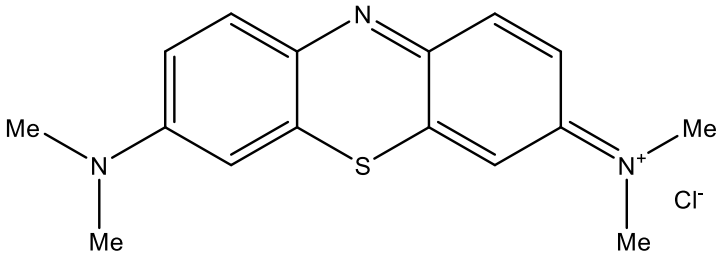

Methylene Blue

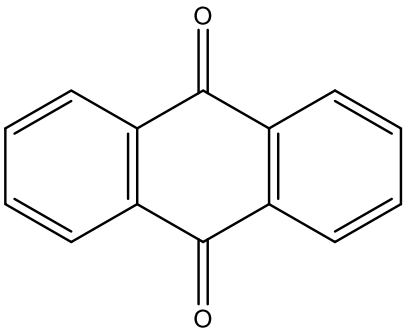

Anthraquinone

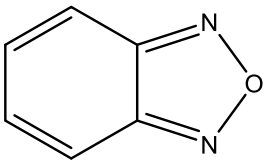

Benzofurazane

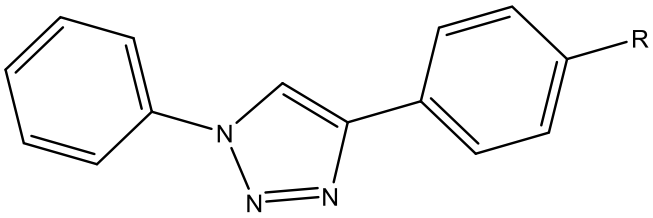

Azidophenyl

Figure 5.1 Examples of redox active tags used in DNA sensing.

Osmium-based[5–7] complexes have been used for the indirect detection of DNA targets by intercalating or binding to the duplex backbone or groove as a separate compound. SNP detection has also been achieved with thymine mispairs due to osmium complexes binding in a highly selective fashion to this nucleobase. The mismatched thymines were free to bind covalently to the OsO_4, 2,2'-bipyridine (see Figure 5.2), which resulted in ~15% increase in current compared with a matching complementary duplex.[8,9] While SNP detection down to picomolar levels is possible with these redox probes, their bulky nature, irreversible binding to the site of interest and the limited range of nucleotides that can be targeted have led to osmium compounds being rarely used for electrochemical SNP detection.[9,10]

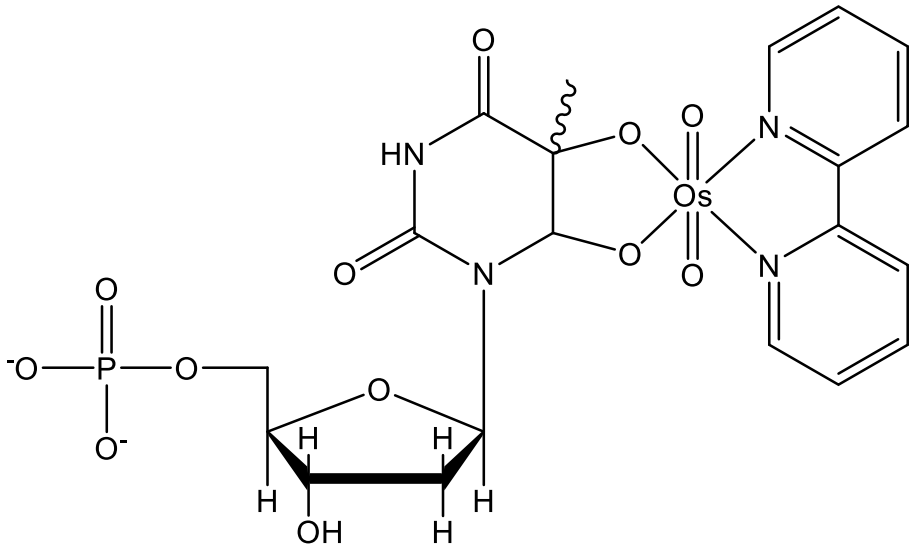

Figure 5.2 The structure resulting from OsO4, 2,2'-bipyridine redox-active probe binding covalently to a thymine nucleobase.

An alternative is an anthraquinone tag, which can be covalently attached to a nucleic acid and has been used to monitor electron transfer reactions.[11–13] It has been shown to offer both stability and reversible electrochemistry with potentials around -200 mV *vs* Ag|AgCl reference electrode. However, careful consideration of the tag linker is

required to prevent intercalation and, as shown by Hocek and co-workers, incorporation into a DNA strand can reduce the reversibility of the electrochemistry and produce poorly resolved peaks in the CV.[11]

Other examples include the use of azidophenyl[14] and benzofurazane[15] groups. However, these all suffer from similar issues, including poorly resolved peaks, high cost and the limited scale on which these tags can be produced.[16] As a result the most common alternatives to Fc redox tags are those based on methylene blue (MB). MB was first discovered in 1876 and since then has found uses as a dye, a medicine (most notably, until recently, as an antidote to cyanide poisoning) and a redox reporter, being used in a very similar way to Fc.[17–24] Although MB exhibits a two electron redox process (Figure 5.3), Ferapontova and co-workers and Kelley and Barton each reported single CV peak sets with reduction potentials of approximately -250 mV *vs* Ag|AgCl[20] and SCE[19] reference electrodes. Fc and MB share many advantages, including well understood and easily detectable electrochemistry, the relative ease with which it can be incorporated into DNA and not very negative reduction potentials. However, MB exists as a charged species (see Figure 5.1 and Figure 5.3) and so must be used in the presence of a counter ion. This can create difficulties for the manufacture of sensing devices since, in many cases, the system can only return to a fully discharged state when the SAM is neutral.[25] MB can also be more expensive and more difficult to functionalise. However, MB has an advantage in terms of its stability *vs* Fc as will be discussed in section 5.1.2.[19,20]

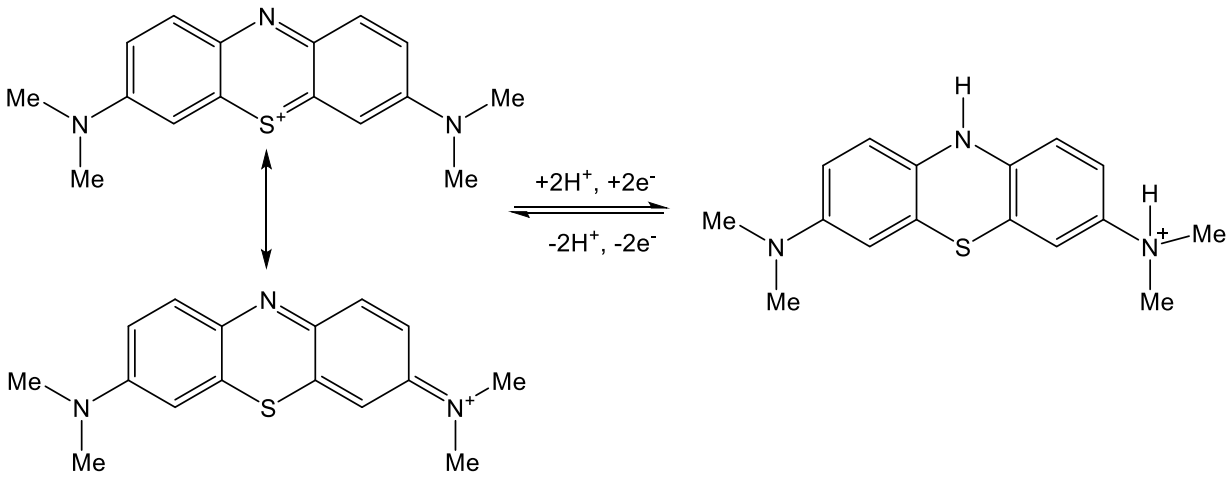

Figure 5.3 Schematic representation of the electrochemistry of MB[26]

5.1.2 Methylene Blue vs *Ferrocene*

Plaxco and co-workers[27] carried out an in depth comparison of two identical 33 nucleobase DNA probes, tagged with a thiol for surface application at the 3' terminus but with either a methylene blue or ferrocene tag attached at the 5' terminus. The DNA sensing capability, long-term stability (180 hours), ability to withstand repeated electrochemical interrogations and reusability were all investigated. The results were striking; ferrocene offered the more sensitive target recognition (an on-off system was used where Fc signal suppression was 87%, whereas MB afforded a change of 70%) but MB was the much more stable of the two and outperformed Fc in all three stability experiments. After 180 hours storage in electrolyte, 100 square wave voltammetry scans and 16 hybridisation and regeneration cycles, the Fc signal had reduced to 90, 50 and 50% of the original signal, respectively, compared with a MB signal reduction of 35, 5 and 10%, respectively. MB was also more stable in complex media (blood serum) with 85% signal recovery after 5 cycles compared with 50% for

Fc. It was also noted that the error associated with electrochemical measurements was consistently higher for Fc although no explanation for this was given.[27]

Bradley and co-workers reported similar findings when comparing Fc and MB attachments to a surface-bound peptide sequence used to monitor protease activity.[18] Both these authors suggested that any reduction in MB signal was more likely to be due to the general loss of thiol from the gold surface as a result of oxidation of the Au-S bond in air and ensuing loss of the labelled DNA from the surface.[28,29] Therefore, further reduction in Fc stability compared to MB was ascribed to the Fc tag's being more easily degraded.

5.1.2.1 Instability of the Ferrocenium Ion

The greater extent of degradation of Fc compared with MB can be understood through examining their charge when undergoing electrochemical interrogation. MB exists as a charged species and can only be used as a redox tag in the presence of a negative counter ion, and thus is reduced to a neutral molecule during the redox process.[21] Fc however is neutral and must be oxidised to a charged species, Fc^{+}, known as a ferrocenium ion.

It is known that the ferrocenium ion is particularly prone to degradation by nucleophilic attack, especially under physiological conditions.[25,30–32] Halide and OH^{-} ions are usually the most problematic since standard electrolytes are normally aqueous and Cl^{-} based; buffers are required to maintain the neutrality of the solution and to ensure that the pH does not become too alkaline, perchlorate (ClO_4^{-}) electrolytes are sometimes used instead.[33,34]

The reaction (shown in Equation 5.1[33]) has been found to occur with the following stoichiometry:

Equation 5.1: $3Fe(Cp)_2^+ + 4\ X^- \rightarrow 2Fe(Cp)_2 + FeX_4^- + 2Cp^\bullet$

This would suggest the Cp rings are initially displaced by the nucleophiles present, before the radicals are subsequently dimerised to $C_{10}H_{12.}$ Indeed, the reaction rate was found to be dependent on the nucleophile.[33,34] This reaction results in the irreversible loss of some of the redox active species and so reduces the current available to monitor. This goes some way to explain the striking differences between the stabilities of Fc and MB. An ideal redox compound would incorporate both the sensitivity and versatility (due to its uncharged nature) of Fc-based tags with the stability and reproducibility afforded by the MB-based tags.

5.1.3 Improved Ferrocene –Based Biosensing

There have been some attempts at improving the stability of ferrocene for electrochemical biosensing; however, many of these involve the covalent binding of ferrocene to large organic molecules,[35] such as cyclodextrin[36–39] or carbon nanotubes[40], and require a complex synthesis. An alternative is to capture the ferrocene unit in a polymer.[41,42] None of these methods are conducive with DNA sensing on a SAM due to the space constraints involved and the difficulties in attaching these molecules to the DNA probe.

However, Schmittel and co-workers recently reported the formation of a SAM containing a 1,1- biferrocenylene unit which may hold the key to unlocking the current status quo. 1,1-Biferrocenylene (or bis(fulvalene)diiron = BFD) was first synthesised

in 1969[43] and then electrochemically characterised in 1992.[44] It possesses mixed valency on primary oxidation to the 1+ ion and has been shown to produce two reversible redox waves corresponding to the available transitions (BFD^0/BFD^I and BFD^I/BFD^{II}). The availability of two analysable peaks (shown in Figure 5.4) raises the possibility of enhanced sensitivity and versatility for DNA sensing.

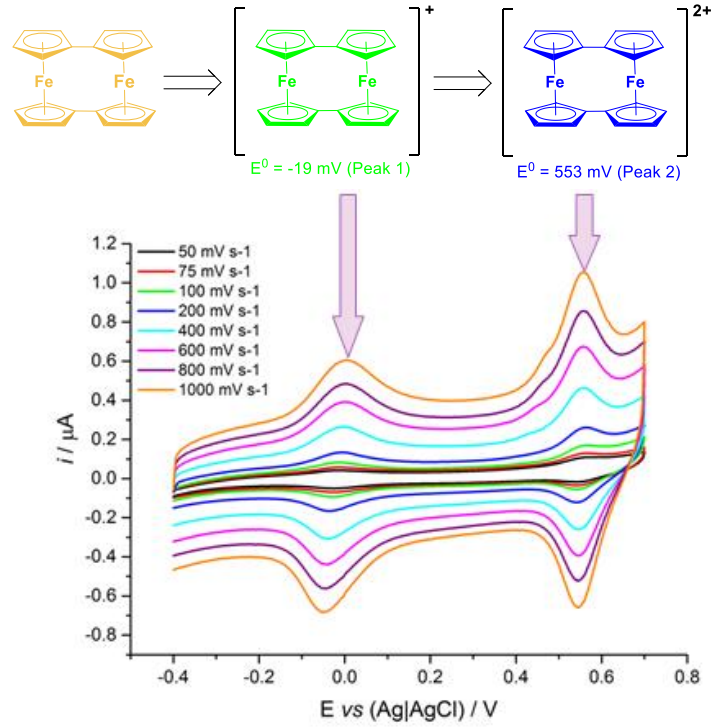

Figure 5.4 Initial studies using DNA probes with BFD tags (attached to the DNA by an 11 carbon atom linker attached at the 5' end of the sequence, not shown in the structures above) which illustrate the BFD oxidation states responsible for both redox waves. The CVs of mixed monolayers were recorded at varying scan rates, between -400 and 700 mV in 1 M $NaClO_4$, 10 mM phosphate buffer, vs Ag|AgCl reference electrode and a platinum counter electrode.

As well as this, BFD monocations have been shown to be more stable than Fc cations by one order of magnitude in solution.[45] This is possibly because the charged species is protected from potential nucleophilic attack by the close proximity of the uncharged ferrocene attached to it.

Schmittel and co-workers further studied BFD stability by comparing four different SAMs attached to the gold surface through the use of an 11 carbon alkane thiol. Two of these SAMS contained a carbonyl group directly next to the BFD group and two contained alkyl chains only. For each of these variants, one had the surface anchor chain attached to the 2' position (α) and one was attached to the 3' position (ß) on the Cp ring (see Figure 5.5).

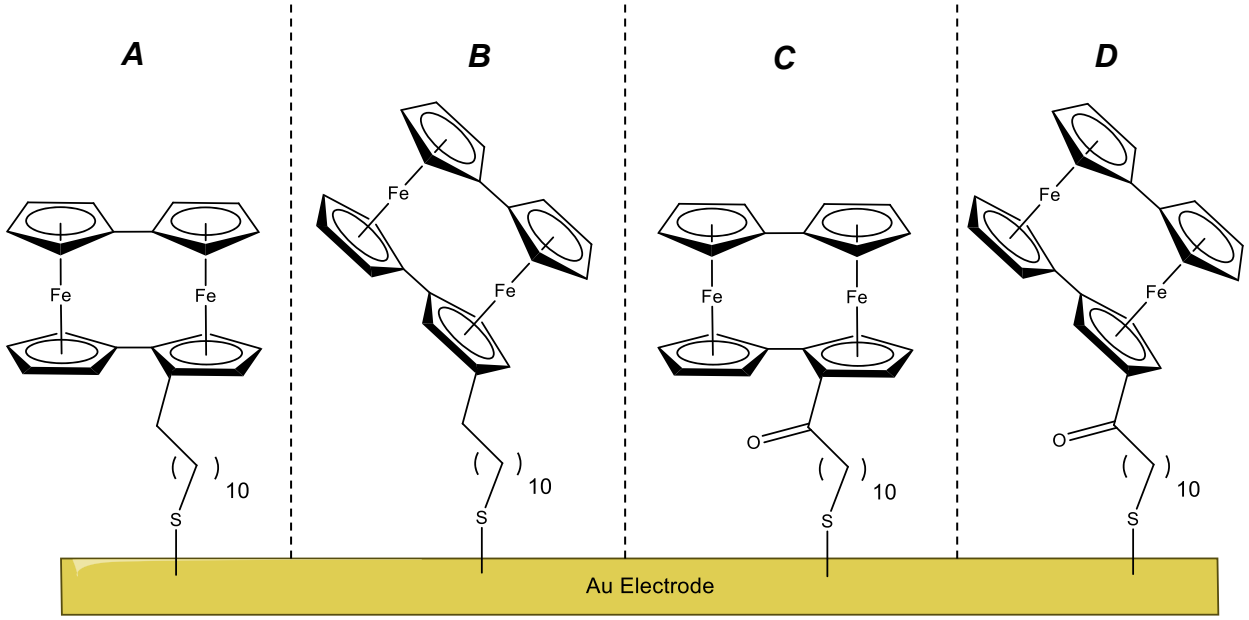

Figure 5.5 BFD variants synthesised and their electrochemical stabilities assessed by Schmittel and co-workers. *A: α alkane thiol, B: ß alkane thiol, C: α carbonyl functionalised alkane thiol, D: ß carbonyl functionalised alkane thiol*

The potential was held such that the BFD unit remained as a monocation for one hour. Comparison of the current intensities before and after this experiment showed near perfect stability between pH 0 and 7 for all the variants, with the alkane BFD SAMs also showing between 85 and 100% SAM present between pH 7 and pH 10. The carbonyl derivatives were less stable in the alkaline range (70-80% for pH 10

and 10-20% for pH 12). The position of the anchor group on the Cp ring appeared to make little difference. It is also interesting to note that changing to a mixed monolayer by introducing a decanethiol molecule further increased the SAM stability (from 85 to 98% in the case of the ß alkyl variant at pH 12), which is promising for DNA sensing since layers with well dispersed probes tend to show increased sensitivity on target binding.[25,46]

5.1.4 Conclusions and Chapter Aims

A viable alternative to the commonly used MB and Fc redox active tags has not yet been found. Both of these species have disadvantages. The former is a charged species and less sensitive than Fc and the latter possesses inherently poor stability in its oxidised state. Despite this less than perfect situation, little progress has been made towards a new redox tag that possesses both sensitivity and stability which is perhaps surprising considering the growth in electrochemical biosensing in recent decades.

However, the recent results from Schmittel and co-workers have shown a remarkable improvement in stability of the oxidised species compared with ferrocene alone across a full pH range. The reported, improved method for functionalisation that they reported also allows for simpler synthesis of a species capable of being tagged onto a DNA probe strand. Therefore, the result is a promising candidate for a stable, reusable and sensitive redox-active biosensor.[25,45]

To date, BFD has been cumbersome to synthesise and difficult to functionalise. However, the work by the Schmittel group in developing a relatively simple method for functionalising BFD may lead to its being a viable alternative for electrochemical biosensing.[45]

The following work aims compare the electrochemical stability of the BFD redox tag with that of the Fc tag when incorporated for the first time into a DNA strand at the 5' position. This study will discuss longevity, stability towards sustained potential and resilience towards multiple interrogations.

Also included below will be a comparison of the sensing capabilities of both probes using anthrax-based DNA targets as a test subject. Not only will this lead to an evaluation of the BFD tags' properties but it will also lay the foundations for future work towards the fast and sensitive detection of a potent, biological warfare agent.

5.2 Results and Discussion

5.2.1 Choice of Target

To study the sensing ability of the BFD unit, the DNA sequences used throughout this chapter correspond to short regions (23mers) of anthrax genomic DNA known to be indicative of a particular anthrax strain (full sequences are given in section 5.2.2).[47]

Anthrax results from infection by a naturally occurring bacterium (*Bacillus Anthracis*, Figure 5.6) and has received widespread attention as a result of its use as a biological warfare agent. Research into this area goes back as far as 1916[48] and bioterrorism is still a real threat with infectious spores being delivered by post as recently as 2001.[49]

Figure 5.6 Photomicrograph of Bacillus Anthracis[50]

The bacterium responsible produces a variety of toxins which cause the body's tissues to swell and break down. It can ultimately kill the host if treatment is not sought.[51] The bacteria are very resilient and can condense to a spore-like form capable of surviving for decades in the ground; livestock can become infected years after an initial contamination, and the unintentional excavation of potential sources is both a health and financial risk for the construction industry.[52,53]

Anthrax is treatable with antibiotics and antitoxins as long as aid is sought quickly.[54] For this reason it is important to have fast and accurate detection methods. Currently such methods largely involve the detection of biomarkers (such as dipicolonic acid; a major component of the anthrax spores, see Figure 5.7)[55,56] using expensive surface enhanced Raman spectroscopy (SERS)[57] or luminescent technology.[55,56]

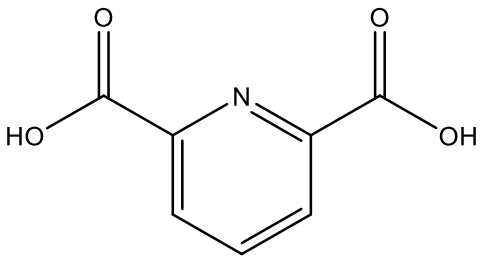

Figure 5.7 Dipicolinic acid; a major component of Bacillus Anthracis *spores and often used as a biomarker*

The detection of biomarkers, such as dipicolinic acid, make identifying a specific strain difficult since all variants are known to produce this molecule. The specificity allowed for through the detection of characteristic single nucleotide polymorphisms (SNPs) using DNA based probes may allow for the identification of the strain and determination of its geographical origin.[47] This, coupled with the speed of electrochemical detection, may offer a faster route to patient treatment and isolation of the infectious species.

5.2.2 Synthesis of the Biferrocenylene Tag

The biferrocenylene unit was provided to us by the Schmittel group as 11-bromoundecanoyl) -1,1'-biferrocenylene and and was subsequently converted into a 5' redox tag suitable for incorporation by automated DNA synthesis by Dr James Carr-Smith using the synthetic method given in Figure 5.8. The same method was used to prepare the corresponding mono-ferrocene redox tag and this was carried out by David Calder.[58]

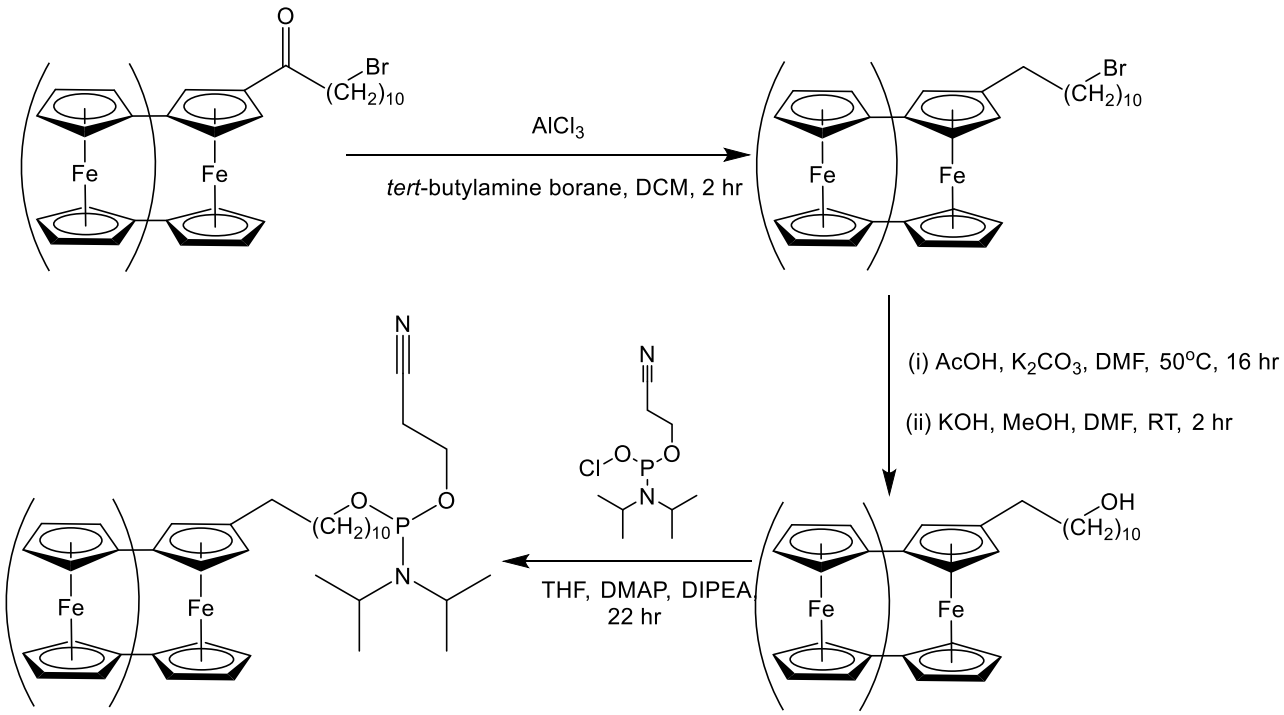

Figure 5.8 Synthetic method for the formation of the ferrocene and biferrocenylene (in brackets) phosphoramidite

5.2.3 Oligonucleotides used

The DNA strands used throughout this work are given in Table 5.1. S1 is complementary to a short section of a sequence from anthrax genomic DNA which has previously been identified as a specific strain. S2 is the complementary target sequence and S3 is a non-complementary control sequence.

Table 5.1 Sequences- S0: non-tagged probe S1: probe, S2: target, S3: non-complementary sequence. SH indicates presence of a C6 disulphide modification which is reduced to free thiol with TCEP before SAM formation.

Oligonucleotide	Sequence (5' – 3')
$S1_{(Fc\ or\ BFD)}$	**(Fc or BFD)** GT TTC TGG ATC TAC TAA TGT TTC - SH
S2	GAA ACA TTA GTA GAT CCA GAA AC
S3	TCC GCT GCA TGC TCC ATT CCA AG

5.2.4 Electrochemical Characterisation of BFD-DNA and Fc-DNA Surfaces

To ensure that no interference peaks were produced by the MCH spacer or the nucleobases themselves cyclic voltammetry (CV) of the unbound species was performed before further investigation (by interrogating mixed SAMs formed with thiolated natural DNA used in Chapter 3),. CVs of the bare Au electrode were also recorded which showed large background currents and peaks, due to the adsorption of ions in solution, which were similar to those seen in the literature.[59] However, the presence of a compact monolayer acts to block the surface of the gold and so prevents these responses, as evidenced by the lack of peaks in both the mixed monolayer and MCH only monolayer. The CVs are included in the appendix, section 8.3.

5.2.3.1 Electrochemistry of $S1_{Fc}$

The mixed monolayers were first characterised by CV at pH 7 in 1M $NaClO_4$, 10 mM phosphate buffer. The CVs of $S1_{Fc}$ mixed monolayers and the resultant scan rate vs current relationship are given in Figure 5.9.

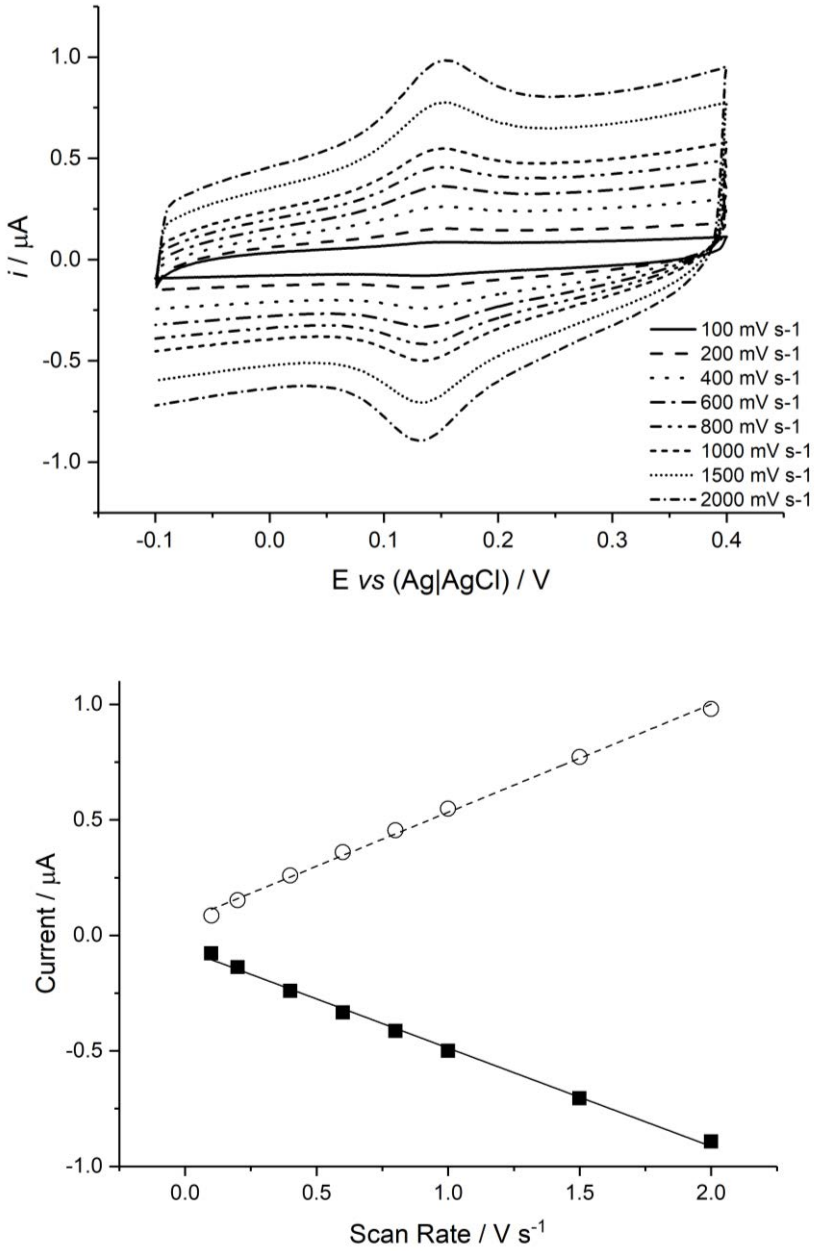

Figure 5.9 Top: CV of $S1_{Fc}$ monolayer recorded at varying scan rates, between -100 and 400 mV in 1 M $NaClO_4$, 10 mM phosphate buffer. Bottom: linear dependence of current on scan rate.

Table 5.2 contains details of the electrochemical characteristics of $S1_{Fc}$ derived from Figure 5.9. Clearly they are surface waves but the peak separation ($\Delta E_p = E_p^a - E_p^c$), 6 mV, and the cathodic to anodic peak ratio (I_p^c / I_p^a), 1.13, are slightly higher than would be expected for a molecule with completely reversible Nernstian behaviour (0 mV and 1 respectively). It has been suggested that this is due to the relatively long

single stranded DNA being flexible and not restricting the positioning of the redox tag very close to the surface. However, these values, and the strongly linear dependence of current on scan rate, still indicate highly reversible behaviour.[60]

Table 5.2 Electrochemical behaviour of S1Fc SAMs. CVs recorded at 100 mV s^{-1}. SWV recorded at 200 Hz frequency with a 1 mV step and 25 mV amplitude. Both were recorded in 1 M $NaClO_4$, 10 mM phosphate buffer, pH 7. Potentials are reported vs Ag|AgCl reference electrode. All values are an average of three replicate measurements.

			CV	
Probe	$E_{1/2}$ / mV	ΔE_p / mV	I_p^c / I_p^a	Γ / x 10^{13} molecules cm^{-2}
$S1_{Fc}$	143 (± 1.5)	6 (± 1.7)	1.13 (± 0.04)	1.36 (± 0.22)

5.2.4.2 Electrochemistry of $S1_{BFD}$

Cyclic voltammetry of mixed monolayers of $S1_{BFD}$ revealed, as was previously reported by Schmittel and co-workers, two well separated redox processes corresponding to $BFD^{0/+}$ and $BFD^{+/2+}$ as shown in Figure 5.10. The electrochemical data for each process is given in Table 5.3.[25] Interestingly, the characteristics of the two redox waves are quite different, as will be discussed below.

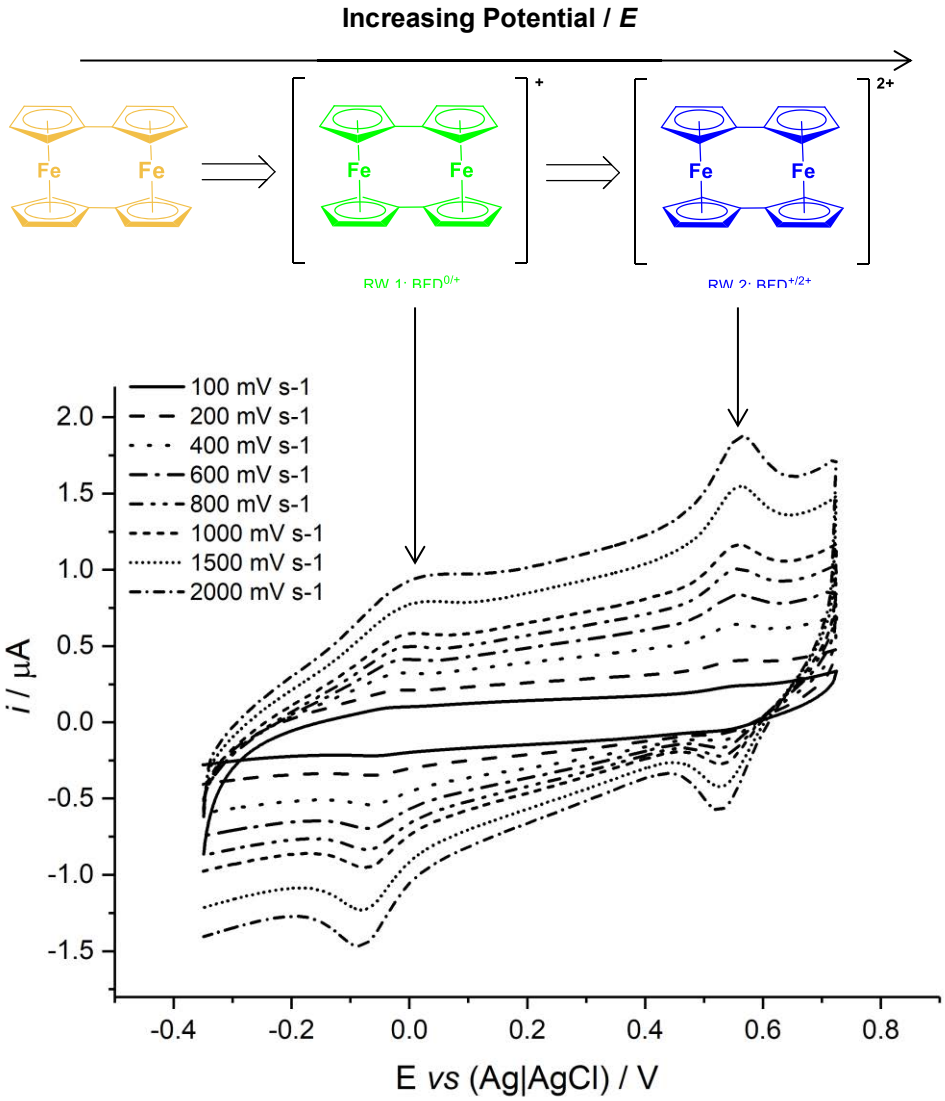

Figure 5.10 CV of $S1_{BFD}$ mixed monolayers recorded at varying scan rates in 1 M $NaClO_4$, 10 mM phosphate buffer. The oxidation states of BFD responsible for each redox wave (RW) are labelled.

Table 5.3 Electrochemical behaviour of $S1_{BFD}$ SAMs. CVs recorded at 100 mV s^{-1} in 1 M NaClO4, 10 mM phosphate buffer. Potentials are reported vs a Ag|AgCl reference electrode. All values are an average of three replicate measurements.

			CV	
RW	$E_{1/2}$ / mV	ΔE_p / mV	I_p^c / I_p^a	Γ / x 10^{13} molecules cm^{-2}
1	-37 (± 7.2)	22 (± 15.2)	0.58 (± 0.04)	2.30 (± 0.60)*
2	549 (± 3.3)	6 (± 3.9)	2.60 (± 0.10)	2.61 (± 0.83)*

It should be noted that the I_p^c / I_p^a values are far from the ideal value of 1. This could be due to several reasons. Often this can be explained by electrochemical reactions of the redox reporter that result in its degradation. However, in this case, multiple scans were recorded on the same $S1_{BFD}$ (as shown in Figure 5.10 below as well as Figure 5.4 and Figure 5.16) and no loss of current intensity for either peak was observed. Neither can this result from underlying redox processes occurring on the DNA or MCH SAMs since control experiments on the unfunctionalised systems (see section 8.3.3) showed no additional peaks across this potential range. The most likely cause is the difficulty in extrapolating a baseline. Owing to the distance of the redox centre from the electrode, both RW currents are fairly small (hence the need for increased scan rates compared with chapters 3 and 4) and the already large potential window prevents expansion to improve the baseline. Indeed, extending the potential range by 25 mV in a positive direction resulted in the appearance of shoulder peaks on the left side of RW 2, resulting from an unidentified process (see section 8.3.4 and Figure 5.4).[60,61]

The determination of the current at each peak maximum allowed plots of current *vs* scan rate to be produced (Figure 5.11). These showed good linear correlations, indicating typical surface-bound behaviour.

However, the gradients of the lines corresponding to the cathodic and anodic processes in each wave vary, in particular for RW 2. This means that the surface coverages calculated from this data are unlikely to be an accurate reflection of the SAM surface packing density. Characterisation using other methods such as XPS and AFM would be required to allow for further conclusions to be drawn about the nature of the SAM.

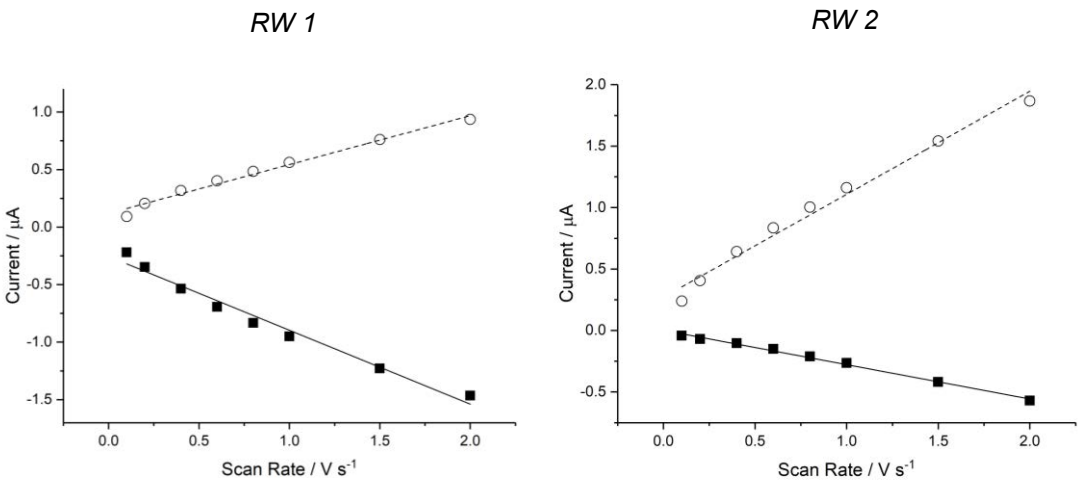

Figure 5.11 Scan rate vs. Current plots for RW 1 and RW 2 where white circles and black squares indicate data derived from anodic and cathodic peaks respectively.

5.2.4.2.1 $\Delta E_{1/2}$ of RW 1 and RW 2

The $E_{1/2}$ values for RW 1 (-37 mV) and RW 2 (549 mV) are more negative and more positive, respectively, than the value for the corresponding Fc SAMs (143 mV). The potential difference between the $E_{1/2}$ of RW 1 and 2 ($\Delta E_{1/2}$) is 586 ± 4 mV, which is slightly higher than that obtained by Schmittel and co-workers with solution-based BFD molecules under similar conditions (0.1 M $NaClO_4$, KH_2PO_4/Na_2HPO_4 buffer at pH 7; CVs were recorded at a scan rate 0.1 V s^{-1} using SAMS formed on a gold working electrode, a platinum counter electrode and Ag wire pseudo reference). However, Schmittel notes that $\Delta E_{1/2}$ decreases on confining BFD thiol to a surface from 590-600 mV to 550-570 mV, respectively.[25] This phenomenon has been reported previously in the literature and has been attributed to the constraints of surface confinement.[25,62] In the BFD unit, the Cp-Cp distance for the Fe^{II} portion of the molecule must expand to allow for the formation of the Fe^{III} (separation increases from 1.65 to 1.70 Å from metal atom to Cp ring). The Cp-Cp distance on the Fe^{III}

portion of the molecule also contracts to accommodate the remaining Fe^{II} and reduce strain (Figure 5.12).[62–64]

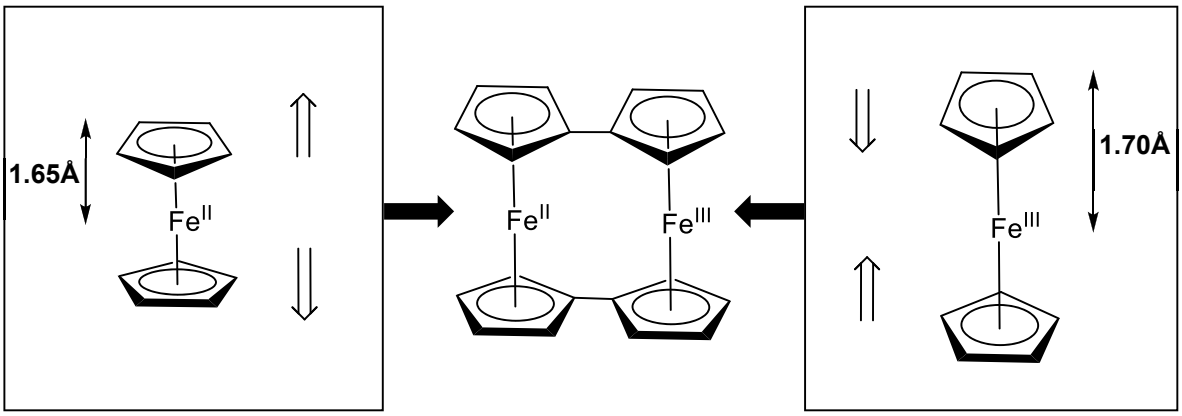

Figure 5.12 Expansion and contraction of the Cp-Cp distance for Fe^{II} and Fe^{III}, respectively, in the BFD^{I} molecule

In solution, the Cp-Cp distances within the BFD molecule can easily expand and contract without restriction, resulting in faster intramolecular electron transfer between the Fc units. This results in a delocalisation of the charge, resulting in the BFD being more resistant to further oxidation, requiring a more positive potential to oxidise both Fe atoms. However, surface confined BFD units are less able to adjust their geometries to support fast, intramolecular charge transfer and so oxidation occurs at a more negative potential. The fact that $\Delta E_{1/2}$ for the $S1_{BFD}$ SAMs are between the two values previously obtained by Schmittel, but closer to that of the freely diffusing BFD species, can be explained by its attachment to a DNA strand. The BFD unit is afforded more freedom to rearrange when attached to the 5' end of a longer 23 base DNA strand than when anchored directly through a shorter alkyl chain, so this more readily facilitates intramolecular electron transfer and therefore results in a larger $\Delta E_{1/2}$.[62]

The comproportionation constant, K_c, which gives an indication of the level of electronic coupling between two metals of different oxidation states in the same compound, can be calculated from $\Delta E_{1/2}$ using the following equation:[65]

Equation 5.2: $$K_c = 10^{\Delta E/59\,mV}$$

K_c for this system is calculated to be 8.56 x 10^9. This large value is indicative of extensive electronic coupling common in mixed valence systems and the resultant fast electron transfer between the Fe atoms.[25,65]

5.2.4.2.2 Implications of the Variance in RW 1 and RW 2 Peak Shape

There is a stark contrast in the ΔE_p values for RW 1 and RW 2 as shown in Table 5.3. For RW 2 the value is close to 0, as is expected for a surface confined species, and there is little error in this value. However, the value for RW 1 is considerably higher and has a large error associated with it. When the peak separations for every scan rate are collated in order, two differing trends became more obvious.[60,66]

As shown in Table 5.4, ΔE_p increases with increasing scan rate for RW 1, which is indicative of quasi-reversible electrochemical behaviour and slower electron transfer kinetics than for the fully reversible RW 2.[66]

Table 5.4 Peak separation values for RW 1 and RW 2 at every scan rate. Average data determined from a minimum of three experiments.

Scan Rate / $V\ s^{-1}$	RW 1 / *mV*	RW 2 / *mV*
0.1	2.5 (± 3.5)	6 (± 4.0)
0.2	4.5 (± 0.5)	7 (± 5.0)
0.4	14.5 (± 2.5)	-3.5 (± 2.5)
0.6	31.5 (± 9.5)	5 (± 1.0)
0.8	28 (± 12.0)	3 (± 2.0)
1	33 (± 13.0)	4.5 (± 2.5)
1.5	41.5 (± 4.5)	4.5 (± 0.5)
2	54 (± 0.0)	7 (± 2.0)

CV interrogations on SAMs formed with a shorter alkyl chain (Figure 5.5), as reported by Schmittel and co-workers, did not produce similar results. Instead, RW 1 for this system displayed fully reversible electrochemistry and low peak separation values. This observation is therefore more likely to be due to the distance of the BFD unit from the electrode surface rather than an inherent characteristic of the unit itself.[25]

The results can be rationalised by considering the charge at the interface. For gold electrodes the potential of zero charge (pzc) value lies between 0.3 and 0.4 V vs Ag|AgCl reference electrode.[67] This means that for RW 1 the electrode interface is likely to be negatively charged whereas it is likely to be positively charged for RW 2. The DNA strand possesses a negatively charged phosphate backbone. Therefore for RW 1, the DNA backbone would be expected to be repelled from the surface due to the negative charge of the surface interface, resulting in the 5' redox tag's being farther from the electrode surface. By contrast, for RW 2 the interface is positively charged and so attracts the backbone towards it, bringing the BFD unit into closer proximity to the electrode surface for more facile electron transfer more indicative of a surface-bound reporter (Figure 5.13).

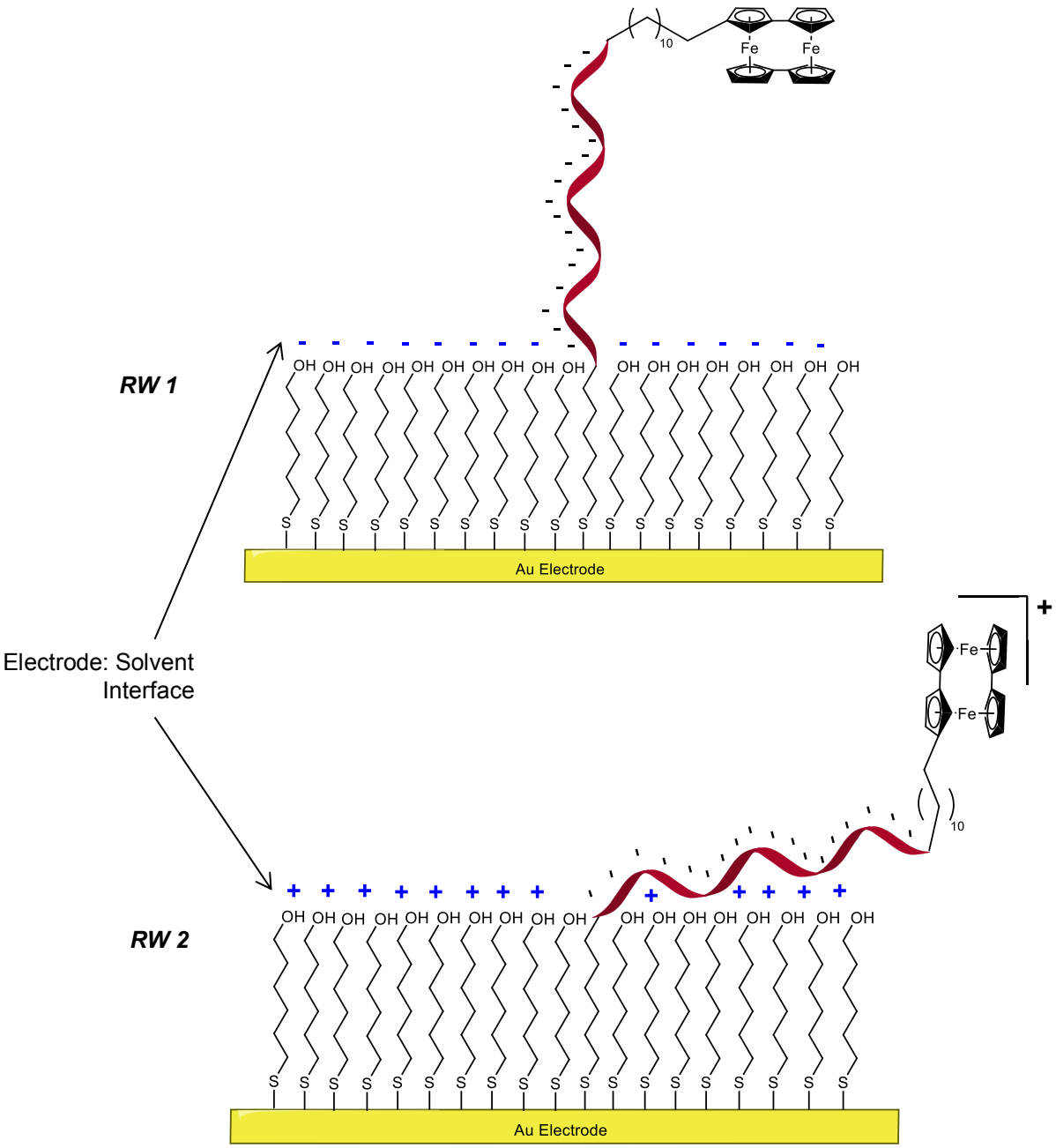

Figure 5.13 Schematic of the effect of electrode charge on the position of the DNA strand with 5' BFD redox tag. Black charge indicate charge due to DNA backbone, Blue charges indicate charge at the electrode solvent interface.

5.2.5 Stability

It was decided to use square wave voltammetry (SWV) for examining SAM stability since it had proved such a sensitive and useful technique in previous work (Chapters 3 and 4). The resultant SWVs are shown in Figure 5.14.The $E_{1/2}$ values closely

correspond with those determined using CV (Table 5.5) and the peak currents are enhanced at least 3-fold compared to CVs recorded at 2000 mV s^{-1}. The same frequency was used in this work as for the work outlined in Chapters 3 and 4. Comparisons of a range of frequencies were made using an $S1_{BFD}$ monolayer and, again, 200 Hz provided the largest signal response without the addition of artefacts. These data are included in section 8.3.

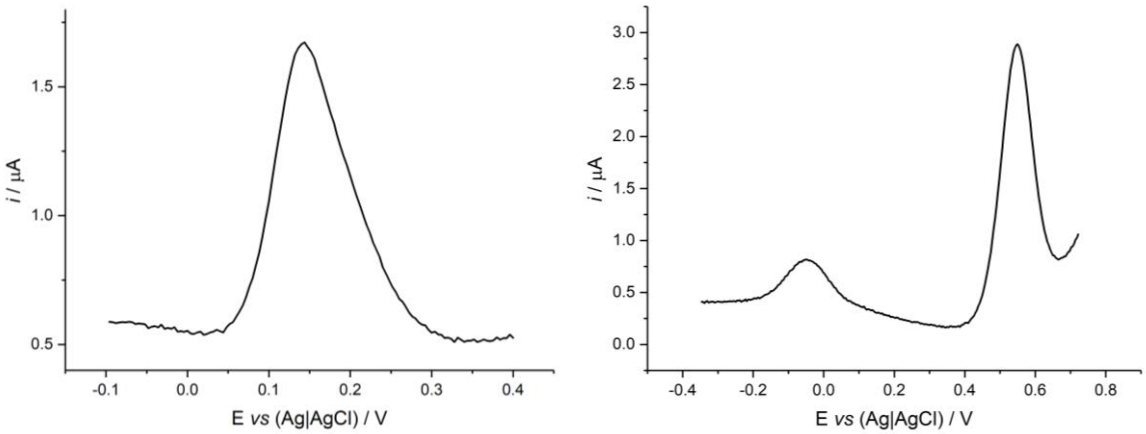

Figure 5.14 SWV of $S1_{Fc}$ (left) and $S1_{BFD}$ (right), recorded at a frequency of 200 Hz, amplitude of 25 mV and step of 1 mV. SWV recorded in 1 M $NaClO_4$, 10 mM phosphate buffer

Table 5.5 Comparison of $E_{1/2}$ data from from CV and SWV. CVs recorded at 100 mV s-1. SWV recorded at 200 Hz frequency with a 1 mV step and 25 mV amplitude. Both were recorded in 1 M NaClO4, 10 mM phosphate buffer. All values are an average of three replicate measurements

Probe	**CV** $E_{1/2}$ / mV	**SWV** $E_{1/2}$ / mV
$S1_{Fc}$	143 (± 1.5)	143 (± 1.9)
$S1_{BFD}$ RW 1	-37 (± 7.2)	-43 (± 7.7)
$S1_{BFD}$ RW 1	549 (± 3.3)	547 (± 3.8)

5.2.5.1 Stability at a Sustained Potential

In order to obtain a direct comparison with work previously carried out by Schmittel and co-workers[25], SWV of both $S1_{Fc}$ and $S1_{BFD}$ SAMs were recorded before and after holding the potential at the peak maximum for 1 hour (143, -43 and 547 mV for $S1_{Fc}$, $S1_{BFD}$ RW 1 and $S1_{BFD}$ RW 2, respectively). The potential hold was carried out in 1 M NaCl instead of 1 M $NaClO_4$ since this was more likely to cause damage to the ferrocene unit and the BFD unit had previously been shown to be more resistant to degradation than Fc in these conditions.[25] The resulting percentage changes in current (as determined from the peak maximum of the SWV) are shown in Figure 5.15.

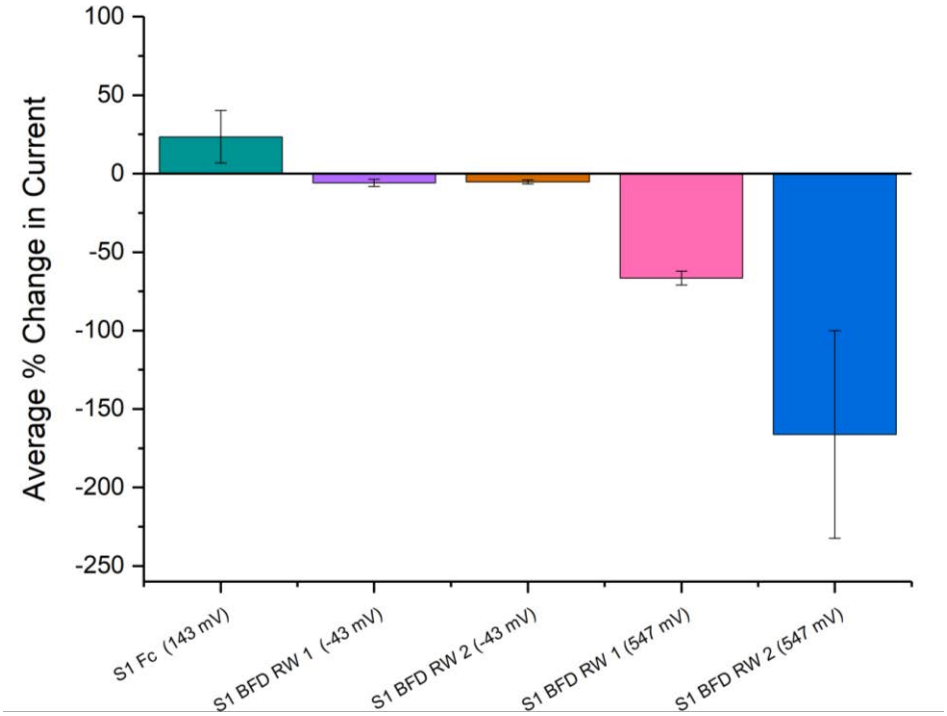

Figure 5.15 The percentage change in current of the peak maximum (of base subtracted SWV) on holding the potential at the peak maximum in 1 M NaCl for 1 hour. Potential hold performed at 143, -43 and 547 mV for $S1_{Fc}$, $S1_{BFD}$ RW 1 and $S1_{BFD}$ RW 2 respectively (BFD peak were compared after holding at both potentials). Potential hold was carried out in 1 M NaCl, 10 mM phosphate buffer. SWV were recorded at a frequency of 200 Hz, amplitude of 25 mV and step of 1 mV in 1 M NaCl, 10 mM phosphate buffer. The data is calculated as the average of three replicate measurements with error bars indicating the standard deviation of the measurements.

Unexpectedly, the $S1_{Fc}$ current showed an increase of 23% but with a large error which again highlights the issues of using Fc as a redox tag (as discussed in section 5.1.2). This observation is currently unexplained but may be a consequence of degradation of the Fc unit, resulting in a loss of full-length probes present on the surface and less competition for space at the electrode interface for electron transfer. This could be probed by AFM to determine the packing density at the surface as well as electrochemical impedance measurements to assess the resistivity of the surface to electron transfer before and after a potential hold.

As previously shown in the literature, $S1_{BFD}$ shows excellent stability and exhibits low error when held at RW 1 potential with a loss in current of 5.9 ± 2.4% and 5.3 ± 1.3% when measured using RW 1 and RW 2, respectively. Although very low and an improvement on current Fc-based redox reporters in DNA, the current loss is not as low as that reported by Schmittel for RW 1 only (0-2% loss in the same experiment, carried out in KH_2PO_4/Na_2HPO_4, 0.1 M $NaClO_4$, scan rate 0.1 V s^{-1}, using BFD units attached to the gold surface through an alkyl chain and interrogated using CV rather than SWV). Schmittel did not investigate the effect on RW 2 and so comparison is not possible.[25,27]

For both of the RWs, the percentage decrease in current is very large after holding at 547 mV (RW 2 potential) for 1 hour. This is to be expected, as the mechanism which had previously protected the BFD, the mixed valency allowing for facile electronic coupling, has now been removed and replaced with a di-cationic species, which would be even more prone to degradation.

The approximately 3-fold increase in current loss of RW 2 compared with RW 1 was probed by CV, which revealed that the anodic background current had increased dramatically (Figure 5.16). This could be due to the presence of degradation products in the electrolyte or the removal of the thiols which would result in higher average capacitance at the interface. It proved impossible to accurately distinguish the peaks accurately above the baseline.

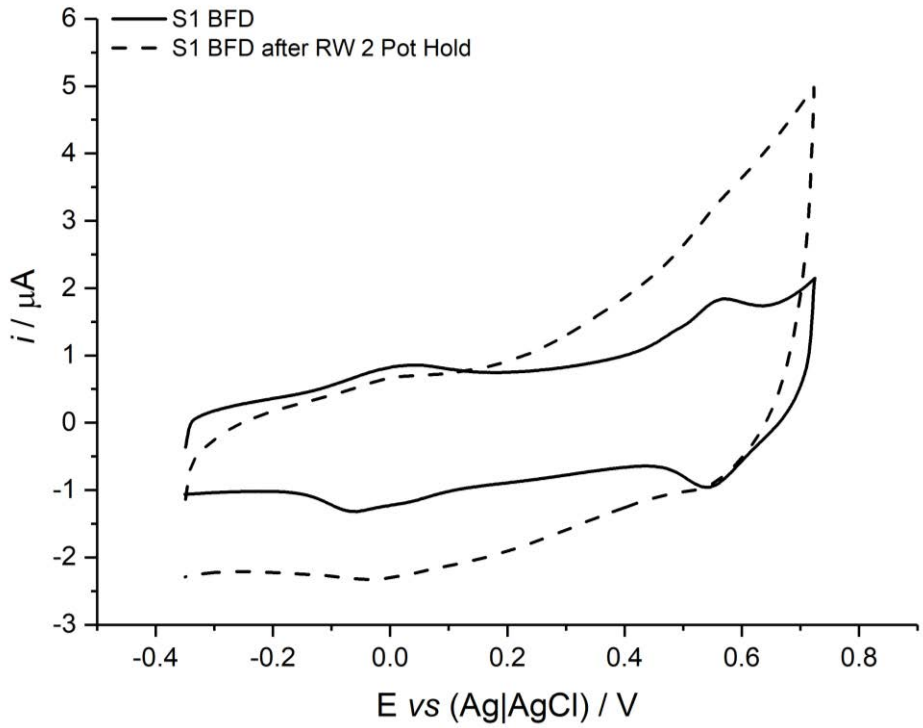

Figure 5.16 CVs of $S1_{BFD}$ recorded before and after RW 2 potential hold in 1 M NaCl. CV were recorded at 2000 mV s^{-1} in 1 M $NaClO_4$, 10 mM phosphate buffer

It is known that SWV can result in negative peaks when the frequency used is far from the 'critical frequency' for a specific molecule (i.e. the frequency which corresponds closely to the rate of electron transfer and so gives highest signal gain).[68] The inability to determine a peak above the baseline and, possibly, the sensitivity of the SWV frequency to degradation products in the electrolyte, which

affected the electron transfer rate for the remaining redox tags, resulted in a peak reversal at higher potentials with high error as demonstrated in Figure 5.17. This explains why the signal loss exhibited in Figure 5.15 is greater than 100%.

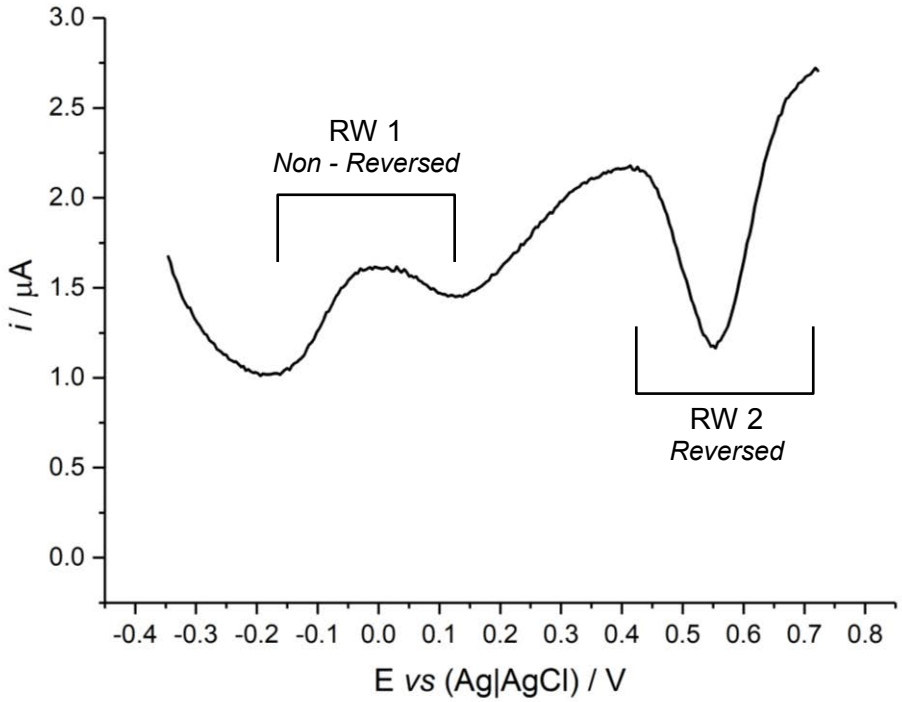

Figure 5.17 SWV of $S1_{BFD}$ recorded after potential hold at RW 2 in NaCl, exhibiting peak reversal between 0.4 and 0.7 V. SWV recorded at a frequency of 200 Hz, amplitude of 25 mV and step of 1 mV in 1 M NaCl, 10 mM phosphate buffer.

5.2.5.2 Stability towards Electrochemical Interrogation

To determine the stability of the BFD unit towards multiple electrochemical interrogations, SAMs of $S1_{Fc}$ and $S1_{BFD}$ were subjected to 150 consecutive SWV scans and the percentage change in current at the peak maxima recorded for comparison. The resulting data is shown in Figure 5.18.

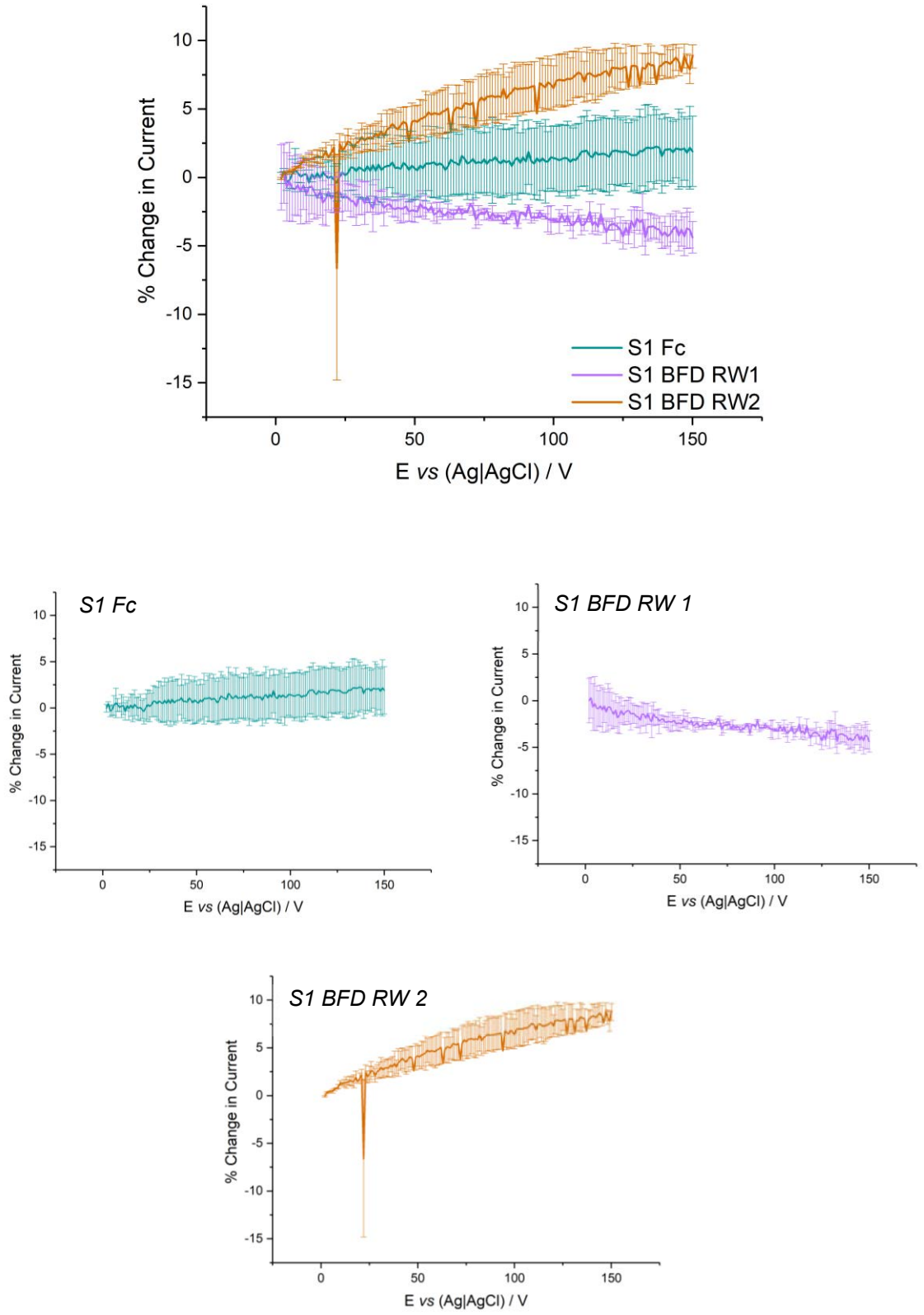

Figure 5.18 Percentage change in current (determined from SWV peak maxima) for 150 consecutive SWV scans, determined from at least three experiments. Top: All SAMs for comparison, Middle Left: $S1_{Fc}$, Middle Right: $S1_{BFD}$ RW 1, Bottom: $S1_{BFD}$ RW 2. SWV recorded at a frequency of 200 Hz, amplitude of 25 mV and step of 1 mV in 1 M $NaClO_4$, 10 mM phosphate buffer.

$S1_{Fc}$ appears to be the most stable SAM towards consecutive interrogations, with a 2% loss of current in 150 scans and consistently small error (maximum error was 3% and the average error was 2.2%). This is not consistent with current literature (which demonstrates a 50% reduction in signal with Fc redox tags). The buffer system in these cases were 10 mM HEPES, 0.5 M $NaClO_4$. It is possible that the reduced $NaClO_4$ concentration or presence of the HEPES (which is known to photo-oxidise to H_2O_2 and which in turn can oxidise Fc), resulted in increased damage to the ferrocene tag. However, neither of these theories can be confirmed without further study.[27,69]

Both $S1_{Fc}$ and $S1_{BFD}$ RW 2 exhibit slight increases in current on increasing number of consecutive scans. This is much more marked for $S1_{BFD}$ RW 2 where the maximum percentage current increase is 8.1% vs 2.3% for $S1_{Fc}$. This could be due to degradation. However, both of these redox systems exhibit surface-bound behaviour (as demonstrated in their CVs) than $S1_{BFD}$ RW 1 and therefore are more sensitive to surface structure and rearrangements. The need to interrogate thiol-based SAMs until a stable current is reached and the ability of Au-thiol based SAMs to rearrange under electrochemical potential (specifically during investigation using scanning tunnelling microscopy (STM)) have been demonstrated previously.[46,70–72] In this case, it is proposed that the rearrangements due to electrochemical interrogation or degradation (also due to electrochemical interrogation) of the probes, which causes loss of redox probes from the electrode surface, may result in diffusion of the DNA probes across the surface, allowing for more redox tags to reach the surface easily. This would enable more facile electron transfer, resulting in an increase in current.

However, this would not be the case for RW 1, which, as discussed previously, is likely to be held away from the surface. There would be very little surface blockage by the DNA strands due to repulsion of the phosphate backbone. As such there is more space for the redox tag reach and to undergo electron transfer at the surface. It can therefore be tentatively assumed that the reduction in current measured using RW 1 is due to degradation of the BFD unit, whereas this effect is cancelled out due to the increase in favourable positions for electron transfer for the surface-bound systems.

The reduction in current as measured by RW 1 is impressively low with a maximum decrease of 4.4 % over 150 scans. Fc tags have been previously shown to exhibit losses of 50% after 100 SWV scans and so the BFD tag would represent an improvement on the status quo, were it not for the corresponding Fc tag in the S1 Fc also giving improved stability under these conditions.[27] The improved stability of the BFD tag is likely due to its mixed valency, as discussed previously, protecting the tag across a large portion of the potential window as well as the presence of a second Fc unit covalently bound to the first which can act to block nucleophilic attack. The BFD tag is therefore a promising tag in terms of its stability towards multiple interrogations.

5.2.5.3 Long Term Stability

The stability of the BFD redox tag to long term storage in air and light was next assessed by storing the SAMs in 1 M NaCl, 10 mM phosphate buffer and exposing the probes to air, at room temperature, for a period of seven days. The sensors were interrogated once a day and the data compared. The results are given in Figure 5.19.

The Au-thiol bond is known to be susceptible to damage due to oxidation of the sulphur and generalised desorption from the gold surface (which as yet, is not fully understood).[28,29] This results in a loss of redox-active species in the monolayer and so some decrease in signal is to be expected.[28,29]

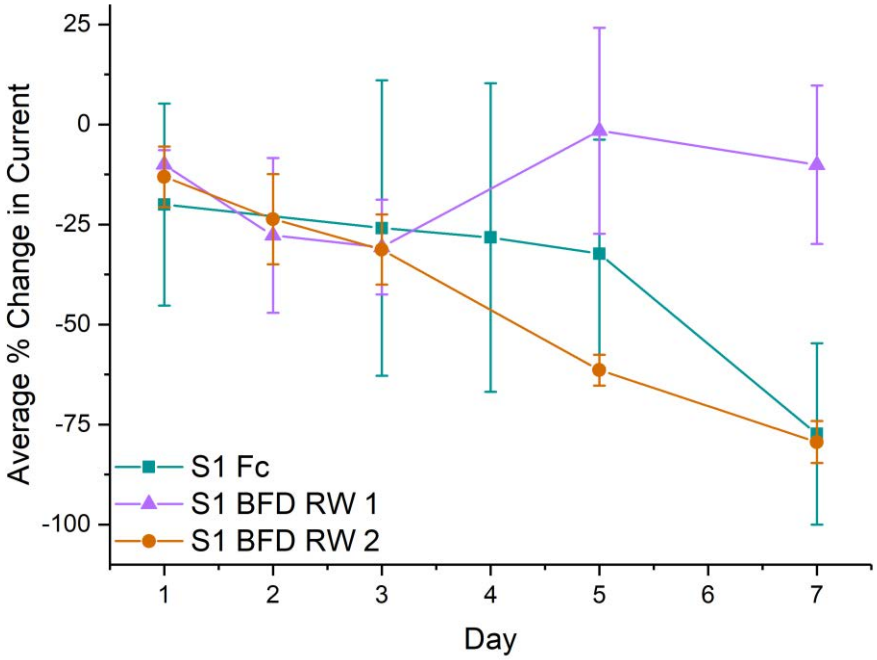

Figure 5.19 Percentage loss in current as measured from the peak maxima of the SWV for $S1_{Fc}$ and $S1_{BFD}$ over 7 days calculated from a minimum of 3 experiments. SWV measured at a frequency of 200 Hz, amplitude of 25 mV and a step of 1 mV in 1 M $NaClO_4$, 10 mM phosphate buffer. Data was calculated form three replicate measurements.

$S1_{Fc}$ and $S1_{BFD}$ RW 2 display similar losses in current (82 ± 28% and 79 ± 5%), which suggests that the use of the BFD unit does not provide an improvement to longevity in NaCl. Both $S1_{Fc}$ and $S1_{BFD}$ RW 2 lose more signal intensity when stored in NaCl for 7 days than $S1_{Fc}$ stored in $NaClO_4$ for 7 days (28 ± 7%), which would suggest these losses are due to instability of the neutral redox tags towards Cl^- ions rather than large loss of thiol attachment. It should be noted that, due to a lack of material, the same experiment but using $NaClO_4$ as a storage buffer was unable to be

completed with $S1_{BFD}$. The loss of signal after seven days for $S1_{Fc}$ in these latter conditions was 28 ± 7.5%. Further studies into whether the effect is the same in $NaClO_4$ would be advantageous to determine whether this high loss of signal for the BFD unit is due to the Cl^- ions present or the storage conditions (i.e. under air, room temperature, in light).

Interestingly RW 1 and RW 2 display very similar losses in current until day 3. After this the current measured from RW 1 increases which results in 10 ± 20 % overall loss by day 7. The unexpected current increase for RW 1 is unexplained but could be due to breakage of the Au-Thiol bonds and loss of some of the redox-active probes. This would reduce the lateral repulsive interactions between the phosphate backbones of the probes and allow for more facile electron transfer when the potential is negative of the pzc, thus resulting in an increase in signal. When the BFD unit is surface-bound (at potentials positive of the pzc and appropriate for RW 2), there are no lateral repulsions due to the negation of the DNA backbone charge and the tag is already in a position to facilitate electron transfer.

5.2.6 DNA target Sensing

The DNA sensing capability of the BFD redox tag was assessed and compared with that of the Fc redox tag by exposing the probes to an excess (100 nM) of fully complementary DNA target, S2 and a non-complementary sequence, S3, for 20 mins. Previous thermal melting studies (T_m) carried out by the Tucker group have shown that the fully complementary target (S2) forms a strong duplex with the S1 Fc and S1BFD probes. T_m values were determined to be 71 ^oC and 70 ^oC, respectively. The duplexes were then electrochemically probed to determine whether binding

could be detected using redox-active tags. As discussed previously, SWV was used due to its enhanced sensitivity. The comparison of the percentage changes in current is given in Figure 5.20.

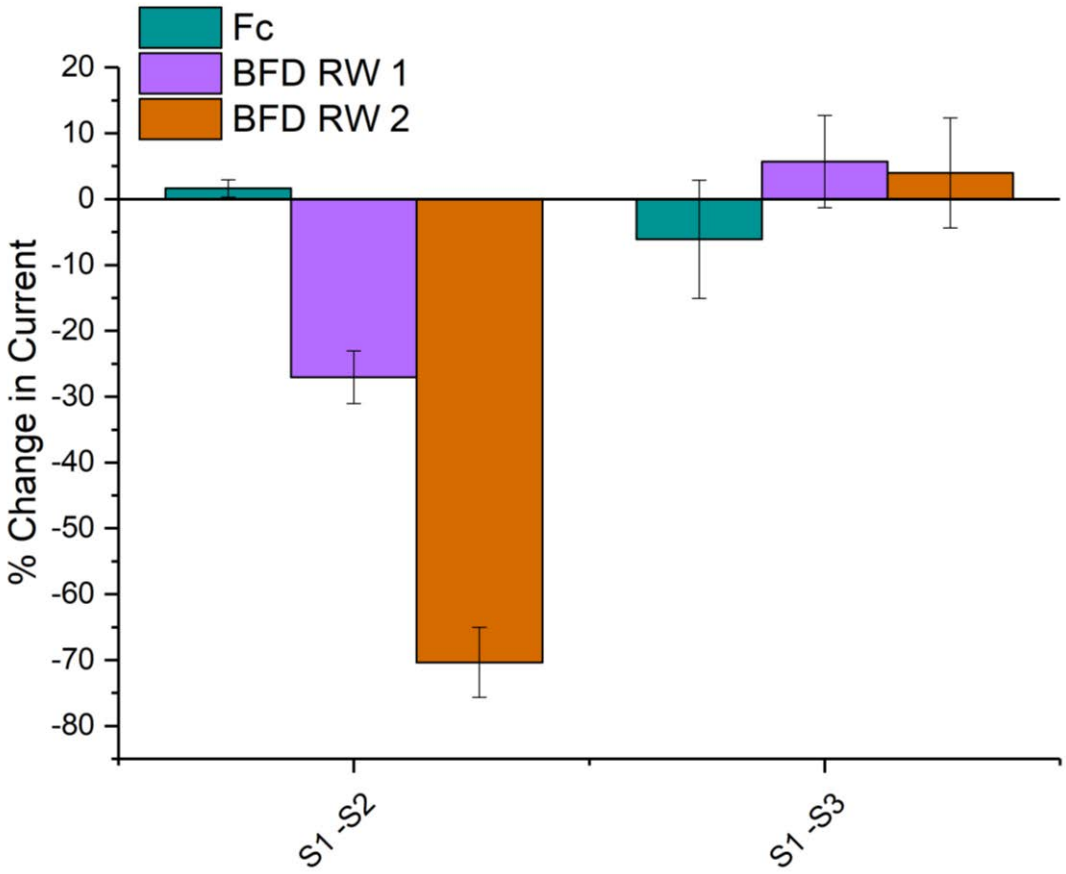

Figure 5.20 Percentage change in current (as measured from the SWV peak maximum) on binding 100 nM complementary (S2) or 100 nM non-complementary (S3) DNA target. SWV recorded at a frequency of 200 Hz, amplitude of 25 mV and step of 1 mV in 1 M $NaClO_4$, 10 mM phosphate buffer. Data is the average of three replicate measurements and the error reported is the standard deviation of these three replicate measurements.

In terms of sensing fully complementary and non-complementary targets, the BFD redox tag offers an improvement on the Fc tag. Both RW 1 and 2 show a marked loss in current on binding with excellent reproducibility (27 ± 4% and 70 ± 5%,

respectively) whereas, within error, there is essentially no change in the current for the duplex utilising Fc (1.6 ± 1.3%).

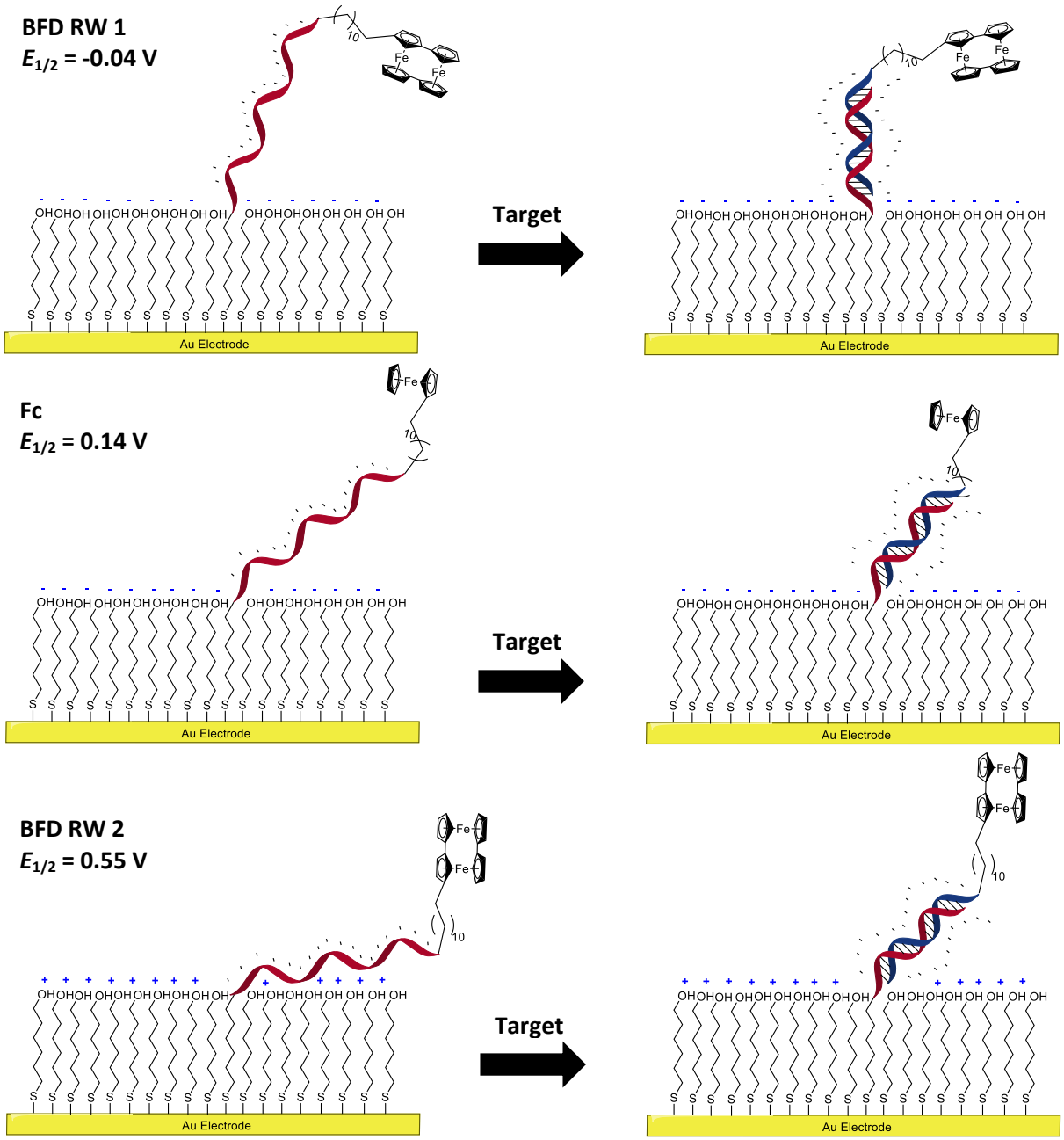

Figure 5.21 Schematic of the suggested position of single and double stranded DNA for top: S1 BFD RW 1, middle: S1 Fc and bottom: S1 BFD RW 2 at oxidation.

The cause of this will require further investigation but may be due to the extra flexibility afforded to S1 Fc at its oxidation potential, resulting in a very small change in environment on duplex formation compared with that of S1 BFD at either the RW 1 or RW 2 oxidation potential, as shown in Figure 5.21. The $E_{1/2}$ values at which both the RW 1 and RW 2 systems are probed are extreme (negative and positive, respectively) on the rational potential scale and so the single stranded probe is either repelled away from the surface or attracted closely to it. The increased rigidity of the duplexes forces the probes away from their positions at their respective oxidation potentials. However, the Fc redox tag is probed at a less negative potential than RW 1 and, as such, the repulsion of the oligonucleotide is not as strong as that of the BFD RW systems. The Fc probe is afforded much more flexibility at the $E_{1/2}$ potential in both single stranded and duplexed form and hence there is little difference in the intensity of the current for both.

The 3-fold difference in current between RW 1 and RW 2 is likely to be due to the more dramatic environmental change of the BFD unit when at higher potential. As discussed previously, the backbone of the single stranded DNA is likely to be lying close to the electrode surface for potentials appropriate for RW 2 due to electrostatic reasons (Figure 5.13). However, hybridisation forms a more rigid species with a wider molecular diameter.[73] This is likely to cause the redox tag to be held farther from the surface and so reduces the ease of electron transfer. The BFD tag is held farther from the surface at potentials appropriate for RW 1 and so the increase in distance from the electrode surface on hybridisation is not as great.

As expected, there was very little change in current when both $S1_{Fc}$ and $S1_{BFD}$ were exposed to the non-complementary target strand, S3, implying no binding is occurring, as expected.

5.3 Conclusions

The stability and sensing capabilities of a BFD unit attached by an alkyl linker to the 5' end of a DNA probe complementary to a short anthrax genetic sequence was investigated. The long term stability in NaCl and ambient conditions, stability to successive electrochemical interrogations and potential hold in NaCl were all investigated and compared with those of the most common redox tags used, Fc.

The aim of this work was to assess whether the BFD unit could improve the current status quo and be used as a redox tag with improved reproducibility and stability akin to MB whilst retaining the sensitivity associated with Fc tags. For this system, while the ability to sense a complementary target is improved when using the BFD unit, the result of the degradation studies give mixed results.

The BFD unit shows no improvement in longevity compared to Fc in these studies when assessing the data resulting from RW 2. However, the data from the BFD system highlights the interesting differences in the behaviour of surface-bound redox-active species and of those more reliant on diffusion, as exemplified by the significant difference in current loss for RW 1 and RW 2 after standing for several days. RW 1 possessed lower error and a decrease in current when being successively interrogated by SWV at 200 Hz compared to RW 2 (which actually increased in current, similarly to the Fc tag), again due to the different sensitivities of surface-bound and solution-based redox tags. It should however be noted that both increase

(less than 10%) and decrease (less than 5%) in signal for RW 2 and 1 respectively still display an excellent stability towards multiple interrogations, notwithstanding the observation of greatly improved stability for the Fc system compared to previous reports.[27]

Degradation due to holding the potential at both RW 1 and RW 2 showed that the BFD unit is extremely stable when in the $BFD^{0/+}$ form for extended periods in NaCl but not as stable when held at more positive potentials appropriate for RW 2.

In conclusion, the lower error generally afforded by the BFD unit in comparison with Fc, enhanced target sensing, stability towards consecutive interrogations and stability in the $BFD^{0/+}$ form for extended periods make BFD an attractive alternative to both MB and Fc on the condition that BFD SAMs are used as soon as possible after assembly. It could also be used a test bed to investigate further the differences in behaviour between surface-bound and solution-based redox tags.

However, further work needs to be done to improve the longevity of these SAMs to allow for long term storage and use. Also, this author suggests that, due to the instability of the $BFD^{+/2+}$ species, using this tag at positive potentials would be difficult.

It is worth noting that, for the BFD system, sensing can be performed at more negative potentials (for RW 1) than those used for Fc, which may aid probe stability and sensing suitability.

5.4 Further Work

To further the investigations of the BFD species as an improved redox reporter, the SAMs described above should be fully characterised using AFM and XPS to determine a more accurate surface coverage and probe distribution. More BFD tag

should also be synthesised to compare with the longevity of the Fc tag in $NaClO_4$ as well as the NaCl data already acquired.

5.5 References

(1) Palecek, E.; Scheller, F.; Wang, J. *Electrochemistry of nucleic acids and proteins: towards electrochemical sensors for genomics and proteomics*; Elsevier, 2005; Vol. 1.

(2) Cummings, T. E.; Elving, P. J. *J. Electroanal. Chem. Interfacial Electrochem.* **1979**, *102*, 237–248.

(3) Hocek, M.; Fojta, M. *Chem. Soc. Rev.* **2011**, *40*, 5802–5814.

(4) Vyskočil, V.; Barek, J. *Crit. Rev. Anal. Chem.* **2009**, *39*, 173–188.

(5) Maruyama, K.; Mishima, Y.; Minagawa, K.; Motonaka, J. *Anal. Chem.* **2002**, *74*, 3698–3703.

(6) Lukasova, E.; Jelen, F.; Palecek, E. *Gen. Physiol. Biophys* **1982**, *1*, 53–70.

(7) Fojta, M.; Havran, L.; Billova, S.; Kostecka, P.; Masarik, M.; Kizek, R. *Electroanalysis* **2003**, *15*, 431–440.

(8) Fojta, M.; Billova, S.; Havran, L.; Pivonˇkova, H.; Cˇernocka, H.; Horáková, P.; Paleček, E. *Anal. Chem.* **2008**, *80*, 4598–4605.

(9) Kostečka, P.; Havran, L.; Bittová, M.; Pivoňková, H.; Fojta, M. *Anal. Bioanal. Chem.* **2011**, *400*, 197–204.

(10) Drummond, T. G.; Hill, M. G.; Barton, J. K. *Nat. Biotechnol.* **2003**, *21*, 1192–1199.

(11) Balintová, J.; Pohl, R.; Horáková, P.; Vidláková, P.; Havran, L.; Fojta, M.; Hocek, M. *Chem. - Eur. J.* **2011**, *17*, 14063–14073.

(12) Vidláková, P.; Pivoňková, H.; Fojta, M.; Havran, L. *Monatshefte für Chem. - Chem. Mon.* **2015**, *146*, 839–847.

(13) Jacobsen, M. F.; Ferapontova, E. E.; Gothelf, K. V. *Org. & Biomol. Chem.* **2009**, *7*, 905–908.

(14) Balintova, J.; Spacek, J.; Pohl, R.; Brazdova, M.; Havran, L.; Fojta, M.; Hocek, M. *Chem. Sci.* **2015**, *6*, 575–587.

(15) Balintová, J.; Plucnara, M.; Vidláková, P.; Pohl, R.; Havran, L.; Fojta, M.; Hocek, M. *Chem. Eur. J.* **2013**, *19*, 12720–12731.

(16) Hocek, M. *J. Org. Chem.* **2014**, *79*, 9914–9921.

(17) Wainwright, M.; Crossley, K. B. *J. Chemother.* **2002**, *14*, 431–443.

(18) González-Fernández, E.; Avlonitis, N.; Murray, A. F.; Mount, A. R.; Bradley, M.

Biosens. Bioelectron. **2016**, *84*, 82–88.

(19) Kelley, S. O.; Barton, J. K.; Jackson, N. M.; Hill, M. G. *Bioconjugate Chem.* **1997**, *8*, 31–37.

(20) Farjami, E.; Campos, R.; Ferapontova, E. E. *Langmuir* **2012**, *28*, 16218–16226.

(21) Lu, Z.; Dong, S. *J. Chem. Soc., Faraday Trans. 1* **1988**, *84*, 2979–2986.

(22) Cummings, T. F. *Occup. Med.* **2004**, *54*, 82–85.

(23) Ozkan, D.; Kara, P.; Kerman, K.; Meric, B.; Erdem, A.; Jelen, F.; Nielsen, P. E.; Ozsoz, M. *Bioelectrochemistry* **2002**, *58*, 119–126.

(24) Gu, J.; Lu, X.; Ju, H. *Electroanalysis* **2002**, *14*.

(25) Breuer, R.; Schmittel, M. *Organometallics* **2012**, *31*, 6642–6651.

(26) Silva, F.; Vieira, S.; Goulart, L.; Boodts, J.; Brito-Madurro, A.; Madurro, J. *Int. J. Mol. Sci.* **2008**, *9*, 1173–1187.

(27) Kang, D.; Zuo, X.; Yang, R.; Xia, F.; Plaxco, K. W.; White, R. J. *Anal. Chem.* **2009**, *81*, 9109–9113.

(28) Willey, T. M.; Vance, A. L.; Van Buuren, T.; Bostedt, C.; Terminello, L. J.; Fadley, C. S. *Surf. Sci.* **2005**, *576*, 188–196.

(29) Mani, G.; Johnson, D. M.; Marton, D.; Dougherty, V. L.; Feldman, M. D.; Patel, D.; Ayon, A. A.; Agrawal, C. M. *Langmuir* **2008**, *24*, 6774–6784.

(30) Hurvois, J. P.; Moinet, C. *J. Organomet. Chem.* **2005**, *690*, 1829–1839.

(31) Holeček, J.; HandlíŖ, K.; Klikorka, J.; Bang, N. D. *Collect. Czechoslov. Chem. Commun.* **1979**, *44*, 1379–1387.

(32) Abbott, N. L.; Whitesides, G. M. *Langmuir* **1994**, *10*, 1493–1497.

(33) Prins, R.; Korswagen, A. R.; Kortbeek, A. G. T. G. *J. Organomet. Chem.* **1972**, *39*, 335–344.

(34) Karpinski, Z. J.; Nanjundiah, C.; Osteryoung, R. A. *Inorg. Chem.* **1984**, *23*, 3358–3364.

(35) Padeste, C.; Grubelnik, A.; Tiefenauer, L. *Biosens. Bioelectron.* **2000**, *15*, 431–438.

(36) Liu, S.; Mo, W.; Chen, F. *J. Instrum. Anal.* **1999**, *18*, 42–45.

(37) Bersier, P. M.; Bersier, J.; Klingert, B. *Electroanalysis* **1991**, *3*, 443–455.

(38) Groom, C. A.; Luong, J. H. T. *Biosens. Bioelectron.* **1994**, *9*, 305–313.

(39) Guorong, Z.; Xiaolei, W.; Xingwang, S.; Tianling, S. *Talanta* **2000**, *51*, 1019–1025.

(40) Tripathi, V. S.; Kandimalla, V. B.; Ju, H. *Biosens. Bioelectron.* **2006**, *21*, 1529–1535.

(41) Fernández, L.; Carrero, H. *Electrochimica Acta* **2005**, *50*, 1233–1240.

(42) Brown, R. S.; Luong, J. H. *Anal. Chim. Acta* **1995**, *310*, 419–427.

(43) Hedberg, F. L.; Rosenberg, H. *J. Am. Chem. Soc.* **1969**, *91*, 1258–1259.

(44) Sakamoto, K.; Nishihara, H.; Aramaki, K. *J. Chem. Soc. Dalton Trans.* **1992**, 1877–1881.

(45) Breuer, R.; Schmittel, M. *Organometallics* **2012**, *31*, 1870–1878.

(46) Ricci, F.; Zari, N.; Caprio, F.; Recine, S.; Amine, A.; Moscone, D.; Palleschi, G.; Plaxco, K. W. *Bioelectrochemistry* **2009**, *76*, 208–213.

(47) Qi, Y.; Patra, G.; Liang, X.; Williams, L. E.; Rose, S.; Redkar, R. J.; DelVecchio, V. G. *Appl. Environ. Microbiol.* **2001**, *67*, 3720–3727.

(48) Bisher, J. *Mil. Hist.* **2003**, *20*.

(49) Cole, L. A. *The Anthrax Letters: A Bioterrorism Expert Investigates the Attacks that Shocked America*; Skyhorse Publishing Inc., 2009.

(50) Centers for Disease Control and Prevention; Public Health Image Library (PHIL). Details https://phil.cdc.gov/phil/details.asp (accessed Jul 24, 2017).

(51) Gao, M.; Schulten, K. *Biophys. J.* **2006**, *90*, 3267–3279.

(52) Guillemin, J. *Anthrax: the investigation of a deadly outbreak*; Univ of California Press, 1999.

(53) Bloomfield, R. Crossrail work stopped after human bones found on site. *The Evening Standard*, 2009.

(54) Centers of Disease Control and Prevention. Treatment https://www.cdc.gov/anthrax/medical-care/treatment.html (accessed Jul 24, 2017).

(55) Seo, H.; Singha, S.; Ahn, K. H. *Asian J. Org. Chem.* **2017**.

(56) Ai, K.; Zhang, B.; Lu, L. *Angew. Chem.* **2009**, *121*, 310–314.

(57) Zhang, X.; Yonzon, C. R.; Duyne, R. P. V. *Plasmonics: Met. Nanostructures Their Opt. Prop.* **2003**.

(58) Calder, D. *The Synthesis of ferrocene and 1,1'-biferrocenylene Tagged DNA*

Strands Towards Electrochemical DNA Sensing; 2014.

(59) Wei, Y.; Yang, R.; Li, X.-Z.; Wang, L.; Huang, X.-J. *Anal.* **2011**, *136*, 3997.

(60) Bard, A. J.; Faulkner, L. R. *Electrochemical methods: fundamentals and applications*; Wiley New York, 1980; Vol. 2.

(61) Wood, P. M. *Biochem. J* **1988**, *253*, 287–289.

(62) Dong, T.-Y.; Chang, L.-S.; Tseng, I.-M.; Huang, S.-J. *Langmuir* **2004**, *20*, 4471–4479.

(63) Mammano, N. J.; Zalkin, A.; Landers, A.; Rheingold, A. L. *Inorg. Chem.* **1977**, *16*, 297–300.

(64) Seiler, P.; Dunitz, J. D. *Acta Crystallogr. Sect. B Struct. Crystallogr. Cryst. Chem.* **1979**, *35*, 1068–1074.

(65) Kaim, W.; Klein, A.; Glöckle, M. *Accounts Chem. Res.* **2000**, *33*, 755–763.

(66) Scholz, F. *Electroanalytical methods*; Springer, 2002.

(67) Kasuya, M.; Sogawa, T.; Masuda, T.; Kamijo, T.; Uosaki, K.; Kurihara, K. *J. Phys. Chem. C* **2016**, *120*, 15986–15992.

(68) White, R. J.; Plaxco, K. W. *Anal. Chem.* **2009**, *82*, 73–76.

(69) Lepe-Zuniga, J. L.; Zigler, J. S.; Gery, I. *J. Immunol. Methods* **1987**, *103*, 145.

(70) Zhang, Q. D.; March, G.; Noel, V.; Piro, B.; Reisberg, S.; Tran, L. D.; Hai, L. V.; Abadia, E.; Nielsen, P. E.; Sola, C.; Pham, M. C. *Biosens. Bioelectron.* **2012**, *32*, 163–168.

(71) Stranick, S. J.; Parikh, An.; Allara, D. L.; Weiss, P. S. *J. Phys. Chem.* **1994**, *98*, 11136–11142.

(72) Wu, Z.-S.; Chen, C.-R.; Shen, G.-L.; Yu, R.-Q. *Biomaterials* **2008**, *29*, 2689–2696.

(73) Anne, A.; Demaille, C. *J. Am. Chem. Soc.* **2006**, *128*, 542–557.

Chapter 6

Enzymatic Digestion of Ferrocene Nucleic Acids

6.1 Introduction

6.1.1 Enzymes

Enzymes are the catalysts of the natural world and have the same overall function as any other catalytic species; the lowering of the activation barrier of a reaction to increase the reaction rate. Enzymes are vitally important macromolecules. Without them, biochemical reactions could not occur fast enough to support the large and complex life forms which exist today. From the transport of CO_2 away from the tissues to the production of DNA, enzymes are present in nearly every part of the body.[1]

6.1.1.1 The Structure of Enzymes

Enzymes are proteins, though a noticeable exception to this is the ribozymes which are made from ribonucleic acid chains (RNA) and are fundamental in the translation of RNA to proteins.[2] Proteins consist of a chain of amino acids, of which there are twenty-two naturally incorporated variations, joined by peptide bonds (Figure 6.1).[1]

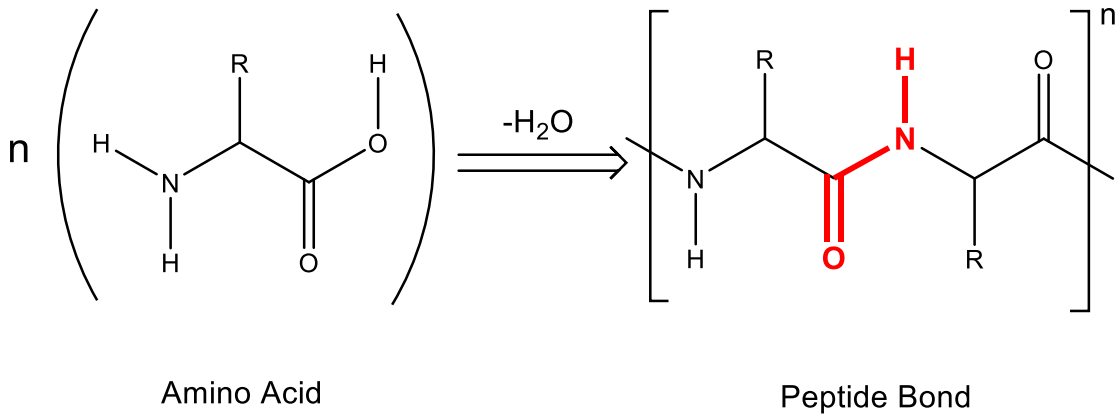

Figure 6.1 The formation of a peptide bond from a generic amino acid (where R is the side chain)

Amino acids can interact with different parts of a polypeptide chain through non-covalent interactions, such as hydrogen bonding. In addition, some amino acids (phenylalanine, tryptophan and tyrosine) have side chains that contain aromatic groups, allowing for π-π stacking. Furthermore, the amino acid cysteine, whose side chain contains a thiol, can form a S-S bond when in close proximity to another cysteine and covalently link previously independent sections of the chain through a 'disulphide bridge'.[3] These interactions, in combination, result in folding alpha-helices and beta-pleated sheets (Figure 6.2) which give a more rigid, secondary structure.

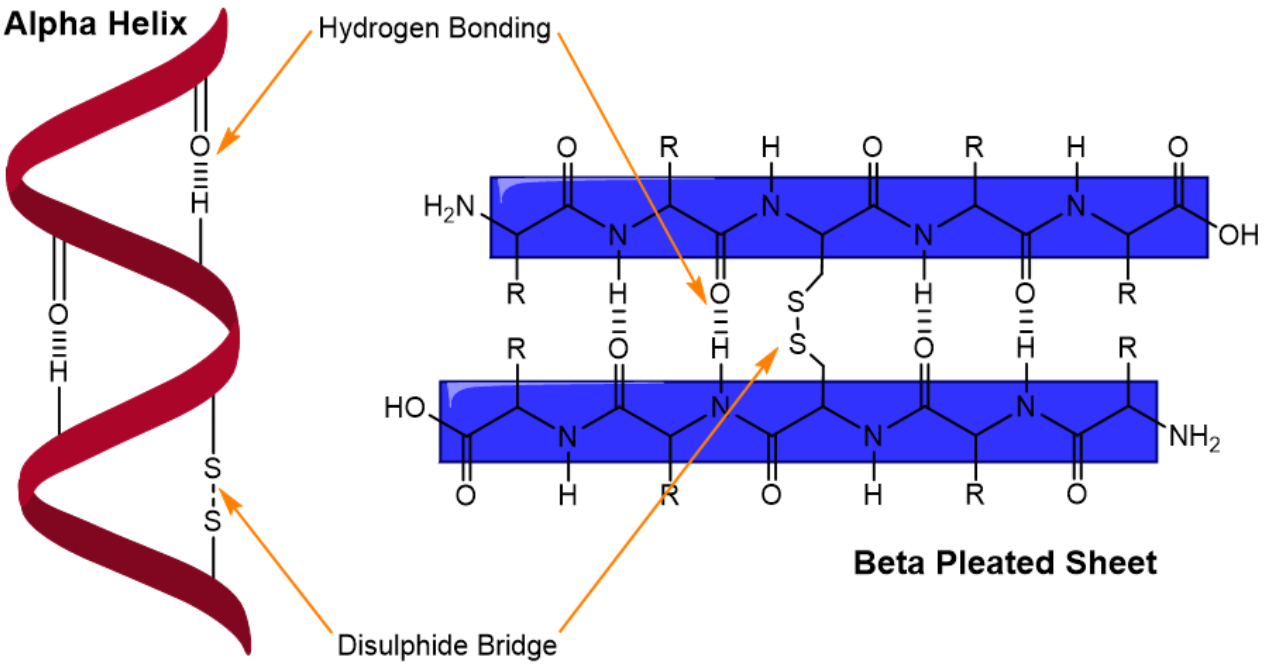

Figure 6.2 The secondary structure of polypeptide chains

Further structural elements include turns and loops, which allow the chain to change direction.[1] This allows the secondary-structure assemblies to interact with each other to give more complicated tertiary structures. The overall shape of the resultant protein is therefore completely dependent on the initial amino acid sequence. The shape of the protein dictates its function and many enzymes are made up of a small collection of proteins interacting. Recently, much research has focussed on the *de novo* design of enzymes to perform specific roles in healthcare and industry.[4–6]

6.1.1.2 Substrate Recognition

The structure of the protein dictates which compound can bind (known as the substrate) to the reactive site (known as the active site). This usually means that enzymes are highly specific biocatalysts.[7] However, enzymes have some flexibility and a number of different methods for substrate recognition have been suggested.

The simplest model, known as the "Lock and Key" model, was the earliest proposal to explain enzyme specificity and relies purely on the premise that the enzyme and substrate must have corresponding geometries in order to fit together, as shown in Figure 6.3.[8] This was further advanced by Koshland in 1958 in an attempt to explain the catalytic nature of the enzymes. It was suggested that preliminary interactions between the substrate and amino acids in the enzyme caused a slight change in the shape of the active site, inducing a better fit with the substrate. This idea also helped to explain the very high specificity of some enzymes.[9]

Additionally, some enzymes require small molecules (known as cofactors) to bind at a site located some distance from the active site (known as the allosteric site). This again allows for a change in the shape of the active site and allows the substrate to

bind. This ability to activate and inhibit the enzyme in the presence of particular molecules is essential for successful regulation of the body.[1,10,11]

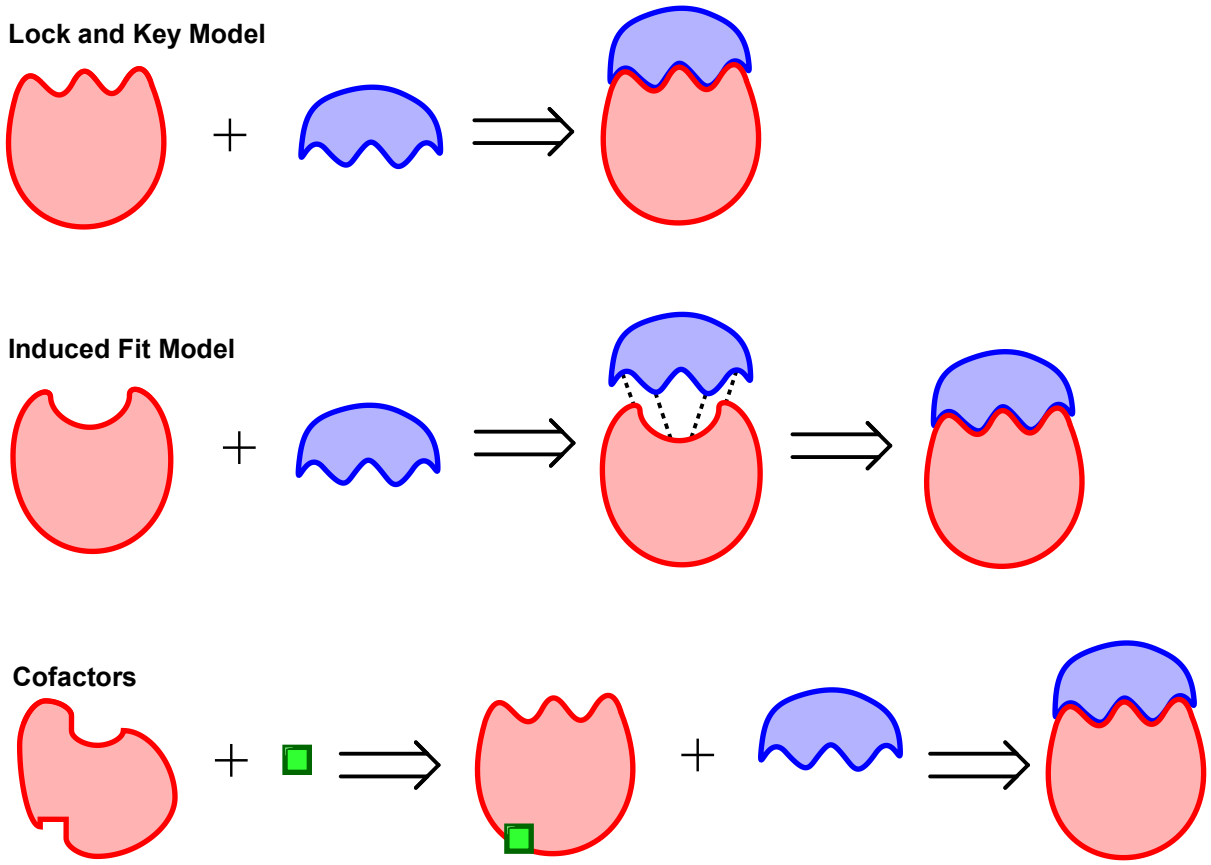

Figure 6.3 A comparison of substrate recognition models where red represents the enzyme, blue the substrate and green the cofactor.

6.1.1.3 Catalytic Behaviour

To be described as a catalyst, a species must lower the activation barrier of a reaction and not be rendered inactive by the process. An enzyme achieves this in several ways:

- Forming a charge-stabilising environment, and, in particular, making the formation of a charged transition state more favourable.[12]

- Binding directly to the substrate, forming a complex which acts as an intermediate and requires less energy to react.[13]
- Distorting the substrate in to a structure which is less reminiscent of the reactants and closer to that of the transition state.[14]
- Orientating reactants so they are in close proximity to each other.[1]

6.1.2 Enzymes and Disease

As enzymes are fundamental to biological function it is inevitable that any malfunction could be potentially harmful. The resultant diseases can be caused by poor regulation of the enzyme or a mistake in the genetic code such as a base insertion or deletion, resulting in the production of a protein with the wrong sequence or even no protein produced at all. These diseases are very often inherited, such as Tay-Sachs disease, which is caused by either a 4 base insertion or a splice mutation in different regions of the genetic code within chromosome 15.[15,16] Consequently, the enzyme *Hexosaminidase*, which breaks down excess gangliosides (lipids which act as cell surface markers), is not formed.[17] The result is that the normally useful gangliosides act as toxins which damage the nervous system and inevitably cause premature death, normally in infancy.[18]

For some diseases, it may be advantageous to modify the production of an enzyme in an attempt to control or cure that illness. This is particularly relevant to diseases which involve the replication of DNA, including cancer and Human Immunodeficiency Virus (HIV). This area of research is also relevant to the emerging field of antisense therapeutics, which relies on using a synthesized nucleic acid strand to block the

replication of a gene. In order to understand this area, the fundamentals of DNA transcription and translation will now be described.

6.1.2.1 RNA

DNA provides the code for every component of the body. In order for these components to be formed, the code must be 'read' by an organelle present in cells called the ribosome. Ribozymes present in the ribosome translate the genetic code into a polypeptide chain by bringing together amino acids which correspond to the initial DNA sequence. However, the ribosome requires a single stranded species to transcribe the information which must also be easily digested by enzymes in order to prevent over expression of a particular gene sequence. The carrier of choice is a messenger ribose nucleic acid (mRNA) strand.

RNA differs from DNA in several key aspects. The sugar unit consists of a ribose group which causes RNA to more readily adopt an A form rather than the B form normally associated with DNA.[19] This and the common occurrence of short, self-complementary sequences within the RNA strand results in it being primarily single stranded. [7]

Another key difference from DNA is the use of uracil (U) instead of thymine (T) (compared in Figure 6.4). Uracil is produced spontaneously through the deamination of cytosine.[20] Since RNA is short lived, the presence of U is not problematic. However, the increased longevity of DNA allows more time for U to be produced spontaneously from C. This would result in genetic mutations of both the initial strand and the complementary strand formed by DNA polymerases, since the corresponding

base for U is A not G. The presence of T in DNA prevents this confusion and allows for the excision of U by DNA repair enzymes.[21]

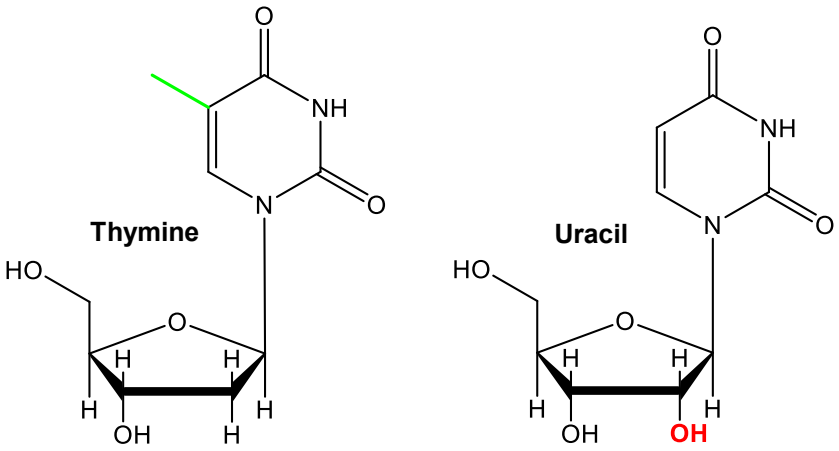

Figure 6.4 A comparison of the structures of thymine and uracil in DNA and RNA respectively. The methyl group of the thymine is highlighted in green and the additional alcohol group on the ribose sugar is highlighted in red.

6.1.2.2 Transcription

Transcription, the method by which mRNA is produced, occurs in the cell nucleus. An RNA polymerase enzyme (Figure 6.5) is used to unwind the DNA double helix structure, exposing the sequence to be used to code for the RNA (the sense strand) as well as its complement (the antisense strand). The RNA polymerase attaches to the sense strand and uses complementary bases, previously free within the cell, to form a new RNA strand (thus the RNA sequence is equivalent to that of the DNA antisense strand). When the polymerase reaches a stop sequence coded in the DNA it releases the three strands, the DNA rewinds into the favourable double helix structure and the resultant RNA strand (known as messenger RNA or mRNA) is transported to the ribosome.[22]

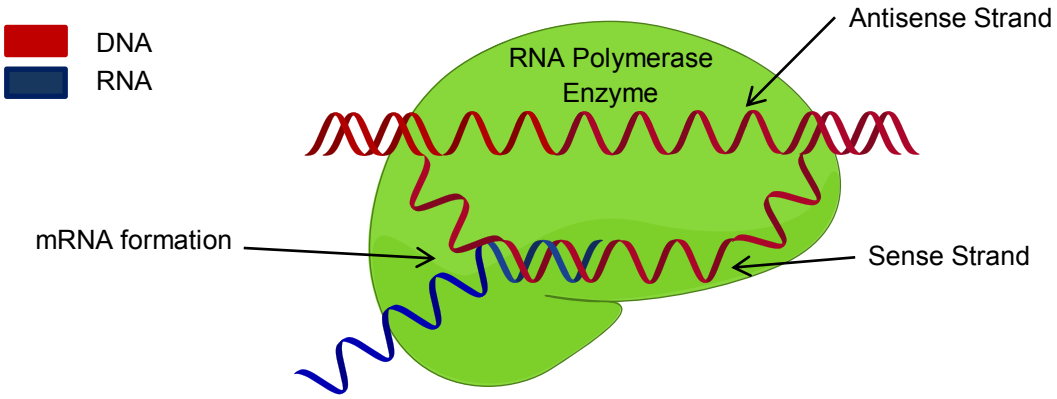

Figure 6.5 Use of RNA polymerase enzymes to form mRNA, the basis of the transcription process

6.1.2.3 Translation

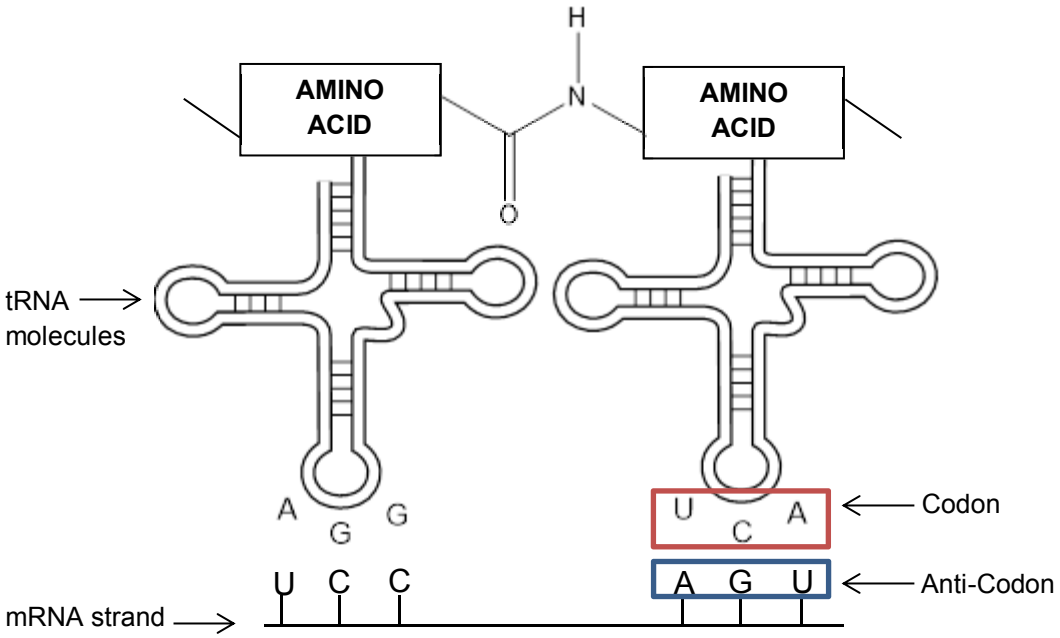

Figure 6.6 An mRNA strand being used by tRNA molecules to code for protein sequences

The ribosomes contain further folded strands of RNA known as transfer RNA (tRNA). Each of these have an amino acid attached at the 3' terminus and a 3 base section known as the codon. These three bases correspond to three bases on the mRNA.

The ribosomes ensure binding occurs in the correct order, which results in a chain of tRNA molecules containing amino acids. These amino acids are in close proximity to each other and the ribosome facilitates a condensation reaction, resulting in the formation of a polypeptide chain. The amino acids are attached to the tRNA through an ester and so the polymerisation process also acts to cleave the peptide chain from the tRNA molecules.[22]

6.1.3 Antisense Therapeutics

Since several difficult to treat and deadly retroviruses, as well as some genetically inherited diseases, utilise the DNA replication pathways already present in the host system, research has started to focus on blocking these routes through the use of antisense therapeutics.

Antisense therapeutics is the design and synthesis of single stranded, antisense modified nucleic sequences (or small interfering RNA sequences (siRNA)) which can bind to the target mRNA to prevent the translation of that sequence into a protein. It is important that the antisense sequences are not recognised by enzymes to prevent their destruction before blocking the mRNA. Recently, Tabrizi and co-workers have been able to show that the use of siRNA can slow the onset of a neurodegenerative disease called Huntington's Disease (HD). HD occurs due to the production of a mutant Huntingtin protein which accumulates in the brain, gradually causing cell death. Tabrizi and co-workers were able to demonstrate that injections of targeted siRNAs directly into the patients spinal fluid, was able to slow the accumulation of the mutant protein by binding to and preventing the translation of the gene responsible for its production.[23–28]

One issue with using natural DNA is that unmodified oligonucleotides are very unstable in biological systems and are broken down by nucleases.[26] In order to stabilise the antisense strands a number of different artificial oligonucleotides have been synthesised and are outlined below.

6.1.3.1 Modified Nucleic Acids for Enzyme Inhibition

The most widely reported modification is the use of a phosphorothioate (PS) backbone in place of the natural phosphate group. These species have the advantages of increased nuclease resistance, being readily taken up by the cell and ability to activate the enzyme *RNase H*, which speeds up the RNA degradation process, rendering it useless before translation can occur.[26] However, the alterations in the backbone have resulted in increased toxicity of these compounds and studies have shown it to cause liver damage, stimulation of the immune system and reduced platelet counts.[29] As a result, some research groups are focussing on nucleic acids with more complicated modifications. The structures of each of the discussed variations are given in Figure 6.7.

Studies have been carried out with a variety of backbone alterations, including replacing the ribose sugar with a six-membered ring (phosphorodiamidate morpholino oligomers (PMO)) and a number of different 2' groups on the ribose moiety. None of these systems have been shown to stimulate *RNase H*, unless in a mixed oligonucleotide and some have displayed toxic side effects in animal studies.[30–32]

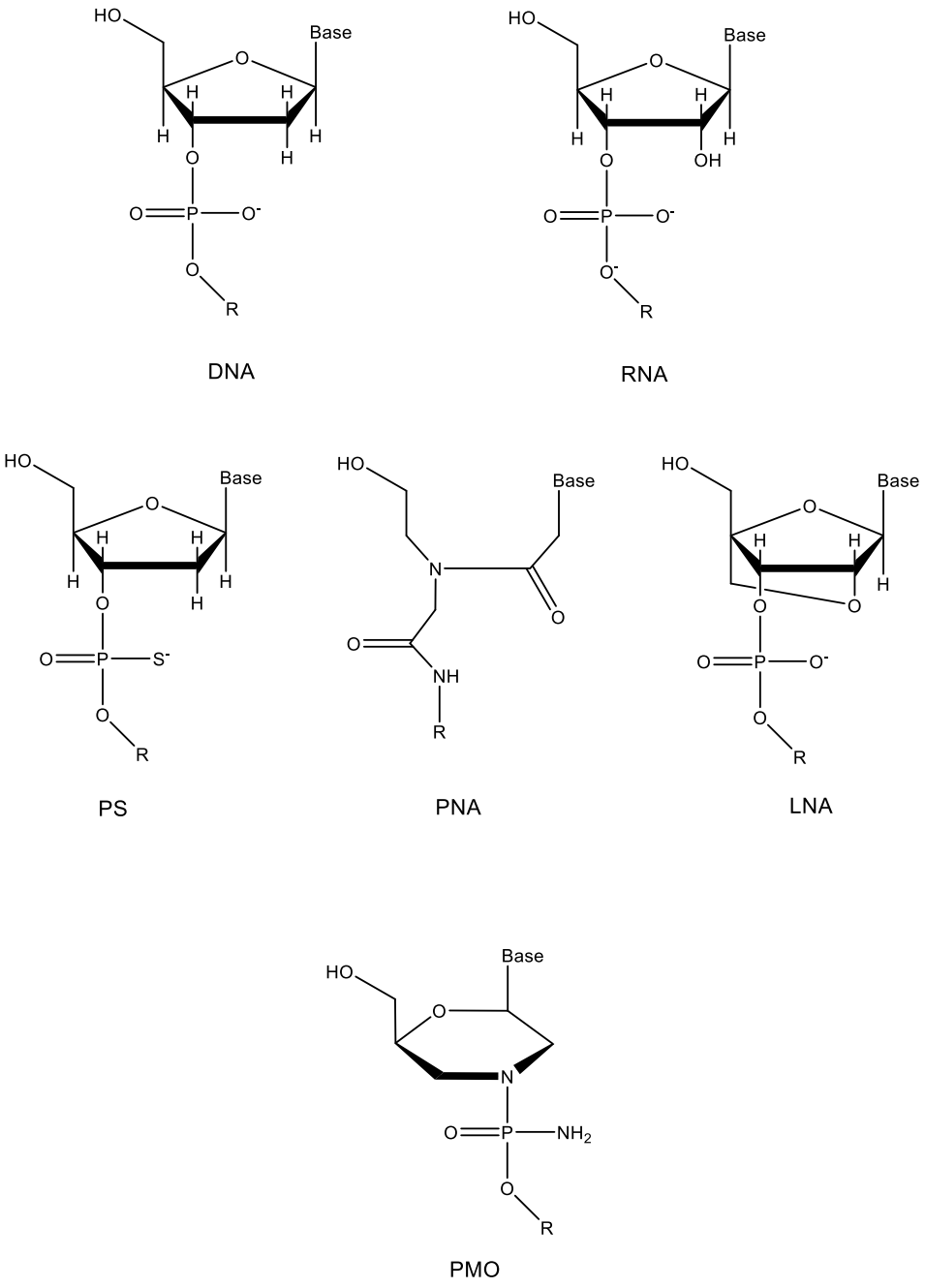

Figure 6.7 Structure of DNA,RNA, phosphorothioate (PS), peptide nucleic acid (PNA),locked nucleic acid (LNA) and morpholino (PMO) nucleic acid modifications

Peptide nucleic acid (PNA), a very flexible alternative to natural DNA, binds strongly and with high specificity to both DNA and RNA. It has also been shown to have

excellent resistance to the action of nucleases.[33] Nielsen and co-workers. found that hybridisation of PNA to the target DNA in duplex form (in a triple helix) prevented transcription as the RNA polymerase enzyme could not 'unzip' the duplex (as in Figure 6.5).[34]

The lack of charge associated with the backbone may also help to reduce the side effects associated with phosphorothioate moieties, rendering PNA non-toxic.[35] However, PNA is poorly soluble and not readily accepted by cells, limiting its use as an antisense agent.[36] However, very recently, Vilaivan and co-workers. demonstrated that the cellular uptake could be vastly improved by post-synthetic addition of pyrrolidinyl groups. This may be a route forward for PNA as an antisense therapy.[37]

Locked nucleic acids (LNA) are a more restricted form of DNA. LNA oligomers form very stable duplexes with RNA, more so than PNA, and are highly resistant to enzymatic degradation.[38,39] LNA, like PNA, does not stimulate the *RNase H* enzyme but has been shown to be more biologically active than PNA by acting as an antisense strand for telomerases. These are proteins with an attached RNA strand which adds sequences to the ends of chromosomes. Unregulated telomerase activity can prevent cell death, resulting in the formation of cancerous cells. By blocking these, LNA moieties have the potential to be potent anti-cancer agents.[38]

6.1.4 Conclusions and Project Aims

As discussed above, the ability of some modified nucleic acids to inhibit the action of enzymes on a DNA strand opens the way to a new branch of medicine: antisense therapeutics.

However, it is clear that the ideal drug candidates have not yet been found. Some species (PNA, LNA and PMO) lack the ability to increase the action of *RNase H*, a vital enzyme which would destroy infectious mRNA before it reached the translation stage. Those moieties that do induce *RNase H* action currently have undesirable side effects.

In conclusion, the ideal species would:

- Not be degraded by species within the cell before reaching the mRNA of interest
- Activate the *RNase H* enzymatic behaviour
- Block the action of polymerases or nucleases to prevent the diseased mRNA from being translated.
- Be readily taken into the cell

Since the ferrocene nucleic acid (FcNA) species have been shown to be robust under experimental conditions, are easily incorporated into DNA and possess a backbone modification which still allows for hydrogen bonding to natural DNA targets, they would appear to be a viable candidate for antisense therapeutics.

The initial studies, which will now be discussed, focussed on the ability of FcNA modified DNA to survive the action of nucleases and so indicate whether this species would be degraded in the cell. Without this ability, FcNA would be redundant as a potential antisense drug.

6.2 Results and Discussion

6.2.1 Sample Preparation

6.2.1.1 Oligonucleotides Used

Both the abasic and thymine modified FcNA species were used to determine whether the presence of the bases had any effect upon the action of the enzymes. The DNA sequences used are shown in Table 6.1. S0 is the natural DNA probe control and S1 is the FcNA probe. S3 is a strand of half-length and was synthesized to use as s comparison for degradation products visualised within the gel. It should be noted that FcNA units with *(S,S) pRpR* chirality (the notation *(S,S)* will be used for convenience) were used due to constraints on the amount of the *(R,R) pSpS* derivative.

Table 6.1 Oligonucleotide sequences used throughout Chapter 6

Oligonucleotide	**Sequence (5' – 3')**
S0	TGG ACT CTT CTC AAT G
$S1_{(TT\ or\ HH)}$	TGG ACT C (**$FcTT_{((S,S))}$ or $FcHH_{((S,S))}$**) CTC AAT G
S2	CAT TGA GAA GAG TCC A
S3	TGG ACT CTT

6.2.1.2 Optimising the visualisation of PAGE Gels

Polyacrylamide gel electrophoresis (PAGE) is technique whereby a current is applied such that one end of the gel is positively charged, attracting negatively charged DNA towards that end. The theory and uses of this technique have been covered in more depth in section 2.5. Briefly, the highly charged and smaller sized strands can travel

more quickly through the gel allowing the user to separate DNA samples based on size and charge. This makes it ideal for monitoring DNA degradation.

Both denaturing and native gels were used during the investigation into enzymatic degradation. Denaturing gels ensure that the samples are in their single stranded forms, with no secondary structure. This is achieved by the addition of high concentrations of urea to the basic acrylamide gel solution before setting. The urea disrupts the hydrogen bonding interactions between bases. Conversely, NaCl is added to a native gel solution to promote and retain structures such as the double helix or DNA rearrangement. Exact experimental conditions are given in section 7.7.2.

It was not possible to visualise any of the FcNA conjugated DNA samples captured in the gel solutions through dye staining. This was believed to be because the Diamond™ nucleic acid dye (Promega Corp.), whose chemical structure and method of action have not been reported, is not capable of binding to short chain oligonucleotides. This became apparent in previous work with DNA strands that were less than 7 bases long. In the case of the 15-mer containing the FcNA in a central position, the dye does not bind to or recognise the FcNA unit and hence not to the 7 base sequences either side of it. Consequently, the method of UV shadow was used to visualise the resultant gels.

UV shadow, described in more detail in section 2.5, has the advantage of preserving the fragments within the gel, allowing for their excision and further study. However, a higher concentration of DNA is required in order for the sample to absorb sufficient amounts of UV light.

In order to try to preserve sample, gels were run using DNA samples equating to 0.5 and 0.1 absorption units (AU). As shown in Figure 6.8, bands using 0.5 AU can clearly be seen in all lanes whereas the bands are very pale or non-existent for 0.1 AU. Hence all experiments were carried out with a sample concentration equating to 0.5 AU. Details of the calculations for this are given in section 7.7.1.

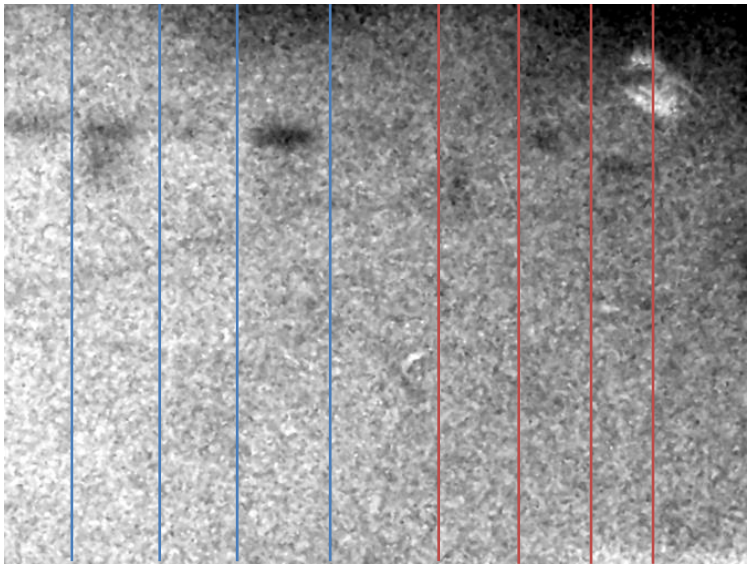

Figure 6.8 0.5 AU (blue lanes) and 0.1 AU (red lanes) of S0 run in a denaturing gel and visualised by UV shadow

6.2.1.3 Enzymes Used

For the initial studies, three enzymes were used to assess the efficacy of the FcNA conjugated DNA. An endonuclease called *DNase I* and two exonucleases called *Exo I* and *Exo III*. Exonucleases will digest from either the 3' or the 5' end of the strand. However, endonucleases are indiscriminate and so will commence the degradation at any point along the DNA chain. *Exo I* and *Exo III* are both active in the 3' to 5' direction but *Exo I* is active on single stranded DNA and *Exo III* on double stranded DNA.[22]

6.2.1.4 Enzymatic Digestion Reaction Conditions

The enzymes were supplied with a reaction buffer (67 mM Glycine-KOH, 6.7 mM $MgCl_2$, 10 mM β-ME, pH 9.5 @ 25°C) and the effects of the buffer contents and increased pH on the FcNA units were unknown. Consequently, controls were run of S0 and $S1_{HH}$ (due to material constraints, it was not possible to complete control with $S1_{TT}$). The samples were incubated under standard conditions in reaction buffer and 0.15 M NaCl (as a possible alternative buffer for diluting the enzyme solution) and compared to non-incubated strands in ultrapure water. These were all carried out with and without the *Exo I* present to determine the effect of altering or removing the buffer on enzyme activity.

The resulting gel is shown in Figure 6.9. The presence of single bands in lanes 2 and 6, at equivalent positions to the corresponding control strands in lanes 1 and 5, confirm both natural DNA and the FcNA modified DNA are stable in the reaction buffer at 37^{o}C for at least 24 hours.

In addition to this, the use of 0.15 M NaCl instead of the supplied reaction buffer has a detrimental effect on nuclease activity. In NaCl, S0 shows partial digestion to a shorter strand as evidenced by a single band positioned lower than the control strand in lane 3 and no equivalent band present in lane 4, where the supplied reaction buffer was used, implying complete digestion. There is a pale, diffuse band present near the bottom of lane 4 which could be attributed to the presence of single nucleotides after complete digestion.

Lanes 7 and 8 are of particular interest. Again, use of the 0.15 M NaCl incubation solution appears to show retardation of the enzyme with $S1_{HH}$. However, it clearly results in 2 bands in lane 7, rather than 1 and instead of complete digestion of the

strand, as is seen with the natural DNA equivalent, a second band is seen at a lower point. This could indicate that enzymatic action on the entire strand is being prevented, an early indication that the FcNA moiety may be capable of enzyme inhibition.[40]

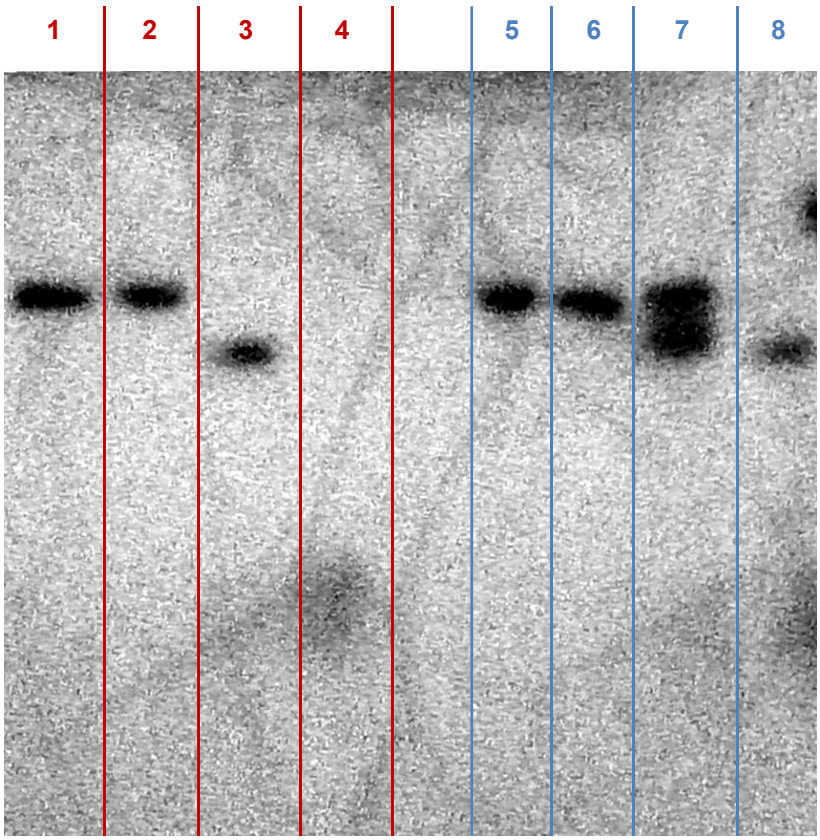

Figure 6.9 Comparison of different sample incubation solutions on Exo I nuclease activity and sample stability carried out using denaturing PAGE, gels run in 1 x TBE Buffer at 200 V for 2 hours, 10 µL sample loaded. Lane 1: S0 in ultrapure water. Lane 2: S0 incubated in reaction buffer. Lane 3: S0 and 0.5 u Exo I incubated in 0.15 M NaCl. Lane 4: S0 and 0.5 u Exo I incubated in reaction buffer Lane 5: $S1_{HH}$ in ultrapure water Lane 6: $S1_{HH}$ incubated in reaction buffer. Lane 7: $S1_{HH}$ and 0.5 u Exo I incubated in 0.15 M NaCl. Lane 8: $S1_{HH}$ and 0.5 u Exo I incubated in reaction buffer

6.2.2 DNase I Digestion Studies

DNase I is an endonuclease present throughout the animal kingdom and is responsible for the breakdown of excess DNA. Although this enzyme shows

increased specificity for bonds between purines and pyrimidines, it can begin digestion at any point along the DNA backbone and can cleave both single and double stranded DNA. [22,41] It is critical that an antisense strand is impervious to this species and would show promise for stability in biological serum.

However, resistance to this enzyme (shown in Figure 6.10) has been mixed among the modified nucleic acids (the structures and function of which are discussed in greater detail in Section 6.1.3.1).

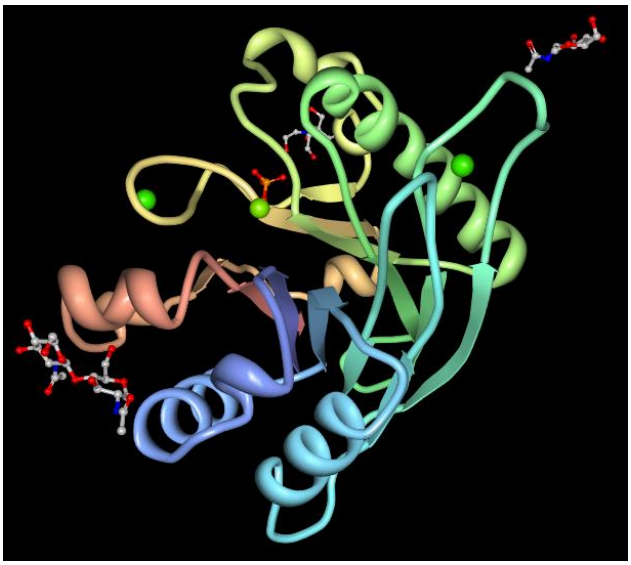

Figure 6.10 Protein structure of Human DNase I with complexing phosphate groups and magnesium ions. PDB Structure: 4AWN[42]

Lee and co-workers. demonstrated that varying the position of the phosphorothioate modified backbone (PS) (the structure of which is shown in Figure 6.11) within a sequence had a huge effect on its enzymatic resistance, more so than the percentage of P-S bonds present. For example, strands of poly(A-PS-T) were *DNase I* resistant whereas poly(PS-A-T) were not, being digested in 30 mins.[43]

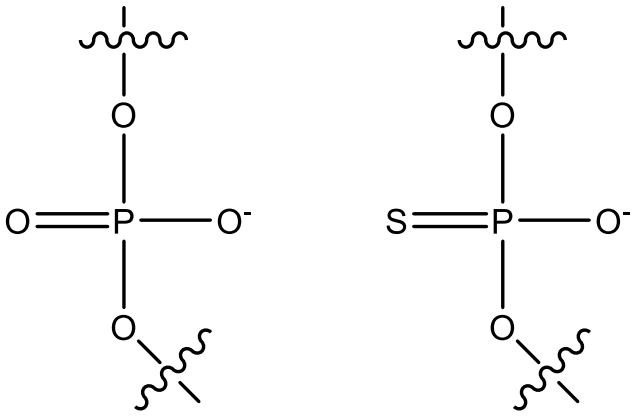

Figure 6.11 The structures of the phosphate backbone found in natural DNA and the modified phosphorothioate backbone for comparison.

Capping DNA at both or either of the 3' and 5' termini with LNA[44,45] and MO[46] units have been shown to greatly increase the stability of the DNA sequence towards DNase I degradation. Whole sequences of PNA are extremely stable in biological conditions but, not suitable for antisense therapeutics as discussed above.[33] Conversely, PNA-DNA chimeras (with a 1:1 DNA: PNA ratio), which possess increased aqueous solubility whilst maintaining duplex stability, are stable for at least three hours but not overnight.[47]

Since these examples involve strand capping or entire sequences of modified structures it would appear unlikely that the presence of only one FcNA unit in a central position would greatly retard the enzymes action. However, a previously investigated octamer, consisting purely of $FcTT_{(S,S)}$ or $FcTT_{(R,R)}$ showed no propensity to forming duplexes with natural DNA.[48] Consequently, a completely altered backbone is not a viable option for antisense therapeutics with this system.

Despite the quandary raised by the points above, both $S1_{TT}$ and $S1_{HH}$ were subjected to DNase I digestion and compared to the digestion of S0.

6.2.2.1 Digestion Studies

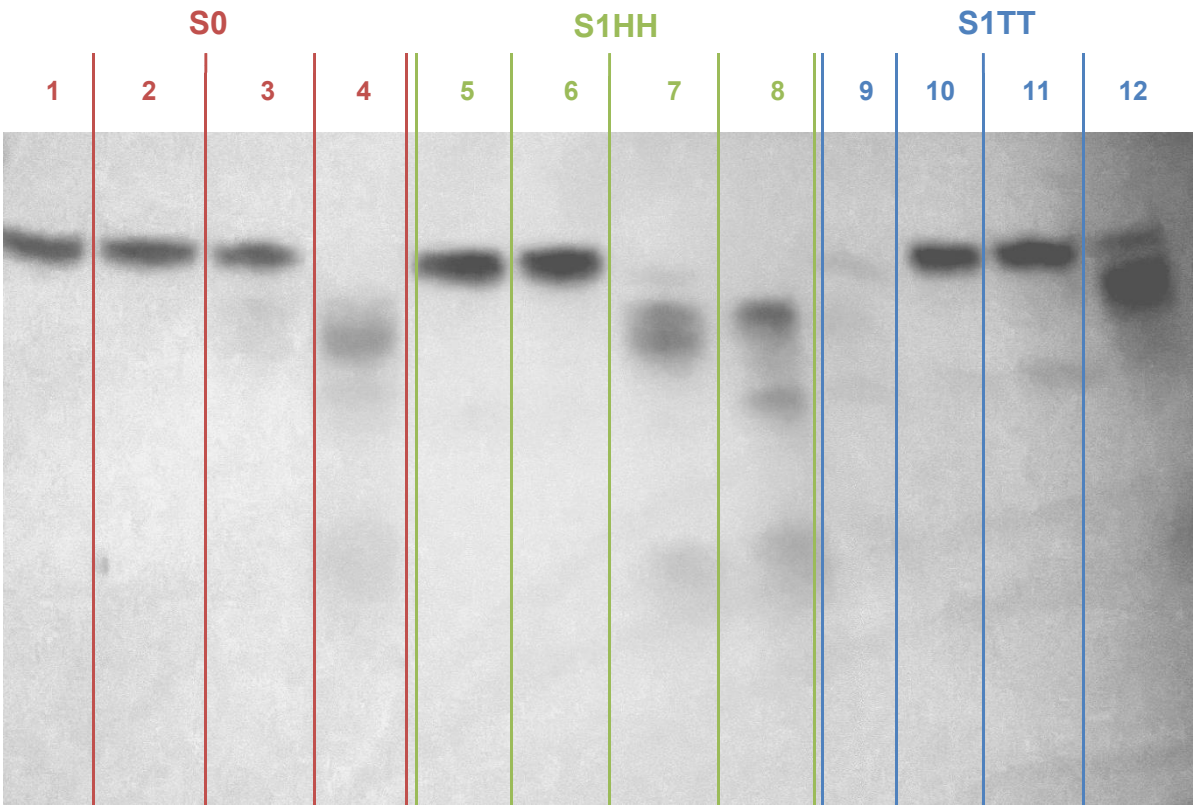

Figure 6.12 Monitoring DNase activity on S0, $S1_{HH}$ and $S1_{TT}$ using denaturing PAGE, gels run in 1 x TBE Buffer at 200 V for 2 hours, 10 µL sample loaded. S0 = Red, $S1_{HH}$ =Green, $S1_{TT}$ = Blue. Lane 1: S0 in ultrapure water. Lane 2: S0 incubated in ultrapure water at 37°C for 48 hrs. Lane 3: S0 and 0.5 u DNase incubated in reaction buffer for 1 hr. Lane 4: S0 and 0.5 u DNase incubated in reaction buffer for 48 hr. Lane 5: $S1_{HH}$ in ultrapure water. Lane 6: $S1_{HH}$ incubated in ultrapure water at 37°C for 48 hrs. Lane 7: $S1_{HH}$ and 0.5 u DNase incubated in reaction buffer for 1 hr. Lane 8: $S1_{HH}$ and 0.5 u DNase incubated in reaction buffer for 48 hr. Lane 9: $S1_{TT}$ in ultrapure water (pale due to a damaged well). Lane 10: $S1_{TT}$ incubated in ultrapure water at 37°C for 48 hrs. Lane 11: $S1_{TT}$ and 0.5 u DNase incubated in reaction buffer for 1 hr. Lane 12: $S1_{TT}$ and 0.5 u DNase incubated in reaction buffer for 48 hr

The resulting gel (Figure 6.12) yielded interesting results. S0 was degraded completely after 48 hours (lane 4) but was still largely intact after 1 hour (lane 3). Although DNase I is capable of degrading both ds and ss DNA, it has much

decreased activity (500 times less) with ss DNA, which affects the time required for full degradation.[41,49]

Interestingly, $S1_{HH}$ is almost completely degraded after 1 hour and seems to be able to activate the DNase I and increase its activity. Studies have shown that this can result from the increased flexibility of a DNA duplex.[49,50] The enhanced flexibility of $S1_{HH}$ (due to reduced steric hindrances and neighbouring base interactions) may allow for the DNA to obtain a structure more complimentary to the enzymes active site and so increase its activity. This is an area which requires further investigation, possibly with the incorporation of varying lengths of spacer phosphoramidites into the DNA backbone to increase strand flexibility.

By contrast, $S1_{TT}$ appeared to increase the resistance of the entire strand to the action of the nuclease. After 1 hour, the whole strand appears to be essentially intact (lane 11) with only a very faint degradation band lower down. Even after 48 hours, some non- degraded oligomer appears to be present as a faint band. There are two degradation bands, close to the complete sequence band, that are more concentrated and not split into many faint bands as for S0 and $S1_{HH}$. This would imply that only partial degradation has occurred, leaving a considerable portion of the sequence intact. Multiple attempts at obtaining a mass spectrum of these two bands were unsuccessful, possibly due to the low concentration and difficulty in separating the bands.

The enhanced stability of $S1_{TT}$ towards DNase I compared to S0 offered further early indications that this system may indeed be able to withstand biological conditions. The tests were then repeated with enzymes relevant to the transcription and translation processes involved in diseases such as HIV, as outlined below.

6.2.3 Exonuclease I (Exo I)

Exonucleases are a class of enzymes which hydrolyse the phosphodiester bonds between nucleotides. This is done sequentially, either 3' to 5' or 5' to 3' rather than the non-specific action associated with DNases. *Exonuclease I* in particular travels 3'-5' and is specifically active on single stranded DNA.[51] In this way nucleotides can be recycled and over expression of proteins is prevented.[52]

It is essential that an antisense strand must be stable towards single stranded exonucleases in order that they are not destroyed before being able to bind successfully with RNA target. Capping strands with just one LNA has been shown to reduce the exonuclease activity of some enzymes and an additional LNA unit resulted in the inhibition of all enzymes with exonuclease behaviours.[53] PNA and morpholino nucleic acids have also been shown to be seemingly completely resistant to the action of exonucleases while phosphorothioates are less resistant.[33,54,55]

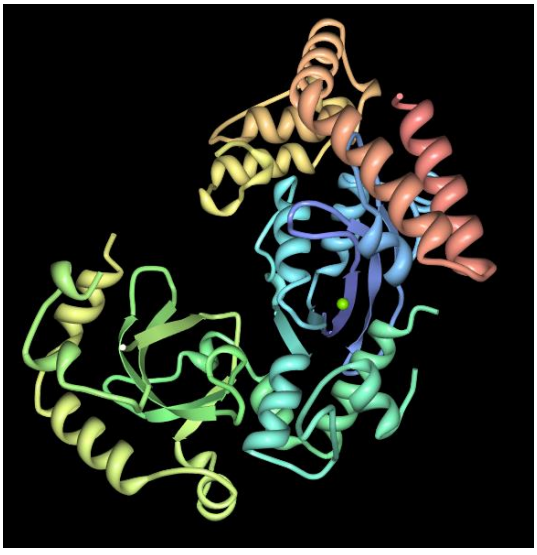

Figure 6.13 Protein structure of Exo I isolated from E.Coli. PDB Structure: 3C95[56]

6.2.3.1 Time Dependency Studies – 0 - 30 minutes

The length of time allowed for enzyme incubation had a very obvious effect with the use of DNase I and demonstrated that some enzymes require more time to completely degrade a sample. Therefore, for *Exo I* nuclease it was decided to undertake a thorough investigation of the level of degradation over short and long time frames. This section deals with the results collected in the first 0-30 minutes of enzyme incubation as shown in Figure 6.14.

It is clear from Figure 6.14 that the S0, $S1_{HH}$ and $S1_{TT}$ samples are not damaged by the extended heating used in these experiments since the band produced in Lane 2 corresponds exactly with the control strand in Lane 1 for each DNA type. Any significant degradation must therefore be due to the enzymatic action of the *Exo I*.

For S0 it is clear that all examples of a full strand have been consumed within 10 minutes leaving shorter degradation products. The bands of the degradation products increase in intensity throughout the experiment as would be expected since the concentration of these species are increasing. There appear to be several degradation bans present, in close proximity to each other, with the top region being most intense between 1 and 5 mins and the bottom region increasing in intensity throughout the time frame. This indicates that the degradation is a gradual process and that the shortening of the strands can be monitored over time.

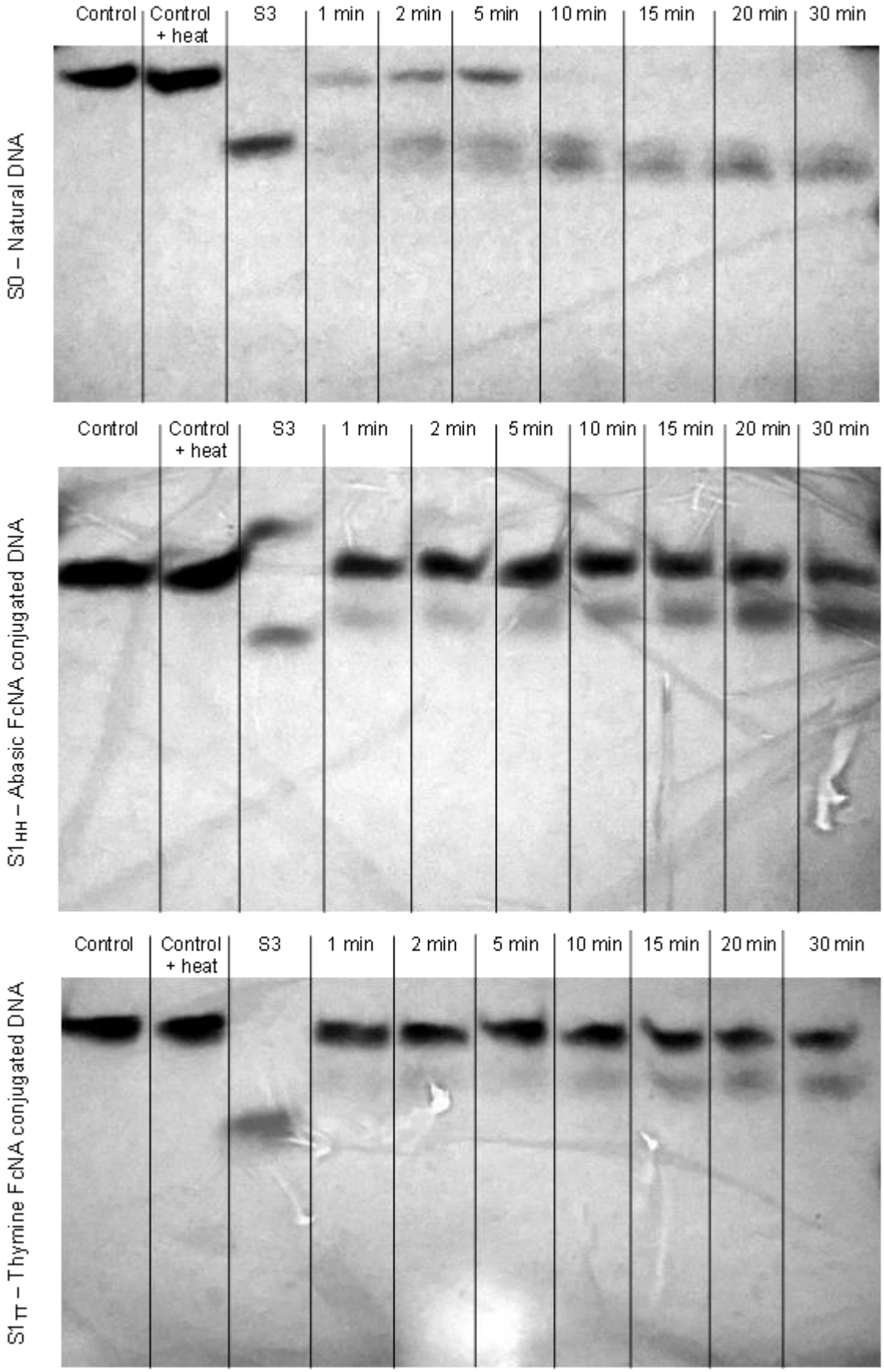

Figure 6.14 Time dependent Exo I degradation of S0 (top), $S1_{HH}$ (middle) and $S1_{TT}$ (bottom) over 30 mins using denaturing PAGE, gels run in 1 x TBE Buffer at 200 V for 2 hours, 10 µL sample loaded. 'Control' indicates S0, $S1_{HH}$ or $S1_{TT}$ respectively, stored in ultrapure water, 'Control + heat' indicates S0, $S1_{HH}$ or $S1_{TT}$ respectively, stored in ultrapure water and heated at 37°C for 72 hours. S3, a strand of half the length of S0 and S1, was also used for comparison.

$S1_{HH}$ and $S1_{TT}$ react very differently to *Exo I* compared with S0. Whilst some degradation is evident, both have a significantly intense band still present after 30 mins which corresponds to a full oligonucleotide. It is clear the presence of even a single FcNA unit in a central position is able to inhibit *Exo I* to a certain extent and implies that the addition of the ferrocene containing unit has a long range structural effect, rather than just affecting those nucleotides in the immediate vicinity. The increased rigidity of the FcNA unit may prevent the remaining nucleotides from orientating so as to allow for the enzyme to digest the strand efficiently. The degradation band increases in intensity much quicker for $S1_{HH}$ than for $S1_{TT}$. As noted for the variation in DNase I activity (section 6.2.2.1), this may be due to the reduce steric hindrance of the $FcHH_{(s,s)}$ unit compared to the $FcTT_{(s,s)}$, enabling the DNA backbone to obtain a better fit for the active site.

6.2.3.2 Time Dependency Studies – 45 minutes – 72 hours

The longer time frame studies were intended to determine whether the FcNA units were able to resist enzyme degradation indefinitely and to produce enough of the degraded species so further analysis could be performed. The results are shown in Figure 6.15. S0 still showed some partially degraded DNA present at 1 hour's incubation but this is not evident after 24 hours, implying that all strands have been completely digested to the monomeric nucleotides.

Conversely, and concordant with the short time scale experiment, both $S1_{HH}$ and $S1_{TT}$ had some undigested strand present after incubation up to one hour and a consistent band of degradation product up to 72 hours. Initially (up to 30 mins), $S1_{HH}$ degrades faster than $S1_{TT}$ (Figure 6.14). However, the level of digestion is comparable after 1 hour for both strands. The *Exo I* enzyme seems unable to digest

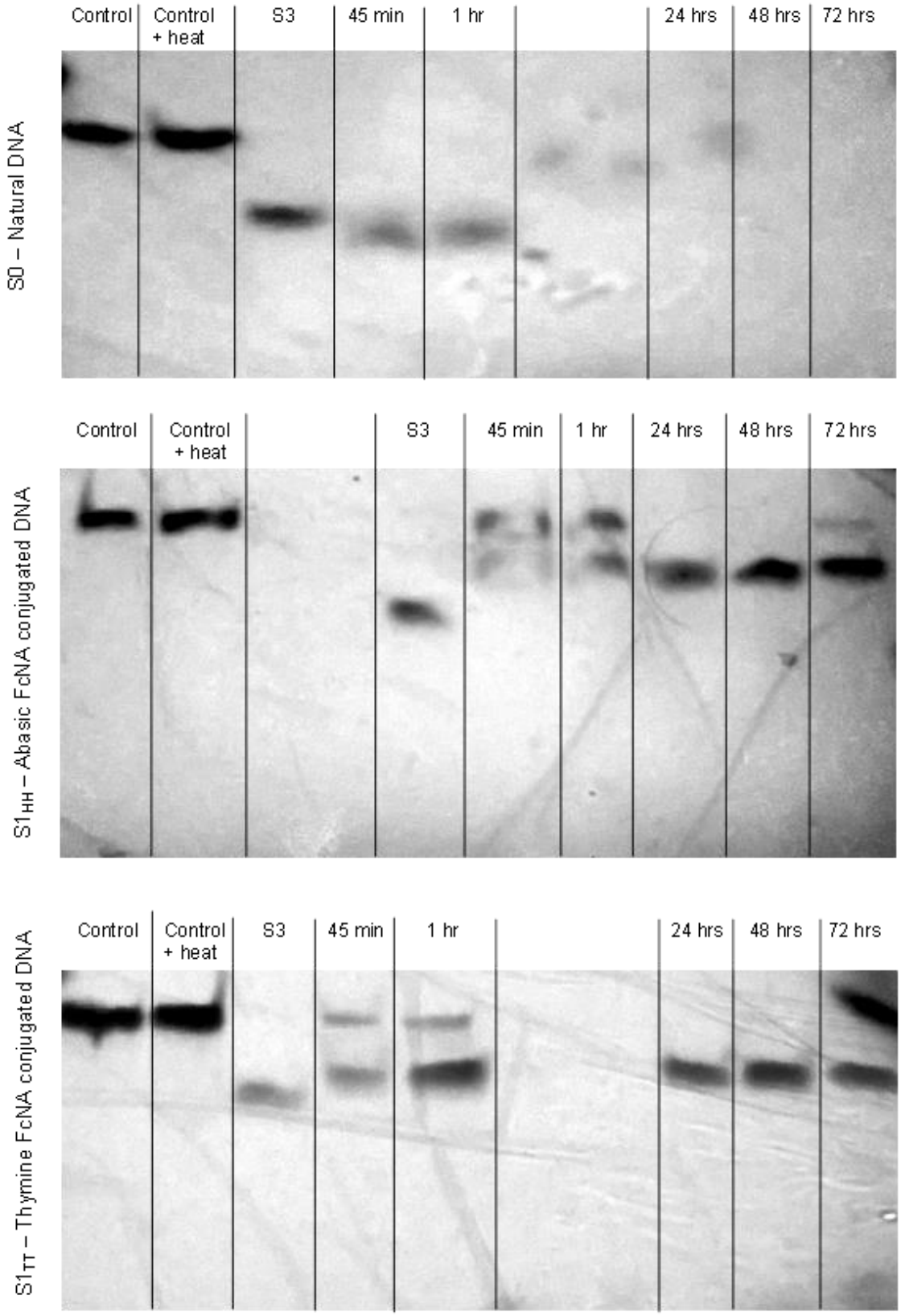

Figure 6.15 Time dependent Exo I degradation of S0 (top), S1HH (middle) and S1TT (bottom) from 45 mins to 72 hrs using denaturing PAGE, gels run in 1 x TBE Buffer at 200 V for 2 hours, 10 µL sample loaded. 'Control' indicates S0, $S1_{HH}$ or $S1_{TT}$ respectively, stored in ultrapure water, 'Control + heat' indicates S0, $S1_{HH}$ or $S1_{TT}$ respectively, stored in ultrapure water and heated at 37°C for 72 hours. S3, a strand of half the length of S0 and S1, was also used for comparison.

past the FcNA unit regardless of whether bases are present or not. To investigate this phenomenon further, the degradation products were excised (see section 7.7.3 for experimental details) and subjected to mass spectrometric analysis.

The band corresponding to the half strand, S3, appears slightly lower than the digested fragments of $S1_{TT}$ and $S1_{HH.}$ This may be suggestive of the presence of the FcNA unit remaining attached to the fragment. As well as the mass difference between an FcNA containing strand and its unmodified equivalent, the ferrocene molecule replaces a phosphate backbone group. The strand contains one less negative charge than the equivalent unmodified DNA sequence and as such is attracted less strongly towards the anode. To confirm the identity of the strand fragments, the bands were excised for mass spectrometric analysis.

6.2.3.3 Mass Spectrometric Data

For $S1_{HH}$ and $S1_{TT}$, the observed mass of the degradation band is 2779 and 3081 g mol^{-1} respectively (see section 8.4.3). A structural proposal for the resulting species containing FcHH is given in Figure 6.16. This structure would satisfy the observed masses and the enzyme's mechanism of action since *Exo I* is known to cleave at the phosphodiester bond.[57]

The enzyme would proceed in the 3'-5' direction and it is interesting that the enzyme cannot digest passed the base preceding the FcNA unit rather than stopping at the FcNA itself. It is possible that the increased rigidity of FcNA backbone structure and the presence of the two additional methyl groups result in the phosphodiester bond between the FcNA and the preceding base (cytosine) being distorted from a natural configuration. C would then be held in a non-natural position and the enzyme would

be unable to recognise this bond. *Exo I* has an extremely narrow active site and so is sensitive to minor structural changes.[57]

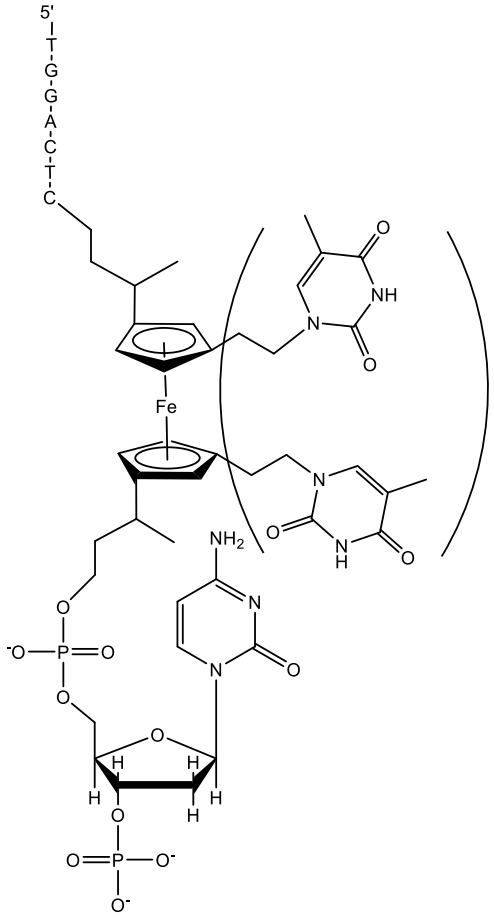

Figure 6.16 Proposed degradation product of S1 after incubation with Exo I (As for $S1_{HH}$ without brackets and $S1_{TT}$ with brackets)

6.2.4 Exonuclease III (Exo III)

Exo III belongs to the same family of enzymes as *Exo I*. However, it only recognises double stranded DNA and acts to digest one of the complementary strands in the 3'→ 5' direction producing mononucleotides (as with *Exo I*).[57] Interestingly, and of great significance to the end goals of this work, *Exo III* also possesses *RNase H* behaviour.[58] Although RNA:FcNA-DNA duplexes have not been assessed with *Exo*

III in this work, which concentrates just on DNA duplexes, it would be a logical next step.

As discussed above (section 6.2.2), morpholino species, PNA and LNA have shown resistance to all exonuclease activity. Indeed, PNA has been used as a protective species to produce short ss DNA directly from genomic ds DNA, thus allowing for simplified genotyping of SNPs by mass spectrometry.[59] Unlike *Exo I*, phosphorothioates have also been shown to be resistant to *Exo III* and can be used to block one of the duplex DNA strands to induce digestion of a specific strand and allow for replication of a target *in vivo.* Interestingly, only one capping phosphorothioate group was required for the prevention of digestion, suggesting that *Exo III* is more sensitive to a structural change of a substrate than *Exo I*.[60]

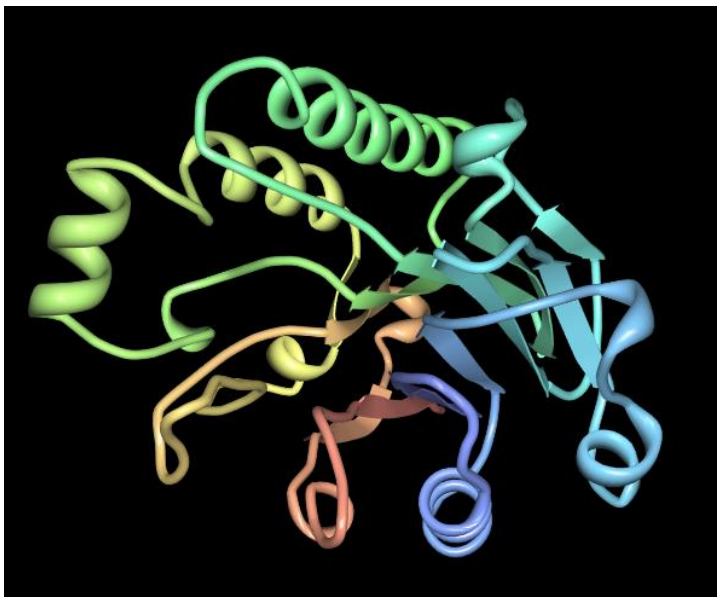

Figure 6.17 Protein structure of Exo II isolated from E. Coli. PDB Structure: 1AKO[61]

6.2.4.1 Digestion Studies

In order to maximise the amounts of sample for mass spectrometric analysis, all samples were incubated in *Exo III* for 72 hours rather than carrying out a time trial study. The resulting gels are given in Figure 6.18.

Interestingly the results correspond more closely with the action of DNase on FcNA than of *Exo I*. After 72 hours incubation, both unmodified DNA and the $FcTT_{(S,S)}$-DNA have bands remaining which correspond to the control band, implying that some ds DNA remains. This is much more prominent for the $FcTT_{(S,S)}$ DNA, where the lower degradation band is much less intense than the ds DNA bands. For S0:S2 there is a ladder of degradation bands (suggesting the presence of DNA strands of different masses) rather than the single band seen for $S1_{TT}$:S2. It is not clear as to why this may be the case. It could be that the first target bases are removed from $S1_{TT}$:S2 but that any further degradation was prevented by the presence of the $FcTT_{(S,S)}$. Also, for S0:S2, there is no unnatural structural arrangement in either of the backbones of the double helix. As such, enzyme attack can occur on either strand, giving rise to a larger range of masses possible through degradation.

The presence of the $FcTT_{(S,S)}$ in $S1_{TT}$:S2 may prevent *Exo III* from attacking the $S1_{TT}$ strand at all. Mass spectrometry was attempted with the degradation products of S0:S2 and $S1_{TT}$:S2 but the data was inconclusive, possibly due to low concentration.

After incubation, there was no full $S1_{HH}$:S2 duplex remaining. As with DNase, it appears that the presence of the $FcHH_{(S,S)}$ unit is able to enhance the enzymatic digestion. This was completely unexpected since, as discussed in section 6.2.4, *Exo III* would appear to be the more structurally sensitive enzyme when compared to *Exo I*. Literature precedence for modified nucleic acids enhancing enzyme activity

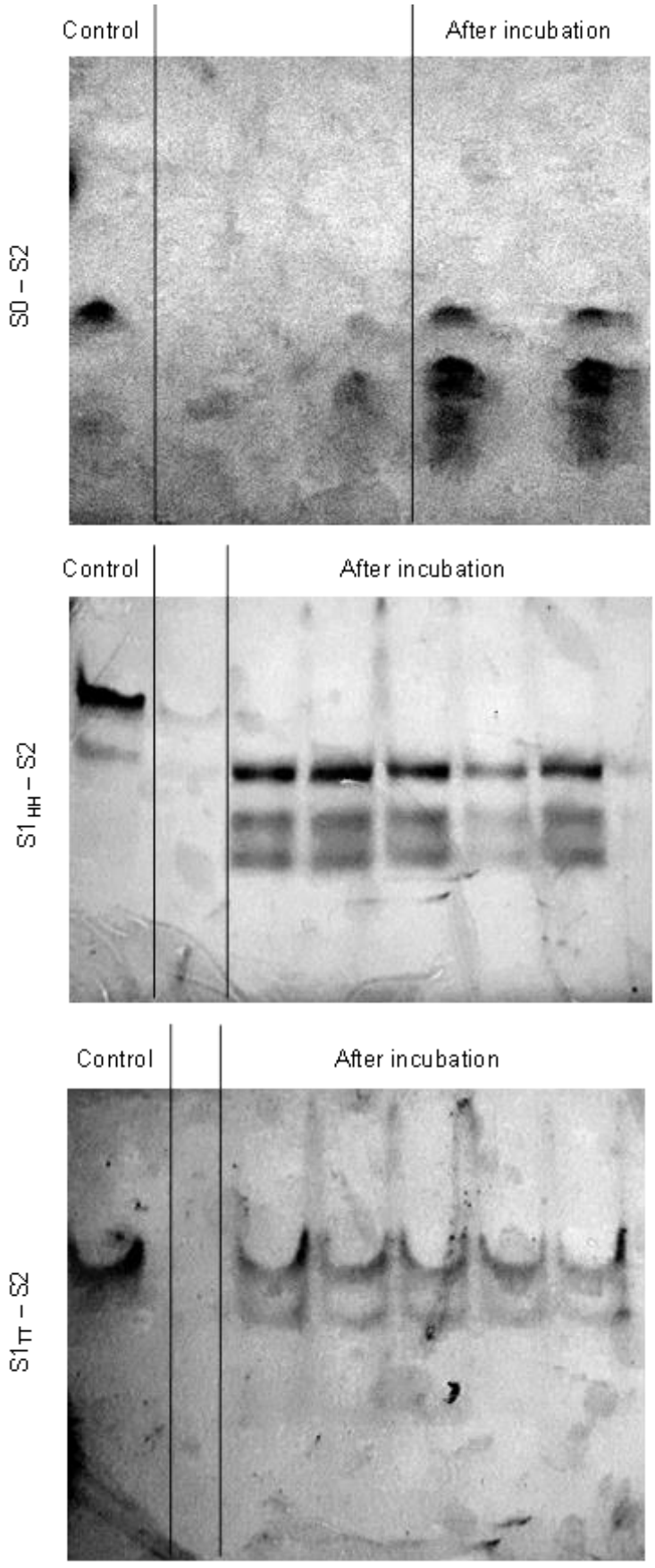

Figure 6.18 Degradation by Exo III of S0:S2 (top), $S1_{HH}$:S2 (middle) and $S1_{TT}$:S2(bottom)duplexes, run on native PAGE gels, in 1 x TBE Buffer at 200 V for 2 hours, 10 µL sample loaded. Control- S0, S1HH or S1TT respectively, stored in ultrapure water. Samples were incubated for 72 hrs at 37°C.

previously has not yet been found making $FcHH_{(S,S)}$ a compelling candidate for further study.

The bands of the upper most digestion product of $S1_{HH}$:S2 were concentrated enough to enable recovery for mass spectrometry.

6.2.4.2 Mass Spectrometric Data

The observed mass of the most intense digestion product of $S1_{HH}$:S2 was 4865 g mol^{-1}. This does not correspond to the individual masses of either $S1_{HH}$ (4630 g mol^{-1}) or S3 (4914 g mol^{-1}) and no suggested fragment has yet been proposed which corresponds to the correct mass (see section 8.4.3). The identity of this species is, as yet, unknown and subject to further investigation.

6.3 Conclusions

DNA containing one of two ferrocene nucleic acid derivatives ($FcHH_{(S,S)}$ and $FcTT_{(S,S)}$) have been exposed to enzymatic digestion by a sporadic DNase and unidirectional ss strand-specific and ds-specific exonucleases. These results have been compared to the same experiments with natural DNA.

The presence of one $FcTT_{(S,S)}$ in a central backbone position was enough to partially inhibit DNase and *Exo III.* It was also enough to prevent *Exo I* from digesting past it, leaving a partial strand fragment, which was identifiable by mass spectrometry. This behaviour is comparable to species such as LNA and PNA who have also been shown to be exonuclease resistant.[9,62–65] This shows early promise for the ability of this system to survive cell conditions.

$FcHH_{(S,S)}$ gave very unexpected results. Whilst behaviour with *Exo I* was similar to $FcTT_{(S,S)}$, there was an increase in the activity of both *DNase* and *Exo III* compared to natural DNA. *Exo III* is known to exhibit *RNase H* behaviour and these results raise the possibility that $FcHH_{(S,S)}$ may be able to promote this in other enzymes *in vivo.* Since the other modified nucleic acids (not including the backbone modification phosphorothioate) have so far been unable to encourage this behaviour, investigation for antisense therapeutics is greatly warranted. A strand containing FcHH could be used to form a duplex with target mRNA and encourage its digestion, prior to translation, through the promotion of *RNase H* behaviour, thus regulating protein production.

6.4 Further Work

To further the investigations of the FcNA species as a potential antisense therapeutic, the following work is suggested:

- Assess whether either FcNA conjugated DNA can be readily accepted by cells with fluorescence-labelled oligonucleotides.
- Assess the ability of $FcHH_{(S,S)}$ to encourage *RNase H* behaviour by synthesising RNA targets and subjected the resulting FcNA:DNA/RNA duplexes to an enzyme possessing *RNase H* activity. This would represent a great step forward for antisense therapeutics.
- Determine whether the incorporation of FcNA units at different points along the DNA strand further affect enzyme activity in an attempt to control digestion rate and the length of the resultant nucleotides. This may have further uses for

the production of oligonucleotides of specific length using *Exo III*, particularly from circular DNA.

- Determine the degradation species of the DNA:$FcHH_{(S,S)}$ duplex when subjected to *Exo III* by further mass spectrometric studies (fragmentation) and NMR to gain further insight into the causes of the differences in enzyme behaviour with these species.

6.5 References

(1) Berg, J. M.; Tymoczko, J. L.; Stryer, L. *Biochemistry 5th edition*; WH Freeman, 2002.

(2) Pyle, A. M. *Science* **1993**, *261*, 709–714.

(3) Jakubke, H.-D.; Sewald, N. *Peptides from A to Z: a concise encyclopedia*; John Wiley & Sons, 2008.

(4) Zanghellini, A.; Jiang, L.; Wollacott, A. M.; Cheng, G.; Meiler, J.; Althoff, E. A.; Röthlisberger, D.; Baker, D. *Protein Sci.* **2006**, *15*, 2785–2794.

(5) Basheer, S. M.; Chellappan, S. Enzyme Engineering. *Bioresources and Bioprocess in Biotechnology*, 2017, 151–168.

(6) Hartley, C. J.; Wilding, M.; Scott, C. *Microbiol. Aust.* **2017**, *38*, 73–75.

(7) Moran, L. A.; Scrimgeour, K. G.; Ochs, R. S. *Biochemistry, Second Edition*; Prentice Hall, Inc, 1994.

(8) Fischer, E. *Ber. Dtsch. Chem. Ges* **1894**, *27*, 2985–2993.

(9) Koshland, D. E. *Proc. Natl. Acad. Sci.* **1958**, *44*, 98–104.

(10) Schwarz, G.; Mendel, R. R.; Ribbe, M. W. *Nature* **2009**, *460*, 839–847.

(11) Tabb, M. M.; Sun, A.; Zhou, C.; Grün, F.; Errandi, J.; Romero, K.; Pham, H.; Inoue, S.; Mallick, S.; Lin, M. *J. Biol. Chem.* **2003**, *278*, 43919–43927.

(12) Warshel, A.; Sharma, P. K.; Kato, M.; Xiang, Y.; Liu, H.; Olsson, M. H. M. *Chem. Rev.* **2006**, *106*, 3210–3235.

(13) Fink, A. L.; Ahmed, A. I. *nat* **1976**, *263*, 294–297.

(14) Wolfenden, R. *Accounts Chem. Res.* **1972**, *5*, 10–18.

(15) Myerowitz, R.; Costigan, F. C. *J. Biol. Chem.* **1988**, *263*, 18587–18589.

(16) Keats, B. J. B.; Elston, R. C.; Andermann, E.; Rao, D. C. *Genet. Epidemiol.* **1987**, *4*, 77–85.

(17) Lehninger, A. L.; Nelson, D. L.; Cox, M. M. *W. Freeman* **2005**.

(18) National Human Genome Research Institute. Learning About Tay-Sachs Disease https://www.genome.gov/10001220/ (accessed Jun 16, 2017).

(19) Shindo, H.; Matsumoto, U. *J. Biol. Chem.* **1984**, *259*, 8682–8684.

(20) Duncan, B. K.; Miller, J. H. *Nature* **1980**, *287*, 560–561.

(21) Békési, A.; Vértessy, B. G. *Sci. Sch.* **2011**, *27*–31.

(22) Brown, T.; Brown Jr., T.; ATDbio Ltd. Nucleic Acids Book.

(23) Agrawal, S.; Kandimalla, E. R. *Mol. Med. Today* **2000**, *6*, 72–81.

(24) Agrawal, S.; Zhao, Q. *Curr. Opin. Chem. Biol.* **1998**, *2*, 519–528.

(25) Crooke, S. T. In *Antisense research and application*; Springer, 1998; pp. 1–50.

(26) Kurreck, J. *Eur J Biochem.* **2003**, *270*, 1628–164420.

(27) Gallagher, J. Huntington's breakthrough may stop disease http://www.bbc.co.uk/news/health-42308341 (accessed Jan 16, 2018).

(28) Miller, J. R. C.; Pfister, E. L.; Liu, W.; Andre, R.; Träger, U.; Kennington, L. A.; Lo, K.; Dijkstra, S.; Macdonald, D.; Ostroff, G.; Aronin, N.; Tabrizi, S. J. *Sci. Reports* **2017**, *7*, 46740.

(29) Jason, T. L.; Koropatnick, J.; Berg, R. W. *Toxicol. Appl. Pharmacol.* **2004**, *201*, 66–83.

(30) Monia, B. P.; Lesnik, E. A.; Gonzalez, C.; Lima, W. F.; McGee, D.; Guinosso, C. J.; Kawasaki, A. M.; Cook, P. D.; Freier, S. M. *J. Biol. Chem.* **1993**, *268*, 14514–14522.

(31) Heasman, J. *Dev. Biol.* **2002**, *243*, 209–214.

(32) Crooke, S. T.; Lemonidis, K. M.; Neilson, L.; Griffey, R.; Lesnik, E. A.; Monia, B. P. *Biochem. J.* **1995**, *312*, 599–608.

(33) Demidov, V. V.; Potaman, V. N.; Frank-Kamenetskil, M. D.; Egholm, M.; Buchard, O.; Sönnichsen, S. H.; Nlelsen, P. E. *Biochem. Pharmacol.* **1994**, *48*, 1310–1313.

(34) Nielsen, P. E.; Egholm, M.; Buchardt, O. *Gene* **1994**, *149*, 139–145.

(35) Sazani, P.; Gemignani, F.; Kang, S.-H.; Maier, M. A.; Manoharan, M.; Persmark, M.; Bortner, D.; Kole, R. *Nat. Biotechnol.* **2002**, *20*, 1228–1233.

(36) Kurreck, J. *Eur. J. Biochem.* **2003**, *270*, 1628–1644.

(37) Suparpprom, C.; Nuanyai, T.; Pansuwan, H.; Vilaivan, T.; Wanichwecharungruang, S.; Ditmangklo, B.; Palaga, T.; Pan-In, P.; Jiangchareon, B.; Vilaivan, C. *Bioconjugate Chem.* **2017**.

(38) Elayadi, A. N.; Braasch, D. A.; Corey, D. R. *Biochemistry* **2002**, *41*, 9973–9981.

(39) Grünweller, A.; Wyszko, E.; Bieber, B.; Jahnel, R.; Erdmann, V. A.; Kurreck, J. *Nucleic acids Res.* **2003**, *31*, 3185–3193.

(40) Prins, R.; Korswagen, A. R.; Kortbeek, A. G. T. G. *J. Organomet. Chem.* **1972**, *39*, 335–344.

(41) Ambion Inc. DNase I Demystified https://www.thermofisher.com/uk/en/home/references/ambion-tech-support/nuclease-enzymes/general-articles/dnase-i-demystified.html (accessed Jun 26, 2017).

(42) Parsiegla, G.; Noguere, C.; Santell, L.; Lazarus, R. A.; Bourne, Y. *Biochemistry* **2012**, 10250.

(43) Latimer, L. J.; Hampel, K.; Lee, J. S. *Nucleic acids Res.* **1989**, *17*, 1549–1561.

(44) Crinelli, R.; Bianchi, M.; Gentilini, L.; Magnani, M. *Nucleic acids Res.* **2002**, *30*, 2435–2443.

(45) Kurreck, J.; Wyszko, E.; Gillen, C.; Erdmann, V. A. *Nucleic acids Res.* **2002**, *30*, 1911–1918.

(46) Chen, J.; Wu, J.; Hong, Y. *Chem. Commun.* **2016**, *52*, 3191–3194.

(47) Moggio, L.; Romanelli, A.; Gambari, R.; Bianchi, N.; Borgatti, M.; Fabbri, E.; Mancini, I.; di Blasio, B.; Pedone, C.; Messere, A. *Pept. Sci.* **2007**, *88*, 815–822.

(48) V. Nguyen, H.; Zhao, Z.; Sallustrau, A.; Horswell, S. L.; Male, L.; Mulas, A.; Tucker, J. H. R. *Chem. Commun.* **2012**, *48*, 12165–12167.

(49) Suck, D. *J. Mol. Recognit.* **1994**, *7*, 65–70.

(50) Hogan, M. E.; Roberson, M. W.; Austin, R. H. *Proc. Natl. Acad. Sci.* **1989**, *86*, 9273–9277.

(51) Lehman, I. R.; Nussbaum, A. L. *J. Biol. Chem.* **1964**, *239*, 2628–2636.

(52) Kushner, S. R.; Nagaishi, H.; Templin, A.; Clark, A. J. *Proc. Natl. Acad. Sci. United States Am.* **1971**, *68*, 824–827.

(53) Di Giusto, D. A.; King, G. C. *Nucleic acids Res.* **2004**, *32*.

(54) Hudziak, R. M.; Barofsky, E.; Barofsky, D. F.; Weller, D. L.; Huang, S.-B.; Weller, D. D. *Antisense Nucleic Acid Drug Dev.* **1996**, *6*, 267–272.

(55) Gebski, B. L.; Mann, C. J.; Fletcher, S.; Wilton, S. D. *Hum. Mol. Genet.* **2003**, *12*, 1801–1811.

(56) Keck, J. L.; Lu, D. *Proc. Natl. Acad. Sci. United States Am.* **2008**, 9169–9174.

(57) Lovett, S. T. *EcoSal Plus* **2011**, *4*.

(58) Weiss, B. *Enzym.* **1981**, *14*, 203–231.

(59) Ren, B.; Zhou, J.-M.; Komiyama, M. *Nucleic acids Res.* **2004**, *32*.

(60) Putney, S. D.; Benkovic, S. J.; Schimmel, P. R. *Proc. Natl. Acad. Sci.* **1981**, *78*, 7350–7354.

(61) Mol, C. D.; Kuo, C.-F.; Thayer, M. M.; Cunningham, R. P.; Tainer, J. A. *Nature* **1995**, 381–386.

(62) Frieden, M.; Christensen, S. M.; Mikkelsen, N. D.; Rosenbohm, C.; Thrue, C. A.; Westergaard, M.; Hansen, H. F.; Ørum, H.; Koch, T. *Nucleic acids Res.* **2003**, *31*, 6365–6372.

(63) Petersen, M.; Wengel, J. *Trends Biotechnol.* **2003**, *21*, 74–81.

(64) Kauppinen, S.; Vester, B.; Wengel, J. *Drug Discov. Today: Technol.* **2005**, *2*, 287–290.

(65) Nielsen, P. E.; Egholm, M.; Berg, R. H.; Buchardt, O. *Nucleic acids Res.* **1993**, *21*, 197–200.

Chapter 7

Experimental

7.1 Ferrocene Nucleic Acid Monomer Synthesis[1–4]

7.1.1 *Materials and Equipment*

Unless otherwise stated, solvents and reagents were obtained from commercial suppliers and used without further purification. Anhydrous solvents were obtained from solvent purification systems, SPS (Innovative Technology). Flash column chromatography was performed using silica gel (Merck, grade 60).^{1}H, ^{13}C and ^{31}P NMR spectra were recorded on Bruker AV 300 or AV 500 spectrometer. Electro-spray mass spectra were measured with a Waters micromass LCT Electro-spray Time-of-Flight (ES-TOF) mass spectrometer. Chiral HPLC enantiomer determination was carried out on a Waters system with Summit P580 pump and 996 Photo Array Detector UV/Vis Multi- Channel Detector using a Phenomenex Lux 5µ Amylose 2. HPLC solvent conditions: an isocratic method of 20% isopropyl alcohol in hexane. Water purified with a Millipore Elix-Gradient A10 system (resistivity > 18 µΩ cm toc ≤ 5 ppb, Millipore, France) was used during DNA/FcNA sample preparation and electrochemical experiments.

The tetra-substituted ferrocene monomer with two thymine base attachments (FcTT *(S,S)* and FcTT *(R,R)*) were synthesized by Dr Van-Huy Nguyen as previously reported.[5]

The synthesis for the FcHH *(S,S)* nucleic acid is given below. The synthesis of the *(R,R)* enantiomer was carried out identically, with the exception of the initial stereochemistry being introduced using the *(R)* -2-Methyl-CBS-oxazaborolidine (where CBS stands for Corey Bakshi Shibata). All characterisation data was the same.

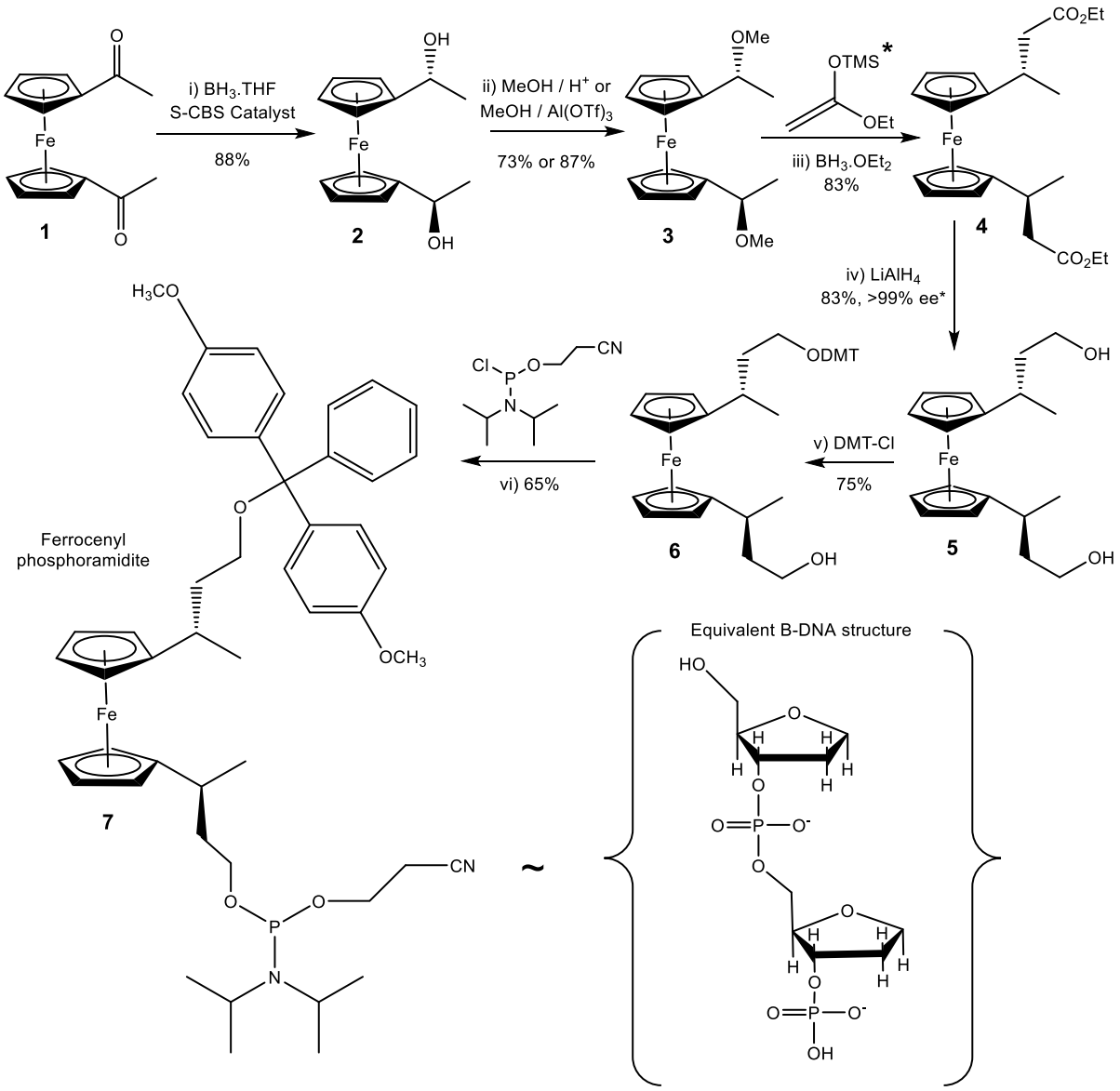

Scheme 7.1 Synthesis route of the FcHH (S,S) ferrocenyl phosphoramidite (for FcHH (R,R) ferrocenyl phosphoramidite the same scheme is used but the S-CBS catalyst is replaced with the R-CBS catalyst). The equivalent two sugar units and a phosphate linker of natural B-D

7.1.2 *(R,R)-1,1'-Bis(α-methylmethanol)ferrocene (2)*

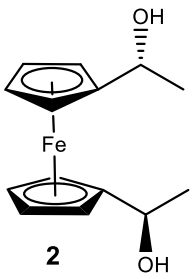

The *(S)*-2-Methyl-CBS-oxazaborolidine (330.00 mg, 1.20 mmol) (where CBS stands for Corey Bakshi Shibata) was dissolved in THF (12.00 mL) and cooled to 0°C under argon. From a syringe charged with $BH_3.SMe_2$ (1.00 M in THF, 4.00 mL) 20% of the final amount

(0.80 mL) was added to the catalyst solution. After 5 min stirring the remaining $BH_3.SMe_2$ and a solution of the **1** (2.00 mmol) in THF (5 mL) were added simultaneously within 20 min. The red colour of the ketone turned to yellow on reduction. After 15 min at 0°C the excess $BH_3.SMe_2$ was quenched by drop-wise addition of methanol (2 mL). After the hydrolysis had ceased the mixture was poured into saturated aqueous NH_4Cl (150 mL) and extracted with ether (200 mL). The organic layer was washed with water (2 x 100 mL) and brine (100 mL), dried, and then concentrated to an oil which was purified by column chromatography (30% ethyl acetate in hexane, 1% TEA) to give a yellow crystalline solid (4.72 g, 17.23 mmol, 88%).

R_f : 0.44 in 1:1 ethyl acetate: hexane. ^1H NMR ($CDCl_3$, 300MHz): δ = 4.7 (q, 2H, *J* = 6.4 Hz, CH), 4.1-4.3 (m, 8H, FcCH), 1.4 (d, 6H, *J* = 6.4 Hz, CH_3). ^{13}C NMR ($CDCl_3$, 101MHz) δ = 95.1 (Cp-ipso), 67.7 (CH-OH), 67.6 (CH-OH), 66.1 (Cp-CH), 65.7 (Cp-CH), 25.5 (CH_3). v_{max}/cm^{-1} = 3347 (OH), 2971 (CH), 2929 (CH). MS (ES) (*m/z*) calcd for $C_{14}H_{14}O_2$ $^{56}FeNa$ 274.1, found 274.1. MS (ES) (m/z) calcd for $C_{14}H_{18}O_2{}^{56}Fe$ (+ Na^+) 297.05, found 297.0557 $[M+Na]^+$.

7.1.3 *(R,R)-1,1'-Bis(α-methylmethoxy)ferrocene (3)*

7.1.3.1 Method 1

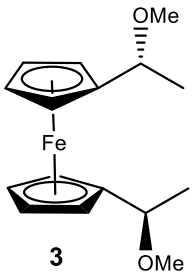

3

2.01g (7.33mmol) of **2** was stirred with 10% acetic acid (4 mL) in methanol at room temperature for 48 hours. The reaction mixture was diluted with H_2O and extracted with DCM. This was dried over $MgSO_4$ and dried *in vacuo*. The resulting oil was purified by column

chromatography (5% ethyl acetate in hexane, 1% TEA) to give a yellow oil (1.61g, 5.38 mmol, 73%).

7.1.3.2 *Method 2*

0.10g (0.37mmol) of **2** was dissolved in 0.6 mL methanol under argon then 0.009g of Al(OTf)3 (0.02mmol) was added. The mixture was stirred for 1.5 hours. This was then dried over $MgSO_4$. Hexane was added and this was dried *in vacuo* to 2 mL. Resulting mixture was purified by column chromatography (5% ethyl acetate in hexane, 1% TEA) to give a yellow oil (0.09g, 0.32 mmol, 86.9%).

R_f: 0.21 in 1:9 ethyl acetate: hexan. ^{1}H NMR ($CDCl_3$, 300MHz): δ = 4.1-4.3 (m, 8H, FcCH), 3.3 (s, 6H, OCH_3), 1.5 (d, 6H, *J* = 6.4 Hz, CH_3). ^{13}C NMR ($CDCl_3$, 101MHz) δ = 89.5 (Cp-ipso), 74.9 (CH-OCH_3), 69.4 (Cp-CH), 68.8 (Cp-CH), 68.6 (Cp-CH), 66.3 (Cp-CH), 55.7 (OCH_3), 20.1 (CH_3). v_{max}/cm^{-1} = 2974 (CH), 2926 (CH), 2815 (CH). MS (ES+) (*m/z*) calcd for $C_{16}H_{22}O_2Fe^{56}$ (+Na^+) 325.09, found 325.0868 $[M+Na]^+$

7.1.4 *((1-ethoxyvinyl)oxy)trimethylsilane*

6 mL of diisopropylamine (44 mmol) in 40 mL of THF was cooled to 0^{o}C under argon. 28 mL (44 mmol) of ^{n}BuLi was added and stirred for 20 min. The mixture was cooled to -78^{o}C and 4 mL (40 mmol) of ethyl acetate was added and stirred for a further 30min. 6 mL (48 mmol) of TMS-Cl was added dropwise and stirred for a further 30min. Mixture was warmed to room temperature and stirred for 1 hour. The resultant mixture was diluted with water (80 mL), extracted with hexane (160 mL) and washed with brine. This was then dried over $MgSO_4$, filtered and dried *in vacuo* then distilled at 45^{o}C. This gave a clear solution (3.66 g).

^{1}H NMR ($CDCl_3$, 300MHz): δ = 4.0 (q, *J* = 7.2 Hz), 3.6 (q, *J* = 0.2 Hz), 3.1 (s, H, CH), 2.9 (s, H, CH), 1.8 (s), 1.15 (dt, 5H, *J* = 20.1, 7.1 Hz, CH_3, CH_2), 0.0 (m, 9H, TMS)

7.1.5 *(S,S)-1,1'-Bis((α-methyl)methylpropanoate)ferrocene (4)*

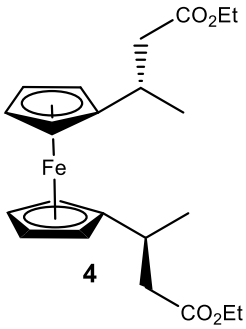

4

3 (0.50 mmol) and ((1-ethoxyvinyl)oxy)trimethylsilane (1.00 mmol) were dissolved in dry CH_2Cl_2 (5 mL) and cooled to -78 ^{o}C under an atmosphere of nitrogen. To the resulting solution was added drop-wise $BF_3.0Et_2$ (0.55 mmol) and the reaction mixture stirred at -78^{o}C for 15 min. The reaction was warmed to room temperature and quenched with saturated $NaHCO_3$ (aq) (10 mL). The product was extracted with CH_2Cl_2 (10 mL), dried over Na_2SO_4 and *in vacuo*. The residue was purified by column chromatography (10% ethyl acetate in hexane, 1% TEA) to give a yellow oil (0.75g, 1.81 mmol, 77%).

^{1}H NMR ($CDCl_3$, 300MHz): δ = 4.2 (q, *J* = 14.7, 7.1 Hz) CH_2), 4.1 (m, FcCH), 3.1 (m, CH), 2.58 (dd, *J* = 14.9, 5.3 Hz, CH_2O_2 (diastereotopic)), 2.32 (dd, *J* = 14.9, 9.2 Hz, CH_2O_2 (diastereotopic)), 1.3 (m, 2xCH3). ^{13}C NMR ($CDCl_3$, 101MHz) δ = 172.7 ($COOC_2H_5$), 94.2 (Cp), 68.1 (Cp), 67.9 (Cp), 67.2 (Cp), 66.3 (Cp), 60.3 (CH_2), 43.6 (CH_2 (diastereotopic)), 30.2 (CH), 20.8 (CH_2CH_3), 14.1 ($CHCH_3$). v_{max}/cm^{-1} = 2976 (CH), 1729 (CO). MS (ES) (*m/z*) calcd for $C_{24}H_{34}O_4Fe^{56}$ 415.11, found 415.1075 $[M]^+$.

7.1.6 *(S,S)-1,1'-Bis(α-methylpropanol)ferrocene (5)*

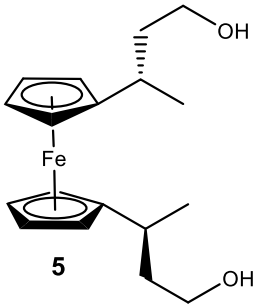

5

0.50g (1.21 mmol) of **4** was dissolved in 20 mL of dry THF. 0.18 g (4.83 mmol) $LiAlH_4$ was added in small portions. The mixture was left stirring under argon overnight. The reaction was

quenched with sodium potassium tartrate and the solution removed from the resultant gel. The solution was washed with diethyl ether, dried over Na_2SO_4 and *in vacuo*. It was then purified by column chromatography (3:1 diethyl ether: hexane).

A yellow oil was produced (0.33 g, 1.01 mmol, 83.5%). R_f: 0.16 in 3:1 diethyl ether: hexane. ^{1}H NMR ($CDCl_3$, 300MHz): δ = 4.03 (m, FcCH), 3.66 (m, CH_2), 2.6 (m, CH), 1.72 (m, CH_2 (diastereotopic)), 1.3 (d, *J* = 6.9 Hz, 2xCH_3). ^{13}C NMR ($CDCl_3$, 101MHz) δ = 95.3 (Cp), 67.9 (Cp), 67.8 (Cp), 61.1 (*C*H_2OH), 41.5 (CH_2 (diastereotopic)), 29.5 (CH), 20.7 (CH_3). v_{max}/cm^{-1} = 3311 (OH), 3089 (Fc CH), 2959 (CH), 2929 (CH), 2872 (CH). MS (EI) (*m/z*) calcd for $C_{18}H_{26}O_2Fe^{56}$ 330.13 found 330.1283 $[M]^+$. HPLC Ret. Time: 65.53 min, >99% enantiomeric purity. $[\alpha]_{20}^{D}$(deg cm^3 g^{-1} dm^{-1}) = 311.6 (*S,S*) and -342.8 (*R,R*) (c = 0.01 g in 1 mL DCM).

7.1.7 *(S,S)-1-(α-methylpropanol)-1'-(α-methylpropanoxy-4,4'-O-dimethoxytrityl) ferrocene (6)*

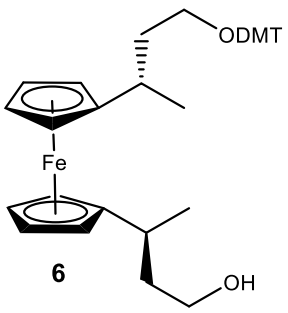

6

0.33 g (1.01 mmol) of **5** and 0.03 g (0.24 mmol) DMAP was dissolved in 5 mL anhydrous THF under argon. 0.34 g (1.00 mmol) DMT-Cl and 0.13 g (1.01 mmol) DIPEA were added to the reaction mixture and stirred under argon overnight at room temperature. The reaction mixture was then quenched with methanol and reduced *in vacuo*. This was then purified by column chromatography (1:1 ethyl acetate: hexane) to give a yellow oil (0.72 g, 1.73 mmol, 75%).

R_f: 0.64 in 1:1 ethyl acetate: hexane. ^{1}H NMR ($CDCl_3$, 300MHz): δ = 7.2-7.5 (m, 9H, Ar-CH), 6.8 (m, 4H, Ar-C*H*), 4.0 (m, 8H, FcCH), 3.8 (s, 6H, OCH_3), 3.7 (m, 4H, C*H*$_2$OH), 3.1 (t, 4H, *J* = 6.4 Hz, CH_2O), 2.6-2.8 (m, 4H, CH (diastereotopic)), 1.6-1.9

(m, 6H, CH_3 (diastereotopic)), 1.3 (d, 3H, *J* = 4.1 Hz, CH_3), 1.1 (d,3H, *J* = 6.8 Hz, CH_3). ^{13}C NMR ($CDCl_3$, 101MHz) δ = 158.3 (ipso-DMT), 145.4 (ipso-Ar), 136.7 (Ar-CH), 130.0 (Ar-CH), 128.2 (Ar-CH), 127.7 (Ar-CH), 126.6 (Ar-CH), 113.0 (Ar-CH), 95.7 (ipso-Cp), 95.1 (ipso-Cp), 67.8 (CH-Cp), 67.7 (CH-Cp), 67.6 (CH-Cp), 66.1 (CH-Cp), 65.8 (CH-Cp), 61.5 (CH), 61.1 (CH), 55.2 (OMe), 41.6 (CH_2), 38.6 (CH_2), 29.6 (CH), 20.9 (CH_3), 20.7 (CH_3). v_{max}/cm^{-1} = 3357 (OH), 2930 (CH). MS (EI) (*m/z*) calcd for $C_{48}H_{44}O_4Fe^{56}$ 632.26, found 632.2590 $[M]^+$.

7.1.8 *(S,S)-1-[(α-methylpropanoxyl)-(β -cyanoethyl)(N,N'- diisopropylamino) phosphine]-1'-(α-methylpropanoxy-4,4'-O-dimethoxytrityl) ferrocene (7)*

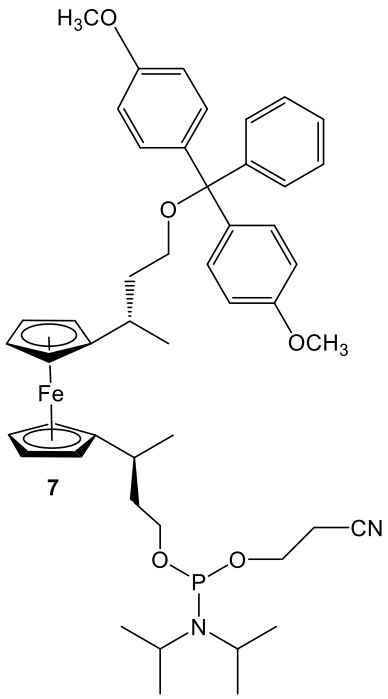

7

0.44 g of **6** (0.70 mmol) was azeotroped with 2 x 10 mL and then redissolved in 10 mL anhydrous acetonitrile. 3 mL of DIPEA (17.41 mmol) and 0.2 mL β- cyanoethyl (N,N-diisopropylamino) chlorophosphine (1.05 mmol) were added to this and stirred at room temperature, under argon, for 2.5 hours. The reaction mixture was then reduced *in vacuo*, extracted with degassed 1 x 10 mL ethyl acetate and washed with degassed $NaHCO_3$ (1 x 10 mL) and degassed brine (1 x 10 mL). This was dried over Na_2SO_4, reduced *in vacuo* and purified by flash column chromatography (2:1 hexane: ethyl acetate).

The product was a yellow oil (107.70 mg, 0.13 mmol, 65%). R_f: 0.08 in 2:1 ethyl acetate: hexane , ^1H NMR (300MHz, CDCl3), δ = 7.2-7.5 (m, 9H, DMT), 6.8 (m, 4H,

DMT), 3.8-4.1 (m, 10H, 8Cp, CH_2OP), 3.8 (s, 6H, OCH_3), 3.5-3.7 (m, 4H, $NCCH_2CH_2OP$, $NCHMe_2$), 3.1 (t, 2H, *J* = 6.5 Hz, CH_2ODMT), 2.60-2.70(m, 4H, $CNCH_2$, $CHMe_2$), 1.6-2.0 (m, 4H, CH_2CH_2O), 1.1-1.3 (m, 18H, 6xCH_3). ^{31}P NMR (121MHz, $CDCl_3$) δ = 147.2 ppm. MS (ES) (*m/z*), calcd for $C_{62}H_{77}N_6O_9Fe^{56}PNa$ 1159.4734, found 1159.4737 (M^+).

The phosphoramidite was then dissolved in anhydrous acetonitrile (1 mL per 100 mg phosphoramidite) and filtered through a 0.2 micron PTFE syringe filter into DNA synthesizer compatible vials. The solvent was then removed under high vacuum and the phosphoramidite was redissolved in anhydrous DCM (1 mL per 100mg). The solvent was once again removed under high vacuum and the final phosphoramidite was stored under argon at -20 ^oC until required.

7.1.9 Chiral Purity

To ensure the enantiomers were chirally pure, analytical HPLC was performed using a Phenomenex Lux 5µm Amylose-1 (250 × 4.6 mm) chiral column on both 1,1'-Bis(α-methylpropanol)ferrocene compounds (5). An isocratic method of 50:50 water and acetonitrile was used over 30 mins. The resulting chromatograms are shown in Figure 7.1. The (R,R) and (S,S) enantiomers were determined to be 83 and 90% enantiomerically pure, respectively.

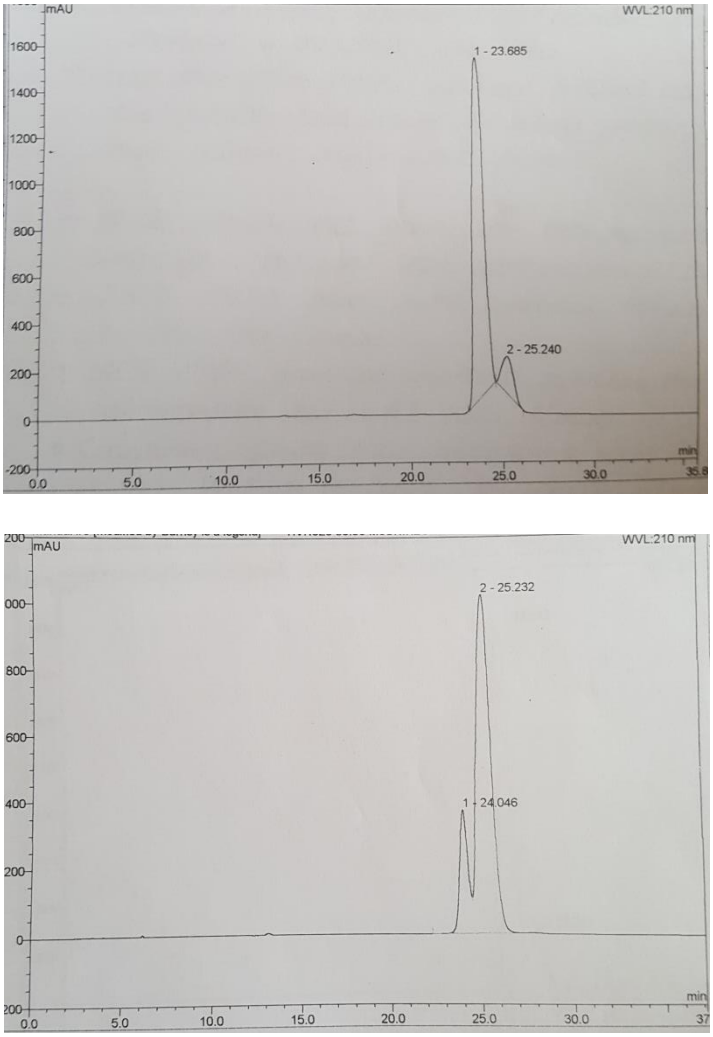

Figure 7.1 Chromatograms showing the chiral purity of Top: (S,S)-1,1'-Bis(α-methylpropanol)ferrocene and Bottom: (R,R)-1,1'-Bis(α-methylpropanol)ferrocene

7.2 Oligonucleotide Synthesis

All DNA and FcNA/DNA conjugates were synthesised using an Applied Biosystems ABI 394 (Foster city, CA, 30 USA) on a 1 μmol scale using solid phase synthesis. Strands intended for attachment onto gold electrodes were modified with 3′ Thiol Modifier C6 S-S disulphide. For activation of nucleosides before coupling 0.25 M ethylthiotetrazole in acetonitrile was used. Capping of unreacted material was carried

out using acetic anhydride and methylimidazole. To protect the oligonucleotide backbone 0.02 M iodine in water was used as an oxidising agent. Standard phosphoramidites of Bz-dA, iBu-dG, Ac-dC 25 and T were used for synthesis. The modified and unmodified phosphoramidites were dissolved in anhydrous acetonitrile to the concentration of 0.1 M prior to the synthesis. For addition of ferrocene modified nucleotides an extended coupling time of 10 min was used, while for standard bases a coupling time of 25 s was used. Oligonucleotides were treated with concentrated ammonia solution for 1 hour to cleave from the resin. DNA/FcNA samples were then deprotected by incubation at 55 ^{o}C for 6 hours. Solvent was then removed on a Thermo Scientific speed vac in preparation for purification.

HPLC purification was carried out on a Waters system with Summit P580 pump and 996 Photo Array Detector UV/Vis Multi- Channel Detector using a Phenomenex Clarity 5µ Oligo RP 150 x 10 mm C18 column. For FcNA/ DNA conjugates the solvent system was a gradient from 95 to 75% 0.1M triethylammonium acetate (TEAA) in acetonitrile followed by an acetonitrile wash (known as ThiolFerro). For DNA the solvent system was a gradient of 30-100% 0.1M TEAA in 15% acetonitrile with a 70-0% gradient of 0.1M TEAA in 5% acetonitrile (known as Oligo60). For the BFD/Fc conjugates and their equivalent DNA strands, the solvent system was 100% 0.1M TEAA in 15% acetonitrile for 10 min followed by an 100-70 % gradient (known as DMT-on). Collected fractions were dried *in vacuo*, diluted to 1 mL in MilliQ water and desalted using a NAP-10 column (GE Healthcare) whilst eluting to 1.5 mL.

Purity of oligonucleotides was determined using Phenomenex Clarity 5µ Oligo RP 150 x 4.6 mm C18 column on the same system as purification.

Mass spectrometry was kindly carried out by staff from the analytical facility in the Chemistry Department at the University of Birmingham. Samples were prepared in 1:1 H_2O:CH_3CN. Spectra were obtained on a Waters Synapt G-2S with a Waters Alliance e2695 pump attached. Data was collected using Mass Lynx 4.1 software and processed using the Maxent programme.

7.3 Electrochemistry

7.3.1 Equipment and Electrolyte Preparation

Electrochemistry was carried out with a 3 electrode system using a BioAnalytical Systems (BASi, USA) Inc. EC epsilon potentiostat with a gold disc, 1.6 mm diameter, working electrode, an Ag/AgCl reference electrode and platinum counter electrode (all provided by BASi, USA). Small glass containers, washed with 1:1 15% ammonia : 12-15% hydrogen peroxide solution for 4 hours and then generously rinsed with and soaked overnight in copious amounts of MilliQ water, were used to hold electrolyte or cleaning solutions. Water purified with a Millipore Elix-Gradient A10 system (resistivity > 18 μΩ cm toc ≤ 5 ppb, Millipore, France) was used throughout.

Electrolyte was prepared by mixing 6 mL of 2.5 M $NaClO_4$ and 1.5 mL of 100 mM phosphate buffer and then diluting to 15 mL to with MilliQ water to obtain a 1 M $NaClO_4$, 10 mM phosphate buffer, pH 7.0 solution.

7.3.2 Electrode Preparation

The working electrodes were polished in a figure of eight fashion using 3 and 1 μm diamond suspensions on a polishing pad (BASi, USA) and 1, 0.3 and 0.05 μm gamma alumina on a microcloth pad (Buehler, UK) before being subjected to

electrochemical cleaning in 0.5 M NaCl (scan rate 2 V s^{-1}, -0.35-1.35 V, 750 cycles) and 0.5 H_2SO_4 (two oxidation steps: 2 V for 5 s followed by -350 mV for 10 s and then a series of scans between -350 and 1500 mV (20 scans at 4 V s^{-1}, 4 scans at 0.1 V s^{-1})). The electrodes were then sonicated in 1:1 ethanol/water for 5 min before being finally washed in stream of MilliQ water for 1 min.

The counter electrode was a platinum wire which was cleaned by annealing with a Bunsen burner before quenching with MilliQ water and was then used immediately. Ag|AgCl Reference electrodes were stored in 3 M KCl and washed thoroughly in a stream of MilliQ water for 1 min before use.

7.3.3 Cyclic Voltammetry

Cyclic voltammograms were recorded at scan rates of 10, 20, 40, 60, 80, 100, 250 and 500 mV s^{-1} over -100-400 mV for ferrocene nucleic acids and 100, 200, 400, 600, 800, 1000, 1500 and 2000 mV s^{-1} over -350-725 mV for biferrocenylene tag experiments.

7.3.3.1 Determining Working Electrode Surface Area

The electroactive surface area was determined for each electrochemistry experiment by performing a CV scan from -350-1500 mV (at a scan rate of 500 mV s^{-1}) in 0.5 H_2SO_4 and determining the charge by integrating the oxide reduction peak as described in section 2.3.3.The literature value used to determine surface area was 482 μC cm^{-2}.[6]

7.3.4 Square Wave Voltammetry

Square wave voltammograms (SWV) were recorded between -100 and 400 mV for ferrocene nucleic acids or -350-725 mV for biferrocenylene tag experiments at a frequency of 200 Hz (unless otherwise stated) with a potential step of 4 mV and amplitude of 25 mV.

7.4 SAM Preparation and Application

7.4.1 SAM Preparation

SAMS were prepared as follows:

1) 2 µL of 100 µM disulphide protected probe oligonucleotide was centrifuged for 30 s with 2 µL of 10 mM TCEP in a 200 µL microcentrifuge tube and incubated for 60 mins to reduce the disulphide bonds. This was then diluted to 200 µL with 1 M $NaClO_4$, 10 mM phosphate buffer, pH 7.0 which had then been degassed for 15 minutes, to give a final DNA concentration of 1 µM.
2) The cleaned electrode was dried with an argon gun and left to incubate for 2 hours in the degassed FcNA/ DNA conjugate solution. (The cleaned electrode was placed in the microcentrifuge tube firmly, parafilm was placed round the electrode and tube to secure it and then the setup was turned upside down so the solution sat on top of the electrode surface).
3) The modified electrode was then washed with copious amounts of water and dried again using an argon gun.
4) The dried electrode was immediately placed into a degassed (15 mins) a 1.46 mL solution of 2 mM 6-mercaptohexan -1-ol in 1 M $NaClO_4$, 10mM phosphate buffer, pH 7.0 (electrolyte buffer) overnight.

5) The excess 6-mercaptohexanol was then washed off with copious amounts of water, dried with an argon gun and then subjected to electrochemistry.

7.4.2 DNA Target Binding Studies

Unless otherwise stated, the prepared working electrode was immersed in 5 mL of 100 nM target DNA dissolved in electrolyte buffer for 20 mins before electrochemical interrogation.

To recover the unhybridised SAM after target detection the electrode was soaked in a solution of 8 M Urea for 10 min before being washed with a stream of MilliQ water for 1 min. The electrode was then interrogated again to ensure the target had been removed.

7.4.3 Data Analysis

OriginPro 9.1 (Massachusetts, USA) was used to analyse all electrochemical data. Square wave voltammetry plots were subjected to background subtraction.

7.5. Mercury Binding Studies

Electrodes with SAMs were prepared as described in 7.4.1 and then soaked in 100 nM target DNA in electrolyte buffer for 20 mins. Unless otherwise stated, 8.8 mg of $Hg(ClO_4)_2$ (CAUTION: TOXIC) was dissolved in 10 mL 1M $NaClO_4$, 10 mM phosphate buffer to give a final concentration of 2 μM $Hg(ClO_4)_2$ solution. Prepared electrodes were then soaked in this solution for 1 hour. The subsequent SAMs were then washed in MilliQ water for 1 min and interrogated in electrolyte buffer using CV or SWV.

7.6 Surface Characterisation

7.6.1 Surface Preparation

For surface characterisation SAMS were prepared on 1 cm^2 100 nm thick polycrystalline gold on silicon wafer pre-coated with titanium (for ellipsometry and contact angle measurements) or 1 cm^2 50 nm thick gold on 1 nm chromium coated glass (XPS measurements) both provided by Georg Albert PVD –Beschichtungen, Germany.

SAMs were prepared as for electrochemistry but with increased volumes to ensure comparable coverages. 2 mL of 1 μM DNA or modified DNA was used for the DNA exposure and 2 mL of 2 mM 6-mercaptohexan-1-ol was used for the overnight soak.

7.6.2 Ellipsometry

Ellipsometry measurements were obtained on a Jobin-Yvon UVISEL ellipsometer with a xenon light source. Data was acquired between 250 and 800 nm with a 70^o angle of incidence.

The data was analysed with a three-phase ambient/SAM/Au model using DeltaPsi (Horiba Ltd, Japan). The SAM was assumed to be uniform and assigned a refractive index of 2.3. The thickness reported is the average and standard deviation was determined from three separate chips prepared with mixed monolayers and three measurements taken on each individual SAM (i.e. 9 measurements in total).

7.6.3 X-Ray Photoelectron Spectroscopy (XPS)

X-ray photoelectron spectra were obtained at the National EPSRC XPS Users' Service (NEXUS) at Newcastle University, an EPSRC Mid-Range Facility.

Data was analysed with CasaXPS (Casa Software Ltd., UK) and access was kindly provided by NEXUS.

7.7 Enzyme Digestion Studies

7.7.1 Enzymatic Digestion

DNase I, Exonuclease I and *Exonuclease III* were all derived from *E.coli* and were provided by New England BioLabs Inc. For each experiment 0.5 AU DNA or modified DNA was used (in both double stranded and single stranded) as calculated using the following equation:

$$\boldsymbol{Volume\ of\ stock\ required\ for\ 1\ AU} = \frac{\boldsymbol{Initial\ Volume\ of\ Stock}}{\boldsymbol{Initial\ Absorbance\ of\ Stock}} \qquad \text{Equation 7.1}$$

The DNA was incubated at 37 ^{o}C with the reaction buffer (67 mM Glycine-KOH, 6.7 mM $MgCl_2$, 10 mM β-ME, pH 9.5 @ 25°C) for 1 hour before the addition of the enzymes. 5 μL of a solution of 100 u mL^{-1} (therefore 0.5 u) of enzyme was used for each experiment.[7] Unless otherwise stated, the enzyme-containing DNA solutions were incubated in a water bath at 37^{o}C for 24 hours before being inhibited by both the addition of 20 μL formamide and heating (80 ^{o}C for 20 mins). The resulting samples were either used immediately or frozen at -20^{o}C until required.

7.7.2 Polyacrylamide Gel Electrophoresis (PAGE)

Gels were run on Hoefer SE400 or Bio-Rad Mini-PROTEAN Tetra Cell System gel kits with a Biorad PowerPac (HV 5000V/500mA/400W). Denaturing gels (for single stranded DNA/FcNA work) were run vertically in a gel consisting of 8 M Urea (14.4 g), 20% acrylamide (15 mL of a 40% stock solution), 1 x Tris Borate EDTA

(TBE) buffer (3 mL of 10 x TBE stock solution) and 1 mL water. Native gels (for all duplex DNA/FcNA work) were run vertically in a gel consisting of 20% acrylamide (15 mL of a 40% stock solution), 150 μL of 5 M NaCl solution, 1 x TBE buffer (3 mL of 10 x TBE stock solution) and 12 mL water. Both gel mixtures were polymerised using 20 μL TEMED and 200 μL 10% APS and then immediately placed in a 1 mm gel rack with a 20 μL well comb and allowed to set for 30 minutes.

5 μL of the appropriate sample was applied to the well and a 5 μL mixture of Bromophenol Blue (BPB) and Xylenecyanol FF (XCFF) dyes was run alongside the samples to determine electrophoresis progress (BPB tends to move with the solvent front whereas XCFF moves at a similar speed to 25 base pairs single strand of DNA). Gels were pre-run for 30 mins at 100 mV in 1 x TBE electrophoresis buffer. After loading the samples, gels were run for 5.25 hours at 100 mV in the same buffer. The gels were then visualised by UV shadow by placing on a silica plate and exposing to UV light.

7.7.3 Sample Excision from Gel

Samples were excised after completing the gel analysis by cutting out the UV active bands with a scalpel. The gel pieces were crushed in a microcentrifuge tube using a melted pipette tip with a pestle and mortar action. 500 μL of 1 x TBE solution was added for every 200 mg of gel pellets and the resultant suspension incubated at 37 overnight. This was then centrifuged at 13,000 g for 1 min before removing the supernatant and placing it in isopropanol at a ratio of 1:2 supernatent:isopropanol. The supernatant solution was dried *in vacuo*, diluted to 1 mL in MilliQ water and desalted using a NAP-10 column (GE Healthcare) whilst eluting to 1.5 mL. The sample was then used for mass spectrometric analysis as described in section 7.2

7.8 References

(1) Locke, A. J.; Richards, C. J.; Hibbs, D. E.; Hursthouse, M. B. *Tetrahedron: Asymmetry* **1997**, *8*, 3383–3386.

(2) Locke, A. J.; Richards, C. J. *Tetrahedron Lett.* **1996**, *37*, 7861–7864.

(3) Locke, A. J.; Gouti, N.; Richards, C. J.; Hibbs, D. E.; Hursthouse, M. B. *Tetrahedron* **1996**, *52*, 1461–1472.

(4) Corey, E. J.; Bakshi, R. K.; Shibata, S. *J. Am. Chem. Soc.* **1987**, *109*, 5551–5553.

(5) V. Nguyen, H.; Zhao, Z.; Sallustrau, A.; Horswell, S. L.; Male, L.; Mulas, A.; Tucker, J. H. R. *Chem. Commun.* **2012**, *48*, 12165–12167.

(6) Oesch, U.; Janata, J. *Electrochimica Acta* **1983**, *28*, 1237–1246.

(7) Putney, S. D.; Benkovic, S. J.; Schimmel, P. R. *Proc. Natl. Acad. Sci.* **1981**, *78*, 7350–7354.

Chapter 8

Appendices

8.1 Ferrocene Nucleic Acids: Surface Stability and Sensing

8.1.1 Oligonucleotide Characterisation

Table 8.1 Characterisation of oligonucleotides used in Chapter 3

Code	Oligo Sequence Number	Sequence (5' – 3')	Predicted Mass / Da	Observed Mass / Da	HPLC Method	Retention Time / min
S0	1254	TGG ACT CTT CTC AAT G -**SH**	5179.4	5179	Oligo60	39.1
$S1TT_{S,S}$	1162-1	TGG ACT C **FcTT$_{(S,S)}$** CTC AAT G -**SH**	5268.53	5268	ThiolFerro	37.0
$S1TT_{R,R}$	1160	TGG ACT C **FcTT$_{(R,R)}$** CTC AAT G -**SH**	5268.53	5268	ThiolFerro	34.5
$S1HH_{S,S}$	1158-1	TGG ACT C **FcHH$_{(S,S)}$** CTC AAT G -**SH**	4964.41	4964	ThiolFerro	35.6
$S1HH_{R,R}$	1156-1	TGG ACT C **FcHH$_{(R,R)}$** CTC AAT G -**SH**	4964.41	4694	ThiolFerro	35.4
S2AA	1173	CAT TGA G**AA** GAG TCC A	4914.3	4914	Oligo60	25.2
S2GG	1251	CAT TGA G**GG** GAG TCC A	4946.3	4945	Oligo60	30.4
S2CC	1195	CAT TGA G**CC** GAG TCC A	4866.2	4866	Oligo60	34.5
S2TT	1174	CAT TGA G**TT** GAG TCC A	4847.2	4847	See Section 8.4.1	
S2TA	1187	CAT TGA G**TA** GAG TCC A	4905.2	4905	Oligo 60	31.6

8.1.2 HPLC Traces

For S2TT see section 8.4.2

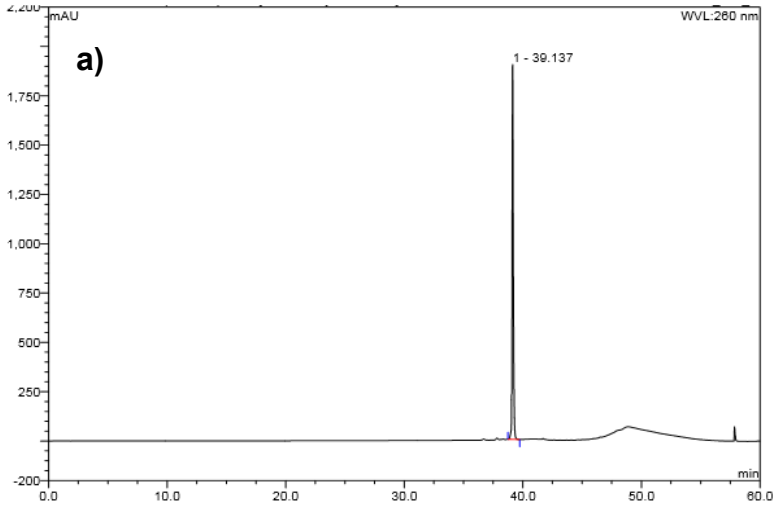

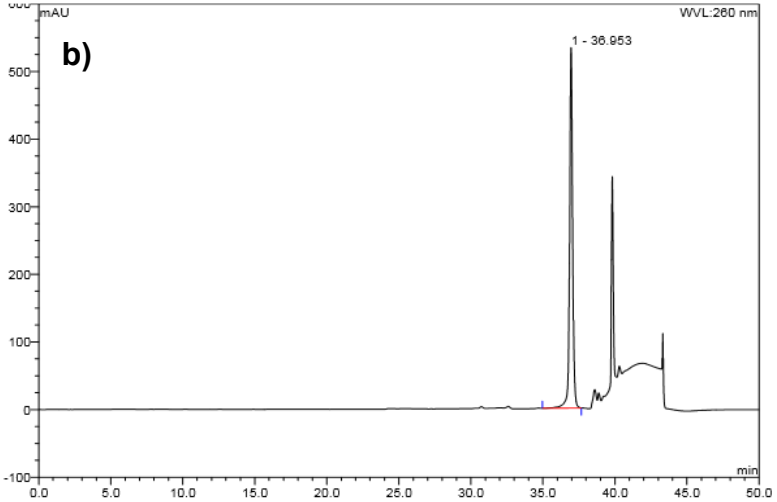

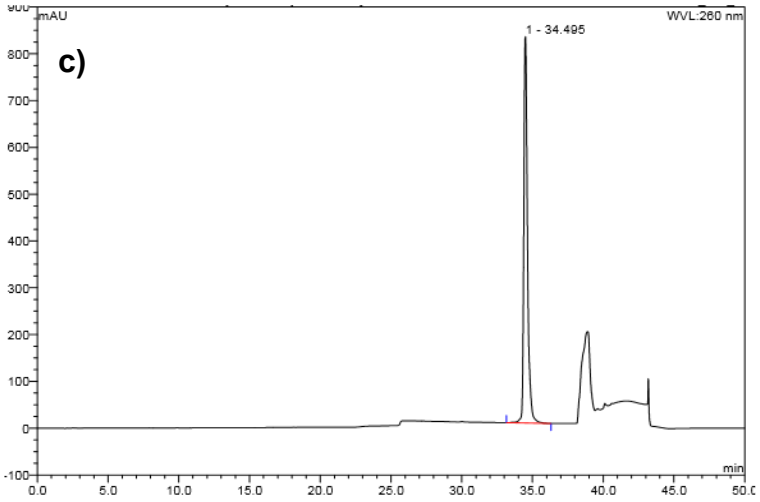

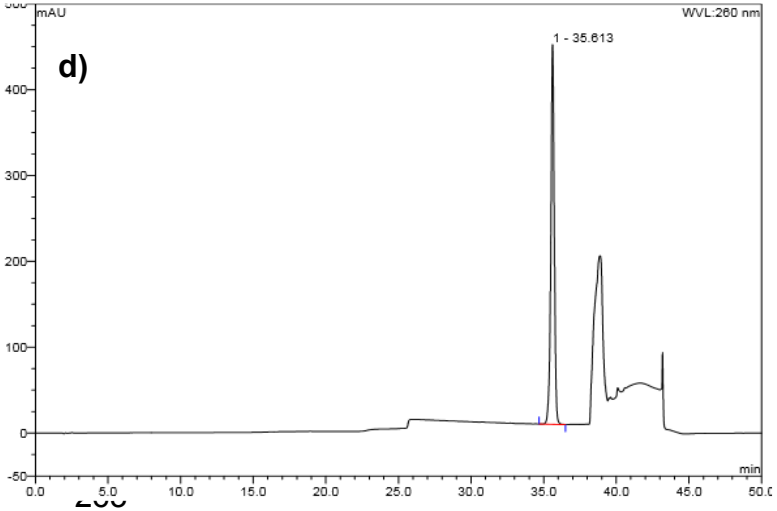

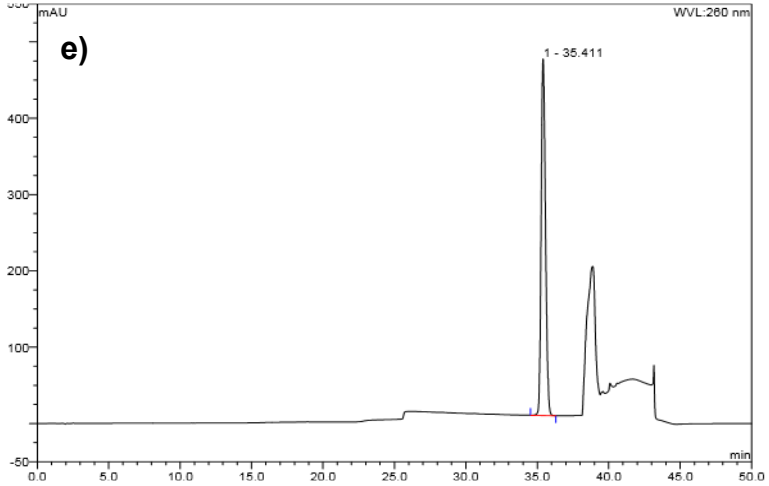
e)
mAU
WVL:260 nm
1 - 35.411
min

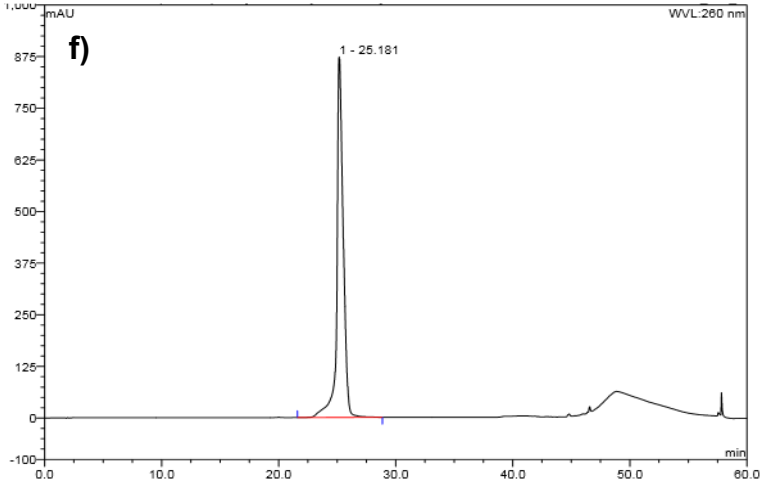
f)
mAU
WVL:260 nm
1 - 25.181
min

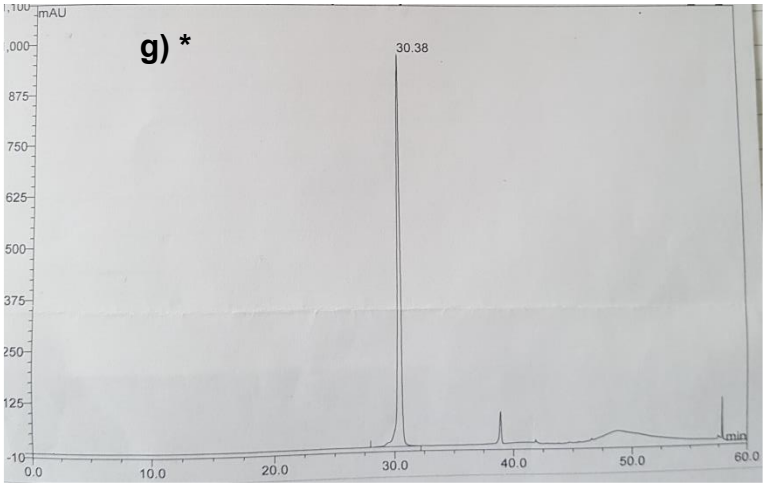
g) *
mAU
30.38
min

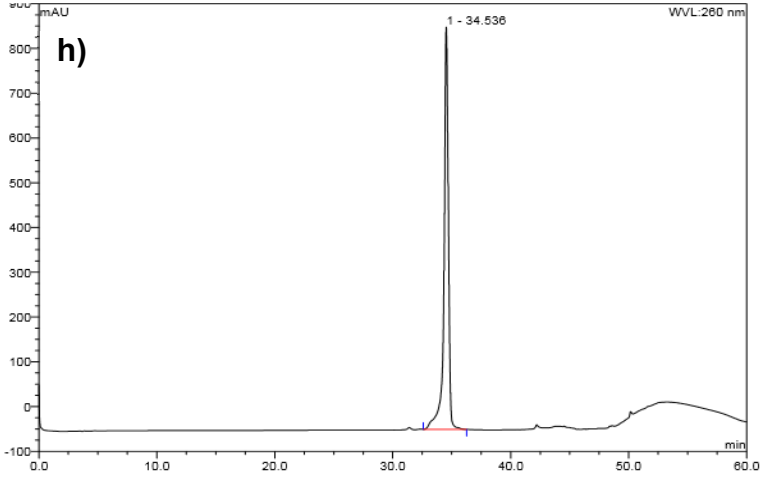
h)
mAU
WVL:260 nm
1 - 34.536
min

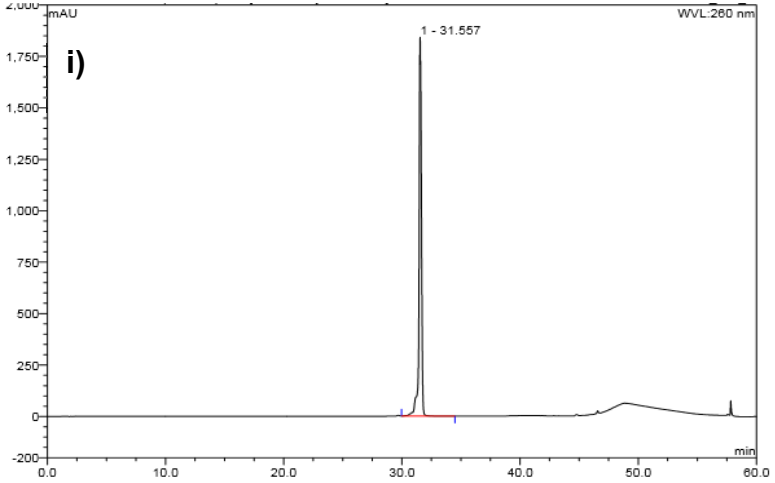

*Figure 8.2 Analytical HPLCs of a) S0 b) $S1TT_{S,S}$ c) $S1TT_{R,R}$ d) $S1HH_{S,S}$ e) $S1HH_{R,R}$ f) S2AA g) S2GG h) S2CC i) S2TA (Those marked with * are photographic copies taken from lab book copies of the HPLC traces due to loss of data from the main computer).*

8.2 Ferrocene Nucleic Acids for Electrochemical Mercury Detection

8.2.1 Oligonucleotide Characterisation

Table 8.2 Characterisation of oligonucleotides used in Chapter 4

Code	Oligo Sequence Number	Sequence (5' – 3')	For Mass and HPLC Data See Section:	For HPLC Trace See Section:
S1TT	1162-1	TGG ACT C **$FcTT_{(S,S)}$** CTC AAT G -**SH**	8.1.1	8.2.1
S1HH	1158-1	TGG ACT C **$FcHH_{(S,S)}$** CTC AAT G -**SH**	8.1.1	8.2.1
S1HH (NT)	1157	TGG ACT C **$FcHH_{(S,S)}$** CTC AAT G	8.4.1	8.4.2
S2	1173	CAT TGA GTT GAG TCC A	8.1.1	8.2.1

8.3 Biferrocenylene Tagged DNA: Surface Stability and Sensing

8.3.1 Oligonucleotide Characterisation

Table 8.3 Characterisation of oligonucleotides used in Chapter 5

Code	Oligo Sequence Number	Sequence (5' – 3')	Predicted Mass / Da	Observed Mass / Da	HPLC Method	Retention Time / min
$S1_{BFD}$	1253	**BFD** GT TTC TGG ATC TAC TAA TGT TTC - SH	7943	7941	DMT-on	18.9
$S1_{Fc}$	1588-1	**Fc** GT TTC TGG ATC TAC TAA TGT TTC - SH	7762	7762	DMT-on	19.6
S2	811	GAA ACA TTA GTA GAT CCA GAA AC	7074	7074	DMT-on	19.4
S3	814	TCC GCT GCA TGC TCC ATT CCA AG	6935	6933	DMT-on	24.0

Purification of 1588-1 was carried out on an Agilent 1260 Infinity system with 1260 Quat pump rather than the Waters system described in Chapter 7. This was due to a change in standard instrumentation but only affected this particular oligonucleotide.

8.3.2 Analytical HPLC Traces

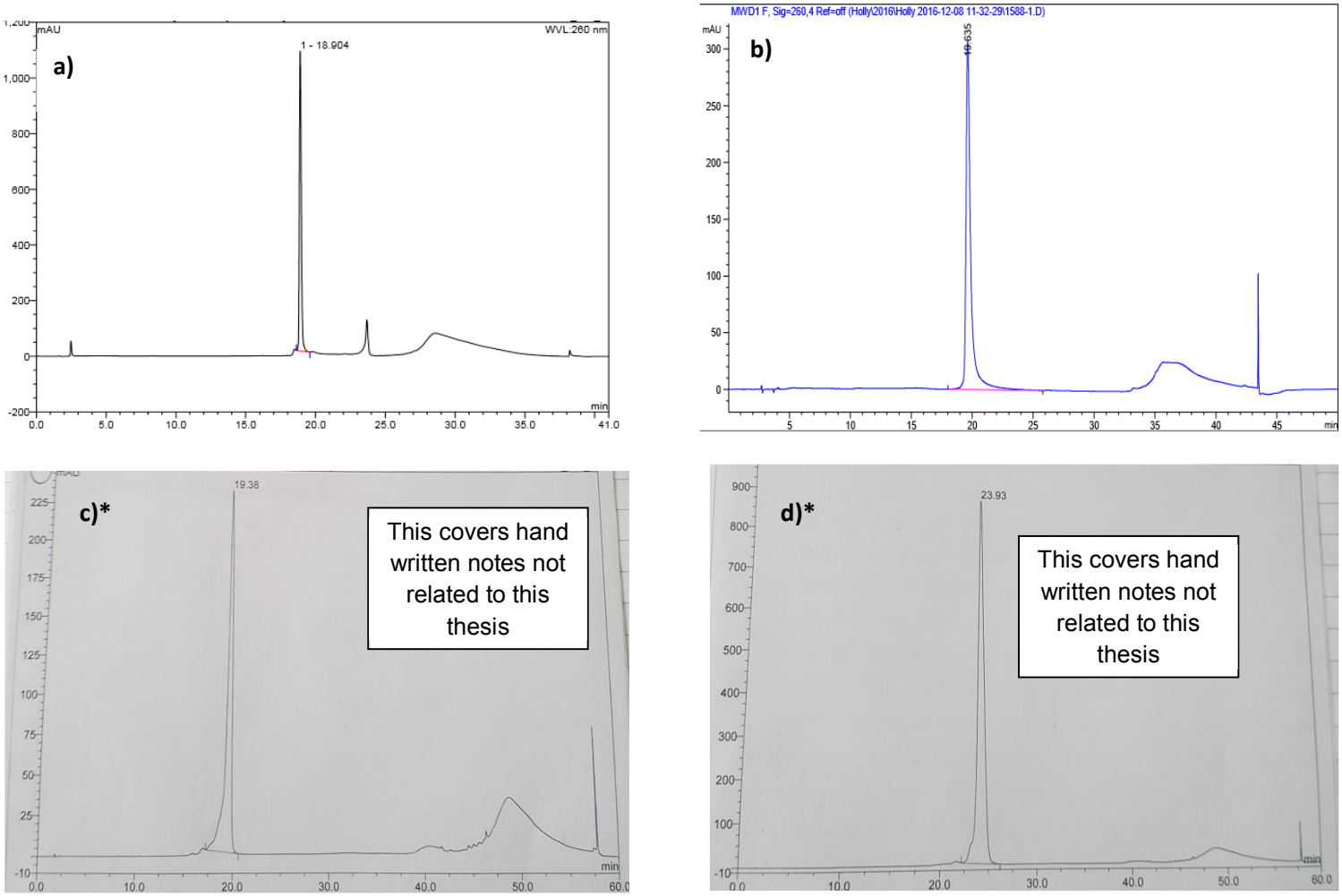

*Figure 8.3 Analytical HPLC of a) $S1_{BFD}$ b) $S1_{Fc}$ c) S2 d) S3. (Those marked with * are photographic copies taken from lab book copies of the HPLC traces due to loss of data from the main computer).*

8.3.3 Controls experiments for BFD and Fc tagged DNA SAMS

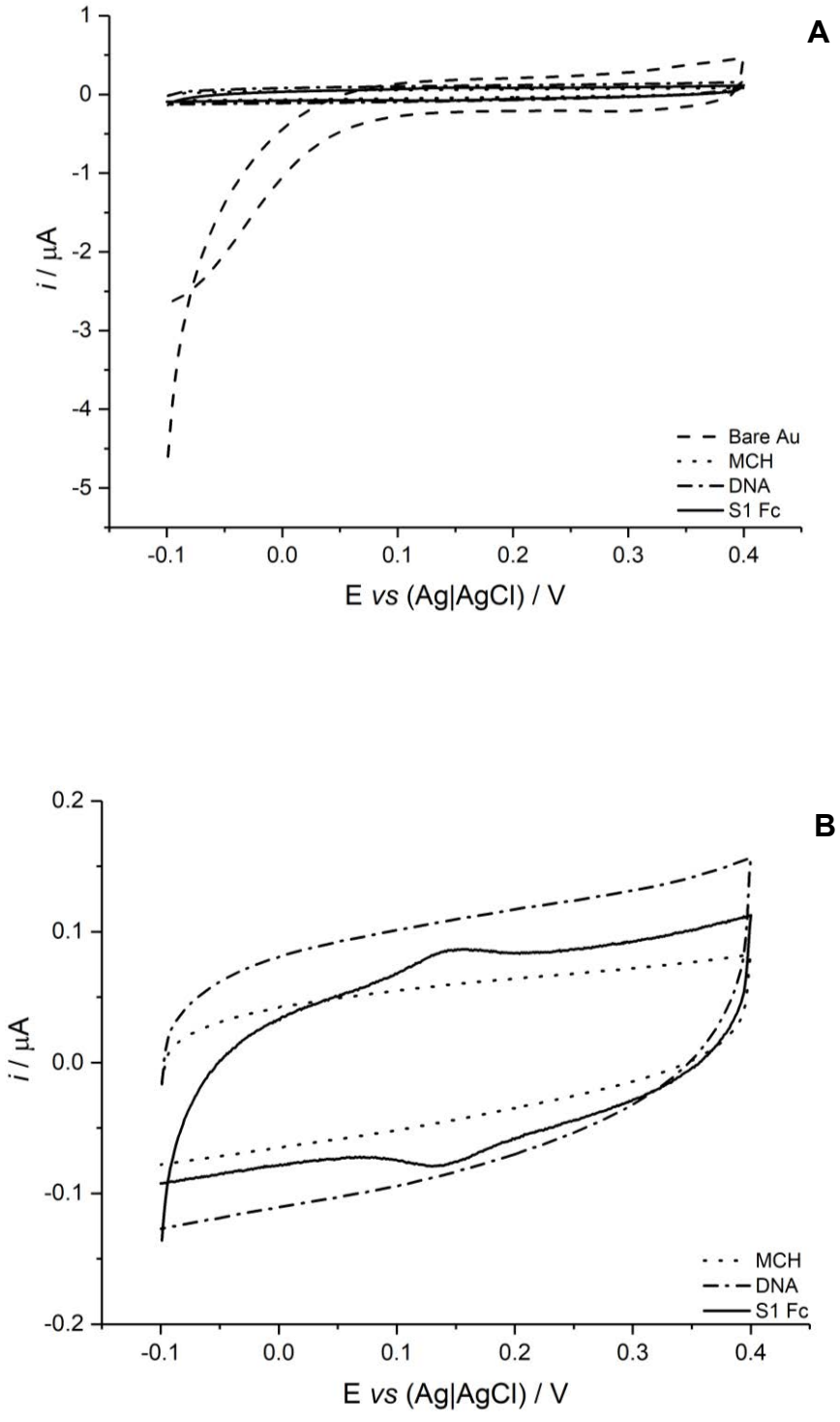

Figure 8.4 Cyclic voltammograms of A: Bare gold, MCH monolayers, natural DNA mixed monolayers and $S1_{Fc}$ mixed monolayers (B: without Bare Au to allow for ease of comparison). CV recorded at 100 mV s^{-1} in 1mM $NaClO_4$, 10 mM phosphate buffer

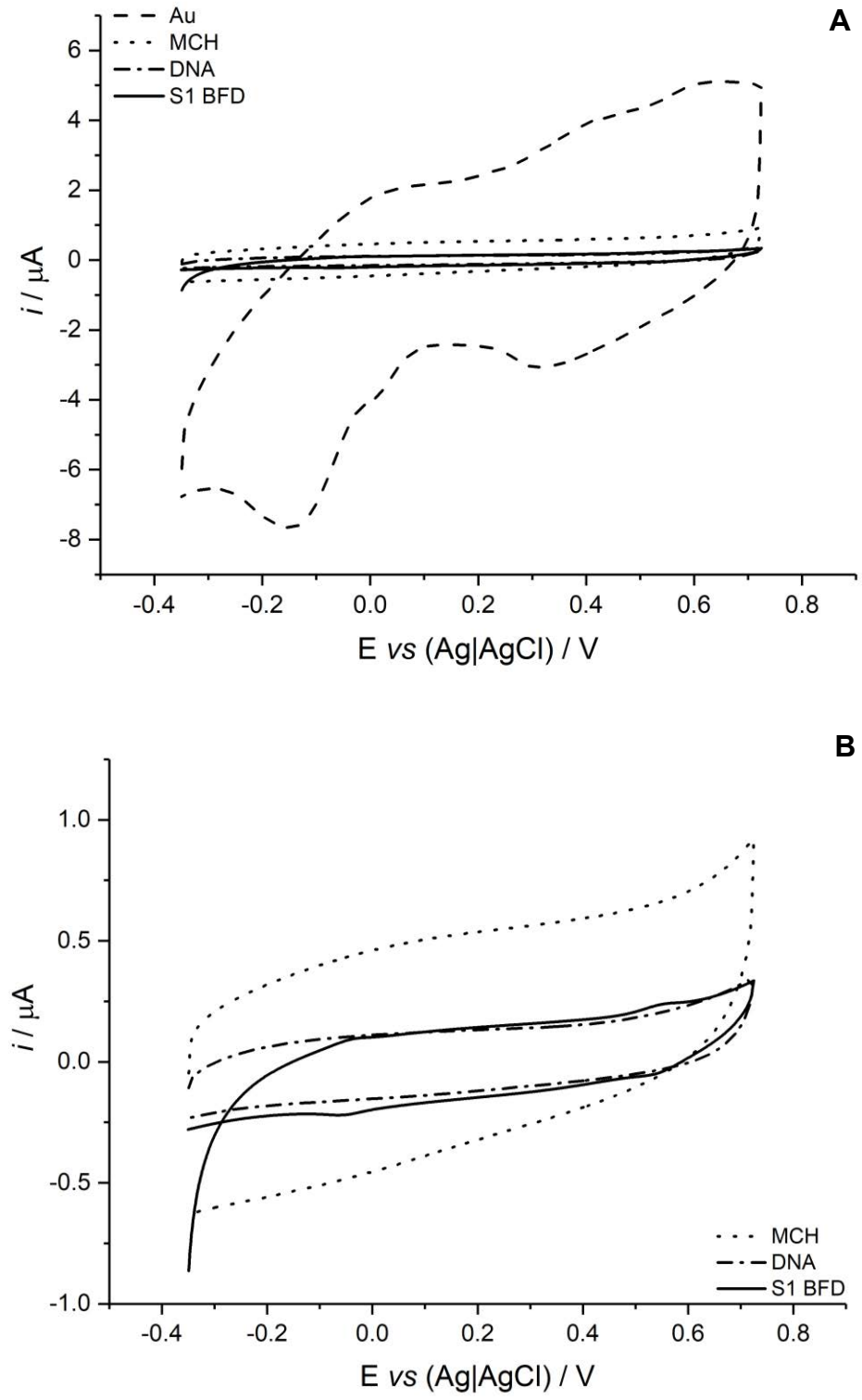

Figure 8.5 Cyclic voltammograms of A: Bare gold, MCH monolayers, natural DNA mixed monolayers and $S1_{BFD}$ mixed monolayers (B: without Bare Au to allow for ease of comparison). CV recorded at 100 mV s-1 in 1mM NaClO4, 10 mM phosphate buffer

8.3.4 Variance of $S1_{BFD}$ with SW frequency

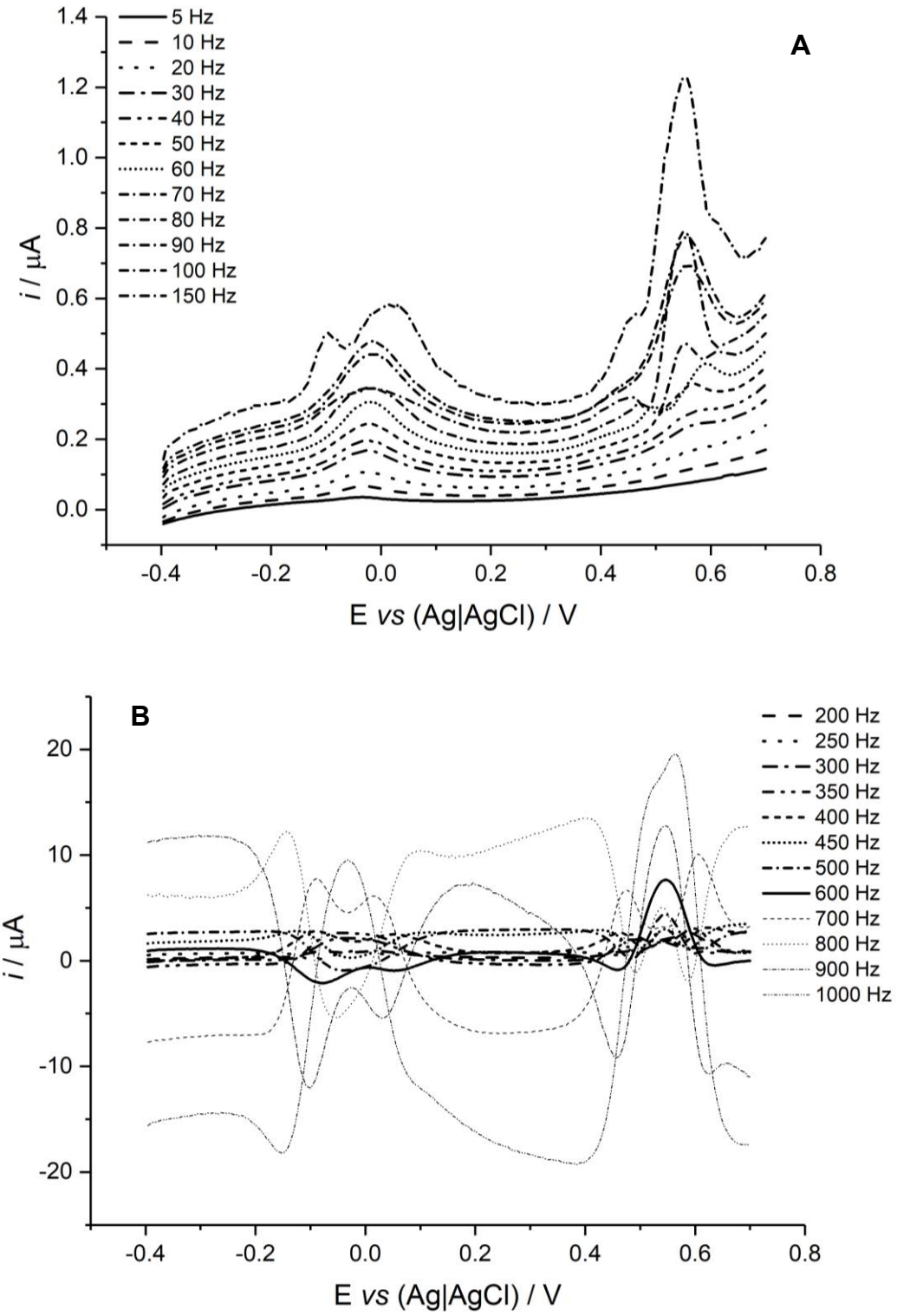

Figure 8.6 SWV of $S1_{BFD}$ mixed monolayers recorded at varying frequencies, a step of 1 mV and amplitude of 25 mV in 1 M $NaClO_4$, 10 mM phosphate buffer

8.3.5 Initial CV of $S1_{BFD}$

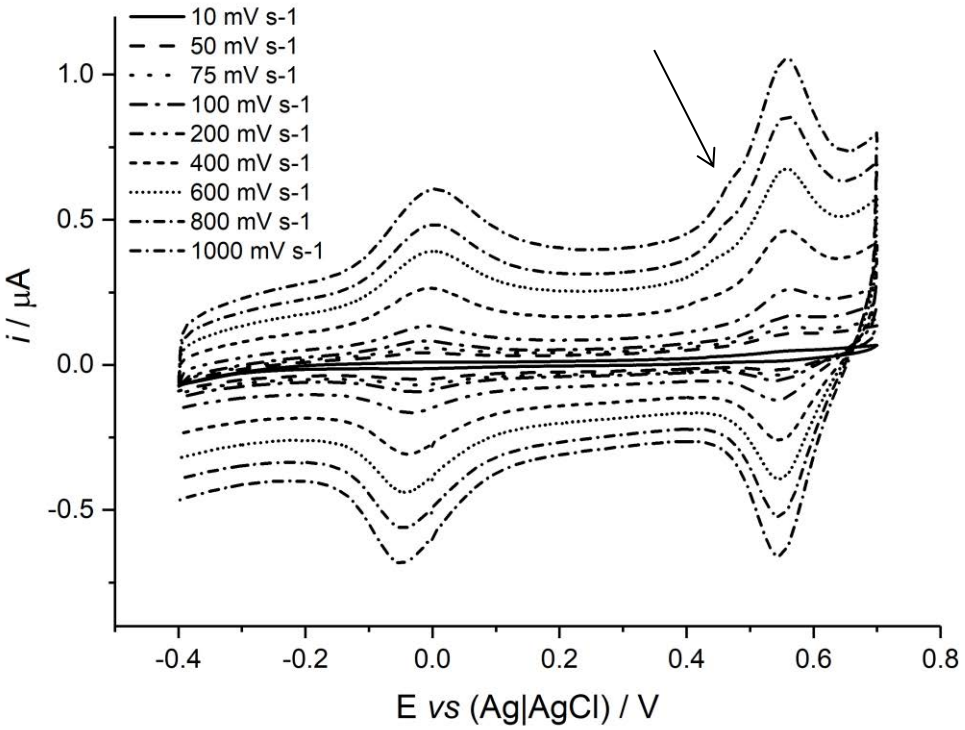

Figure 8.7 Initial CV of $S1_{BFD}$ used to determine most appropriate scan rate range. Shoulder peak (denoted by an arrow) due to extended potential window highlighted. CVs recorded in 1 M $NaClO_4$, 10 mM phosphate buffer.

8.4 Enzymatic Digestion of Ferrocene Nucleic Acids

8.4.1. Oligonucleotides Characterisation

Table 8.4 Characterisation of oligonucleotides used in Chapter 6

Code	Oligo Sequence Number	Sequence (5' – 3')	Predicted Mass / Da	Observed Mass / Da	HPLC Method	Retention Time / min
S0	1174	TGG ACT CTT CTC AAT G	4847	4847	Oligo60	25.7
$S1_{HH}$	1157	TGG ACT C **FcHH** CTC AAT G	4631	4630	ThiolFerro	30.1
$S1_{TT}$	1161	TGG ACT C **FcTT** CTC AAT G	4936	4934	ThiolFerro	30.0
S2	1239	CAT TGA GAA GAG TCC A	4914	4914	Oligo60	25.3

8.4.2. Analytical HPLC Traces

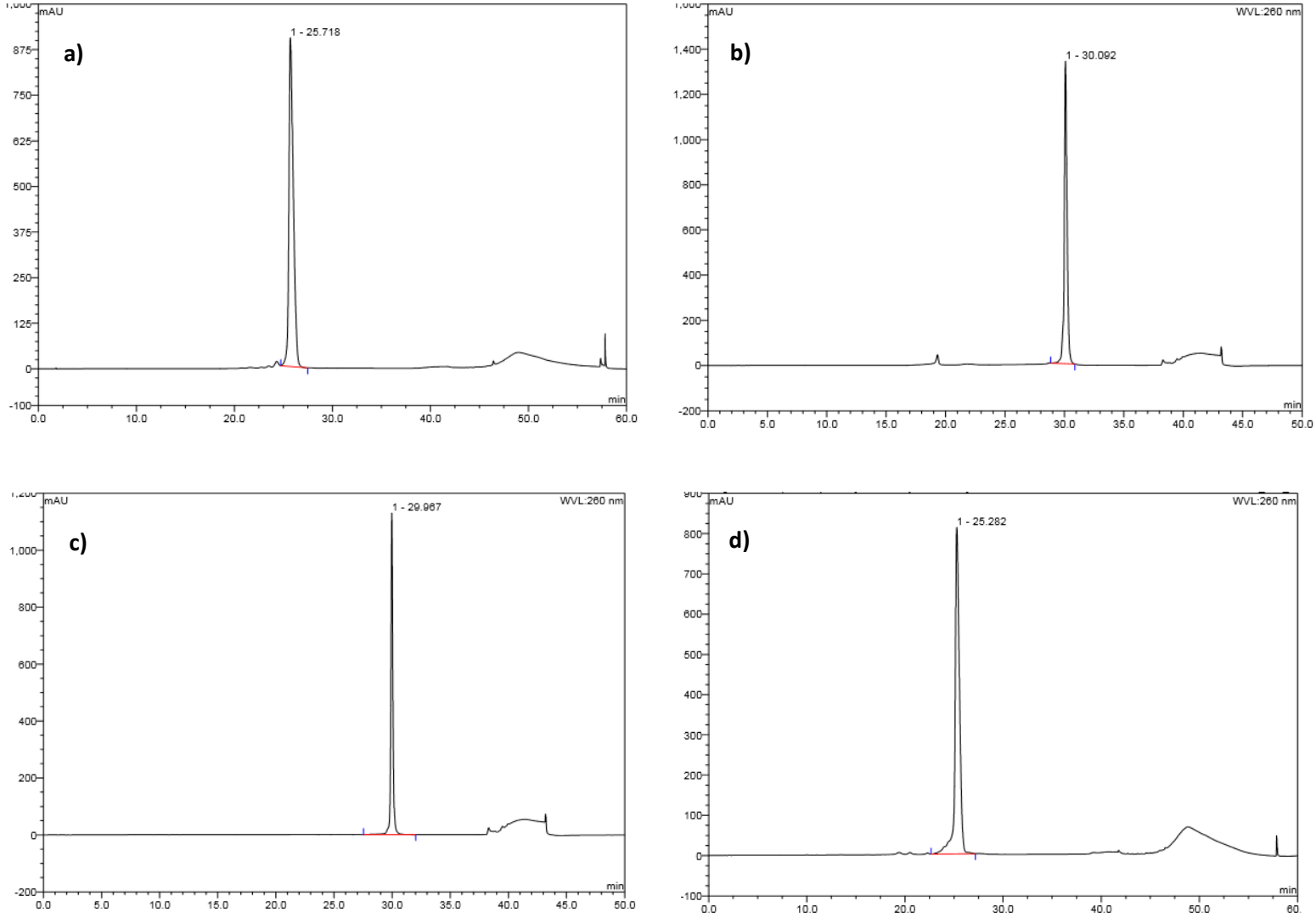

Figure 8.8 Analytical HPLC traces of a) S0, b) $S1_{HH}$, c) $S1_{TT}$ and d) S2

8.4.3. Mass Spectrometric Data for Exo I Digestion Products

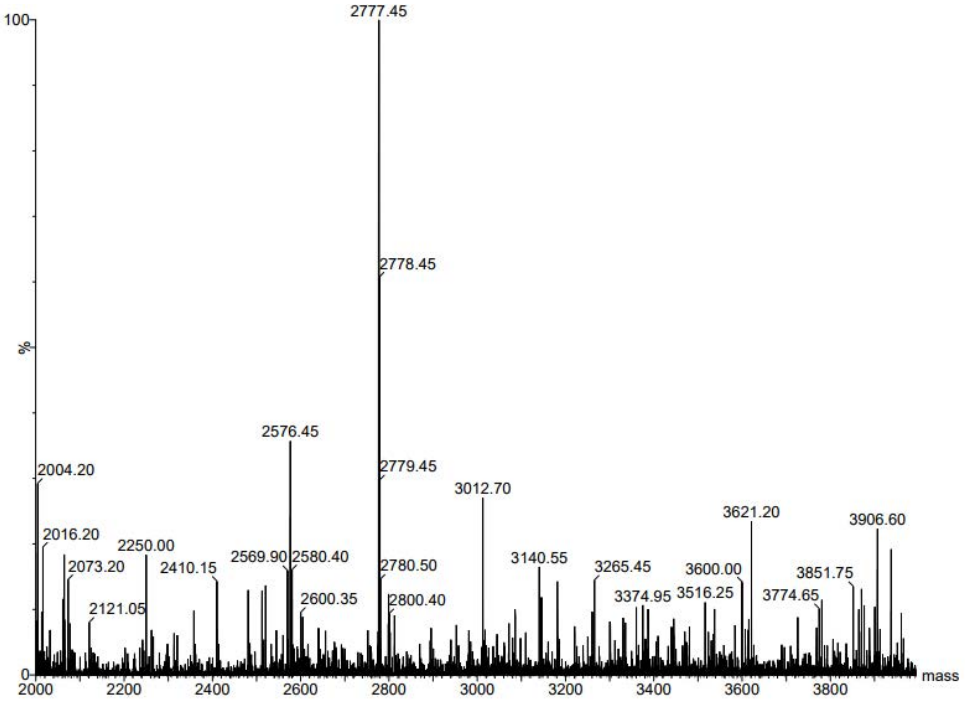

Figure 8.9 Deconvoluted ESI mass spectrum of degradation product when $S1_{HH}$ is digested by Exo I for 72 hours at 37°C

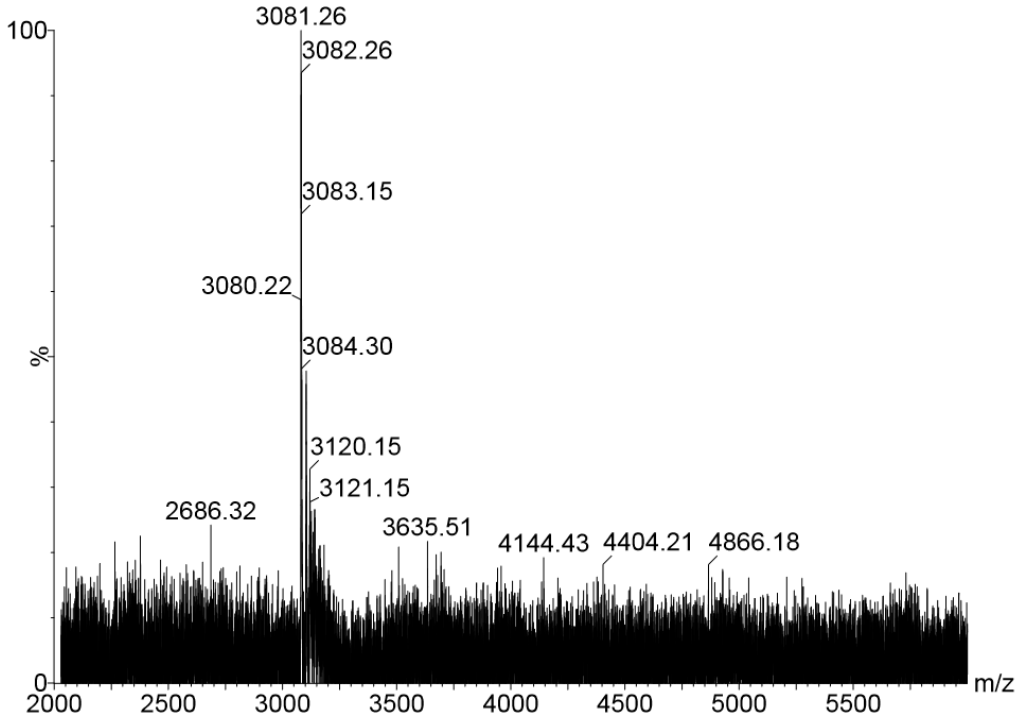

Figure 8.10 Deconvoluted ESI mass spectrum of degradation product when $S1_{TT}$ is digested by Exo I for 72 hours at 37°C

8.4.4. Mass Spectrometric Data for Exo III Digestion Products

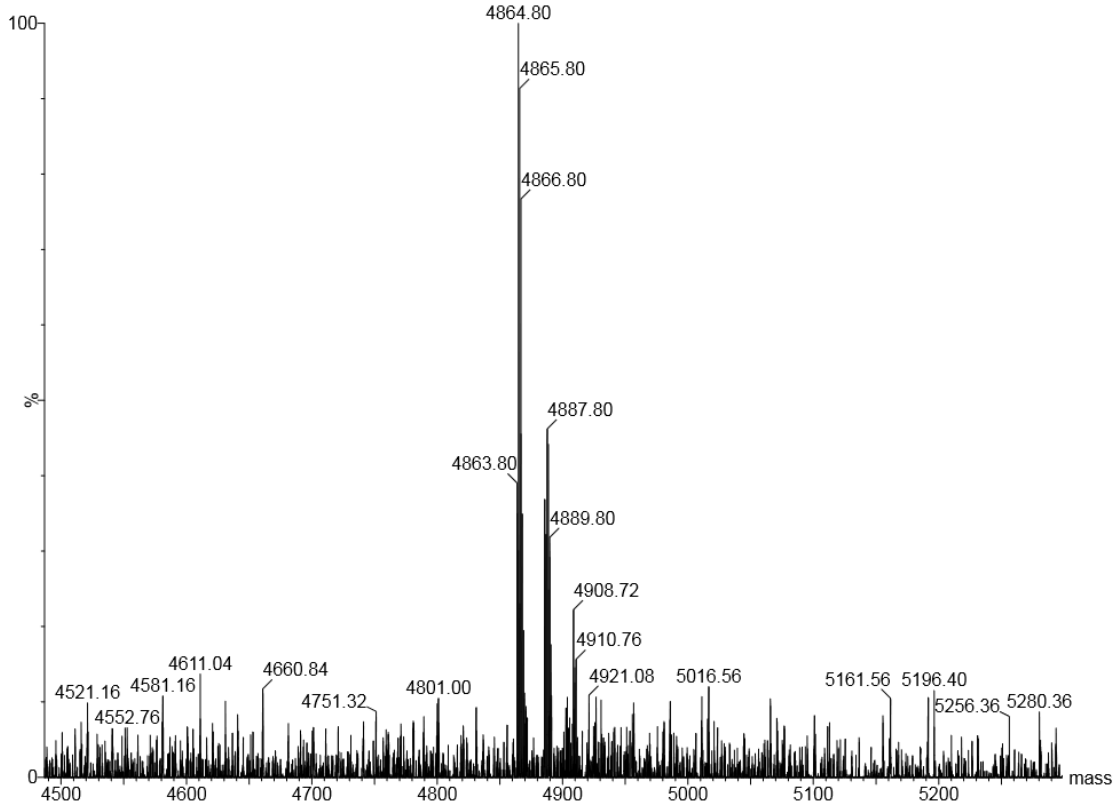

Figure 8.11 Deconvoluted ESI mass spectrum of degradation product when $S1_{HH}$ is digested by Exo III for 72 hours at 37°C

8.5 List of Publications

Publications:

1. Jonathan L. Kedge, Huy V. Nguyen, Zahra Khan, Louise Male, Media K. Ismail, **Holly V. Roberts**, Nikolas J. Hodges, Sarah L. Horswell, Youcef Mehellou, James H. R. Tucker, '*Organometallic Nucleoside Analogues: Effect of Hydroxyalkyl Linker Length on Cancer Cell Line Toxicity*', Eur. J. Inorg. Chem., 2017: 466–476. doi:10.1002/ejic.201600853
   (This work does not relate to work discussed in this thesis)
2. Luca Pisciottania, Maxime Douarrea, Brigitte Bibala, Clotilde Davies, **Holly Roberts**, Brice Kauffmann, Sarah L. Horswell, James H. R. Tucker and Nathan D. McClenaghan. '*Macrocyclic Hamilton-type Receptors Comprising a Ferrocene Pivot'*, Supramolecular Chemistry, under review, due for publication 2018.
   (This work does not relate to work discussed in this thesis)

Oral Presentations:

1. H.V. Roberts, *Ferrocene Conjugated DNA Probes for Electrochemical Sensing*, 5th Euro Biosensors and Bioelectronics Conference, 2016, Valencia, Spain.

Poster Presentations:

1. H. V. Roberts, J. Carr-Smith, J-L. H. A. Duprey, V-H. Nguyen, S. L. Horswell and J. H. R. Tucker. *Development of Modified Ferrocenes DNA Probes for Electrochemical SNP Sensing,* presented at*:*
    a. 12th Nucleic Acids Forum, 2015, London, UK
    b. Next Generation Tools for DNA Diagnostics, 2015, Edinburgh, UK
    c. RSC MASC 2015, 2015, Durham, UK
    d. Id^2, 2015, Birmingham
    e. 13th Nucleic Acids Forum, 2016, London, UK
    f. Chemical Nanoscience Symposium 6, 2016, Newcastle, UK